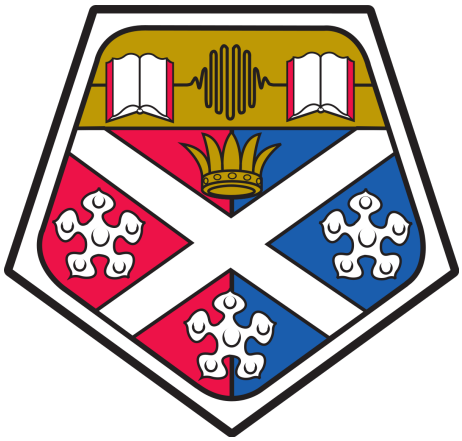

Expanding Adiabatic Horizons:

Computing counterdiabatic driving in new models

PhD Thesis

Ewen D C Lawrence

Strathclyde Open Quantum Systems

Department of Physics

University of Strathclyde, Glasgow

February 12, 2026

This thesis is the result of the author's original research. It has been composed by the author and has not been previously submitted for examination which has led to the award of a degree.

Contents

Acknowledgements

A PhD is often described as both a journey and a marathon, and many people expect this knowledge will prepare them for what is to come. At the very least, I felt this way at the beginning. I believed I could overcome my own naivety by knowledge of those who came before me. Now sitting at the end, reflecting on this time period, I can see the ironic nature of such a notion. Any journey will have unseen turns, no matter how hard you strive to 'cure' your own ignorance. Knowledge of the challenges can help, but to overcome them, it is necessary to build the resilience needed to tackle them as they appear, and to get back up when you get knocked down. During my PhD, there have been many times I have had to learn this lesson, with many tests along the way. I am greatly proud of the academic achievement this thesis represents, however I believe the resilience I have gained to be my biggest personal growth. So, in my certain naivety and ignorance of the future ahead, I still feel prepared for the challenges that life has lined up for me, with the greater knowledge of overcoming adversity I now possess. Surely these words will age like fine wine.

Firstly I would like to thank my supervisor Peter Kirton for his fundamental support during my studies. The direction of my PhD changed many times, and you were always there to help and guide no matter where we ended up. I have greatly enjoyed our meetings over the past years, both from an academic and a personal view, and I am truly grateful to have had you as my supervisor. I also wish to thank Callum Duncan, for introducing me to the subject of this thesis and the many thought-provoking chats we had about it. I thank my second supervisor Andrew Daley, and the QOQMS group for providing both a stimulating and welcoming environment at Strathclyde. Likewise I wish to thank members of the CNQO group, in particular Grant Henderson,

Lorenzo Carfora, Kathryn McInroy and Alessandro Civolani for making the office a truly enjoyable place to work.

There were many people who made my time in Glasgow a special experience, and I thank you all for the many boardgame sessions, bad movie nights, and other social activities. I want to thank my fellow SOQS group member, Simon, for many an enjoyable game session ranging from Dark Souls to Brass Birmingham, alongside the interesting physics discussions we had. Likewise, I thank Gerard for the many board games we played, and for always being around for a chat about how work was going. I thank Ieva for the many helpful discussions on the AGP, and being able to talk about the frustrations we had during our studies. Also I thank Ryan, as there were many activities I got up to whilst at Glasgow, but few I enjoyed and remember more than playing snooker and pool with him. We may need a lot of practice to even become amateurs, but I will always remember the games alongside our chats. Another unforgettable recurring event would surely be the bad movies nights, which I thank Tomas for hosting with his trademark enthusiasm and whimsy. Your approach to life and its challenges, greatly shaped how I now view the world, and I thank you greatly for it. In a similar vein, I thank Sridevi for always being there to listen and discuss, be it about physics or anything else, and somehow always have an interesting thing to say. Additionally I wish to thank my family for their continued support. I thank Gran and Andrew for providing a wonderful place to visit both in early childhood and more recently. I greatly thank my brothers Kit, Pip and Tom for providing non-stop humour and wit in my life, with a bit of chaos sprinkled in here and there. I will always remember our trip up to Loch Lomond with Silvi and Soph, which was truly a wonderful memory to share with all of you. To my mother Val who has supported me no matter the circumstances, free from any pressures to be anyone other than who I am, I thank you dearly. Likewise to my father Chuff, for encouraging me at a young age to complete maths puzzles, pushing me to learn whenever I could, and challenging my views and ideas through my whole life, I cannot thank you enough.

The final person I wish to thank, is Sebastian. That we could share this time during our studies together as flatmates, colleagues and more importantly as friends,

has been pivotal in this journey. You are never afraid to share your opinion, or to stand up to those around you when it is necessary. Even when times are tough, you find a childlike sense of joy, always finding something to laugh about the world. Whilst we were not always the best motivation for the academic side, as our adventures in Bloodbourne would attest, the times we did work in tandem lead to some of my most proud academic achievements during the PhD. I hope you understand how grateful I am for your presence, and the many lessons about physics, the world and life as a whole that you have taught me.

List of Figures

List of Figures

Chapter 1

Introduction

There any many technologies we use on a daily basis that make use of quantum mechanics, such as the electronic device this thesis is likely being read on, that have drastically shaped the way we live over the last hundred years. However, we have barely scratched the surface of potential applications, with many phenomena being secluded to laboratory experiments or sometimes still only theoretical. There are many steps on the path between explaining the underlying theory, and applying it to the everyday world. Even at the time of writing, some 350 years after Newton wrote down the laws of classical mechanics, engineers and physicists still find new applications of his theory.

Whilst there are surely many more years of development ahead, we wish to highlight some of the most successful quantum applications up to the time of writing. Firstly there is the field of semiconductor physics, which has played a fundamental role in our advancement of electronics, allowing for smaller and more dense computing units [1–3]. Another quantum technology that has had numerous applications are lasers, which have been used for studying quantum optics [4, 5], applications in communication networks [6, 7], and even in medical procedures [8, 9]. Applications of quantum phenomena in measurement devices lead to the field of quantum sensing [10, 11], with resulting technologies such as atomic clocks [12, 13] and magnetometers [14, 15]. The field of quantum communication [16], has explored the use of quantum cryptography to protect our data [17, 18], and quantum entanglement to transfer information across large distances [19]. Currently, one of the most sought after technologies is that of

quantum computers [20, 21], with the ability to overcome the exponential scaling of quantum problems, either universally with digital quantum computers [22, 23], or more specifically with analogue quantum computers [24, 25]. This lists a few of the key applications so far of quantum mechanics, but what steps need to be taken to further the number of quantum applications? Of course, there are many answers to this question, with many different interesting and useful areas of quantum physics, but we shall look at one step in particular, namely the control over a quantum system [26, 27].

In almost all experiments, some parameter will need to be varied, whether to prepare a state [28–30], or to look at out of equilibrium phenomena [31, 32]. However many losses occur into unwanted states during these processes, for example arising from coupling to a external environment [33, 34], or from diabatic excitations [35, 36]. To combat environmental coupling, protocols can be developed to avoid states with high loss such as with STIRAP [37–39], or feedback can be used to return the lost information [40, 41], alongside other methods [42–44]. However, even for a closed or near to closed system, diabatic excitations still need to be accounted for by designing a pulse to use the excitations productively [45, 46], adding an extra feedback step to address the populations of unwanted states [47, 48], or driving the pulse adiabatically to reduce the effect of the excitations [49–51]. Narrowing down the topic of this thesis again, we will look at adiabatic driving and how to increase driving speed whilst retaining the adiabatic following. This field of speeding up adiabatic pulse are known as shortcuts to adiabaticity [52, 53], and can range in application in many forms. Some example include using invariants and scaling [54, 55], or fast-forward techniques [56, 57].

We in particular are interested in counterdiabatic driving [58, 59], where an extra operator is added to the Hamiltonian to counteract any diabatic excitations. Counterdiabatic driving first appeared as an idea in quantum chemistry by Demirplak and Rice [60], but was also independently formulated under the name ‘transitionless driving’ at the same time by Berry [61]. The operator that provides the counterdiabatic driving is referred to as the Adiabatic Gauge Potential (AGP) [36, 58]. The AGP can provide significant insights into the dynamics of a Hamiltonian [36], which is still an ongoing area of research, with current examples including the strength of diabatic losses [62], or

a measure for quantum chaos [63–65]. As such the AGP is a very valuable operator to compute, however it is often not straightforward to do so, as its dimension is near the size of the full Hilbert space for most non trivial cases. In addition, whilst in principle it is always possible to apply a counterdiabatic drive, in practise the AGP can be difficult to implement [59]. This has led to approximate forms being developed, for example using only local operators [58], generating relevant operators form nested commutators [66], or Krylov methods [67, 68]. Whilst these methods do not have the ability to perfectly remain in a given eigenstate of a Hamiltonian, they can still greatly improve adiabatic procedures [69], or be used in conjugation with other control methods to help simplify the optimisation procedure [70, 71].

A large focus in AGP research has been targeted towards quantum information [62, 71–73], as improving quantum gate fidelity allows more accurate results, and shortening pulse sequence prevents losses in current quantum hardware from decoherence [74–76]. This has been one reason why the majority of AGP research has been focused on spin-1/2 models, such that qubits in quantum computers can be addressed. However there any many models beyond spin-1/2 that are of interest to physicists, with some implementations of quantum information using larger spins such as with qutrits [77, 78], or including the environment in the equations for a true open systems description [34, 79]. As such to be able to describe other quantum systems such as bosonic or fermionic physics, it is important to expand the current scope of AGP physics beyond spin-1/2 models, developing methods that work across many different types of systems. This is a key theme of this thesis, expanding the current scope of physical models the AGP has been applied to, and providing methodology within these new bases.

1.1 Thesis outline

The remainder of this thesis is divided in to six chapters, that take the reader step by step through the physics of the AGP, allowing understanding of the results and conclusions in the later chapters. Chapter 2 will explain the background theory, starting from the Schrödinger equation and working the way to a definition of the AGP. To do

this we look at what adiabaticity is, how diabatic excitations limit the speed of adiabatic protocols, why the AGP can be used to resolve this problem, and some methods used to compute the AGP. Then in Chapter 3 we explain the method we developed in Ref. [80], that we use as a base method for the later results. The method highlights some key aspects of the AGP, and how we can think about the underlying operators that form the AGP. Whilst the majority of AGP research currently focus on spin-1/2 physics, due to the wide range of applications and the relative simplicity compared to other models, we also describe the necessary steps for tackling large spin models using generalised Gell-Mann matrices.

Once the background theory and methods are explained, we move onto the three results chapters. Each chapter focuses on a different type of physical system: Chapter 4 for spin models, Chapter 5 for bosonic models, which are combined together in Chapter 6 for hybrid models. This means there are a wide variety of models discussed in thesis, each with its own complexity, unique problems and specific applications. A large amount of work in Chapter 4 is focused on the spin-1/2 Ising model with different graph configurations, which we previously presented in Ref. [80]. We also discuss the XXZ model, comparing the results between having spin-1/2 and spin-1 particles. We find as expected that the spin-1 model provides extra complexity, and far worse scaling than the spin-1/2 version.

Computing the AGP in bosonic models leads to some signifiant differences to the spin models, with issues from the infinite nature of bosonic Hilbert spaces and the standard creation and annihilation operators being non stationary. In Chapter 5 we discuss all of this, providing examples for a coherently driven bosonic mode, showing it is possible to compute the AGP in bosonic systems. We find that all quadratic bosonic models have a finite AGP of relatively small order, and provide a closed form solution for Real Hermitian Hamiltonians. Using the information then of the previous two chapters, in Chapter 6 we combine these together into hybrid systems of spins and bosons. While care needs to be taken with each of the subsystems, no new issues arise in the methodology, allowing computation in this new subset of models. Hybrid systems are vital to our understanding of open quantum systems, meaning this is a

crucial step in expanding AGP physics towards speeding up open system protocols. We focus on a single spin-1/2 inside a bosonic cavity, with and without the rotating wave approximation applied, giving results for the Jaynes Cummings and Rabi models respectively. We find that even though the Jaynes Cummings model has a conserved excitation number, this can be broken via varying the cavity frequency. In the Rabi model, we approximate the cavity as a large spin, meaning the results can also be used to describe pure spin models as well, with the result approach the bosonic case as the spin size is increased. We provide an analytical form of the set of equations to solve for the AGP in the Rabi model, which allows the spin size to be pushed high to ensure the validity of the approximation. Finally in Chapter 7, we collect together our conclusions from the results of the thesis. We see how the necessary ground work has been laid out for the AGP to be computed and used in many new physical models, however much more research is required to find practical applications in the new models.

Chapter 2

The Adiabatic Gauge Potential

As outlined in the introduction, the main topic of this thesis is on the Adiabatic Gauge Potential (AGP). This chapter will start from the time dependent Schrödinger to explain adiabatic dynamics, working through gauge potentials and counterdiabatic driving, giving a full explanation of the physics of the AGP. The last part of this chapter then focuses on how to compute the AGP, before deep diving into the main method we use in this thesis next chapter.

2.1 Dynamics of non static Hamiltonians

A static quantum system is described by a Hamiltonian $\hat{H}$ that is independent of time, eg. $\hat{H}(t) = \hat{H} \forall t$. The dynamics of the system can be solved by the time dependent Schrödinger equation

$$i\hbar \frac{d}{dt} |\Psi(t)\rangle = \hat{H} |\Psi(t)\rangle , \tag{2.1}$$

where $|\Psi(t)\rangle$ is the wave function at time t. The general solution to this equation is given by

$$|\Psi(t)\rangle = \sum_n c_n^0 |n\rangle e^{-iE_n t/\hbar}, \tag{2.2}$$

where c_n^0 is a coefficient that represents how much of a particular mode is present, given by

$$c_n^0 = \langle n|\Psi(0)\rangle , \tag{2.3}$$

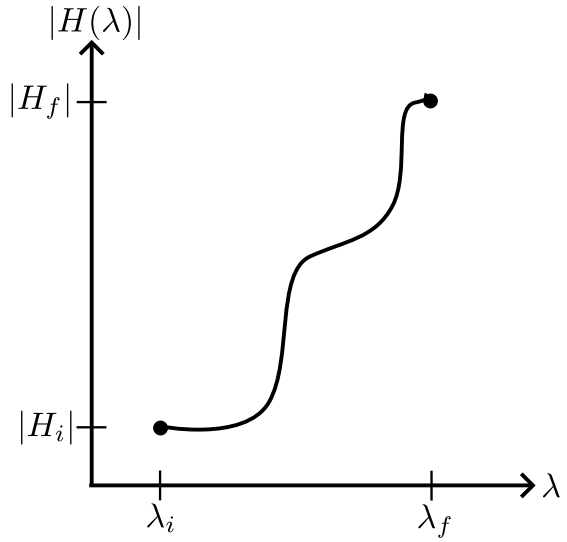

Figure 2.1: Sketch of the parametrisation of the Hamiltonian by λ, where the Hamiltonian is defined by λ at all points. The control sequence can then be thought of travelling along this line, at some arbitrary speed $\dot{\lambda}(t)$, where the initial and final times correspond to the respective initial and final Hamiltonians. By using this intermediate variable λ, further computation can be done independent of path and speed

and E_n, $|n\rangle$ are energy eigenvalues and eigenstates of the time independent Schrödinger equation

$$\hat{H}\,|n\rangle = E_n\,|n\rangle\,. \tag{2.4}$$

From Eq. (2.2) we see that there is no change in magnitude between eigenstates, as c_n^0 is time independent so $|\,\langle n|\Psi(t)\rangle\,| = |c_n^0|$. Instead only the relative phase of the eigenstates varies, with it being dependent on the eigenvalue E_n. This means if a Hamiltonian can be efficiently diagonalised, the dynamics are then trivial to compute.

The situation is more complex if the Hamiltonian varies with time [81, 82]. We focus on the common case for quantum control [27], where for $t \leq 0$ the Hamiltonian will be given by $\hat{H}(t \leq 0) = \hat{H}_i$, which will then undergo some variation up to some final time t_f, where for $t \geq t_f$ the Hamiltonian will stay in the form $\hat{H}(t \geq t_f) = \hat{H}_f$. This is often written in terms of an intermediate control variable $\lambda(t)$ which itself is dependent on time. This variable is defined as being $\lambda(t = 0) = \lambda_i$ and $\lambda(t = t_f) = \lambda_f$, such that the initial and final values of λ correspond to the associated Hamiltonian ($\hat{H}(\lambda = \lambda_i) = \hat{H}_i$ and $\hat{H}(\lambda = \lambda_f) = \hat{H}_f$). A sketch of this is given in Fig. 2.1, which

illustrates how λ defines a path that takes the Hamiltonian form the initial to the final form. How this path is traversed is placed into the functional form of $\lambda(t)$ and $\dot{\lambda}(t)$, allowing later results to be defined independent of path and speed for the same Hamiltonian parametrisation.

The time dependent Schrödinger equation also describes the time dynamics of this varying system, where now the Hamiltonian is dependent on $\lambda(t)$

$$i\hbar\frac{d}{dt}\left|\Psi(t)\right\rangle = \hat{H}\left(\lambda(t)\right)\left|\Psi(t)\right\rangle. \tag{2.5}$$

This means the general solution now has $\lambda(t)$ dependence as well

$$\left|\Psi(t)\right\rangle = \sum_n c_n\left(\lambda(t)\right)\left|n\left(\lambda(t)\right)\right\rangle e^{i\Phi_n(\lambda(t))}, \tag{2.6}$$

where $c_n\left(\lambda(t)\right)$ and $\Phi_n\left(\lambda(t)\right)$ are the time dependent magnitude and phase of mode the n eigenstate. Whilst it is true that this still describes all possible solutions to the equation, without knowing the form of the $\lambda(t)$ dependence, the only real information this is saying is that the solution can be expressed in an eigenbasis at each time step.

As the Hamiltonian is varying with $\lambda(t)$, so are the eigenstates $\left|n\left(\lambda(t)\right)\right\rangle$, as such we have an instantaneous eigenbasis at each specific value of $\lambda(t)$. These instantaneous eigenstates can be calculated, similar to the static Hamiltonian case, using the time-independent Schrödinger equation

$$\hat{H}\left(\lambda(t)\right)\left|n\left(\lambda(t)\right)\right\rangle = E_n\left(\lambda(t)\right)\left|n\left(\lambda(t)\right)\right\rangle. \tag{2.7}$$

Using the idea of instantaneous eigenstates, we can now split the problem into three different cases distinguished by the speed of the variation ($\dot{\lambda}(t)$): Adiabatic dynamics, Diabatic dynamics and Quench dynamics.

2.1.1 Adiabatic dynamics

The first case is when the variation of $\lambda(t)$ is sufficiently slow such that the dynamics are adiabatic. In general, sufficiently slow means following the standard adiabatic

condition, which can be stated as [83]

$$i\hbar\dot{\lambda}\frac{\langle m_\lambda|\,\partial_\lambda\hat{H}_\lambda\,|n_\lambda\rangle}{\left(E_m(\lambda)-E_n(\lambda)\right)^2}\ll 1, \tag{2.8}$$

with $|m_\lambda\rangle$ the eigenstate closest in energy to the eigenstate $|n_\lambda\rangle$, with non zero matrix element $\langle m_\lambda|\,\partial_\lambda\hat{H}_\lambda\,|n_\lambda\rangle$. If there are multiple degenerate $|m_\lambda\rangle$ for which this is true, use the $|m_\lambda\rangle$ state that maximises the expression, as this will have the largest contribution. Note that we have dropped the explicit time dependence of λ for clarity, and shall continue this for the majority of the thesis. This expression is of the same form as the second order correction in perturbation theory [84], as such this expression can be read as "If the second order perturbation correction to the closest state is sufficiently smaller than the inverse of $\dot{\lambda}$, the dynamics will be adiabatic".

When this adiabatic condition is followed, we can apply the approximation that the distribution between eigenstates stays constant, eg. $c_n(t)\approx c_n(t_0=0)=c_n$. Note that in the limit of $t_f\to\infty$ and $\dot{\lambda}(t)\to 0$, this approximation is exact, meaning the slower the variation is applied, the better the approximation. We can then write a solution in the form

$$|\Psi(t)\rangle\approx\sum_n c_n\,|n\,(\lambda(t))\rangle\,e^{i\Phi_n(\lambda(t))}. \tag{2.9}$$

As we are looking at the case of a quantum control sequence, the most important result is finding out what the state is at the end of the variation ($|\Psi(t>t_f)\rangle$). At this point the Hamiltonian is again static, in the form $\hat{H}_f$ meaning the solution is simply

$$|\Psi(t>t_f)\rangle\approx\sum_n c_n\,|n\rangle_f\,e^{-i\left(E_n^f t/\hbar-\Phi_n^f\right)}, \tag{2.10}$$

where E_n^f and $|n\rangle_f$ are the eigenvalues and eigenstates of H_f, and $\Phi_n^f=\Phi_n(\lambda_f)$ is the phase at the the end of the variation. This means the only remaining factor from the variation is the the relative phase offset given by Φ_n^f.

Whilst it is possible to calculate this phase offset, often with adiabatic dynamics the system is initialised in a particular eigenstate n_0, such that $c_n=\delta_{n,n_0}$ is a Kronecker delta function. In this case, the phase can be completely ignored as it is purely global,

and will not affect any observables. As such we can state that the system will end in the equivalent eigenstate of $\hat{H}_f$ that it was initialised in H_i

$$\text{if} \quad |\Psi(t<0)\rangle = |n_0\rangle_i\,, \quad \text{then} \quad |\Psi(t>t_f)\rangle \approx |n_0\rangle_f\,. \tag{2.11}$$

We note that there are situations where following the adiabatic condition is not possible, and these results will not work. If there is a phase transition that occurs with the eigenstate that is being followed, then there is a energy gap to the nearest relevant energy level closing. In such a case the denominator of the adiabatic condition is zero in the thermodynamic limit, meaning the whole expression explodes towards infinity unless $\dot{\lambda}(t) \to 0$ at a rate related to the critical exponents such that the expression stays finite, however then it will take an infinite amount of time to cross the phase transition. As such, care must be taken to either avoid phase transitions, or to take them into account with further calculations [85].

Whilst the above results do provide the relevant dynamics, we do this by enforcing the adiabatic condition and as such limit the scope to only a group of relatively simple dynamics, which follow the eigenstates up to a relative phase. So the question arises, why would such dynamics be useful? We describe this partially in the introduction to this thesis, but we will focus in on a specific case here. The simplest application of adiabatic dynamics in quantum physics, is that of preparing the ground state of a complex Hamiltonian, where there is no trivial way to initialise in this state. It may be possible to find a related Hamiltonian of a similar form, with a ground state we can prepare the experiment in. Then the simple Hamiltonian can be used as the initial Hamiltonian to a control procedure, which is driven adiabatically to the final Hamiltonian of the complex Hamiltonian, meaning the resulting state will be the complex ground state we wish to study. For example, suppose we wish to study an interacting Hamiltonian, so we start by preparing the ground state with the interaction turned off, and then we adiabatically turn on the interactions to reach the desired ground state. This allows the study of more complex ground states, which for example can encode the solution to combinatorial optimisation problems [86–89].

2.1.2 Quench dynamics

On the other end of the spectrum to adiabatic dynamics, we have quench dynamics, where the Hamiltonian is changed almost instantaneously such that $t_f \approx 0$. There are in fact different scales within the class of quench dynamics, however in this thesis we just mention abrupt quenches which are the fastest case, where the timescale of the Hamiltonian change is the smallest in the problem [90]. In the case of a quench, there is no time for the system to react to the change, and as such the state $|\Psi(t=0)\rangle \approx |\Psi(t=t_f)\rangle$. However, this now evolves under the new Hamiltonian H_f and as such, decomposing into the new eigenbasis allows us to write dynamics beyond t_f.

We will again focus on the case of a single eigenstate $|n_0\rangle$ for the initial state. The solution is then given by

$$|\Psi(t>t_f)\rangle = \sum_n {}_f\langle n|n_0\rangle_i \, |n\rangle_f \, e^{-iE_n^f t/\hbar}. \tag{2.12}$$

This can be seen as simply a decomposition into the new basis, where then each eigenstate rotates according to its eigenvalue like in the static Hamiltonian case. For an example of the use of quenches, suppose in an experiment we want to initialise the system in some excited state $|e\rangle$. We can find a different Hamiltonian H_i where $|e\rangle$ is its groundstate, and then quench to our desired Hamiltonian H_f.

If the initial state instead contained a superposition of eigenstates, then the resulting decomposition would be dependent on both the initial distribution and relative phases. This would lead to interference between the states, but ultimately it will just change the final values of the magnitudes of eigenstates and the phase. As such, it is far easier to just adjust the single initial eigenstate, rather than combining more into a superposition in most cases.

2.1.3 Diabatic dynamics

The final case, is everything in between adiabatic and quench dynamics, which we refer to as diabatic dynamics. By using the adiabatic case as a reference point, we can think of the speed in diabatic dynamics as causing excitations between instantaneous eigen-

states. These excitations can affect both the distribution of the eigenstates ($c_n(\lambda(t))$) and the relative phases ($\Phi(\lambda(t))$). As this case encompasses all other dynamics, there again is no easy solution. However as we shall see soon, there are approaches to convert diabatic dynamics to adiabatic dynamics whilst going faster than the adiabatic condition allows. To get to that result, we must first explore what are gauge potentials, to build up the rest of the ground work.

2.2 Gauge potentials

When transforming between different frames of reference, the equations of motion can change such that the resulting physics between the frames agree. In physics we always assume our reference frame is stationary, and as such all our equations of motion be it classical or quantum build from this assumption. This assumption however breaks down if we try to describe the physics in multiple frames with relative acceleration, and in this case we can use a gauge potential to ensure the physics remains the same.

For example lets consider the classical mechanics problem of a merry-go-round. Imagine a person is riding on the merry-go-round; they will feel a force pushing them outwards whilst they rotate around, however the outside observer would not be able to detect the force. This discrepancy arises because there is relative acceleration between the two frames, so the equations of motion in the two frames are different, although they in the end describe the same outcome. These generators of these extra forces are known as gauge potentials, and they ensure accelerating frames obey the same laws of physics as stationary ones.

In quantum mechanics, different bases are the same as different reference frames. As such, a basis varying in time will result in a gauge potential appearing in the Schrödinger equation. To explain gauge potentials we shall outline the derivation as shown in [72]. Let $|\psi_0\rangle$ be a wave function, then it always has a decomposition into a stationary basis $|n\rangle_0$ given by

$$|\psi_0\rangle = \sum_n c_n |n\rangle_0 . \tag{2.13}$$

There then exists a unitary transformation, to some other basis $|m\rangle_\ell$ such that

$$|m\rangle_\ell = \sum_n U_{nm}(\ell)\,|n\rangle_0\,, \tag{2.14}$$

$$|n\rangle_0 = \sum_m U^*_{nm}(\ell)\,|m\rangle_\ell\,. \tag{2.15}$$

We refer to $|m\rangle_\ell$ as the moving frame, as the basis is dependent on the value of ℓ which describes some parametrised path similar to the use of λ in control procedures. The values $U_{nm}(\ell)$ can be thought of as matrix elements of a matrix $\hat{U}(\ell)$, where each column transforms a stationary basis state to the moving basis, and each row vice versa.

We can then write the wave function now in the moving frame

$$\left|\tilde{\psi}_\ell\right\rangle = \sum_{nm} c_n U^*_{nm}(\ell)\,|m\rangle_\ell = \sum_m \tilde{c}_m(\ell)\,|m\rangle_\ell\,, \tag{2.16}$$

with $\tilde{c}_m(\ell)$ giving the moving frame distribution ($\tilde{c}_m(\ell) = \sum_n U^*_{nm}(\ell)c_n$). We can then write the shorthand of this as

$$\left|\tilde{\psi}_\ell\right\rangle = \hat{U}^\dagger_\ell\,|\psi_0\rangle\,, \tag{2.17}$$

$$|\psi_0\rangle = \hat{U}_\ell\left|\tilde{\psi}_\ell\right\rangle. \tag{2.18}$$

With the description of the two bases complete, we introduce the gauge potential $\hat{\mathcal{U}}_\ell$ as generators of continuous unitary transformations, which are given by $\hat{\mathcal{U}}_\ell = i\hbar\partial_\ell$. We then apply this to the moving state vector $\left|\tilde{\psi}_\ell\right\rangle$ giving

$$i\hbar\left(\partial_\ell\left|\tilde{\psi}_\ell\right\rangle\right) = i\hbar\left(\partial_\ell\left(\hat{U}^\dagger_\ell\,|\psi_0\rangle\right)\right), \tag{2.19}$$

which as c_n is independent of ℓ, we can apply the product rule to extract it from the derivative, and convert back to the moving basis

$$i\hbar\left(\partial_\ell\hat{U}^\dagger_\ell\right)|\psi_0\rangle = i\hbar\left(\partial_\ell\hat{U}^\dagger_\ell\right)\hat{U}_\ell\left|\tilde{\psi}_\ell\right\rangle. \tag{2.20}$$

Now the derivative is split apart from the basis, we can define the resulting operator

as the negative of the gauge potential $\hat{\mathcal{U}}_\ell$

$$i\hbar\left(\partial_\ell \hat{U}_\ell^\dagger\right)\hat{U}_\ell = -\tilde{\hat{\mathcal{U}}}_\ell. \tag{2.21}$$

By noting the identity

$$\partial_\ell\left(\hat{U}_\ell^\dagger \hat{U}_\ell\right) = \partial_\ell \hat{\mathbb{I}} = 0 \implies \hat{U}_\ell^\dagger\left(\partial_\ell \hat{U}_\ell\right) = -\left(\partial_\ell \hat{U}_\ell^\dagger\right)\hat{U}_\ell \tag{2.22}$$

and dropping the explicit brackets, we get

$$\tilde{\hat{\mathcal{U}}}_\ell = i\hbar \hat{U}_\ell^\dagger \partial_\ell \hat{U}_\ell. \tag{2.23}$$

This expression also shows that the gauge potential is a hermitian operator. Note we can also transform the gauge potential into the lab frame to get

$$\hat{\mathcal{U}}_\ell = \hat{U}_\ell \tilde{\hat{\mathcal{U}}}_\ell \hat{U}_\ell^\dagger = i\hbar\partial_\ell. \tag{2.24}$$

These gauge potentials can both be defined via their matrix elements

$${}_\ell\langle m|\,\hat{\mathcal{U}}_\ell\,|n\rangle_\ell = {}_0\langle m|\,\tilde{\hat{\mathcal{U}}}_\ell\,|n\rangle_0\,. \tag{2.25}$$

As we discussed at the start of this section, these gauge potentials appear when applying a unitary transformation to the Schrödinger equation. In the transformed basis, we can write the Schrödinger equation as

$$i\hbar d_t\left(\hat{U}_\ell\left|\tilde{\psi}_\ell\right\rangle\right) = \hat{H}\left(\hat{U}_\ell\left|\tilde{\psi}_\ell\right\rangle\right), \tag{2.26}$$

$$\left(i\hbar\dot{\ell}\partial_\ell \hat{U}_\ell + i\hbar\hat{U}_\ell d_t\right)\left|\tilde{\psi}_\ell\right\rangle = \hat{H}\hat{U}_\ell\left|\tilde{\psi}_\ell\right\rangle. \tag{2.27}$$

If we then apply from the left the operator $\hat{U}_\ell^\dagger$ we get

$$\begin{aligned} i\hbar\hat{U}_\ell^\dagger\dot{\ell}\partial_\ell\hat{U}_\ell + i\hbar\hat{U}_\ell^\dagger\hat{U}_\ell d_t\left|\tilde{\psi}_\ell\right\rangle &= \hat{U}_\ell^\dagger\hat{H}\hat{U}_\ell\left|\tilde{\psi}_\ell\right\rangle, \\ \dot{\ell}\tilde{\hat{\mathcal{U}}}_\ell + i\hbar d_t\left|\tilde{\psi}_\ell\right\rangle &= \tilde{\hat{H}}_\ell\left|\tilde{\psi}_\ell\right\rangle, \end{aligned} \tag{2.28}$$

where $\tilde{\hat{H}}_\ell$ is the transformed Hamiltonian. Rearranging this, we can see that in the moving frame the Schrödinger reads as

$$i\hbar d_t \left|\tilde{\psi}_\ell\right\rangle = \left(\tilde{\hat{H}}_\ell - \dot{\ell}\tilde{\hat{\mathcal{U}}}_\ell\right)\left|\tilde{\psi}_\ell\right\rangle. \tag{2.29}$$

This extra term of the gauge potential, is what leads to the diabatic excitations we briefly discussed in Sec. 2.1.3. So if we can adjust the gauge potential, we can affect the diabatic excitations of our time dependent system.

So to summarise, using Gauge potentials allows transformation between different frames of reference without affecting the physics. To adjust our equations of motion, the Schrödinger equation, we add in the extra resulting Gauge potential. This finishes our discussion directly on gauge potentials, and we now turn our attention to bringing together the past two sections, to define the Adiabatic Gauge Potential.

2.3 Defining the AGP, counterdiabatic driving and other properties

When discussing gauge potentials so far we have allowed for any unitary transformation $\hat{U}_\ell$. Now we limit ourselves to transformations that take us between the stationary lab frame and the energy eigenbasis of the Hamiltonian. We denote this transformation as $\hat{U}_\lambda$ with the λ signifying this difference, and we write the gauge potential as $\hat{\mathcal{A}}_\lambda$, which is the Adiabatic Gauge Potential. The reason for this name will become apparent shortly when discussing counterdiabatic driving.

Due to the Hamiltonian represented in the energy eigenbasis being diagonal, we can derive a more useful expression for the matrix elements of the AGP compared to the general gauge potentials. We start with the expression

$${}_\lambda\langle m|\, \hat{H}_\lambda\, |n\rangle_\lambda = 0, \tag{2.30}$$

which is clearly true if $m \neq n$. Then by differentiating this with respect to λ we get

$$\begin{aligned} (\partial_\lambda {}_\lambda\langle m|)\,\hat{H}_\lambda\,|n\rangle_\lambda + {}_\lambda\langle m|\left(\partial_\lambda \hat{H}_\lambda\right)|n\rangle_\lambda + {}_\lambda\langle m|\,\hat{H}_\lambda\,(\partial_\lambda\,|n\rangle_\lambda) = 0 \\ E_n(\lambda)\,(\partial_\lambda {}_\lambda\langle m|)\,|n\rangle_\lambda + {}_\lambda\langle m|\left(\partial_\lambda \hat{H}_\lambda\right)|n\rangle_\lambda + E_m(\lambda)\,{}_\lambda\langle m|\,(\partial_\lambda\,|n\rangle_\lambda) = 0, \end{aligned} \tag{2.31}$$

where $E_n(\lambda), E_m(\lambda)$ are the eigenvalues of the associated eigenstates. We can use the fact that ${}_\lambda\langle m|n\rangle_\lambda = 0$ to find

$$\partial_\lambda\,({}_\lambda\langle m|n\rangle_\lambda) = 0 \implies (\partial_\lambda {}_\lambda\langle m|)\,|n\rangle_\lambda = -\,{}_\lambda\langle m|\,(\partial_\lambda\,|n\rangle_\lambda)\,. \tag{2.32}$$

Then using Eq. (2.24) to substitute the partial derivate with the AGP we get

$${}_\lambda\langle m|\,(\partial_\lambda\,|n\rangle_\lambda) = \frac{-i}{\hbar}\,{}_\lambda\langle m|\,\hat{\mathcal{A}}_\lambda\,|n\rangle_\lambda\,. \tag{2.33}$$

Finally putting all this together and rearranging, we get

$${}_\lambda\langle m|\,\hat{\mathcal{A}}_\lambda\,|n\rangle_\lambda = i\hbar\frac{{}_\lambda\langle m|\,\partial_\lambda \hat{H}_\lambda\,|n\rangle_\lambda}{E_n(\lambda) - E_m(\lambda)}. \tag{2.34}$$

This expression may in fact look rather familiar, as we have seen an extremely similar form for the adiabatic condition given in Eq. (2.8). This is no coincidence, as the AGP can be seen as a measure of the adiabaticity of the system. In fact an alternative wording of the adiabatic condition is the statement: If the largest element of the AGP is much smaller than the relevant energy gap divided by the rate of change of λ, then the condition holds. We also note that this expression does not give the diagonal elements of the AGP, as clearly it is divergent. The diagonal elements of the AGP are in fact the Berry connections [61], and affect only the relative phase of the eigenstates. As such, similar to what we did in the adiabatic dynamics, they are often ignored and set to zero.

So now if we can easily diagonalise $\hat{H}_\lambda$, we have an expression for the AGP, but why is this useful? Well, the AGP provides a large amount of insight into the dynamical properties of a system [72], and has applications as a signature of quantum chaos [65, 91,

92], or as a measure of quantum phase transitions for simple models [93]. However, likely the most common use case of the AGP is to compute the counterdiabatic Hamiltonian. This is given by

$$\hat{H}_{CD}(\lambda) = \hat{H}_\lambda + \dot{\lambda}\hat{\mathcal{A}}_\lambda. \tag{2.35}$$

This Hamiltonian is interesting because if we apply the unitary to transform to the co-moving frame, we get

$$\hat{H}_{CD}(\lambda) \to \tilde{\hat{H}}_\lambda + \dot{\lambda}\tilde{\hat{\mathcal{A}}}_\lambda - \dot{\lambda}\tilde{\hat{\mathcal{A}}}_\lambda = \tilde{\hat{H}}_\lambda. \tag{2.36}$$

We see the AGP added to the counterdiabatic Hamiltonian, cancels out with its counterpart from the transformation. This means in the co-moving frame, the system evolves under a purely diagonal Hamiltonian. If the Hamiltonian is then varied at any arbitrary speed $\dot{\lambda}$, it will experience no diabatic excitations, leading to adiabatic dynamics for all speeds of driving. There is one small caveat, if a phase transition occurs along the path varied across, the AGP will diverge and not be able to be implemented in the thermodynamic limit. However outside of this case, any adiabatic procedure can be sped up dramatically by adding these extra operators.

Whilst we have an expression for the AGP in the diagonal basis, this limits the problems that can be addressed to where diagonalization at all instantaneous times is feasible. If we again look at Eq. 2.34, we can rearrange and work back a few steps and get

$$\begin{aligned}
{}_\lambda\langle m|\, \hat{\mathcal{A}}_\lambda E_n(\lambda)\, |n\rangle_\lambda - {}_\lambda\langle m|\, E_m(\lambda)\hat{\mathcal{A}}_\lambda\, |n\rangle_\lambda &= i\hbar\, {}_\lambda\langle m|\, \partial_\lambda \hat{H}_\lambda\, |n\rangle_\lambda \\
{}_\lambda\langle m|\, \hat{\mathcal{A}}_\lambda \hat{H}_\lambda\, |n\rangle_\lambda - {}_\lambda\langle m|\, \hat{H}_\lambda \hat{\mathcal{A}}_\lambda\, |n\rangle_\lambda &= i\hbar\, {}_\lambda\langle m|\, \partial_\lambda \hat{H}_\lambda\, |n\rangle_\lambda \\
{}_\lambda\langle m|\, \left[\hat{\mathcal{A}}_\lambda, \hat{H}_\lambda\right] |n\rangle_\lambda &= {}_\lambda\langle m|\, i\hbar\partial_\lambda \hat{H}_\lambda\, |n\rangle_\lambda\,,
\end{aligned} \tag{2.37}$$

which as we already know represent the off-diagonal elements of the AGP. To build a full matrix of $i\hbar\partial_\lambda\hat{H}_\lambda$, we include the diagonal elements $\hat{M}_\lambda = -\sum_n \frac{\partial E_n(\lambda)}{\partial\lambda} |n\rangle_\lambda\, {}_\lambda\langle n|$

to get

$$i\hbar\partial_\lambda \hat{H}_\lambda = \left[\hat{\mathcal{A}}_\lambda, \hat{H}_\lambda\right] - i\hbar\hat{M}_\lambda. \tag{2.38}$$

If we then apply a left hand commutator with $\hat{H}_\lambda$, we can see that $\left[\hat{H}_\lambda, \hat{M}_\lambda\right] = 0$ due to the form of $\hat{M}_\lambda$, leaving just

$$\left[\hat{H}_\lambda, i\hbar\partial_\lambda \hat{H}_\lambda - \left[\hat{\mathcal{A}}_\lambda, \hat{H}_\lambda\right]\right] = 0. \tag{2.39}$$

The expression inside the right hand side of the commutator is often expressed, as the quantity [94]

$$\hat{G}\left(\hat{\mathcal{A}}_\lambda\right) = \hbar\partial_\lambda \hat{H}_\lambda - i\left[\hat{H}_\lambda, \hat{\mathcal{A}}_\lambda\right], \tag{2.40}$$

such that the condition simply reads as $\left[\hat{H}, \hat{G}\left(\hat{\mathcal{A}}_\lambda\right)\right] = 0$. This expression in Eq. 2.39 provides a general condition, as it is not basis dependent, which is exactly satisfied by the AGP. It is also used as a building block for most methods of computing the AGP without diagonalization, which we shall discuss in Sec. 2.5.

The AGP is an extremely useful quantity, however it is a operator of the size of the Hilbert space. As such it is often useful to define an $\mathcal{L}_2$ norm which we shall refer to as the AGP norm, defined as

$$||\hat{\mathcal{A}}_\lambda||^2 = \frac{\mathrm{Tr}[\hat{\mathcal{A}}_\lambda^2]}{\dim \hat{H}_\lambda}. \tag{2.41}$$

The exact form of the AGP norm is not important, and definitions differ by factors between different papers. We decide to additionally normalise by the dimension of the Hilbert space, to allow comparisons between different system sizes. There may be more appropriate ways of normalising this expression in specific cases, to allow for better comparison, but we are not aware of a better general expression for all types of systems. For a physical description of the AGP norm, it can be seen as the measure of the adiabaticity of a system, where the larger the value the more diabatic excitations are present. It is related to the combined adiabatic conditions between all eigenstates, and as such when it is zero all eigenstates behave perfectly adiabatically.

So far we have expressed the AGP as along a one dimensional path defined by λ, but sometimes having instead multiple directions can be useful. Suppose we have

a Hamiltonian that is parametrised by $\lambda_1, \lambda_2, \ldots, \lambda_n$ which we write as the vector $\vec{\lambda}$. Then $\dot{\lambda}$ is replaced by $\dot{\vec{\lambda}} = \left(\dot{\lambda}_1, \dot{\lambda}_2, \ldots, \dot{\lambda}_n\right)$, and the AGP is expressed as a vector of operators $\hat{\mathcal{A}}_{\vec{\lambda}} = \left(\hat{\mathcal{A}}_{\lambda_1}, \hat{\mathcal{A}}_{\lambda_2}, \ldots, \hat{\mathcal{A}}_{\lambda_n}\right)$. This means the AGP can be broken up into specific directions for simpler calculations in each direction, then combined later to get the full result.

We have now introduced the AGP alongside some of its properties and shown how it can be used to speed up adiabatic control sequences. We will now look at a small example of a simple two level system, to see how these results are computed and used.

2.4 Example: 2 level system AGP

The 2 level system we wish to study for this example is given by Hamiltonian, expressed in vector notation as

$$\hat{H} = \begin{pmatrix} \Delta & \omega \\ \omega & -\Delta \end{pmatrix} = \Delta\hat{\sigma}^z + \omega\hat{\sigma}^x, \tag{2.42}$$

in the basis of $|\uparrow\rangle, |\downarrow\rangle$ which are the eigenstates of $\hat{\sigma}^z$, where $\hat{\sigma}^z$ and $\hat{\sigma}^x$ are the Pauli matrices. Note that ω is an energy as we are now using the natural units of $\hbar = 1$, which we shall continue onwards for the rest of the thesis. This system has two states with energies of Δ and $-\Delta$ with a driving of ω between them. When $\Delta \gg \omega$ the Hamiltonian is effectively just a $\hat{\sigma}^z$ operator, meaning the ground state is simply $|\downarrow\rangle$. On the other hand when $\omega \gg \Delta$ the Hamiltonian is now effectively just a $\hat{\sigma}^x$ operator, meaning the ground state is now proportional to $|\uparrow\rangle - |\downarrow\rangle$. This means we can drive adiabatically between these two state by following the ground state whilst varying $\frac{\omega}{\Delta}$.

To be explicit, the Hamiltonian has the eigenenergies

$$\lambda_\pm = \pm\sqrt{\Delta^2 + \omega^2}, \tag{2.43}$$

with corresponding eigenstates

$$|+\rangle = \cos(\theta)\,|\uparrow\rangle + \sin(\theta)\,|\downarrow\rangle\,, \tag{2.44}$$

$$|-\rangle = \sin(\theta)\,|\uparrow\rangle - \cos(\theta)\,|\downarrow\rangle\,, \tag{2.45}$$

where θ is given by $\tan(2\theta) = \frac{\omega}{\Delta}$. This shows how as the ratio of $\frac{\omega}{\Delta}$ increases the groundstate $|\downarrow\rangle$ gets closer to the superposition state $|\uparrow\rangle - |\downarrow\rangle$.

We then compute the AGP for varying $\lambda = \omega$, meaning we have

$$\partial_\omega \hat{H} = \hat{\sigma}^x. \tag{2.46}$$

Then using Eq. (2.34), to give

$$\begin{aligned}
\langle -| \hat{\mathcal{A}}_\omega |+\rangle =& i \frac{\langle -| \hat{\sigma^x} |+\rangle}{\sqrt{\Delta^2+\omega^2} + \sqrt{\Delta^2+\omega^2}} \\
=& -i \frac{\cos(2\theta)}{2\sqrt{\Delta^2+\omega^2}}, && (2.47)\\
\langle +| \hat{\mathcal{A}}_\omega |-\rangle =& i \frac{\cos(2\theta)}{2\sqrt{\Delta^2+\omega^2}}. && (2.48)
\end{aligned}$$

Additionally we can simplify this expression by computing $\cos(2\theta)$ in terms of Δ and ω, with the correct normalisation,

$$\begin{aligned}
\tan 2\theta =& \frac{\omega}{\Delta} = \frac{\sin(2\theta)}{\cos(2\theta)}, && (2.49)\\
\sin(2\theta) =& \frac{\omega}{\sqrt{\omega^2+\Delta^2}}, && (2.50)\\
\cos(2\theta) =& \frac{\Delta}{\sqrt{\omega^2+\Delta^2}}. && (2.51)
\end{aligned}$$

Applying this to the matrix element we now get

$$\begin{aligned}
\langle +| \hat{\mathcal{A}}_\omega |-\rangle = -\langle +| \hat{\mathcal{A}}_\omega |-\rangle =& -i \frac{\frac{\Delta}{\sqrt{\omega^2+\Delta^2}}}{2\sqrt{\Delta^2+\omega^2}} \\
=& -i \frac{1}{2} \frac{\Delta}{\Delta^2+\omega^2}. && (2.52)
\end{aligned}$$

We can then express the AGP as an operator in the form of outer products this gives

$$i \frac{1}{2} \frac{\Delta}{\Delta^2+\omega^2} \left(|+\rangle \langle -| - |-\rangle \langle +| \right). \tag{2.53}$$

Now we can transform back into the stationary $|\uparrow\rangle, |\downarrow\rangle$ basis, by computing and applying the inverse transformation. The original transformation into the eigenbasis is

given by

$$\begin{pmatrix} |+\rangle \\ |-\rangle \end{pmatrix} = \begin{pmatrix} \cos(\theta) & \sin(\theta) \\ \sin(\theta) & -\cos(\theta) \end{pmatrix} \begin{pmatrix} |\uparrow\rangle \\ |\downarrow\rangle \end{pmatrix}, \tag{2.54}$$

and this is a involutory matrix, so its inverse is itself. This means the inverse transformation is

$$\begin{pmatrix} |\uparrow\rangle \\ |\downarrow\rangle \end{pmatrix} = \begin{pmatrix} \cos(\theta) & \sin(\theta) \\ \sin(\theta) & -\cos(\theta) \end{pmatrix} \begin{pmatrix} |+\rangle \\ |-\rangle \end{pmatrix}. \tag{2.55}$$

Applying this to the eigenbasis expression for the AGP we get

$$\begin{aligned} \hat{\mathcal{A}}_\omega =& \begin{pmatrix} \cos(\theta) & \sin(\theta) \\ \sin(\theta) & -\cos(\theta) \end{pmatrix} \tilde{\hat{\mathcal{A}}}_\omega \begin{pmatrix} \cos(\theta) & \sin(\theta) \\ \sin(\theta) & -\cos(\theta) \end{pmatrix} \\ =& i\frac{1}{2}\frac{\Delta}{\Delta^2+\omega^2} \begin{pmatrix} 0 & -1 \\ 1 & 0 \end{pmatrix} \\ =& \frac{1}{2}\frac{\Delta}{\Delta^2+\omega^2}\hat{\sigma}^y. \end{aligned} \tag{2.56}$$

From this we can state the counterdiabatic Hamiltonian using Eq. (2.35) simply as

$$\hat{H}_{CD} = \hat{H} + \dot{\omega}\hat{\mathcal{A}}_\omega = \Delta\hat{\sigma}^z + \omega\hat{\sigma}^x + \dot{\omega}\frac{1}{2}\frac{\Delta}{\Delta^2+\omega^2}\hat{\sigma}^y, \tag{2.57}$$

which will have adiabatic like dynamics at any value of $\dot{\omega}$.

We can verify the result as well using the general condition given in Eq. (2.39)

$$\begin{aligned} \left[\hat{\mathcal{A}}_\omega, \hat{H}\right] =& i\frac{\Delta}{\Delta^2+\omega^2}\left(\Delta\sigma_x - \omega\sigma_z\right), \\ i\partial_\omega\hat{H} - \left[\hat{\mathcal{A}}_\omega, \hat{H}\right] =& i\frac{\omega^2}{\Delta^2+\omega^2}\hat{\sigma}^x + i\frac{\Delta\omega}{\Delta^2+\omega^2}\hat{\sigma}^z, \\ \left[\hat{H}, i\partial_\omega\hat{H} - \left[\hat{\mathcal{A}}_\omega, \hat{H}\right]\right] =& \left[\Delta\hat{\sigma}^z + \omega\hat{\sigma}^x, i\frac{\omega^2}{\Delta^2+\omega^2}\hat{\sigma}^x + i\frac{\Delta\omega}{\Delta^2+\omega^2}\hat{\sigma}^z\right] \\ =& 0. \end{aligned} \tag{2.58}$$

Finally we can compute the norm of the AGP defined in Eq. (2.41) to be

$$||\hat{\mathcal{A}}_\omega||^2 = \frac{1}{8}\frac{\Delta^2}{(\Delta^2+\omega^2)^2}. \tag{2.59}$$

This shows that if Δ is kept small compared to ω, the AGP norm is small and the dynamics are approximately adiabatic in nature. However when the Δ and ω are close in value, there is the largest amount of diabatic excitations. However, whilst computing the AGP by its matrix elements for the two level system worked, it was rather complicated computation for a simple final result, and was only possible due to it having an exact analytical form for the eigenbasis.

2.5 Computing the AGP

In many systems, diagonalising the Hamiltonian is infeasible, as such we require methods to compute the AGP beyond the form of its matrix elements. There are a few different approaches to this problem that differ in two main areas: how the basis is generated, and how the operator coefficients are obtained. The first of these two differences refers to an approximate AGP which consists of a subset of the full operator space, which we discuss in Sec. 2.5.1, with discussions of the exact case in Sec. 2.5.2. The second difference will change the step taken during computation but will not change the final output of the AGP, as this will be the same for a given operator basis. This is shown in Secs. 2.5.3 and 2.5.4 where we show the two most common set of steps. Note in the next chapter we also present the approach we proposed in Ref. [80] called the Orthogonal Commutator Expansion (OCE) in Sec. 3.1, which combines different aspects of previous methods, allowing a scale between the approximate and exact AGP which can be computed numerically efficiently.

2.5.1 Approximate AGP

The AGP in general for given Hilbert space of dimension d, can contain as many independent operators as the full operator space d^2. It is important to note, the dimension d scales exponentially with the number of degrees of freedom in many-body systems, and such so does the number of operators needed to represent the AGP. To circumvent this, a subset of operators can be chosen to define an approximate AGP, which we

denote with $\hat{\chi}_\lambda$, given by

$$\hat{\chi}_\lambda = \sum_k \alpha_k(\lambda)\hat{\mathcal{O}}_k. \tag{2.60}$$

Here $\alpha_k(\lambda)$ represents the coefficient of the kth operator $\hat{\mathcal{O}}_k$ in the chosen subset. An optimal choice of this subset however is not clear *a priori*, with this being problem specific and dependent on the degree of accuracy required.

One solution to this problem is proposed in Ref. [66], where they show that the AGP can be equivalently defined as

$$\hat{\mathcal{A}}_\lambda = \lim_{\epsilon\to 0^+} \int_0^\infty \mathrm{d}t\ \mathrm{e}^{-\epsilon t}(\mathrm{e}^{-i\hat{H}_\lambda t}\partial_\lambda \hat{H}_\lambda \mathrm{e}^{i\hat{H}_\lambda t} - \hat{\mathcal{M}}_\lambda), \tag{2.61}$$

with $\hat{\mathcal{M}}_\lambda$ cancelling the diagonal elements, which are not relevant in the formulation of the AGP, from the first term. So only focusing on the off diagonal elements of the first term in the integral, we can further expanded this using a form of the Baker-Campbell-Hausdorff formula [95]

$$\mathrm{e}^{\hat{X}}\hat{Y}\mathrm{e}^{-\hat{X}} = \sum_{n=0}^\infty \frac{1}{n!}\underbrace{\left[\hat{X},\left[\hat{X},\ldots\left[\hat{X},\hat{Y}\right]\right]\right]}_{n} = \sum_{n=0}^\infty \frac{\left[(\hat{X})^n,\hat{Y}\right]}{n!}, \tag{2.62}$$

where $\left[(\hat{X})^n,\hat{Y}\right]$ is shorthand for the nested commutators. This allows part of the integrand to be written as

$$\begin{aligned}\mathrm{e}^{-i\hat{H}_\lambda t}\partial_\lambda \hat{H}_\lambda \mathrm{e}^{i\hat{H}_\lambda t} &= \sum_{n=0}^\infty \frac{\left[(-i\hat{H}_\lambda t)^n, \partial_\lambda \hat{H}_\lambda\right]}{n!} \\ &= \sum_{n=0}^\infty \frac{(-it)^n}{n!}\left[(\hat{H}_\lambda)^n, \partial_\lambda \hat{H}_\lambda\right].\end{aligned} \tag{2.63}$$

Placing this back into the expression for the AGP (Eq. (2.61))

$$\begin{aligned}\hat{\mathcal{A}}_\lambda &= \lim_{\epsilon\to 0^+} \int_0^\infty \mathrm{d}t\ \mathrm{e}^{-\epsilon t}(\sum_{n=0}^\infty \frac{(-it)^n}{n!}\left[(\hat{H}_\lambda)^n, \partial_\lambda \hat{H}_\lambda\right] - \hat{\mathcal{M}}_\lambda) \\ &= \lim_{\epsilon\to 0^+} \int_0^\infty \mathrm{d}t\ \mathrm{e}^{-\epsilon t}\sum_{l=0}^\infty \frac{(-it)^{(2l+1)}}{(2l+1)!}\left[(\hat{H}_\lambda)^{(2l+1)}, \partial_\lambda \hat{H}_\lambda\right].\end{aligned} \tag{2.64}$$

As the even nested commutators give diagonal elements, we cancel them with $\hat{\mathcal{M}}_\lambda$ giving a new index l which only covers the odd nested commutators. Now whilst this expression is still not particularly useful for computing the AGP, Claeys *et al.* [66] note that by combining all the scalar values into one coefficient α_l for each l, this provides an expansion of the AGP

$$\hat{\mathcal{A}}_\lambda = i\sum_{l=0}^{\infty} \alpha_l \left[(\hat{H}_\lambda)^{(2l+1)}, \partial_\lambda \hat{H}_\lambda\right]. \tag{2.65}$$

This expansion can then be truncated at a finite order, giving an ansatz of the AGP where the α_l can be obtained.

Whilst this ansatz provides a full basis for the AGP, the operators at each value of l are not necessarily orthogonal to each other. This means there is an unnecessary dependence between the operators, that complicates solving for the values of α_l leading to unstable convergence of the results in even simple examples such as the one dimensional Ising model.

In Ref. [96] they show how to enforce orthogonality in a Krylov based method of generating the AGP basis [97]. The general idea is closely related to the nested commutator ansatz, using repeated commutation with the Hamiltonian to give these operators, but additionally subtracting previous operators. They define their approximate basis over operators $\hat{O}_k$ with odd values of k giving the AGP

$$\hat{\mathcal{A}}^\ell_\lambda = i\sum_{k=1}^{\ell} \gamma_k \hat{O}_{2k-1}. \tag{2.66}$$

where ℓ represents the order of the approximation. To facilitate a concise algorithm they introduce the notation

$$(\hat{A}|\hat{B}) = \frac{\mathrm{Tr}\left(\hat{A}^\dagger \hat{B}\right)}{d}, \tag{2.67}$$

$$\left\|\hat{A}\right\| = \sqrt{(\hat{A}|\hat{A})}, \tag{2.68}$$

$$\hat{\mathcal{L}}|\hat{O}) = [\hat{H}, \hat{O}], \tag{2.69}$$

with Hilbert space dimension d. Using these they provide an algorithm for the process of computing the operators $\hat{O}_k$, shown in Alg. 1. This provides an orthogonal constructed basis for the AGP, that can be used to solve to a given order of approximation. At the same time as this work on Krylov basis generation was being done, we created our own approach to fixing this problem of orthogonalisation, which we discuss in detail in Sec. 3.1.

Algorithm 1 Krylov basis generation

$\hat{A}_0 \leftarrow \partial_\lambda \hat{H}$
$b_0 \leftarrow \left\|\hat{A}_0\right\|$
$\hat{O}_0 \leftarrow \hat{A}_0 / b_0$
$\hat{A}_1 \leftarrow \hat{\mathcal{L}}|\hat{O}_0)$
$b_1 \leftarrow \left\|\hat{A}_1\right\|$
$\hat{O}_1 \leftarrow \hat{A}_1 / b_1$
for $k \in 2 \dots 2\ell$ **do**
    $\hat{A}_k \leftarrow \hat{\mathcal{L}}|\hat{O}_{k-1}) - b_{k-1}|\hat{O}_{k-2})$
    $b_k \leftarrow \left\|\hat{A}_k\right\|$
    $\hat{O}_k \leftarrow \hat{A}_k / b_k$
end for

2.5.2 Lie algebra

Now that we have disused what an approximate AGP looks like, lets briefly discuss the structure of a basis that describes the exact AGP. Whilst in many cases it is not possible to compute the exact AGP, having some understanding about the form of it can help point towards optimal approximate forms. We have seen in Eq. (2.65), all operators that the AGP consist of can be computed via commutation with the Hamiltonian. This operator space is known as the dynamical Lie algebra [98], where the Lie bracket is given by

$$\hat{\mathcal{L}} = [\hat{H}, \cdot\,]. \tag{2.70}$$

All forms of the AGP are defined over this Lie algebra, with different approximations only differing by which subset is chosen up to a basis transformation. Previous works have shown there are links between the size of the Lie algebra, the controllability of a system [99], and also the degree of quantum chaos in the system [100].

2.5.3 Variational approach

We now turn our attention to the problem of solving for the coefficients of the AGP for a given basis, where we shall use the form given in Eq. (2.60) for consistent notation. There are two commonly used approaches to this problem, the first of which is a variational approach developed in Ref. [94]. The idea of this approach is to define an appropriate cost function S (the action) for the AGP coefficients to be minimised over, which is defined as

$$\hat{G}(\hat{\chi}_\lambda) = \partial_\lambda \hat{H} - i\left[\hat{H}, \hat{\chi}_\lambda\right], \tag{2.71}$$

$$S(\hat{\chi}_\lambda) = \mathrm{Tr}\left[\hat{G}(\hat{\chi}_\lambda)^2\right]. \tag{2.72}$$

The values of the α_k that minimise this cost function, will give the best AGP for a given basis, whether that is approximate or the full AGP basis in which case it be equivalent to the exact condition given in Eq. (2.39) . To help motivate this form, we can define the quantity

$$F(\hat{\chi}_\lambda) = \frac{1}{\dim(\hat{\chi}_\lambda)} \mathrm{Tr}\left(\left[\hat{H}_\lambda, \hat{G}(\hat{\chi}_\lambda)\right]^2\right). \tag{2.73}$$

This quantity $F(\hat{\chi}_\lambda)$ is the norm of the condition in Eq. (2.39), and gives a measure of how far away from the exact AGP we are. In Ref. [72] it is shown that this quantity is proportional to the average rate of change of eigenstate populations. Therefore the smaller this quantity is, the more adiabatic the dynamics are, giving a measure of the success of an approximate expression for the AGP.

2.5.4 Algebraic approach

The second approach to computing the coefficients of the AGP, was first developed in Ref. [93], where by writing the equation

$$\mathbf{M}\vec{\alpha} = \vec{u}, \tag{2.74}$$

with $\vec{\alpha}$ being the vector of AGP coefficients α_k, they turn the problem into a matrix equation. The matrix $\mathbf{M}$ and condition $\vec{u}$ are given by

$$M_{i,j} = \mathrm{Tr}\left([\hat{H}, \hat{\mathcal{O}}_i][H, \hat{\mathcal{O}}_j]\right), \tag{2.75}$$

$$u_k = i\,\mathrm{Tr}\left([\hat{H}, \partial_\lambda \hat{H}]\hat{\mathcal{O}}_k\right). \tag{2.76}$$

Note that this equation is not always directly solvable due to either symmetries in the operators or diagonal elements being arbitrary. The authors solve the first issue by reducing equivalent operators in the operator basis by taking into account the symmetries of the Hamiltonian. Then enforcing the diagonal elements are zero, which is the normal choice for the AGP as seen previously in Eq. (2.61), an extra condition is obtained

$$\mathrm{Tr}\left[\hat{H}, \hat{\chi}_\lambda\right] = 0. \tag{2.77}$$

Both the variational and algebraic approaches provide the same result, but have different cases where each is appropriate. As such a combination of any of the basis shown in Sec. 2.5.1 and approaches here can be used interchangeably.

2.6 Summary of AGP background theory

In this chapter we have built up to a basic understanding of what the AGP is, and how it can be used in different cases. We looked at the different rates of change of time dependent Hamiltonian lead to different general dynamics, where when the change is near instant, a quench occurs that acts like a basis change. On the other hand, if the change is slow we get Adiabatic dynamics that follow the time independent solution, and in between these two extremes we have diabatic dynamics where there are some excitations between eigenstates induced from the changing Hamiltonian.

We described the use of Gauge potentials to facilitate computing physics in different accelerating reference frames, with the special case of the AGP being the transformation to the co-moving frame. This showed how adding the AGP to our Hamiltonian in our stationary lab frame, leads to cancellation in the co-moving frame resulting in adiabatic

dynamics, and we refer to this process as counterdiabatic driving.

We have looked at what methods there are to compute the AGP in different scenarios, ranging from approximate to exact representations. These different methods have each got their own benefits and drawbacks, but there has been little comparison between different methods, as different research groups tend to stick to one particular method. During this thesis, we try to apply a range of different methods to explore the different strengths of these methods. However the OCE method we developed, which the next chapter is dedicated to, will appear the most often as we have the most familiarity with it.

Chapter 3

The Orthogonal Commutator Expansion

In the previous chapter we have described the AGP, some useful properties and applications for it, and also some methods to computing the operator. One method we left out of that chapter is the Orthogonal Commutator Expansion (OCE), which we developed in our publication Ref. [80], and this current chapter is dedicated to and based on. The main goal of the OCE was to have a method that can systematically compute the exact AGP, whilst having different degrees to approximation when this is unfeasible. We build from the approximate AGP described in Sec. 2.5.1, and in particular the nested commutator ansatz given in Eq. 2.65, with the goal of addressing the difficult optimisation problem that arise from the non-orthogonality between the different ansatz operators.

To address this problem, we decompose the nested commutators into an trace-orthogonal basis and remove any duplicate operators from the ansatz, which we discuss in Sec. 3.1. This leads to being able to define a matrix equation similar to the algebraic approach described in Sec. 2.5.4, but with a simpler final form of the matrix due to the added conditions of trace-orthogonality and operators ordered by the nested commutator expansion. The name Orthogonal Commutator Expansion arises from these key differences to the previous methods, whose effect will be discussed in Sec. 3.2. In this thesis there are some common bases we shall use when defining the AGP, so we

outline a few of these in Sec. 3.4, to provide a single point of reference for calculations done later in the thesis. We then end this chapter with a discussion of how to implement the OCE numerically in Sec. 3.3.2, including a general algorithm for those interested in implementing the method themselves.

3.1 Deriving the OCE

The first steps of this chapter is to illustrate how the OCE works, and alongside this derive the necessary equations for the method. We will use an example two site Hamiltonian to help explain the steps, which is of the form

$$\hat{H} = J\hat{\sigma}_1^z\hat{\sigma}_2^z + \Delta\left(\hat{\sigma}_1^x + \hat{\sigma}_2^x\right) + \lambda\left(\hat{\sigma}_1^z + \hat{\sigma}_2^z\right), \tag{3.1}$$

$$\partial_\lambda \hat{H} = \hat{\sigma}_1^z + \hat{\sigma}_2^z, \tag{3.2}$$

where $\hat{\sigma}_i^\gamma$ is the Pauli matrix γ acting on site i. This Hamiltonian is a very simple two site spin-1/2 Ising model, where the AGP can also be computed using any of the other methods described in this thesis, and as such is a good model for comparisons. As we discussed in the introduction to this chapter, there are two key details that define the OCE: trace-orthogonality and the generating of operators via nested commutation.

Tackling the first detail then, trace-orthogonality is defined as

$$\mathrm{Tr}\left(\hat{O}_i^\dagger \hat{O}_j\right) = t_{i,j}\delta_{i,j}, \tag{3.3}$$

for two operators $\hat{O}_i$, $\hat{O}_j$ in the Hamiltonian Hilbert space, where $t_{i,j}$ is some scalar value and $\delta_{i,j}$ is the Kronecker delta function. By enforcing this condition, it leads to a simplification in the elements of matrix equation, which reduces the overall computational complexity of the problem. As the trace product can be viewed as two dimensional generalisation of the one dimensional inner/dot product, so trace-orthogonality can be analogously compared to the orthogonality condition for state vectors $\langle m|n\rangle = \delta_{m,n}$.

Whilst strictly speaking only the trace-orthogonality property is required, to save on tracking each of the values $t_{i,j}$ in the equation, it is easier still to use a trace-orthonormal

basis, meaning $t_{i,j} = 1 \,\forall\, i, j$

$$\mathrm{Tr}\left(\hat{O}_i^\dagger \hat{O}_j\right) = \delta_{i,j}. \tag{3.4}$$

If a basis is trace-orthogonal, it is always possible to normalise the operators to enforce the stronger condition of trace-orthonormality. Additionally in the case that the scalar factors are the same for all basis vectors $t_{i,j} = t \,\forall\, i, j$, it will not affect the final result of the OCE, meaning it can be ignored for the convenience of not needing to normalise the basis. In fact we shall use this in our example calculation, as the basis of the Pauli matrices is trace-orthogonal but not trace-orthonormal, with the scalar factor being $t_{i,j} = 2 \,\forall\, i, j$, so we can work directly in this basis without extra factors begin added.

Returning to our example Hamiltonian, we turn to look at the second detail of generating the AGP operators via nested commutation. As we discussed in Sec 2.5.2, we can see this step as generation of a Lie algebra (our basis) via repeated use of the Lie bracket (the commutator) with the Hamiltonian. By ordering our basis/Lie algebra by when they first appear in the nested commutation/Lie bracket, we are able to compute that many of the matrix elements we find later are exactly zero, so there is good reason for this structured ordering of the basis. We can compute the first two nested commutators to be

$$\left[\hat{H}, \partial_\lambda \hat{H}\right] = -i\Delta\left(\hat{\sigma}_1^y + \hat{\sigma}_2^y\right), \tag{3.5}$$

$$\left[\hat{H}, \left[\hat{H}, \partial_\lambda \hat{H}\right]\right] = -J\Delta\left(\hat{\sigma}_1^x \hat{\sigma}_2^z + \hat{\sigma}_1^z \hat{\sigma}_2^x\right) + \Delta^2\left(\hat{\sigma}_1^z + \hat{\sigma}_2^z\right) - \lambda\Delta\left(\hat{\sigma}_1^x + \hat{\sigma}_2^x\right). \tag{3.6}$$

This shows our first example of the non-orthogonal nature of the original commutator ansatz given in Eq. (2.65), as $\hat{\sigma}_1^z$ and $\hat{\sigma}_2^z$ have appeared in both $\partial_\lambda \hat{H}$ and $\left[\hat{H}, \left[\hat{H}, \partial_\lambda \hat{H}\right]\right]$. In fact for the Pauli matrices, every single previous operator seen in even (odd) nested commutators will appear in all future even (odd) nested commutators. It will become more clear why this is the case shortly when we describe commutators in terms of structure constants, where the reversibility of commutation is made apparent. As in the OCE we are decomposing the nested commutators into the given basis, we only need to track an operator the first time it appears. As such we find the set of operators B_ℓ that appear after ℓ nested commutations (taking odd operators to be Hermitian) to

be

$$B_0 = \{i\hat{\sigma}_1^z, i\hat{\sigma}_2^z\}, \tag{3.7}$$

$$B_1 = \{\hat{\sigma}_1^y, \hat{\sigma}_2^y\}, \tag{3.8}$$

$$B_2 = \{i\hat{\sigma}_1^x\hat{\sigma}_2^z, i\hat{\sigma}_1^z\hat{\sigma}_2^x, i\hat{\sigma}_1^x, i\hat{\sigma}_2^x\}, \tag{3.9}$$

$$B_3 = \{\hat{\sigma}_1^z\hat{\sigma}_2^y, \hat{\sigma}_1^y\hat{\sigma}_2^z, \hat{\sigma}_1^x\hat{\sigma}_2^y, \hat{\sigma}_1^y\hat{\sigma}_2^x\}, \tag{3.10}$$

$$B_4 = \{i\hat{\sigma}_1^z\hat{\sigma}_2^z, i\hat{\sigma}_1^x\hat{\sigma}_2^x, i\hat{\sigma}_1^y\hat{\sigma}_2^y\}. \tag{3.11}$$

As seen previously in Eq. (2.65), the AGP is then defined over all the sets where ℓ is odd. We also note the action (see Eq. (2.72)) is defined on the sets where ℓ is even, as it is computed via a single commutation with the AGP. This hopefully makes clear what we mean by decomposing the nested commutators into a given basis.

The resulting matrix equation given in the OCE, is effectively a special case of the algebraic approach, which results in simpler matrix elements. Commutation can be expressed in the form of structure constants f_{ab}^c, which are totally antisymmetric values, such that commutation between two operators $\hat{O}_a$,$\hat{O}_b$ as

$$\left[\hat{O}_a, \hat{O}_b\right] = i\sum_c f_{ab}^c \hat{O}_c. \tag{3.12}$$

This means the commutation relations of all operators in the Hilbert space can be defined via all the non-zero values of the structure constants f_{ab}^c. For example the Pauli basis commutations is defined by $f_{xy}^z = 2$, where all other non-zero values are given by swapping the order of the indices and flipping the sign for every swap eg. $f_{xy}^z = 2 \implies f_{yx}^z = -2$.

Whilst the full structure constants define all the values we require for computation in the OCE, they are actually overly expressive for our use case. This is because we only take commutations of the form $[\hat{H}, \cdot]$, so one index is always fixed. To simplify the form, first lets express the Hamiltonian $\hat{H}$ in our chosen basis as

$$\hat{H} = \sum_j h_j \hat{O}_j, \tag{3.13}$$

where h_j are real valued scalars, as we take $\hat{O}_j$ and $\hat{H}$ to be Hermitian. Similar results are be able to be computed for a non-Hermitian basis and Hamiltonian where h_j can be complex valued, but we will not explore that case here.

We can then insert this expression of the Hamiltonian into Eq. 3.12, with $\hat{O}_a = H$ and the other indices rewritten as $b, c = k, l$, this gives

$$\left[\hat{H}, \hat{O}_k\right] = i \sum_l \sum_j h_j f_{jk}^l \hat{O}_l. \tag{3.14}$$

From this expression we can define what we call the reduced structure constants c_k^l as

$$c_k^l = \sum_j h_j f_{jk}^l, \tag{3.15}$$

reducing the expression for the commutation to

$$\left[\hat{H}, \hat{O}_k\right] = i \sum_l c_k^l \hat{O}_l. \tag{3.16}$$

Whilst it is useful to define the reduced structure constants in terms of the full structure constants, it is also helpful to have an expression based purely on the operators themselves. To achieve this we take a trace product of Eq. (3.16) with a specific operator $\hat{O}_{l'} \in B_\ell$, which means $\hat{O}_{l'}^\dagger = \pm \hat{O}_{l'}$ depending on whether ℓ is odd or even. Applying this trace product we get,

$$\begin{aligned} \mathrm{Tr}\left(\left[\hat{H}, \hat{O}_k\right] \hat{O}_{l'}^\dagger\right) &= \mathrm{Tr}\left(i \sum_l c_k^l \hat{O}_l \hat{O}_{l'}^\dagger\right) \\ \pm \mathrm{Tr}\left(\left[\hat{H}, \hat{O}_k\right] \hat{O}_{l'}\right) &= \pm \mathrm{Tr}\left(i \sum_l c_k^l \hat{O}_l \hat{O}_{l'}\right) \end{aligned} \tag{3.17}$$

so the $\pm$ ends up just cancelling anyway. Finishing the calculation we get

$$\begin{aligned} \mathrm{Tr}\left(\left[\hat{H}, \hat{O}_k\right] \hat{O}_{l'}\right) =& i \sum_l c_k^l \mathrm{Tr}\left(\hat{O}_l \hat{O}_{l'}\right) \\ =& i c_k^{l'}, \end{aligned} \tag{3.18}$$

which we can relabel l' back to l to give simply

$$c_k^l = -i \operatorname{Tr}\left(\left[\hat{H}, \hat{O}_k\right] \hat{O}_l\right). \tag{3.19}$$

We have previously described our basis in terms of the sets B_ℓ, where B_ℓ commutes onto the sets $B_{\ell-1}$ and $B_{\ell+1}$. As such, if the operators $\hat{O}_k \in B_\ell$ then $\left[\hat{H}, \hat{O}_k\right] \in B_{\ell-1} \cup B_{\ell+1}$, which for now we will simplify to just $\hat{O}_k^{B_{\text{odd}}}$ and $\hat{O}_l^{B_{\text{even}}}$. This means the elements of the matrix $\mathbf{M}$ first described in the algebraic approach to the AGP, see Eq. (2.75), can be written as

$$\begin{aligned} M_{p,k} &= \operatorname{Tr}\left([\hat{H}, \hat{\mathcal{O}}_p][H, \hat{\mathcal{O}}_k]\right) \\ &= \operatorname{Tr}\left(-\sum_l c_p^l \hat{O}_l^{B_{\text{even}}} \sum_m c_k^m \hat{O}_m^{B_{\text{even}}}\right) \\ &= \operatorname{Tr}\left(-\sum_l \sum_m c_p^l c_k^m \hat{O}_l^{B_{\text{even}}} \hat{O}_m^{B_{\text{even}}}\right) \\ &= -\sum_l \sum_m c_p^l c_k^m \operatorname{Tr}\left(\hat{O}_l^{B_{\text{even}}} \hat{O}_m^{B_{\text{even}}}\right). \end{aligned} \tag{3.20}$$

As $\hat{O}_l^{B_{\text{even}}}$ is even we know it is an anti-Hermitian operator meaning we can write

$$\operatorname{Tr}\left(\hat{O}_l^{B_{\text{even}}} \hat{O}_m^{B_{\text{even}}}\right) = -\operatorname{Tr}\left(\left(\hat{O}_l^{B_{\text{even}}}\right)^\dagger \hat{O}_m^{B_{\text{even}}}\right) = -\delta_{l,m}. \tag{3.21}$$

Combining this back into our expression, results in the final expression of

$$M_{p,k} = \sum_l c_p^l c_k^l. \tag{3.22}$$

Similarly we can compute $\vec{u}$ by using Eq. (2.76), where we first need to get an expression for $\partial_\lambda \hat{H}$. Using the decomposition of $\hat{H}$ given in Eq. (3.13), we can find

$$\partial_\lambda \hat{H} = \sum_l \partial_\lambda h_l \hat{O}_l^{B_0}. \tag{3.23}$$

We can then substitute this expression into Eq. (2.76) to get

$$\begin{aligned} u_k =& i \operatorname{Tr}\left([\hat{H}, \partial_\lambda \hat{H}] \hat{O}_k^{B_{\text{odd}}}\right) \\ =& i \operatorname{Tr}\left(\sum_l \partial_\lambda h_l \left[\hat{H}, \hat{O}_l^{B_0}\right] \hat{O}_k^{B_{\text{odd}}}\right) \\ =& i \sum_l \partial_\lambda h_l \operatorname{Tr}\left(\left[\hat{H}, \hat{O}_l^{B_0}\right] \hat{O}_k^{B_{\text{odd}}}\right) \\ =& i \sum_l \partial_\lambda h_l \left(-i c_l^k\right) \\ =& \sum_l \partial_\lambda h_l c_l^k. \end{aligned} \tag{3.24}$$

We note that the expression for the matrix elements $M_{p,k}$ in Eq. (3.22), are defined going from odd operators (k) to even operators (l), so we wish to swap the indices in c_l^k. To do so we can look at the definition in Eq. (3.15) and see that swapping l and k will flip the sign of the full structure constant f_{jk}^l, and as such $c_l^k = -c_k^l$. So we can write the initial condition in terms of odd to even reduced structure constants equivalently as

$$u_k = -\sum_l \partial_\lambda h_l c_k^l. \tag{3.25}$$

This result combined with Eq. (3.22) defines the matrices required to solve the matrix equation of the different coefficients of the AGP in a given basis, as was seen in the previous chapter in Eq. (2.74).

With this the steps of the OCE have been laid out, with now only the matrix equation is left to be solved. This provides a complete set of instructions to solve any Hamiltonian that is desired, however it is not guaranteed to be computationally feasible. As such we shall now look at some of the details of the OCE, what generalisations about the method can we make, and how to approximate the result when the computational demand grows beyond reach.

3.2 Exploring the details of the OCE

The form of the matrix elements given in Eq. (3.22), is reasonably straightforward being made up of reduced structure constants only. However, if we look at the scaling of how many operations are required to compute this matrix, we see quickly that the problem is still computationally expensive in its current form. Let B_l have N_{even} and N_{odd} operators for l even and odd respectively. Then the matrix is of size $N_{\text{odd}} \times N_{\text{odd}}$ where each element required a sum over N_{even} operators. This naive computation leads to scaling of the form $\mathcal{O}(N_{\text{odd}}^2 N_{\text{even}})$, which at first appears to be polynomial and not too bad. However for general systems N_{even},$N_{\text{odd}} \propto d^2$, where d is the Hilbert space of the system, which itself grows exponentially ($d = 2^N$ for N spin-1/2 particles), it is clear that this scaling should be reduced as much as possible.

Over these next few subsections, we will explore different simplifications and details of the method: the shape of matrix in Eq. (3.22), how symmetries can be used to reduce the size of computation, creating approximate AGP by truncating the matrix equation, and dealing with complex valued Hamiltonians.

3.2.1 The block tridiagongal form of the matrix equation

The first step to simplification, is to remove all elements where it is known *a priori* they are zero valued. As we have described OCE organises the operators into operator sets B_l that are ordered by number of nested commutation. This means that the commutator of any given operator set exactly maps on to operators in its consecutive sets, given mathematically as

$$[\hat{H}, \hat{O}_k^{B_l}] \in B_{l-1} \cup B_{l+1}. \tag{3.26}$$

As such, the structure constants are zero between any non-consecutive operator sets. Using this fact, we can note Eq. (3.22) has only non-zero elements between operator sets that share a consecutive set, or more simply put, the matrix elements between any two non consecutive odd operator sets are always zero. Similarly Eq. (3.25) is only non-zero for operators in the first set B_1, as this is the only consecutive set to B_0

where $\partial_\lambda \hat{H}$ is defined. This means that the matrix $\mathbf{M}$ is block tridiagonal, which can be efficiently solved [101], with additionally only non zero $\vec{u}$ for the first block. This is one of the key results of OCE, that by ordering the operator sets in this particular way, the complexity of the resulting matrix equation is reduced dramatically.

3.2.2 How to exploit symmetries in the Hamiltonian

In many cases the Hamiltonian will have some form of symmetry that it is invariant under. This can be related directly to the type of Hamiltonian (the Ising model has a $\mathbb{Z}_2$ symmetry) or the geometry the Hamiltonian is on (a chain having a reflection symmetry). We find that symmetries present in a Hamiltonian are also present its associated AGP, which can be used to reduce the complexity of computing the AGP.

Firstly, we show that the AGP respects the same symmetries as the Hamiltonian, by considering the condition given in Eq. (2.39). For clarity we restate the condition here

$$[\hat{H}, \partial_\lambda \hat{H} - i[\hat{H}, \hat{\mathcal{A}}]] = 0. \tag{3.27}$$

Suppose we apply a transformation such that $\hat{H}$,$\hat{\mathcal{A}}$ transforms to $\hat{H}'$,$\hat{\mathcal{A}}'$ respectively, and we specify that the transformation is symmetry preserving such that $\hat{H} = \hat{H}'$. Under this transformation the condition becomes

$$[\hat{H}, \partial_\lambda \hat{H} - i[\hat{H}, \hat{\mathcal{A}}']] = 0. \tag{3.28}$$

However as the AGP is unique up to a basis transformation, we can state $\hat{\mathcal{A}} = \hat{\mathcal{A}}'$, and can conclude that the AGP shares the Hamiltonian symmetries.

The main consequence of the AGP sharing symmetries, is that all its individual operators can be rewritten in a symmetric form. To do this we would combine non-symmetric operators together to form new symmetric operators. For example, suppose we have a two spin-1/2 particles coupled together, such that there is a geometric reflection symmetry between the two particles. In this case, the operator $\hat{\sigma}_1^x \hat{\sigma}_2^x$ is symmetric, but $\hat{\sigma}_1^x \hat{\sigma}_2^z$ is not. However we can combine this non-symmetric operator with $\hat{\sigma}_1^z \hat{\sigma}_2^x$, to get $\hat{\sigma}_1^x \hat{\sigma}_1^z + \hat{\sigma}_1^z \hat{\sigma}_2^x$, which is now symmetric.

Ideally the Hamiltonian is already written in a symmetric basis, or can easily be transformed into it, and then the OCE can be applied in this basis. However as the specific symmetric basis is dependent on a particular Hamiltonian, the structure constants may not be a known result and have to be calculated for that specific Hamiltonian. As the OCE relies heavily on the reduced structure constants, it is often easier to pick a basis where the structure constants are already known, and then make use of the symmetries during the method itself.

The most straightforward approach, is to express the symmetric reduced structure constants in terms of their non-symmetric parts. This is only necessary for the AGP operators (B_ℓ where ℓ is odd), as the matrix elements in Eq. (3.22) already sum over the even operators. So we can write the symmetric odd operators as a sum over the non-symmetric odd as discussed previously,

$$\hat{O}^{B_{\text{odd}}}_{S_k} = \sum_{k' \in \{S_k\}} \hat{O}^{B_{\text{odd}}}_{k'}, \tag{3.29}$$

where $\{S_k\}$ is the set of symmetric indexes to be combined. Substituting this form into Eq. (3.19) we get

$$c^l_{S_k} = -i \operatorname{Tr}\left(\left[\hat{H}, \sum_{k' \in \{S_k\}} \hat{O}^{B_{\text{odd}}}_{k'}\right] \hat{O}_l\right) = \sum_{k' \in \{S_k\}} -i \operatorname{Tr}\left(\left[\hat{H}, \hat{O}^{B_{\text{odd}}}_{k'}\right] \hat{O}_l\right) = \sum_{k' \in \{S_k\}} c^l_{k'}. \tag{3.30}$$

The linear nature means we can simply add together the structure constants to get the values for symmetric operators.

This symmetric combination of odd operators reduces the number of AGP coefficients that need to be solved for, which reduces the size of the matrix equation. When a Hamiltonian has a very high degree of symmetry, this greatly reduces the overall scaling of the problem. In the next three chapters where we discuss results of computing the AGP in different systems, we will see how this allows the computation to be pushed much further than may be naively expected from the inherent exponential scaling of the operator space.

3.2.3 How to approximate via truncation

One clear approximation that can be applied, is truncating the generation of the Lie algebra, meaning we take a maximum number of nested commutations, giving B_l a maximum l value of l_{trunc} which is smaller than the true maximum. This gives a structured approach to building an approximate AGP, however we have not studied the effect of this approximation outside of computing it for some simple examples. In many cases the size of the full Lie algebra will be unfeasible to tackle, so this at least gives an approach to solving these problems even if there is a better approximation that can be made.

3.2.4 How to handle complex valued Hamiltonians

Most of the reasoning we have presented so far has partially assumed a real Hamiltonian. This has not been an explicit assumption, and all the results are still true for a complex Hamiltonian, however there are some oddities that arise. A key fact is when a Hamiltonian is fully real, its AGP is fully imaginary [72]. For every case the AGP must be hermitian, so this limits the overall operators for real Hamiltonians, for example to operators with an odd number of $\hat{\sigma}^y$ for spin-1/2 systems. Due to the nature of commutation, the commutator of any two hermitian operators $\hat{O}^1, \hat{O}^2$ is anti-hermitian:

$$\left[\hat{O}^1, \hat{O}^2\right]^\dagger = (\hat{O}^1\hat{O}^2 - \hat{O}^2\hat{O}^1)^\dagger = -(\hat{O}^1\hat{O}^2 - \hat{O}^2\hat{O}^1) = -\left[\hat{O}^1, \hat{O}^2\right]. \tag{3.31}$$

This means that the sets B_ℓ alternate between hermitian and anti-hermitian operators. We can always multiply an operator by i to change between hermitian and anti-hermitian, so we are free to choose that odd values of ℓ have hermitian operators. This ensures the AGP defined over odd ℓ values of B_ℓ operators sets is hermitian with real α coefficients.

When the Hamiltonian is real, the limits on the operators leads to even and odd values of l containing completely different operators, so the distinction of factors of i is not necessarily required. However for complex Hamiltonians the AGP can also be complex, meaning the same real operator can appear in both odd and even values of

l, with a difference of a factor i. As such, when dealing with complex Hamiltonians it is important to treat the complex nature of the operators, and track both $\hat{\sigma}^x$ and $i\hat{\sigma}^x$ separately.

To show an example of this, lets consider a simple spin-1/2 Hamiltonian of the form

$$\hat{H} = \hat{\sigma}^x + \hat{\sigma}^y + \lambda\hat{\sigma}^z. \tag{3.32}$$

We can see that $\partial_\lambda \hat{H} = \hat{\sigma}^z$, so lets take this as $B_0 = \{\hat{\sigma}^z\}$ and ignore factors of i to see the problems that occur. We can find B_1 to be

$$B_1 = \{\hat{\sigma}^x, \hat{\sigma}^y\}, \tag{3.33}$$

and there are no more non-repeating operators that are generated from nested commutation. This result suggests the AGP is of the form $\hat{\mathcal{A}}_\lambda = \alpha_x\hat{\sigma}^x + \alpha_y\hat{\sigma}^y$ with no component of $\hat{\sigma}^z$.

However, if we instead track the factors of i that appear from commutation, we find a conflicting result. Starting from $i\hat{\sigma}^z$ such that B_ℓ is Hermitian for odd ℓ, we find the operator sets to be

$$B_0 = \{i\hat{\sigma}^z\}, \tag{3.34}$$

$$B_1 = \{\hat{\sigma}^x, \hat{\sigma}^y\}, \tag{3.35}$$

$$B_2 = \{i\hat{\sigma}^x, i\hat{\sigma}^y\}, \tag{3.36}$$

$$B_3 = \{\hat{\sigma}^z\}. \tag{3.37}$$

This shows that the AGP is actually of the form $\hat{\mathcal{A}}_\lambda = \alpha_x\hat{\sigma}^x + \alpha_y\hat{\sigma}^y + \alpha_z\hat{\sigma}^z$, showing how ignoring the complex nature of the coefficients can lead to incorrect results in the AGP.

3.2.5 Diagrammatic description of the OCE

It can be helpful to visualise the OCE with a diagrammatic representation, which is shown in Fig. 3.1. Here the operator sets B_ℓ are represented by the rectangles and

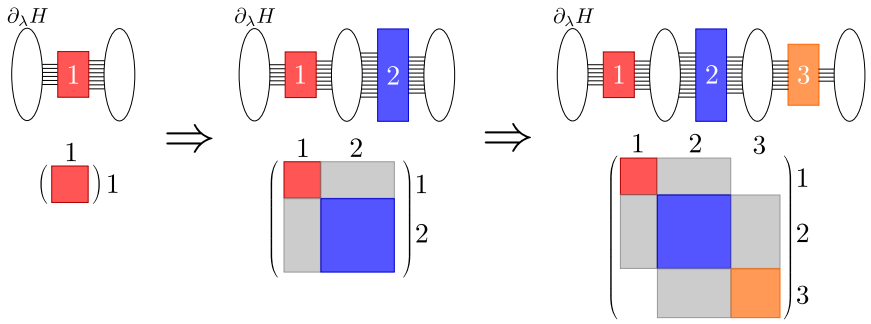

Figure 3.1: Graphical illustration of the OCE algorithm, with rectangles (ovals) representing operator sets B_l with odd (even) l, with lines showing the connection of commutation. To solve for the coefficients of the AGP which are defined over the odd operator sets (rectangles), a matrix equation is created. This matrix has elements that involve a sum over consecutive even sets (ovals), which gives the matrix a block tridiagonal form.

ovals for odd and even values of ℓ respectively, with lines between them showing the commutation from operators in one set to the next. Note that only the odd sets here are labelled, as these are the operator sets that make up the AGP. As discussed in the previous paragraph, there is only commutation between consecutive sets, meaning only consecutive odd sets have non-zero matrix elements between them. Going from left to right in this picture we see how we grow the basis, and compute the matrix elements at the same time as they both require the same process of commutation with the Hamiltonian. Eventually there will be no new operators generated and the final $B_{\ell_{\max}}$ will be reached, which means the entire Lie algebra has been spanned and solving the matrix equation will give the exact AGP.

3.3 Computation of the OCE

When implementing a method, whether that be analytically or numerically, there are practical details of the computation that arise. We write this section to try and collect together some of the mathematical details around commutation that are needed to use the OCE in practise. We will explain how to compute the commutator in coupled bases, where the structure constants are only known for operators on single sites. We then give an overview of different ways of implementing commutation numerically, to

be able to automate the process of generating B_ℓ and the reduced structure constants required. To conclude this section, we then give a step by step algorithm of the OCE, for a short form summary of all the steps highlighted in this chapter.

3.3.1 The commutator in coupled bases

In many-body physics, it is common to represent the Hamiltonian as a Kronecker/tensor product over the individual sites/particles. However it is unlikely commutation is directly defined across this many-body space, and instead is defined for each site. If this is the case, we need a way of commuting operators in terms of the single site, such that we can apply the OCE.

First lets define two generic operators $\hat{O}^a$ and $\hat{O}^b$ in terms of a Kronecker product over N sites/particles. We write these as

$$\hat{O}^{a/b} = \hat{O}_1^{a,b} \otimes \hat{O}_2^{a,b} \otimes \dots \hat{O}_N^{a,b} = \bigotimes_k \hat{O}_k^{a,b}, \tag{3.38}$$

where the subscript k indicates the operator on the kth site.

We then use the mixed-product property of the Kronecker product [102], to be able to multiply together $\hat{O}^a$ and $\hat{O}^b$,

$$\hat{O}^a\hat{O}^b = \bigotimes_k \hat{O}_k^a\hat{O}_k^b. \tag{3.39}$$

Applying this to the commutator we get

$$[\hat{O}^a, \hat{O}^b] = \hat{O}^a\hat{O}^b - \hat{O}^b\hat{O}^a = \bigotimes_k \hat{O}_k^a\hat{O}_k^b - \bigotimes_k \hat{O}_k^b\hat{O}_k^a. \tag{3.40}$$

We can then express the products on each sites as additions of commutators and anti-commutators

$$\begin{aligned} \hat{O}_k^a\hat{O}_k^b =& \frac{1}{2}\left(\left[\hat{O}_k^a, \hat{O}_k^b\right] + \left\{\hat{O}_k^a, \hat{O}_k^b\right\}\right), \\ \hat{O}_k^b\hat{O}_k^a =& \frac{1}{2}\left(\left[\hat{O}_k^b, \hat{O}_k^a\right] + \left\{\hat{O}_k^b, \hat{O}_k^a\right\}\right) \end{aligned} \tag{3.41}$$

$$= \frac{1}{2}\left(-\left[\hat{O}_k^a, \hat{O}_k^b\right] + \left\{\hat{O}_k^a, \hat{O}_k^b\right\}\right), \tag{3.42}$$

where $\left\{\hat{O}_k^a, \hat{O}_k^b\right\}$ is the anti-commutator between $\hat{O}_k^a$ and $\hat{O}_k^b$. To simplify the notation, we define $\hat{C}_k = \left[\hat{O}_k^a, \hat{O}_k^b\right]$ and $\hat{A}_k = \left\{\hat{O}_k^a, \hat{O}_k^b\right\}$. We can then express the commutator in Eq. (3.40) as

$$[\hat{O}^a, \hat{O}^b] = \bigotimes_k \frac{1}{2}\left(\hat{A}_k + \hat{C}_k\right) - \bigotimes_k \frac{1}{2}\left(\hat{A}_k - \hat{C}_k\right). \tag{3.43}$$

The Kronecker product does not have a mixed sum property, meaning $\bigotimes_k \hat{O}_k^a + \bigotimes_k \hat{O}_k^b \neq \bigotimes_k \left(\hat{O}_k^a + \hat{O}_k^b\right)$, so we will simplify this expression in a different way.

First we define $\hat{p}$ to be a ordered permutation of the form

$$\hat{p} = \bigotimes_k \hat{p}_k \quad \text{where} \quad \hat{p}_k = \hat{A}_k \text{ or } \hat{C}_k. \tag{3.44}$$

Then we let $\mathcal{P}$ be the set of all possible permutations of this form. Using this, we can write

$$\bigotimes_k \frac{1}{2}\left(\hat{A}_k + \hat{C}_k\right) = \left(\frac{1}{2}\right)^N \sum_{\hat{p}\in\mathcal{P}} \hat{p}, \tag{3.45}$$

$$\bigotimes_k \frac{1}{2}\left(\hat{A}_k - \hat{C}_k\right) = \left(\frac{1}{2}\right)^N \sum_{\hat{p}\in\mathcal{P}} (-1)^{n_c^{\hat{p}}} \hat{p}, \tag{3.46}$$

where $n_c^{\hat{p}}$ is the number of commutators ($\hat{C}_k$) present in $\hat{p}$.

As shown Eq. (3.43), the commutator is the difference between these two expressions. This means when $n_c^{\hat{p}}$ is even, the two expressions cancel, and we are left with only the odd values of $n_c^{\hat{p}}$. If we let $\mathcal{P}_{\text{odd}}$ be the set of $\hat{p}$ with odd $n_c^{\hat{p}}$, then we get the final expression

$$[\hat{O}^a, \hat{O}^b] = \left(\frac{1}{2}\right)^{N-1} \sum_{\hat{p}\in\mathcal{P}_{\text{odd}}} \hat{p} \tag{3.47}$$

With this general expression in hand, we can work out how many permutations ($\hat{p}$) are needed. For a given N sites/particles, there are 2^N different permutations, of which approximately half will be odd. Clearly this exponential scaling is not feasible to use

in general, however there are cases where we can simplify the form further to a more practical number.

The simplest case occurs when the commutator and anti-commutator are disjoint, meaning $\hat{C}_k \neq 0 \implies \hat{A}_k = 0$ and $\hat{A}_k \neq 0 \implies \hat{C}_k = 0$. This implies that only one permutation ($\hat{p}$) is non-zero, and as such the scaling goes from exponential to exactly order one. The Pauli matrices are an example that satisfy this condition, so all many-body spin-1/2 models are accessible with this approach.

Another simplified form can be found for two-body operations. We can write

$$\hat{O}^a = \hat{\mathbb{I}} \otimes \cdots \otimes \hat{O}^a_{k_1} \otimes \cdots \otimes \hat{O}^a_{k_2} \otimes \cdots \otimes \hat{\mathbb{I}}, \tag{3.48}$$

where k_1 and k_2 are the sites/particles the operator interacts with. As $\left[\hat{\mathbb{I}}, \hat{O}\right] = 0$ and $\left\{\hat{\mathbb{I}}, \hat{O}\right\} = 2\hat{O}$ for any operator $\hat{O}$, we can reduce Eq. (3.47) to

$$\begin{aligned}[\hat{O}^a, \hat{O}^b] =& \frac{1}{2}\Big(\hat{O}^b_1 \otimes \cdots \otimes \hat{C}_{k_1} \otimes \cdots \otimes \hat{A}_{k_2} \otimes \cdots \otimes \hat{O}^b_N \\ &+ \hat{O}^b_1 \otimes \cdots \otimes \hat{A}_{k_1} \otimes \cdots \otimes \hat{C}_{k_2} \otimes \cdots \otimes \hat{O}^b_N\Big).\end{aligned} \tag{3.49}$$

So only the result is completely dependent on the operators at sites k_1 and k_2, and can only affect those sites. This again is a large reduction from a exponential number of permutations down to simply two.

There are of course other cases where the form of commutation will be simpler than the general expression, for example any n-body operator where $n < N$. As such, it is feasible to build up larger many-body Hilbert spaces, even if the commutation relations are only known for single site operators. However in all cases, knowledge of both the commutator and anti-commutator is required. Where the fully anti-symmetric structure constants f^c_{ab} we have defined in Eq. (3.12) describes commutation in a given basis, the fully symmetric structure constants d^c_{ab} can describe anti-commutation as

$$\left\{\hat{O}^a, \hat{O}^b\right\} = 2\hat{\mathbb{I}}\delta_{ab} + \sum_c d^c_{ab}\hat{O}^c. \tag{3.50}$$

With the values then of f^c_{ab} and d^c_{ab}, it is possible to extend single site/particles bases

to describe many-body Hamiltonians.

3.3.2 Numerical representation of bases

The OCE algorithm can be used analytically, but due to the large dimension of the AGP this often is not possible. In general the algorithm will be implemented numerically for a basis, that can then be used for multiple Hamiltonians. The first step in the OCE is to decide how the chosen basis will be represented on the computer.

The simplest general representation is to use an array of integers, where each array index represents a different site, and the integer represents the type of operator for that site. This can also equivalently be done with string values to make them more readable to the user. Lets show this for the Pauli matrices on four sites

$$[1, 2, 0, 3] = \hat{\sigma}^x \otimes \hat{\sigma}^y \otimes \hat{\mathbb{I}} \otimes \hat{\sigma}^z. \tag{3.51}$$

Here the integers $0, 1, 2, 3$ represent $\hat{\mathbb{I}}, \hat{\sigma}^x, \hat{\sigma}^y, \hat{\sigma}^z$ respectively. Depending on implementation in code, the size of the integers is different, so we shall assume the code uses $U8$ (unsigned 8-bit) type integers. This means we can represent up to 256 operators, which is more than sufficient for each site in most cases. With this the memory usage for a N-body operator is N bytes, however clearly this greatly overuses memory for small local site dimension.

One implementation that is slightly more efficient for memory, but is more cumbersome to use, is to collect multiple sites into the same integer. Lets stick with the spin-1/2 example, so we have an operator dimension of four per site. We can group together every four sites, such that every two bits of the integer represents a different site. For example

$$01100011 = 109 = \hat{\sigma}^x \otimes \hat{\sigma}^y \otimes \hat{\mathbb{I}} \otimes \hat{\sigma}^z. \tag{3.52}$$

With such a representation, we have at most less than one byte of memory inefficacy. In almost all modern architecture, a byte is the smallest size anything can be, so we have maximum memory efficiency for representing a generic operator.

To be able to apply the OCE we also require the ability to commute operators.

In general this can be done by hashmaps or dictionaries, where the key represents the input operator and the value is the commuted result. To save on needing to define every single operator, we can define the dictionary only over the size of the largest many-body operator in the Hamiltonian and then combine the results together. For example if we wish to define a commutation of $[\hat{\sigma}^z \otimes \hat{\sigma}^z, \cdot]$ we can write a dictionary

```
{ Ix :  zy ,  Iy :  zx ,  xI :  yz ,  xz :  yI ,
  yI :  xz ,  yz :  xI ,  zx :  Iy ,  zy :  Ix } ,
```

with a default value of zero for all other two-body operators. The key of the dictionary represents the operator the commutator is applied to, and the value that returns is the commuted operator, so for example {Ix: zy} represents $\left[\hat{\sigma}^z \otimes \hat{\sigma}^z, \hat{\mathbb{I}} \otimes \hat{\sigma}^x\right] = \hat{\sigma}^z \otimes \hat{\sigma}^y$. This provides a very flexible approach commuting an operator, which can be refined for specific cases to reduce overhead, like using the symmetry of a given operator. However this does require the generation of a new commutator dictionary for each new Hamiltonian operator, but these dictionaries are often quite small due to their local nature.

There are certain representations that provide both memory efficient implementation, and simple approaches to commutation without dictionaries. The most important example of this, due to the prevalence of spin-1/2 models, is the Binary Symplectic Form (BSF) [103]. In this form an operator is written out in terms of $\hat{\sigma}^x$ and $\hat{\sigma}^z$ on each site. Let $\hat{P}$ be a many-body Pauli operator

$$\hat{P} = \bigotimes_k \hat{P}_k, \tag{3.53}$$

where $\hat{P}_k$ is a Pauli operator on site k.

We can then write each $\hat{P}_k$ as

$$\hat{P}_k = (-i)^{\theta + x \cdot z} (\hat{\sigma}^z)^z (\hat{\sigma}^x)^x \tag{3.54}$$

where there is a real valued phase $\theta \in \mathbb{Z}_4$ and small x and z are either $0, 1$. The extra factor in the phase is to account for the fact $\sigma_z \sigma_x = i\sigma_y$. As the phases of all

the individual $\hat{P}_k$ are multiplied together in the Kronecker product, we only need to track the global phase of $\hat{P}$ which we denote θ_P. Lets define P^x and P^z to be binary numbers, where the kth values are given by the x and z values for the associated kth site. This means that a general N-body Pauli operator can be written with a global phase θ_P and two binary numbers P^x,P^z of length N.

When commuting two operators in BSF, there are a few different values we need to compute. We will quote these values and explain their importance here, and show our full working out for these results in App. A.1. Firstly we let $\hat{A}$,$\hat{B}$ be BSF operators, we can then write their commutator as

$$\hat{C} = \left[\hat{A}, \hat{B}\right]. \tag{3.55}$$

In Sec. 3.3.1, we showed the commutator between coupled Pauli operators is only non zero if there are an odd number of commutations on individual sites. It is possible to show that the number of commutations is given by

$$N_{\text{com}} = \text{countones}\left((A^x \wedge B^z) \oplus (B^x \wedge A^z)\right), \tag{3.56}$$

where $\wedge$ is an AND operation, countones counts the number of ones in the binary representation. As such only when N_{com} is odd, the commutator is non-zero, so N_{com} mod 2 is a effective boolean value for whether commutation is non-zero. Then it can also be shown that the x and z values for C are given by using the XOR ($\oplus$) operations

$$C^x = A^x \oplus B^x, \tag{3.57}$$

$$C^z = A^z \oplus B^z. \tag{3.58}$$

The final value required is the new global phase θ_C, which is a combination of the globals phases of $\hat{A}$ and $\hat{B}$, with the addition of tracking the factors of $+i$ and $-i$ that arise during commutation. This results in the expression

$$\theta_C = \theta_A \cdot \theta_B \cdot (+i)^{N_{\text{positive}}} (-i)^{N_{\text{coms}} - N_{\text{positive}}}, \tag{3.59}$$

where N_{positive} is the number of $+i$ factors that occur (we omit the form of N_{positive}, as it requires quite a few steps to compute).

The BSF as such provides a very handy representation for Pauli operators, that can commute any two coupled Pauli operators using simple binary operators. For more complicated bases, where the Hamiltonian is reasonably local the dictionary approach is also a good approach. These approaches provide a suitable way of computing the needed reduced structure constants and ordered operators sets B_ℓ.

3.4 Structure constants in some example bases

In the following three chapters we discuss results obtained for different Hamiltonians using the OCE, which are defined over a few different bases. As the OCE requires commuting operators, and as such understanding of both the fully anti-symmetric and symmetric structure constants, f^c_{ab} (Eq. (3.12)) and d^c_{ab} (Eq. (3.50)) respectively, we list here these values for the majority of bases used in the thesis: the Pauli matrices, Gell-Mann matrices and generalised Gell-Mann matrices. The one basis omitted in this section which is used elsewhere in this thesis, is the creation ($\hat{a}^\dagger$) and annihilation operators ($\hat{a}$), due to added complications we shall discuss in Chap. 5. Due to the fully anti-symmetric nature of f^c_{ab}, swapping any two indices will flip the sign of the value, meaning any permutation of the same indices can be figured out, for example $f^a_{bc} = -f^b_{ac} = f^c_{ab}$. In the other case d^c_{ab} is fully symmetric, so all permutations of the indices share the same value. This ability to permute values of f^c_{ab} and d^c_{ab}, allows us to only state one value per unique combination of indices, where all other related values can be calculated when required.

3.4.1 The Pauli matrices

The Pauli matrices are generators of the $SU(2)$ group, and in physics represent spin-1/2 systems, which are prevalent in a large majority of AGP calculations in the literature [69, 92, 94]. In many of the examples already shown, we have used the Pauli matrices, so the basis should be familiar to the reader at this stage. For completeness,

and to have a single reference point, we briefly recap the results here. The basis is given by

$$\hat{\sigma}^x = \begin{pmatrix} 0 & 1 \\ 1 & 0 \end{pmatrix}, \hat{\sigma}^y = \begin{pmatrix} 0 & -i \\ i & 0 \end{pmatrix}, \hat{\sigma}^z = \begin{pmatrix} 1 & 0 \\ 0 & -1 \end{pmatrix}. \tag{3.60}$$

The non-zero values of the fully anti-symmetric structure constants are

$$f^z_{xy} = 2. \tag{3.61}$$

The fully symmetric structure constants are zero valued for all indexes, because the anti-commutator is only non-zero when two indexes repeat

$$\left\{\hat{\sigma}^i, \hat{\sigma}^j\right\} = 2\delta_{i,j}\hat{\mathbb{I}}. \tag{3.62}$$

Lastly the spin-1/2 operators are directly proportional to each of the Pauli matrices

$$\hat{S}^j = \frac{\hbar}{2}\hat{\sigma}^j \tag{3.63}$$

3.4.2 The Gell-Mann matrices

The next basis we state here is the Gell-Mann matrices, which is used to describe the physics spin-1 particles or other three level systems generally [104]. These matrices are analogous to the Pauli matrices but for the $SU(3)$ group. Whilst they have many similarities to the Pauli matrices there are major differences, importantly for the OCE the commutator and anti-commutator are no longer disjoint, so the simplified form for spin-1/2 systems is lost. The matrices are defined as

$$\hat{\lambda}^1 = \begin{pmatrix} 0 & 1 & 0 \\ 1 & 0 & 0 \\ 0 & 0 & 0 \end{pmatrix}, \hat{\lambda}^4 = \begin{pmatrix} 0 & 0 & 1 \\ 0 & 0 & 0 \\ 1 & 0 & 0 \end{pmatrix}, \hat{\lambda}^6 = \begin{pmatrix} 0 & 0 & 0 \\ 0 & 0 & 1 \\ 0 & 1 & 0 \end{pmatrix},$$

$$\hat{\lambda}^2 = \begin{pmatrix} 0 & -i & 0 \\ i & 0 & 0 \\ 0 & 0 & 0 \end{pmatrix}, \hat{\lambda}^5 = \begin{pmatrix} 0 & 0 & -i \\ 0 & 0 & 0 \\ i & 0 & 0 \end{pmatrix}, \hat{\lambda}^7 = \begin{pmatrix} 0 & 0 & 0 \\ 0 & 0 & -i \\ 0 & i & 0 \end{pmatrix},$$

$$\hat{\lambda}^3 = \begin{pmatrix} 1 & 0 & 0 \\ 0 & -1 & 0 \\ 0 & 0 & 0 \end{pmatrix}, \hat{\lambda}^8 = \frac{1}{\sqrt{3}} \begin{pmatrix} 1 & 0 & 0 \\ 0 & 1 & 0 \\ 0 & 0 & -2 \end{pmatrix}. \tag{3.64}$$

The non zero elements of the fully anti-symmetric structure constants are

$$\begin{aligned} f_{14}^7 =& f_{16}^5 = f_{24}^6 = f_{25}^7 = 1, \\ f_{12}^3 =& 2, \\ f_{34}^5 =& f_{37}^6 = 1, \\ f_{45}^8 =& f_{67}^8 = \sqrt{3}. \end{aligned} \tag{3.65}$$

Lastly, the non zero elements of the symmetric structure constants are

$$\begin{aligned} d_{14}^6 =& d_{15}^7 = d_{25}^6 = 1, \\ d_{24}^7 =& -1 \\ d_{34}^4 =& d_{35}^5 = 1, \\ d_{36}^6 =& d_{37}^7 = -1, \\ d_{11}^8 =& d_{22}^8 = d_{33}^8 = \frac{2}{\sqrt{3}}, \\ d_{44}^8 =& d_{55}^8 = d_{66}^8 = d_{77}^8 = -\frac{1}{\sqrt{3}}, \\ d_{88}^8 =& -\frac{2}{\sqrt{3}}. \end{aligned} \tag{3.66}$$

When writing a spin-1 Hamiltonian, they will often be expressed in terms of the spin operators $\hat{S}^x, \hat{S}^y, \hat{S}^z$, so we note here the conversion to the Gell-Mann matrices as

$$\hat{S}^x = \frac{\hbar}{\sqrt{2}} \begin{pmatrix} 0 & 1 & 0 \\ 1 & 0 & 1 \\ 0 & 1 & 0 \end{pmatrix} = \frac{\hbar}{\sqrt{2}} \left(\hat{\lambda}^1 + \hat{\lambda}^6 \right), \tag{3.67}$$

$$\hat{S}^y = \frac{\hbar}{\sqrt{2}} \begin{pmatrix} 0 & -i & 0 \\ i & 0 & -i \\ 0 & i & 0 \end{pmatrix} = \frac{\hbar}{\sqrt{2}} \left(\hat{\lambda}^2 + \hat{\lambda}^7 \right), \tag{3.68}$$

$$\hat{S}^z = \hbar \begin{pmatrix} 1 & 0 & 0 \\ 0 & 0 & 0 \\ 0 & 0 & -1 \end{pmatrix} = \hbar \left(\hat{\lambda}^3 + \sqrt{3}\hat{\lambda}^8 \right). \tag{3.69}$$

3.4.3 The generalised Gell-Mann matrices

The Generalised Gell-Mann matrices (GGM) [105, 106] is a basis for all $\mathfrak{su}(N)$, being the generalised version of both the Pauli matrices ($\mathfrak{su}(2)$) and the Gell-Mann matrices ($\mathfrak{su}(3)$). As such they can be used to represent any N level system, so they are ideal for higher order spin models. They are split into three classes: Symmetric (S_{nm}), Anti-Symmetric (A_{nm}) and Diagonal (D_n), which have the forms

$$\hat{S}_{S_{nm}} = \frac{1}{2} \left(|m\rangle \langle n| + |n\rangle \langle m| \right), \tag{3.70}$$

$$\hat{S}_{A_{nm}} = -i\frac{1}{2} \left(|m\rangle \langle n| - |n\rangle \langle m| \right), \tag{3.71}$$

$$\hat{S}_{D_n} = \frac{1}{\sqrt{2n(n-1)}} \left(\sum_{k=1}^{n-1} |k\rangle \langle k| + (1-n) |n\rangle \langle n| \right), \tag{3.72}$$

where $|n\rangle$,$|m\rangle$ are number states, with the condition $1 \leq m < n \leq N$. To make it easier to index each of the matrices, the indexes S_{nm},A_{nm},D_n can be written as

$$S_{nm} = n^2 + 2(m-n) - 1, \tag{3.73}$$

$$A_{nm} = n^2 + 2(m-n), \tag{3.74}$$

$$D_n = n^2 - 1. \tag{3.75}$$

As such all numbers between 1 and N^2-1 represent an index for different basis vectors, with each number uniquely falling into one of the three classes.

The non-zero values of f_{ijk} are given by [106]

$$f^{A_{km}}_{S_{nm}S_{kn}} = f^{A_{km}}_{S_{nm}S_{nk}} = f^{A_{kn}}_{S_{nm}S_{km}} = \frac{1}{2}, \tag{3.76}$$

$$f^{A_{kn}}_{A_{nm}A_{km}} = \frac{1}{2}, \tag{3.77}$$

$$f^{D_m}_{S_{nm}A_{nm}} = -\sqrt{\frac{m-1}{2m}}, \tag{3.78}$$

$$f^{D_n}_{S_{nm}A_{nm}} = \sqrt{\frac{n}{2(n-1)}}, \tag{3.79}$$

$$f^{D_k}_{S_{nm}A_{nm}} = \sqrt{\frac{1}{2k(k-1)}}, m < k < n. \tag{3.80}$$

For the first two lines, the range of values of k can be figured out by using the condition $1 \leq i_2 < i_1 \leq N$, where i_1, i_2 are the first and second indexes respectively (this is just a generalisation of the condition $1 \leq m < n \leq N$).

Anti-commutation is then completely defined by the non-zero values of d_{ijk}, which are given by [106]

$$d^{S_{km}}_{S_{nm}S_{kn}} = d^{A_{km}}_{S_{nm}A_{kn}} = d^{A_{nk}}_{S_{nm}A_{mk}} = \frac{1}{2}, \tag{3.81}$$

$$d^{A_{km}}_{S_{nm}A_{nk}} = -\frac{1}{2}, \tag{3.82}$$

$$d^{D_m}_{S_{nm}S_{nm}} = d^{D_m}_{A_{nm}A_{nm}} = -\sqrt{\frac{m-1}{2m}}, \tag{3.83}$$

$$d^{D_k}_{S_{nm}S_{nm}} = d^{D_k}_{A_{nm}A_{nm}} = \sqrt{\frac{1}{2k(k-1)}}, m < k < n, \tag{3.84}$$

$$d^{D_n}_{S_{nm}S_{nm}} = d^{D_n}_{A_{nm}A_{nm}} = \frac{2-n}{\sqrt{2n(n-1)}}, \tag{3.85}$$

$$d^{D_k}_{S_{nm}S_{nm}} = d^{D_k}_{A_{nm}A_{nm}} = \sqrt{\frac{2}{k(k-1)}}, n < k, \tag{3.86}$$

$$d^{D_k}_{D_nD_k} = \sqrt{\frac{2}{n(n-1)}}, k < n, \tag{3.87}$$

$$d^{D_n}_{D_nD_n} = (2-n)\sqrt{\frac{2}{n(n-1)}}. \tag{3.88}$$

Like commutation, the exact range of k where it is not clear, can be figured out by the condition $1 \leq i_2 < i_1 \leq N$, where i_1, i_2 are the first and second indexes respectively.

Similar to the Gell-Mann matrices, these are often used in higher order spin models. The general form for a spin operator for a spin-s particle, have matrix elements (a, b)

$$\left(\hat{S}^x\right)_{ab} = \frac{\hbar}{2}\left(\delta_{a,b+1} + \delta_{a+1,b}\right)\sqrt{(s+1)(a+b-1) - ab}, \tag{3.89}$$

$$\left(\hat{S}^y\right)_{ab} = \frac{i\hbar}{2}\left(\delta_{a,b+1} - \delta_{a+1,b}\right)\sqrt{(s+1)(a+b-1) - ab}, \tag{3.90}$$

$$\left(\hat{S}^z\right)_{ab} = \hbar(s+1-a)\delta_{a,b} = \hbar(s+1-b)\delta_{a,b}, \tag{3.91}$$

where $1 \leq a, b \leq 2s+1$, meaning $N = 2s+1$. The total spin s can take on any integer or half integer and $s \geq 0$.

Converting $\hat{S}^x$ and $\hat{S}^y$ to the generalised Gell-Mann matrices is

$$\hat{S}^x = \hbar \sum_{k=1}^{N-1} \sqrt{(s+1)(2k) - (k+1)(k)}\hat{S}_{S_{k+1,k}}, \tag{3.92}$$

$$\hat{S}^y = \hbar \sum_{k=1}^{N-1} \sqrt{(s+1)(2k) - (k+1)(k)}\hat{S}_{A_{k+1,k}}. \tag{3.93}$$

For $\hat{S}^z$ we can show the result is (see App. A.2)

$$\hat{S}^z = \hbar \sum_{k=2}^{N} \sqrt{\frac{k(k-1)}{2}}\hat{S}_{D_k}. \tag{3.94}$$

This concludes this section on a few example bases, and simultaneously the end of this chapter. The OCE can be summarised as a simplification to the more general algebraic approach, resulting from the restriction on a trace-orthogonal basis, and the ordering of the operator sets B_ℓ. As such, the OCE provides the best results when the major computational difficultly is arising from solving the matrix equation or minimising the associated action of the AGP. However, for simpler systems it is clear the more general algebraic approach will be quicker to implement, and may perform faster overall. In the following chapter we shall make use of different methods depending on which we think is most applicable to the problem, so the results of Chap. 2 will also be highly relevant. We now begin the results chapter of this thesis, looking at computing and using the AGP in different spin models.

Chapter 4

The AGP in spin models

In this chapter we compute the AGP in different spin models, and analyse the results to gain insight into the models diabatic excitations. Any spin model can be expressed only using the spin operators $\hat{S}^x$, $\hat{S}^y$, $\hat{S}^z$ which obey the commutation relation [107]

$$\left[\hat{S}^j \hat{S}^k\right] = i\hbar\epsilon_{jkl}\hat{S}^l, \tag{4.1}$$

where ϵ_{jkl} is the Levi-Civita symbol. Spin is an intrinsic angular momentum that is quantised to a number of levels depending on the maximum value of spin S. For spin-1/2 particles, they have two possible spin states, up and down, making them a two level system. As we saw in the previous chapter (Sec. 3.4.1), the spin-1/2 operators are directly proportional to the Pauli matrices and as such we often simply use Pauli matrices and not the full spin operators. For a given spin-S, there are exactly $2S + 1$ levels, ranging from $-S$ to S in steps of one, and can be represented by the generalised Gell-Mann matrices (Sec. 3.4.3).

There are many different spin models of interest to researches, but for this thesis we will look at two types: the transverse field Ising model, and the XXZ model. The first part of this chapter will focus on the transverse field Ising model, with different geometries defined by an associated graph. Then in the second part, we shall explore how the XXZ model compares to the Ising model, finding completely different forms of scaling for the number of operators needed for the AGP. Additionally we will look

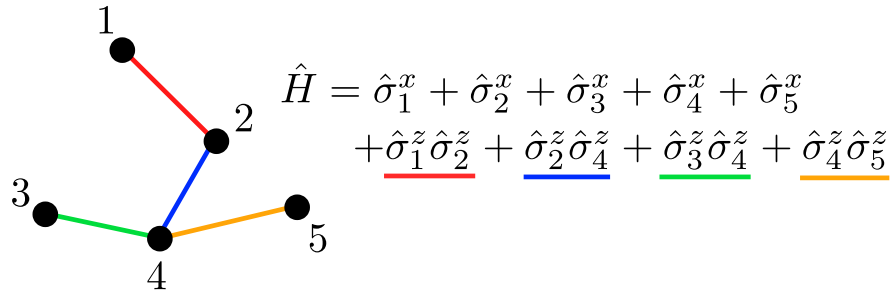

Figure 4.1: A schematic of the transverse field Ising model, where connections are defined by edges on the associated graph. The exact positioning of graph nodes and edges does not change the Hamiltonian, only which edges are present.

at the differences between spin-1/2 and spin-1 XXZ models, showing the increase in computational complexity as the size of spin increases.

4.1 Spin-1/2 Ising model on graphs

The first model we discuss is the widely used transverse field Ising model [108–110], with arbitrary connections between different spins defined by an associated graph. One interesting property of the Ising model is the ability to express combinatorial optimisation problems in terms of finding the ground state of a particular associated graph [111–114]. As such, quantum annealing can be used to adiabatically vary the Hamiltonian, from starting in a trivial ground state, to a solution to a combinatorial optimisation problem [86–89]. To map between the different Hamiltonians we require the ability to turn on or off the connections between different spins. We define connections on an associated graph so we can include graphs that go beyond the usual crystalline structure studied in condensed matter physics. There are a range of experimental setups that have tried implementing this quantum annealing problem, including superconducting qubits [115–117], trapped ions [118–120], and Rydberg atoms [121, 122]. As such understanding the diabatic operators in such systems is of great importance to improving these procedures, so this provides a useful example to study.

We can write the Hamilton of the transverse field Ising model for a given graph as

$$\hat{H}(\lambda) = -J \sum_{(i,j)} \hat{\sigma}_i^z \hat{\sigma}_j^z + \lambda \sum_i^N \hat{\sigma}_i^x, \tag{4.2}$$

where σ^x and σ^z are the usual Pauli matrices, J is the coupling constant which can be positive or negative giving a ferromagnetic or antiferromagnetic interaction, N is the number of sites or vertices in the graph, and (i, j) are the indexes of sites connected by an edge on a given graph. In Fig. 4.1 we show an example schematic of this Hamiltonian, where the operators each edge is associated with are shown by colour coding. For the Hamiltonian, we use spin-1/2 particles but larger spins are also possible, but will be more computationally expensive. We wil only look at ferromagnetic interactions so we set $J = 1$, but the complexity is equal for computing the AGP in an antiferromagnetic setup. If the underlying graph is a chain, the Hamiltonian becomes the 1D transverse field Ising model, which has a ground state phase transition when $N \to \infty$. Ground state phase transitions are also known to appear in the all-to-all Ising model, which is given for a complete graph of connections, so there are multiple examples that can be studied within this model as well. We shall look at four different graphs: the Ring, the Chain, the Complete and a specific Asymmetric graph. Note that the results here are reproduced from our paper Ref. [80].

4.1.1 Scaling of the number of diabatic operators

The first quantity we can compute is the maximum number of diabatic operators required for a given graph. The largest number of non linear dependent operators in a given system is the Hilbert space dimension ($d = 2^N$) squared, which gives our most strict upper bound in this case of 4^N. Likewise the most strict lower bound is always zero, for the case where no diabatic excitations occur and the system is always adiabatic. However as we discussed in Sec. 3.2 the dimension of the AGP is reduced by a few different factors. For the case of the Ising model, the Hamiltonian is fully real and as such the AGP must be fully imaginary. The only Hermitian and imaginary Pauli operator is $\hat{\sigma}^y$, and as such a valid diabatic operator must contain an odd number of

$\hat{\sigma}^y$ across the sites of the graph. Another general non graph dependent reduction is the $\mathbb{Z}_2$ symmetry, which leads to the symmetry operator $\hat{S} = \bigotimes_i \hat{\sigma}_i^x$ which performs a spin flip on all sites, such that $\hat{S}^\dagger \hat{H} \hat{S} = \hat{H}$. As such both $\hat{\sigma}^x$ and $\hat{\mathbb{I}}$ are symmetric under $\hat{S}$ but $\hat{\sigma}^y$ and $\hat{\sigma}^z$ are not ($\hat{S}^\dagger \hat{\sigma}_i^y \hat{S} = -\sigma_i^y$ and $\hat{S}^\dagger \hat{\sigma}_i^z \hat{S} = -\sigma_i^z$). This is addressed by an even total of $\hat{\sigma}^y$ and $\hat{\sigma}^z$ across all the sites, which alongside the limitation of $\hat{\sigma}^y$ from the real Hamiltonian this means the number of both $\hat{\sigma}^y$ and $\hat{\sigma}^z$ must be odd, to combine to give a total even number. Therefore, using combinatorics we can find the maximum number of individual operators/coefficients to solve for, to be

$$N_{\mathcal{A}}^{\max} = \sum_{n_y}^{N} \sum_{n_z}^{N-n_y} \frac{N!}{n_y! n_z! (N - n_y - n_z)!} 2^{N-n_y-n_z}, \tag{4.3}$$

where N is the total number of sites, n_y, n_z are restricted to odd values and represent the number of $\hat{\sigma}^y$, $\hat{\sigma}^z$ respectively in a given string of operators. This can be simplified to

$$N_{\mathcal{A}}^{\max} = 2^{N-1}(2^{N-1} - 1). \tag{4.4}$$

Asymptotically, this gives 4^{N-1} operators so this is a reduction of about four times from the strict upper bound. We note this form is not derived from Eq. (4.3) , but from matching the numerical results, please see App A.3 for further details. Whilst these reductions reduce the complexity of the problem, they do not affect the fundamental exponential scaling of the problem. However specific graphs will fall somewhere between this maximum and the minimum value, with better scaling for highly symmetric graphs.

To illustrate the generic scaling of small sized graphs, Fig. 4.2(b) shows the number of diabatic terms ($N_{\mathcal{A}}$) for all non-isomorphic graphs up to size $N = 8$. This is done numerically by generating the Lie algebra from repeated commutation, and then grouping any operators that are equivalent under graph symmetries. The numerically computed values are indicated by black dots, with solid lines for scaling of graphs derived in the following subsections. The value of $N_{\mathcal{A}}$ lies within the purple region which is bounded by the maximum $N_{\mathcal{A}}^{\max}$, and a new lower bound given by the most symmetric graph

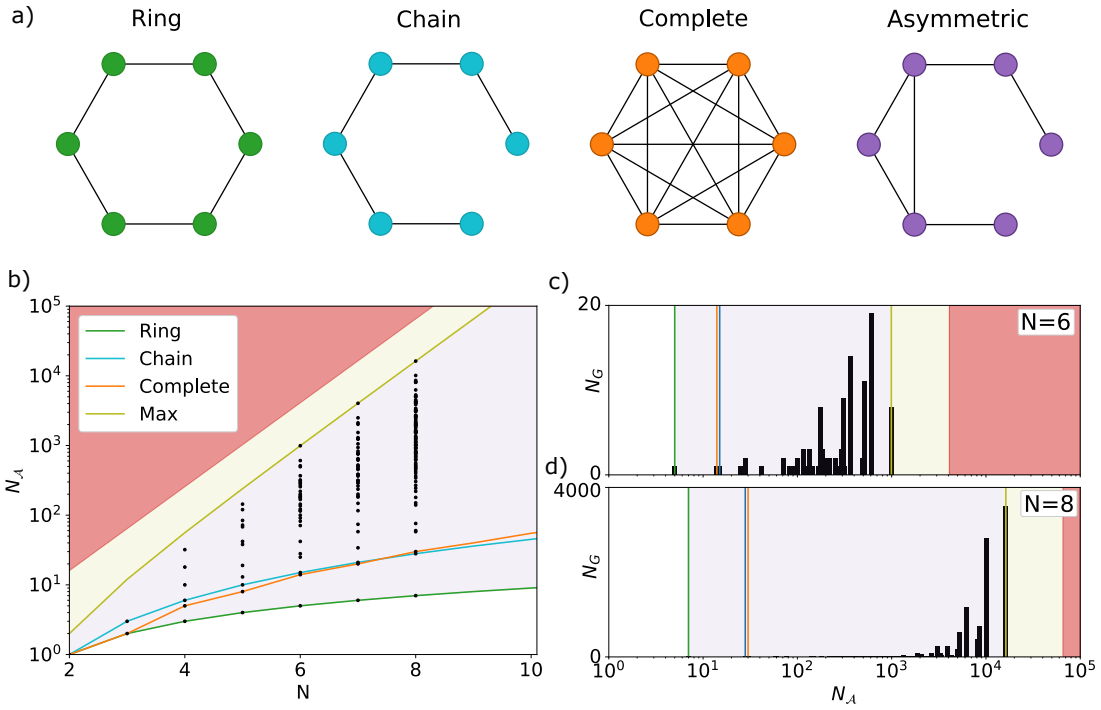

Figure 4.2: a) Diagrams of three classes of graphs studied (Ring, Chain, Complete), and a specific asymmetric graph which has the maximum possible number of coefficients for $N = 6$. b) The scaling of the number of unique operators ($N_{\mathcal{A}}$) required to construct the exact AGP vs. graph size. Black dots represent values for specific graphs, the coloured lines represent the three special cases and the maximum. The purple region shows the possible values of $N_{\mathcal{A}}$, yellow shows the region between the maximum possible for the Ising model studied here and the full size of operator space, and red region shows values larger than the operator space. c) For all $N = 6$ graphs, the number at each value of $N_{\mathcal{A}}$. d) Same as c) but with $N = 8$.

structure, the ring graph. We also note that for $N \geq 6$ there are points that lie on this upper bound, which are asymmetric with enough connectivity to span all possible operators (see Sec. 4.1.5).

Figure 4.2(b) shows the possible values $N_{\mathcal{A}}$ can take, but not the amount of graphs those values have. This information is given for $N = 6$ and $N = 8$ in Figs. 4.2(c)–(d), where the larger bar indicates more graphs of that value. We find that the distribution of values skews towards the maximum value as N increases. This is to be expected, as a known result from graph theory states the portion of asymmetric graphs increases along with graph size [123]. Due to this fact, large random graphs are effectively always asymmetric graphs, and as such are almost always the most difficult problems to solve.

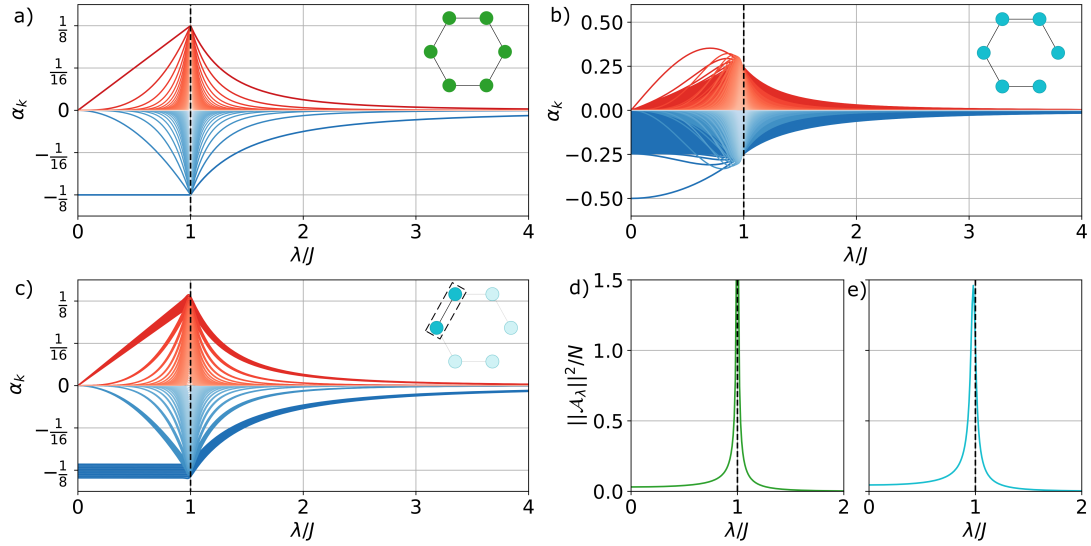

Figure 4.3: a) Coefficients of unique operators in the thermodynamic limit of the ring graph. Blue and red differentiate between operators with even and odd length respectively, the color fades as the length of the operator increases. The critical point is indicated at $\lambda = 1$ b) Coefficients of unique operators in the $N = 100$ chain graph, with the same colouring as before. Panel c) shows what happens when the operators are limited to those which only have support on the middle 10 sites for the $N = 100$ chain, same colouring as before, d) Norm of the AGP for the ring graph and e) AGP norm of the $N = 100$ chain graph.

As such, approximations must be made to make the computation feasible, but these must be done case by case for the best results. However many models of interest have a high degree of symmetry, in which the computation is far simpler and more tractable, as we will see in the following subsections.

4.1.2 The Ring graph

The first type of graph we shall discuss is the Ring graph, which has connections between sites $(i, i+1)$ and a connection between sites $(1, N)$, making it equivalent to the 1D ising chain with periodic boundary conditions. This model has been well studied in the literature [124, 125] and serves as a good first graph to study, in fact we find evidence that this is the simplest type of graph for computing the AGP for the Ising model. The Ring graph has a N-fold rotation symmetry by the operation of $i \to i+1 \pmod N$ (starting counting at 1, such that $N+1 \pmod N = 1$), and also N reflection

symmetries around any single site j giving the operation $i = j \pm l \rightarrow i = j \mp l \pmod N$. This provides a high degree of symmetry to the graph, greatly suppressing the number of diabatic operators that appear.

Another form of suppression of operators arises from the 1D nature of the graph, which we will find when studying what operators appear from repeated commutation. One way to represent these commutations is represent the different Pauli matrices by colour, which can help visualise the operators (if the reader struggles to distinguish the operators here, please see App. A.4 for a non colour based derivation). We use the colour representation

$$\bullet = \hat{\mathbb{I}}, \qquad \textcolor{blue}{\bullet} = \hat{\sigma}^x, \qquad \textcolor{green}{\bullet} = \hat{\sigma}^y, \qquad \textcolor{red}{\bullet} = \hat{\sigma}^z. \tag{4.5}$$

This means we can represent our Ising Hamiltonian by

$$\hat{H} = J\textcolor{red}{\bullet}\!-\!\textcolor{red}{\bullet} + \lambda\textcolor{blue}{\bullet}, \qquad \partial_\lambda \hat{H} = \textcolor{blue}{\bullet}. \tag{4.6}$$

Note we have used the symmetries of the graph to group together all the $\hat{\sigma}^z\hat{\sigma}^z$ and $\hat{\sigma}^x$ operators, as all sites are equivalent here, such that $\textcolor{red}{\bullet}\!-\!\textcolor{red}{\bullet} = \sum_k^N \hat{\sigma}_k^z\hat{\sigma}_{k+1}^z$. This allows a simpler representation where we do not need to write unnecessary identities and sums.

Ignoring the coefficients, we define a truth table to show us how to apply commutation

$$
\begin{aligned}
[\textcolor{blue}{\bullet}, \textcolor{red}{\bullet}] &= \textcolor{green}{\bullet}, & [\textcolor{blue}{\bullet}, \textcolor{green}{\bullet}] &= \textcolor{red}{\bullet},\\
[\textcolor{red}{\bullet}\!-\!\textcolor{red}{\bullet}, \bullet\!-\!\textcolor{blue}{\bullet}] &= \textcolor{red}{\bullet}\!-\!\textcolor{green}{\bullet}, & [\textcolor{red}{\bullet}\!-\!\textcolor{red}{\bullet}, \textcolor{blue}{\bullet}\!-\!\bullet] &= \textcolor{green}{\bullet}\!-\!\textcolor{red}{\bullet},\\
[\textcolor{red}{\bullet}\!-\!\textcolor{red}{\bullet}, \bullet\!-\!\textcolor{green}{\bullet}] &= \textcolor{red}{\bullet}\!-\!\textcolor{blue}{\bullet}, & [\textcolor{red}{\bullet}\!-\!\textcolor{red}{\bullet}, \textcolor{green}{\bullet}\!-\!\bullet] &= \textcolor{blue}{\bullet}\!-\!\textcolor{red}{\bullet},\\
[\textcolor{red}{\bullet}\!-\!\textcolor{red}{\bullet}, \textcolor{red}{\bullet}\!-\!\textcolor{blue}{\bullet}] &= \bullet\!-\!\textcolor{green}{\bullet}, & [\textcolor{red}{\bullet}\!-\!\textcolor{red}{\bullet}, \textcolor{blue}{\bullet}\!-\!\textcolor{red}{\bullet}] &= \textcolor{green}{\bullet}\!-\!\bullet,\\
[\textcolor{red}{\bullet}\!-\!\textcolor{red}{\bullet}, \textcolor{red}{\bullet}\!-\!\textcolor{green}{\bullet}] &= \bullet\!-\!\textcolor{blue}{\bullet}, & [\textcolor{red}{\bullet}\!-\!\textcolor{red}{\bullet}, \textcolor{green}{\bullet}\!-\!\textcolor{red}{\bullet}] &= \textcolor{blue}{\bullet}\!-\!\bullet.
\end{aligned}
$$

This can give helpful intuition that we can think of the commutators as just swapping colours.

We can then compute the first seven applications of the commutator for the Ising

Hamiltonian on a ring graph, to work out the general pattern of applying the commutator. We will only retain new operators to get the operator sets B_ℓ, which we discussed in the previous chapter. Doing so gives the result

$$B_1: \quad [\bullet\!\!-\!\!\bullet + \bullet, \bullet] = \bullet\!\!-\!\!\bullet + \bullet\!\!-\!\!\bullet, \tag{4.7}$$

$$B_2: \quad [\bullet\!\!-\!\!\bullet + \bullet, B_1] = \bullet + \bullet\!\!-\!\!\bullet + \bullet\!\!-\!\!\bullet + \bullet\!\!-\!\!\bullet\!\!-\!\!\bullet, \tag{4.8}$$

$$B_3: \quad [\bullet\!\!-\!\!\bullet + \bullet, B_2] = \bullet\!\!-\!\!\bullet\!\!-\!\!\bullet + \bullet\!\!-\!\!\bullet\!\!-\!\!\bullet, \tag{4.9}$$

$$B_4: \quad [\bullet\!\!-\!\!\bullet + \bullet, B_3] = \bullet\!\!-\!\!\bullet\!\!-\!\!\bullet + \bullet\!\!-\!\!\bullet\!\!-\!\!\bullet\!\!-\!\!\bullet, \tag{4.10}$$

$$B_5: \quad [\bullet\!\!-\!\!\bullet + \bullet, B_4] = \bullet\!\!-\!\!\bullet\!\!-\!\!\bullet\!\!-\!\!\bullet + \bullet\!\!-\!\!\bullet\!\!-\!\!\bullet\!\!-\!\!\bullet, \tag{4.11}$$

$$B_6: \quad [\bullet\!\!-\!\!\bullet + \bullet, B_5] = \bullet\!\!-\!\!\bullet\!\!-\!\!\bullet\!\!-\!\!\bullet + \bullet\!\!-\!\!\bullet\!\!-\!\!\bullet\!\!-\!\!\bullet\!\!-\!\!\bullet, \tag{4.12}$$

$$B_7: \quad [\bullet\!\!-\!\!\bullet + \bullet, B_6] = \bullet\!\!-\!\!\bullet\!\!-\!\!\bullet\!\!-\!\!\bullet\!\!-\!\!\bullet + \bullet\!\!-\!\!\bullet\!\!-\!\!\bullet\!\!-\!\!\bullet\!\!-\!\!\bullet. \tag{4.13}$$

We see that the operators are limited to chains with $\hat{\sigma}^x$ operators in the bulk, indicated by the blue dots, and either $\hat{\sigma}^y$ or $\hat{\sigma}^z$ on the ends, indicated by the green or red dots. The operators that appear at odd number of nested commutations that give the diabatic terms, have a $\hat{\sigma}^y$ at one end and $\hat{\sigma}^z$ at the other, that are equivalent under the reflection symmetry.

Using this result, means the AGP can be represented as

$$\hat{\mathcal{A}} = \sum_{k=1}^{N-1} \alpha_k \hat{O}_k, \tag{4.14}$$

$$\hat{O}_k = \sum_{i}^{N} \left(\hat{\sigma}_i^y \hat{\sigma}_{i+1}^x \dots \hat{\sigma}_{i+k-1}^x \hat{\sigma}_{i+k}^z + \hat{\sigma}_i^z \hat{\sigma}_{i+1}^x \dots \hat{\sigma}_{i+k-1}^x \hat{\sigma}_{i+k}^y \right). \tag{4.15}$$

For an explicit example of what these operators look like, for $N = 3$ we can write out $\hat{O}_k$ as

$$\hat{O}_1 = \hat{\sigma}_1^y \hat{\sigma}_2^z + \hat{\sigma}_1^z \hat{\sigma}_2^y + \hat{\sigma}_2^y \hat{\sigma}_3^z + \hat{\sigma}_2^z \hat{\sigma}_3^y + \hat{\sigma}_3^y \hat{\sigma}_1^z + \hat{\sigma}_3^z \hat{\sigma}_1^y, \tag{4.16}$$

$$\hat{O}_2 = \hat{\sigma}_1^y \hat{\sigma}_2^x \hat{\sigma}_3^z + \hat{\sigma}_1^z \hat{\sigma}_2^x \hat{\sigma}_3^y + \hat{\sigma}_2^y \hat{\sigma}_3^x \hat{\sigma}_1^z + \hat{\sigma}_2^z \hat{\sigma}_3^x \hat{\sigma}_1^y + \hat{\sigma}_3^y \hat{\sigma}_1^x \hat{\sigma}_2^z + \hat{\sigma}_3^z \hat{\sigma}_1^x \hat{\sigma}_2^y. \tag{4.17}$$

As each value of k has a single operator $\hat{O}_k$, and there are $N - 1$ values of k, we

can state that the number of diabatic terms in the Ring graph is exactly

$$N_{\mathcal{A}}^{\text{ring}} = N - 1. \tag{4.18}$$

This is clearly a signifiant reduction from the exponential scaling of the worst case, and in fact we believe this to be the lower bound for the Ising model, as seen in Fig. 4.2.

With the simplicity of the Ring graph so far, it may not come as a surprise that the values of α_k has a closed-form analytical solution

$$\alpha_k = \frac{\lambda^{k-1}}{8} \frac{\lambda^{2(N-k)} - 1}{\lambda^{2N} - 1}. \tag{4.19}$$

For the derivation of this result please refer to App. A.5.

Due to the closed form solution, we can study the thermodynamic limit of this result taking $N \to \infty$, and explore the phase transition. Applying the limit we find

$$\lim_{N\to\infty} \alpha_k = \begin{cases} (-1)^k \frac{\lambda^{k-1}}{8}, & 0 \leq \lambda \leq 1 \\ (-1)^k \frac{\lambda^{-k-1}}{8}, & \lambda > 1 \end{cases}. \tag{4.20}$$

These values are displayed in Fig. 4.3(a), where we see the split between operators of an odd or even length leading to positive or negative values respectively. Additionally we see that the magnitude of the values drop as the length ($l = k + 1$) increases, showing the lesser importance of many body terms on the diabatic effects. However at the critical point all the coefficients share the same magnitude of $|\alpha_k(\lambda_c)| = \frac{1}{8}$, showing how all operators instantaneously become relevant as the length scales at the critical point change.

We can then use this to also compute the norm of the AGP, which should diverge with a critical exponent at the critical point due to the discontinuous change in the ground state. We find the value to be

$$\lim_{N\to\infty} \frac{||\hat{\mathcal{A}}_\lambda||^2}{N} = \begin{cases} \frac{1}{32} \frac{1}{1-\lambda^2}, & 0 \leq \lambda \leq 1 \\ \frac{1}{32\lambda^2} \frac{1}{\lambda^2-1}, & \lambda > 1 \end{cases}. \tag{4.21}$$

Defining δ_λ as the difference to the critical point, we get:

$$\delta_\lambda = \lambda - \lambda_c \tag{4.22}$$

$$\lim_{\delta_\lambda \to 0} \frac{||\hat{\mathcal{A}}_\lambda||^2}{N} = \frac{1}{64}\frac{1}{|\delta_\lambda|}. \tag{4.23}$$

In Fig. 4.3(d) we show the divergence of the norm around the critical point at $\lambda = J$. Additionally we see how the values are non-zero for all values of $\lambda < J$, whereas the values asymptotically reach zero for large values of λ. As such on the small scales there are large diabatic effects that take place, however once λ is far greater than the energy scale of J, the Hamiltonian is effectively just N separate spin-1/2 particles in a magnetic field, leading to no diabatic effects.

4.1.3 The Chain graph

The next case we shall look at is the Chain graph, which is similar to the Ring graph, but without the periodic boundary conditions that couple together the sites labelled $(1, N)$. This greatly reduces symmetry of the graph to just a single reflection symmetry around the centre point of the chain. Thankfully the argument of the form of the terms in the Ring graph applies also to the chain graph as it only depends on the 1D nature of the problem. This means we need to count the number of operators of the form of each individual operator in Eq. (4.15), that exist on the chain of length N. There are exactly $N + 1 - l$ operators of size l leading to scaling of the form

$$N_{\mathcal{A}}^{chain} = \frac{N}{2}(N-1). \tag{4.24}$$

Note that the factor of two from the symmetry cancels out with the two types of operators possible ($\hat{\sigma}_i^y \hat{\sigma}_{i+1}^x \dots \hat{\sigma}_{i+k-1}^x \hat{\sigma}_{i+k}^z$ and $\hat{\sigma}_i^z \hat{\sigma}_{i+1}^x \dots \hat{\sigma}_{i+k-1}^x \hat{\sigma}_{i+k}^y$).

There is no closed form solution to the computation of α_k in the Chain graph, however we can efficiently compute this numerically allowing large sizes of N. Results of these calculations are shown in Fig. 4.3(b) for $N = 100$. Similar to the Ring graph, the coefficients flip sign dependent on odd/even length of operator, however operators of

a given size l have a splitting between there values. There is another peak in the values near to where the critical point would be in the infinite limit, however the derivative at this peak is not discontinuous as would be expected in an infinite limit. This is further shown in Fig. 4.3(e) which shows the norm of the AGP, which does appear to diverge near the critical point. The result is very similar to the result of the Ring graph as may be expected.

One interesting result can be shown if we limit the allowed sites of the diabatic operators to near the centre of the chain. This means we discard any operator which is not the identity outside of a defined central region. We show this for the middle 10 sites of a $N = 100$ long chain in Fig. 4.3(c). This result now looks much closer to the Ring graph, which is to be expected as near the centre of the chain, operators have very little influence from the edges. As such we can see this in the infinite limit as the local operators not being able to tell the difference between the periodic and non periodic boundary conditions. Whilst we would expect the results between the Chain and Ring graphs to be different, we can see that for the bulk of the graphs, there is no effective difference once N is large enough.

4.1.4 The Complete graph

Another graph type that is of interest is the Complete graph, which is more commonly referred to as an all-to-all model. This graph consists of all possible connection between sites, such that each site and edge is equivalent to every other site and edge respectively. This large degree of symmetry, in fact, allows a description in terms of disjoint collective spin operators. Notably the ground state of the model lies within the $\frac{N}{2}$ total spin sector, so often this model is simplified to just being a single large spin, which transforms the Ising all-to-all model to a Lipkin-Meshkov-Glick (LMG) model [126]. The LMG model possesses a ground state phase transition, and as such shows the Ising all-to-all model also posses the same phase transition. Whilst it is sufficient to describe the Hamiltonian in this collective spin model, this mapping breaks down if the symmetry of the graph is broken at all. This leads us to want a full description of model in terms of the spin-1/2 operators as well, to allow for the possibility of changing the strength of

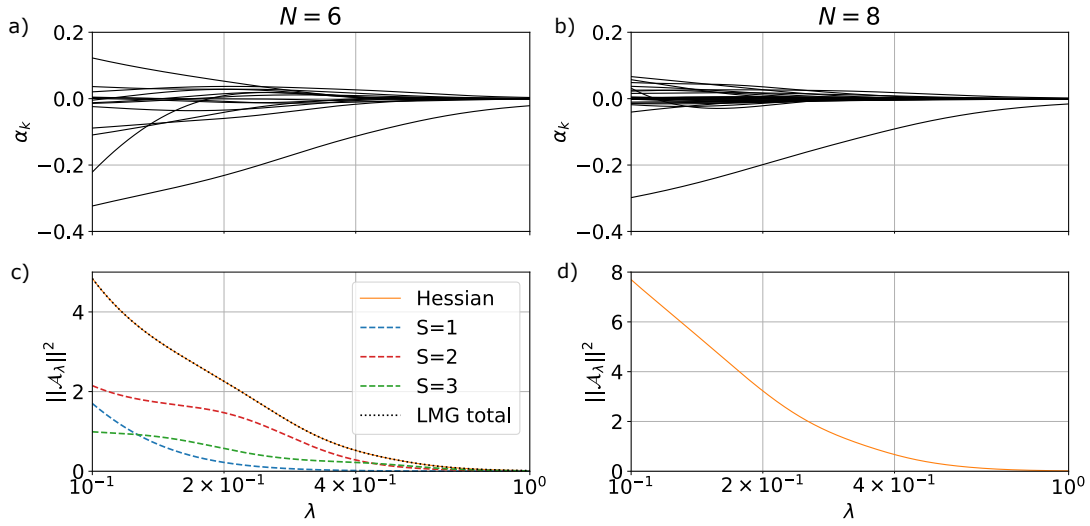

Figure 4.4: Coefficients of the different operators in the AGP for the complete graph for a) $N = 6$ and b) $N = 8$. The dominant operator in both cases is $\hat{\sigma}^y\hat{\sigma}^z$. Panel c) shows the AGP norm for $N = 6$ graph. Along with this are the norms obtained for relevant LMG models as described in the main text. Panel d) gives the AGP norm for the $N = 8$ graph.

specific connections. We shall as such show the calculation in terms of both collective spin and spin-1/2 operators.

The collective spin hamiltonian is given by

$$\hat{H}_{\text{complete}} = \sum_{s}^{N/2} C_s^N \hat{H}^s_{\text{LMG}}, \tag{4.25}$$

where the spin s takes positive integer or half integer values for each of the disjoint spin sectors, and the multiplicity C_s^N is the number of ways ti arrange N spin-1/2 particles to get a total spin s. The individual LMG Hamiltonians are given by

$$\hat{H}^s_{\text{LMG}} = \frac{J}{N}\left(\hat{S}^z_s\right)^2 + \lambda \hat{S}^x_s, \tag{4.26}$$

where we note a factor of $\frac{1}{N}$ has been added to ensure the critical point of the ground state transition is not dependent on N. As the collective spin model is mainly for comparison in this section, we limit the computing of the AGP to using diagonalization to compute the matrix elements given in Eq. (2.34).

Focusing now again on the spin-1/2 representation, we can figure out the number of diabatic operators required for an exact AGP. As the Complete graph has all possible connections, we can expect that the Lie algebra is not restricted in the way we saw for the 1D models and in fact should consist of all possible operators (excluding the identity operator, as this always has a commutator of zero). Whilst this may seem catastrophic for the scaling at first glance, the symmetry in the graph means that the position of different spin operators does not matter, only the total number. We know that the base restriction is the number of $\hat{\sigma}^y$ and $\hat{\sigma}^z$ operators must be both odd, but there is no restriction on $\hat{\sigma}^x$ and $\hat{\mathbb{I}}$ other than the overall total operators must be equal to N. So we can express this as

$$N_{\mathcal{A}}^{\text{complete}} = \sum_{n_y}^{N} \sum_{n_z}^{N-n_y} (N + 1 - n_y - n_z) \tag{4.27}$$

This expression can then be simplified to

$$N_{\mathcal{A}}^{\text{complete}} = \begin{cases} \frac{N}{2}(\frac{N}{2}+1)\left(\frac{N+1}{2} - \frac{N+1}{3}\right), & N\text{even} \\ \frac{N-1}{2}\frac{N+1}{2}\left(\frac{N+1}{2} - \frac{N}{3}\right), & N\text{odd} \end{cases}. \tag{4.28}$$

where we see a different scaling between odd and even values of N. This can be best explained by thinking in terms of the collective spin operators. When N is even the collective spin takes integer values, giving bosonic particles, whereas when N is odd the collective spin instead get half integer values, giving fermionic particles. This difference in the nature between the two types of particles changes how the counting statistics works, leading to different forms of the expression but the general scaling is still cubic. For an alternate explanation from a more mathematical point of view, note that number of odd integer values between 1 and N is given by floor $\frac{N+1}{2}$, meaning the sum in Eq. (4.27) only gets more terms every other increase in N, however the value of the summand still increases. This difference in scaling means when comparing between different N values, we should stick to either even or odd values.

Using the OCE to numerically solve the Complete graph and numerical diagonal-

ization for the LMG model, we plot these results in Fig. 4.4. The α_k values here are non coloured as it is difficult to distinguish between different lines with so many terms, however we note the major contribution comes from the $\hat{\sigma}^y\hat{\sigma}^z$ operator for both $N = 6$ and $N = 8$. This seems to indicate that, even in this highly non-local model, the two body operator is still the most important term. In Fig. 4.4(c) we compare the AGP norm values between the different representations, where the results for the different spin sector include the multiplicity factor C_s^N, meaning the total is equal to the complete graph as expected.

An interesting feature of these results, is in contrast to what we saw for the Chain and Ring graphs, the critical point in the ground state of the LMG model (which occurs at $\lambda = \frac{1}{2}$) does not appear as a peak in the AGP norm for the Complete graph. Now these are very small models studied here, so we do not expect a strong indication of the phase transition, but we would expect the first signs of a divergence appearing. This effect is coming from a washing out of the higher spin LMG models from the large multiplicity of the smaller spin sectors. Each of the individual LMG models has a divergence appearing at their respected critical points S/N, but for small N the multiplicity C_s^N grows faster than the divergence. As such the AGP norm is dominated by contributions from $S = 1$ and $S = 2$ sectors, which have peaks around zero, that skew the peak of the overall norm. The phase transition does still occur in the ground state, but observing this divergence in the results for the full Complete graph is far more difficult.

4.1.5 Example of an Asymmetric graph

In the previous three subsections we have looked at the classes of graph that have desirable properties such as high symmetry or suppression of terms from the 1D nature. We now turn our attention to the most difficult problems to solve, where we have zero graph symmetries and there are no suppression of terms occurring, meaning the maximum number of diabatic operators are present. This describes a subset of the Asymmetric graphs, as some Asymmetric can still suppress terms due to 1D like geometry. One particular graph that fits into this subset is shown in Fig. 4.2(a), where

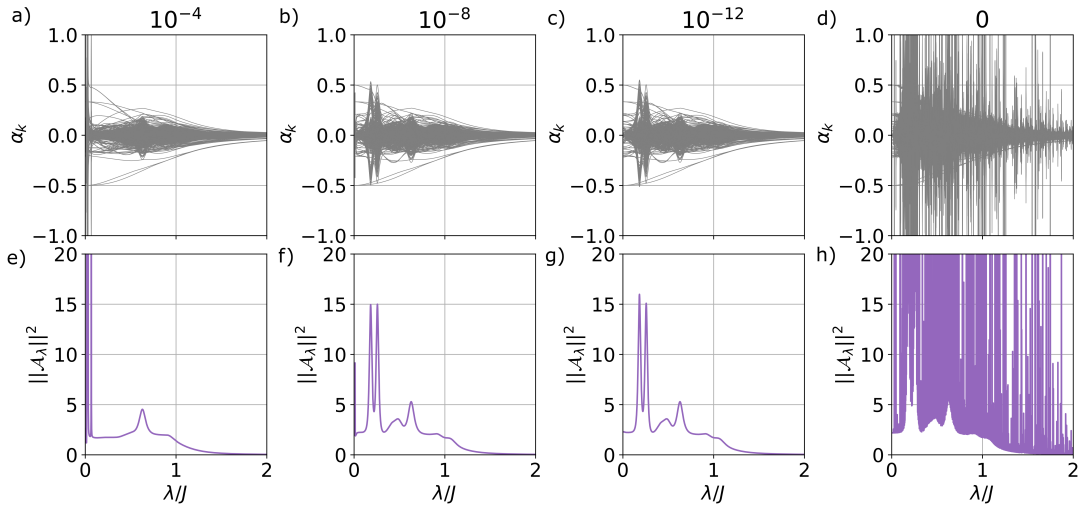

Figure 4.5: Coefficients, α_k, a)–d) and AGP norm e)–h) obtained for the asymmetric graph (as illustrated in Fig. 4.2(a)). Each column represents a different threshold value for removing entries from the Hessian matrix. The values for these thresholds are indicated at the top of each column.

there is one extra connection added to a $N = 6$ Chain graph. This graph has 992 individual diabatic operators to optimise over, making it difficult to solve but still very feasible if the matrix equation can be found.

We use OCE to automatically solve this problem the same as with any of the other graphs, which removes any of the major complexity of the problem. However we must be careful with the numerical implementation as the solution to the matrix equation is extremely sensitive to floating point error. In Fig. 4.5 we show the results for both the α_k values and the AGP norm, for different threshold values, where all matrix elements below this relative threshold are set to zero. We see that if the threshold is too large at 10^{-4} we miss some of the features present at smaller threshold values and have an instability near zero. On the opposite end, if we have no threshold at all, the results are widley unstable varying in orders of magnitude, but only increase the value of the norm and never decreases compared to larger thresholds. The general shape of the curves is then reasonably similar for thresholds 10^{-8} and 10^{-12}, indicating this is a good approximation for the true result of the calculation. Further in depth numerical study can be done to figure out how to converge the result towards the true values.

Whilst these results appear to show an extremely unstable solution to the diabatic terms for this Asymmetric graph, the fidelity of following the ground state seems to indicate otherwise. We find that for all the threshold values shown, the groundstate fidelity achieved during simulation to be approximately $1-10^{-5}$ for $\dot{\lambda}=10$. This shows that whilst the AGP norm and the α_k values are very sensitive to numerical errors, the adiabatic following of the ground state is rather robust. This is likely due to the ground state not being influenced by the operators that are numerically unstable.

It is important to emphasise again that this asymmetric graph is only one connection away from the chain graph, but exhibits widely different behaviour. If we however scale up this Asymmetric graph by continually adding one site on either end of the graph, we can preserve the asymmetric nature of the graph, whilst decreasing the influence of the extra connection. We as such, expect the chain graph to be a good approximation for large N. This approximation of changing a single connection of the graph we believe is an incredibly interesting area for further study, to see if this can be used to approximate more difficult graph geometries.

With this result, we conclude our study on the Ising model on different graph geometries. We have shown how within the same family of Hamiltonians, different associated graphs lead to vastly different computational complexity computing the AGP. For the simplest case of the Ring graph, we computed the AGP in thermodynamic limit, allowing us to find the critical exponent of the AGP at the phase transition. In the other one dimensional model, the Chain graph, we found quadratic scaling to the number of coefficients of the AGP, allowing large but still finite computations. The Complete graph provided a rather unexpected result, as the norm of the AGP did not clearly show the presence of the groundstate phase transition, highlighting the difference between the LMG model and the Complete graph (all-to-all model). Finally we look at a small N example of the worst scaling graph type, the asymmetric graphs, where extra care was needed to be taken to ensure numerical stability for measure of the AGP, but the counter diabatic behaviour was more resilient to numerical errors. As such, the Ising model has provided a wide range of interesting results, but we now wish to look at a different type of spin model, to further expand our understanding of

the AGP.

4.2 Exploring the AGP in the XXZ model

The majority of our spin studies have involved the Ising graph Hamiltonian shown in the previous section, however we wish to push to other Hamiltonians. By doing so, we explore the limitations of the OCE method and begin to identify which features are general to all spin models and which are specific to the Ising model. One model which is of particular interest is the XXZ model, which consists of $\hat{\sigma}^x \otimes \hat{\sigma}^x$, $\hat{\sigma}^y \otimes \hat{\sigma}^y$ and $\hat{\sigma}^z \otimes \hat{\sigma}^z$ operators connecting sites, with the magnitude of the x and y directions being equal [127, 128]. This model provides a simple description of magnetisation, from the spins aligning in the z direction, when the z connection is strong enough [129, 130]. There are also many other properties/features of interest in the XXZ model such as: ballistic spin transport [131], the existence of long range order [132], or entanglement in the ground state [133].

The general XXZ model is described by the Hamiltonian [128]

$$\hat{H}_{XXZ} = -J \sum_{(i,j)} \left(\hat{S}_i^x \hat{S}_j^x + \hat{S}_i^y \hat{S}_j^y + \Delta \hat{S}_i^z \hat{S}_j^z \right), \tag{4.29}$$

where $\hat{S}_i^x$, $\hat{S}_i^y$, $\hat{S}_i^z$ are the spin operators for a spin of size s, (i,j) are all the connections between sites which are defined by an associated graph, J is a constant positive energy scale ($J > 0$), and Δ varies the model between ferromagnetic ($\Delta > 0$) and anti-ferromagnetic ($\Delta < 0$). There are two key models which are limiting cases of the above Hamiltonian: the XX model ($\Delta = 0$) [134], and the Heisenberg model ($\Delta = 1$) [135]. Depending on the size of the spin operators, the nature of the model varies. For example, a spin-1/2 ring, there is an spontaneous symmetry breaking at $\Delta = 1$, where the system is gapped for $\Delta > 1$ and has a degenerate ground state for $\Delta < 1$ [136]. There exists a similar transition for spin-1 particles, however there is an extra phase that appears, and in fact a triple point that occurs [137]. In the following subsections we will look at both the spin-1/2 and spin-1 cases, exploring what are the lower and upper bounds on the number of coefficients for the AGP, and how these vary when

adding extra operators beyond the XXZ model.

4.2.1 Computing the AGP in the all-to-all spin-1/2 XXZ model

The spin-1/2 XXZ model is the simplest of these family of models, but what graph gives the best scaling for the AGP? We can use our knowledge gained from the Ising model, to make a naive guess that the Ring is also the simplest model. However there is a trivial graph that has zero diabatic affects for the spin-1/2 XXZ model, the complete graph. The simplest way of showing this is to look at a collective spin picture of the model.

Similar to the Ising model, we have a set of disjoint collective spin Hamiltonians, however in this case they are of the form

$$\hat{H}^{(s)} = -J\left(\hat{S}^2 - \left(\hat{S}^z\right)^2 + \Delta\left(\hat{S}^z\right)^2\right), \tag{4.30}$$

where the total spin operator $\hat{S}$ is given by $\hat{S}^2 = \left(\hat{S}^x\right)^2 + \left(\hat{S}^y\right)^2 + \left(\hat{S}^z\right)^2$As the value J only determines the energy scale, it will not affect the diabatic dynamics of the model, unless the sign changes, so we shall take the value as being constant. On the other hand, Δ will cause diabatic excitation in the XXZ model in general, with it being the control parameter for a ground state phase transition in certain geometries. For this reason, we choose to vary Δ and find the AGP associated with this.

We can find that the commutator of $\hat{H}^{(s)}$ with the partial derivate with respect to Δ, is equal to zero

$$\left[\hat{H}^{(s)}, \partial_\Delta \hat{H}^{(s)}\right] = \left[-J\left(\hat{S}^2 - \left(\hat{S}^z\right)^2 + \Delta\left(\hat{S}^z\right)^2\right), -J\left(\hat{S}^z\right)^2\right] = 0, \tag{4.31}$$

as $\left[\hat{S}^2, \hat{S}^z\right] = 0$. This means that the dynamical Lie algebra is the empty set, and as such there are no diabatic operators. This can also be seen from the fact the Hamiltonian is already diagonal, and as such no diabatic excitations are expected to occurs.

Another approach to this is to compute the same quantity in the Pauli basis. The

commutator now looks like

$$\sum_{i,j,l,k} \left(\left[\hat{\sigma}_i^x \hat{\sigma}_j^x, \hat{\sigma}_l^z \hat{\sigma}_k^z \right] + \left[\hat{\sigma}_i^y \hat{\sigma}_j^y, \hat{\sigma}_l^z \hat{\sigma}_k^z \right] \right). \tag{4.32}$$

The commutations are zero if $i = l$ and $j = k$ or $i = k$ and $j = l$, so we need only one pair to be the same, and the others remain free. So we combine one index ($j = l$), and write

$$\sum_{i,j,k} \left(\left[\hat{\sigma}_i^x \hat{\sigma}_j^x, \hat{\sigma}_j^z \hat{\sigma}_k^z \right] + \left[\hat{\sigma}_i^y \hat{\sigma}_j^y, \hat{\sigma}_j^z \hat{\sigma}_k^z \right] \right). \tag{4.33}$$

We can then also swap the indexes around in the second term (as all index combinations occur from all-to-all coupling) to get

$$\sum_{i,j,j,k} \left(\left[\hat{\sigma}_i^x \hat{\sigma}_j^x, \hat{\sigma}_j^z \hat{\sigma}_k^z \right] + \left[\hat{\sigma}_j^y \hat{\sigma}_i^y, \hat{\sigma}_i^z \hat{\sigma}_k^z \right] \right). \tag{4.34}$$

Computing the commutators then leaves us with

$$\sum_{i,j,j,k} \left(-\hat{\sigma}_i^x \hat{\sigma}_j^y \hat{\sigma}_k^z + \hat{\sigma}_j^y \hat{\sigma}_i^x \hat{\sigma}_k^z \right) = 0. \tag{4.35}$$

As such this result also agrees that there are no diabatic terms for the spin-1/2 complete graph. Note that for larger spins this proof does not work, as $\left[\hat{S}^x \otimes \hat{S}^x, \hat{S}^z \otimes \hat{S}^z \right]$ and $\left[\hat{S}^y \otimes \hat{S}^y, \hat{S}^z \otimes \hat{S}^z \right]$ are not always zero, and spin-1/2 is a special case.

4.2.2 Scaling of the AGP in the spin-1/2 XXZ model

As we have just seen the best graph for the XXZ model is in fact the Complete graph rather than the Ring graph. So the question arises, what is the scaling of the number of coefficients needed for the AGP in the spin-1/2 XXZ on the Ring graph? We do not strive to derive an analytical expression in this case, but instead look at this purely numerically. Previously with the Ising model, we studied how many counter diabatic operators are needed to represent the exact AGP over all different graphs, and we can repeat this for the XXZ model.

We previously found a maximum in the Ising model that took into account the

symmetries of the model, notably being a real Hamiltonian and having parity symmetry from spin flips, given in Eq. (4.4). We will now additionally note the different upper scaling limit of the number of coefficients of the AGP for a real Hamiltonian without any symmetry, is given by

$$\mathcal{N}_{\text{limit}}^{\text{real}}(N) = (2^{N-1})(2^N - 1), \tag{4.36}$$

for N sites (see App A.3 for derivation). These two limits of real valued Hamiltonians with and without parity symmetry, will be plotted alongside the Hilbert space dimension on all the following plots, to provide a upper limit on the number of coefficients.

The upper left plots in Fig. 4.6 shows the number of operators required to represent the AGP for the base XXZ model. We note that due to the y axis being a log scale, the complete graph does not show due to being zero for all N. Somewhat surprisingly, the XXZ model has better overall scaling compared to the Ising model, with it not reaching the real parity limit the Ising model did. This is explained by the XXZ model having a $U(1)$ symmetry which is stronger than the parity symmetry, leading to further suppression of the number of coefficients. However the results for the Ring and Chain graphs are significantly worse than in the Ising model, showing how if limited to one dimensional models, the XXZ model is far more complicated to apply counter diabatic pulses.

We wish to explore the family of closely related models to the XXZ, to see how breaking different symmetries affects the overall scaling of the graphs. To do so we look at adding one body operators to every site, which will not affect the graph symmetries, but these terms can break the $U(1)$ symmetry and the assumption of a real Hamiltonian. As all directions in the x-y plane are equivalent, we distinguish operators by being parallel or perpendicular to this plane. The perpendicular direction is $\hat{\sigma}^z$ for this setup, however the exact choice of operators parallel to the plane is not directly important, as long as they are orthogonal to each other, so we choose to first add an $\hat{\sigma}^x$ then a $\hat{\sigma}^y$. We note each of these fields are independent and can vary like any other operators we

have treated before, giving an overall Hamiltonian that looks like

$$H_{XXZ}^{\text{extended}} = -J\sum_{(i,j)}\left(\hat{\sigma}_i^x\hat{\sigma}_j^x + \hat{\sigma}_i^y\hat{\sigma}_j^y + \Delta(\lambda)\hat{\sigma}_i^z\hat{\sigma}_j^z\right) + \gamma_x(\lambda)\sum_i \hat{\sigma}_i^x + \gamma_y(\lambda)\sum_i \hat{\sigma}_i^y + \gamma_z(\lambda)\sum_i \hat{\sigma}_i^z. \tag{4.37}$$

Returning to Fig. 4.6, the rows and columns vary which single body operators are included, with rows changing perpendicular operators ($\hat{\sigma}^z$) and columns changing parallel operators ($\hat{\sigma}^x$, $\hat{\sigma}^y$). We see that for all the operators added, we can even reach what appears to be the Hilbert space dimension, although it is limited to at most 4^N-1 as $\hat{\mathbb{I}}$ never has any affect on the diabatic dynamics. There is similarity between scaling when the number of fields added is equal. For example looking at the bottom left plot ($\hat{\sigma}^z$) and the top middle plot ($\hat{\sigma}^x$) which both have one term added, the maximum points appear roughly the same. However specific graph types are affected by the operator being perpendicular or parallel, notably the complete graph which when the plane symmetry is broken by $\hat{\sigma}^x$ its AGP is no longer zero valued, unlike when adding $\hat{\sigma}^z$ as it is diagonal and commutes with the operators.

To help illustrate this point further, we observe how the three different special graphs we have pointed out before, namely the Ring, Chain and Complete graphs, vary with the different operators added. Some of the lines are the same across the different plots, showing how certain operators do not affect the scaling at all, for example the complete graph adding $\hat{\sigma}^z$ keeps the zero AGP (seen in the two plots on the left). On the other hand, some graphs vary massively, with the Chain and Ring graphs having five distinct scaling lines. We note that the Complete graph is the lower bound of all the Hamiltonians in each case (at least up to $N = 10$), indicating that the Ring graph being the lower bound for the Ising model may be a special case. This could be interpreted that more generally we may expect the Complete graph to be the best case graph in other Hamiltonian types.

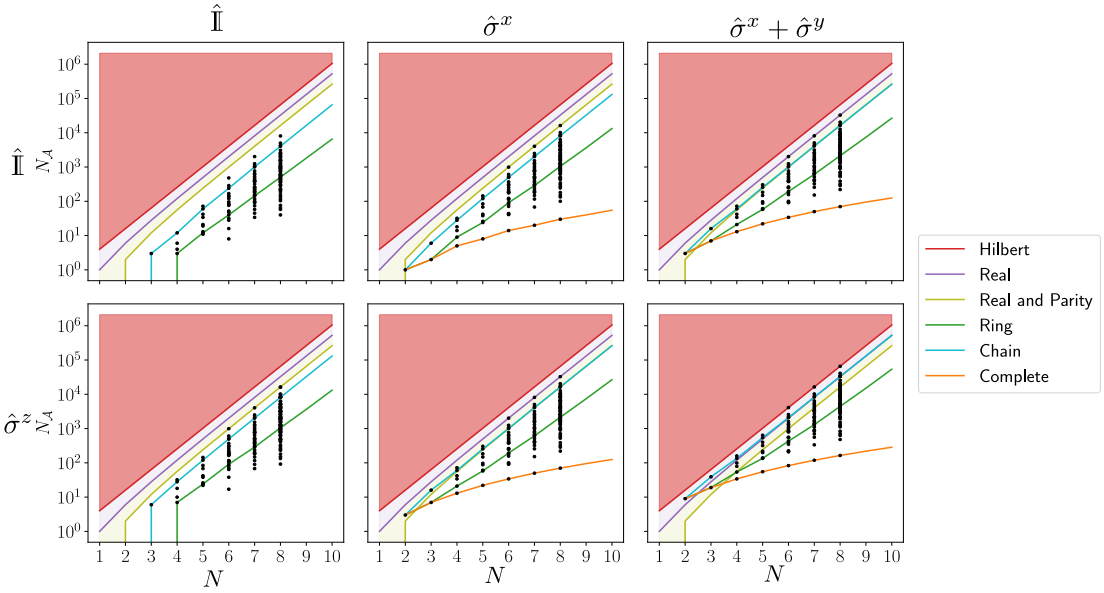

Figure 4.6: Plot showing the scaling of number of AGP terms for the spin-1/2 XXZ model. The different rows and columns have different extra one body operators additionally added. The first row has no perpendicular (to the XY plane) field added and second row adds a $\hat{\sigma}^z$ field. Similarly the first column has no parallel (to the XY plane) field added, the second column has a $\hat{\sigma}^x$ field added, and the third column has both $\hat{\sigma}^x$ and $\hat{\sigma}^y$ fields added. All the extra fields have independent magnitudes, and as such break up the different symmetries of the model leading to worse scaling as more fields are added.

4.2.3 Exploring the AGP in the spin-1 XXZ model

Now we look at the spin-1 XXZ model, and as such we are required to use a different basis than the Pauli basis. For spin-1 we can use the Gell-Mann matrices, which are described in Sec 3.4 alongside the forms of the spin operators. Using this information, we can write the model (with $\hbar = 1$) as

$$\hat{H}_{XXZ} = -J \sum_{j}^{N} \left(\frac{1}{2} \left(\hat{\lambda}_j^1 + \hat{\lambda}_j^6 \right) \left(\hat{\lambda}_{j+1}^1 + \hat{\lambda}_{j+1}^6 \right) + \frac{1}{2} \left(\hat{\lambda}_j^2 + \hat{\lambda}_j^7 \right) \left(\hat{\lambda}_{j+1}^2 + \hat{\lambda}_{j+1}^7 \right) + \Delta \left(\hat{\lambda}_j^3 + \sqrt{3} \hat{\lambda}_j^8 \right) \left(\hat{\lambda}_{j+1}^3 + \sqrt{3} \hat{\lambda}_{j+1}^8 \right) \right). \tag{4.38}$$

We setup the OCE using a array of numbers from 0 to 8 representing the Gell-Mann matrix on each site. As the Hamiltonian is only made of two body operations, we can define our commutation dictionary as being applied to a tuple of values. We can then

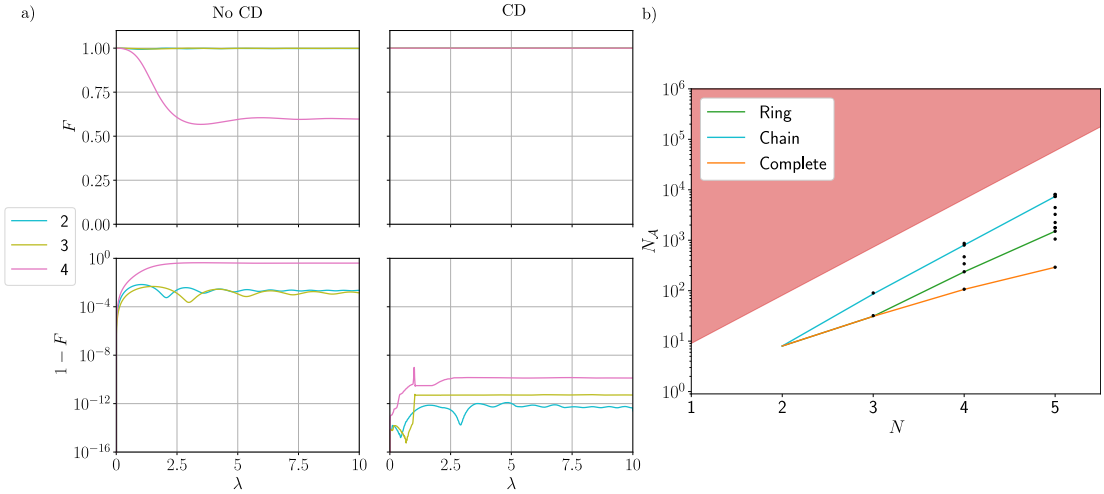

Figure 4.7: Panel a) shows plots of the following of the ground state with and without a counter diabatic pulse being applied, for a chain of spin one particles with XXZ connections. We see that like for the Ising model spin-1/2, we can achieve perfect ground state following, up to numerical errors. In panel b) we show scaling of the spin-1 XXZ model with all non isomorphic graphs. We see similar to results to the spin-1/2 case, with the chain being near the worst and the complete being the best case. We are far more limited in the number size we can achieve due to the increase in the number of operators spin-1 Hilbert spaces contain.

use this implementation to automate everything from this step onwards. However due to the scaling of the operator space dimension of this problem 9^N, it is already rather difficult to compute even small sized graphs. As such, outside of special cases where the symmetry of specific graphs reduces the scaling, computing the result in general for large N is unfeasible.

In Fig. 4.7-a we show the results of computing the AGP for a chain graph. As expected, when applying the AGP to the Hamiltonian to get a counter diabatic Hamiltonian, we follow the ground state of the system up to a numerical error on the order of 10^{-12} which scales with system size. We see that this gets worse as the dimension gets larger, leading to larger numerical errors. When looking at all the graphs, we are much more limited in how large we can go due to the 9^N Hilbert space scaling for spin-1. As such in Fig. 4.7-b we only show the results for up to $N = 5$, again highlighting the three special case graphs. We see the same similar pattern to the spin-1/2 results, except the complete graph having a non zero AGP. Again the chain is near the worst

possible graph for such a Hamiltonian.

With this result, we reach the end of the section and the chapter on spin models. We have shown that even in relatively simple models like the Ising and XXZ models, the AGP is a computationally difficult quantity to calculate outside of specific high symmetry graphs. The scaling of the number of coefficients varies widely amongst different graphs, with almost the full Hilbert space dimension begin reached in the worst cases. Now that the AGP has been computed in these spin models, it can be used to gain insight into the dynamics, and how to optimise adiabatic pulse sequences to reduce losses in these models.

Chapter 5

The AGP in bosonic models

In the previous chapter we have explored multiple spin models, and seen how the AGP can be used to improve control procedures and understanding of the systems in question. Now we wish to broaden our scope of models, to also describe bosonic physics which have many applications in areas such as quantum optics [4] and ultra-cold gases [138]. In addition to purely bosonic models, in many experiments it is very difficult to fully separate the system from its environment, which are often modelled as bosonic in nature [79]. We leave the discussion of open systems to the next chapter, where we discuss hybrid models, however it is important to note the main motivation of this chapter is to build the perquisite understanding of bosonic models required to compute the AGP in hybrid models.

For these reasons we shall study bosonic models, starting with describing the main differences of bosonic AGP physics compared to spin. The large majority of research for the AGP is focused on spin (especially spin-1/2), so this is not a particularly developed field in terms of the AGP. That being said, we will link back to some counter-diabatic results where possible, however many of the questions raised in this section are still active areas of research. Once we have a rough description of bosonic AGP physics, we shall look at the simplest non-trivial model, the harmonic oscillator. We will then expand this model to an exact description of quadratic bosonic models, providing a near closed form solution. This will then give the ground work on bosonic models to be used for the hybrid systems described in the next chapter.

5.1 Comparing bosonic and spin AGPs

As may be expected, there are differences between computing the AGP for spin and bosonic models. To be able to compute a bosonic AGP it is important to take two key factors into account: the creation and annihilation operators are non-stationary, and the Hilbert space is always infinite. Without carefully taking into account these differences, it is easy to make mistakes when computing the AGP, so we shall briefly outline these in the next two subsections. We shall then follow this with an example of a simple bosonic mode with the addition of a positional driving.

5.1.1 Non-stationary basis vectors

The first difference we shall discus, is how the creation and annihilation operators are non-stationary, specifically with respect to the boson frequency ω. As these operators are not independent of ω, when computing the AGP for varying ω we need to take this dependence into the partial derivative.

To work out the dependence for $\hat{a}$, we can write it in the canonical co-ordinates position ($\hat{x}$) and momentum ($\hat{p}$), which are stationary with respect to ω. This gives

$$\begin{aligned}\partial_\omega \hat{a} &= \partial_\omega \left(\sqrt{\frac{m\omega}{2\hbar}} \left(\hat{x} + \frac{i}{m\omega}\hat{p} \right) \right) \\ &= \frac{1}{2}\sqrt{\frac{m}{2\hbar\omega}} \left(\hat{x} - \frac{i}{m\omega}\hat{p} \right) \\ &= \frac{1}{2\omega}\hat{a}^\dagger, \end{aligned} \tag{5.1}$$

where m is the mass. Similarly this can be computed for $\hat{a}^\dagger$, where we find the result as expected is the Hermitian conjugate of the expression in Eq. (5.1), $\partial_\omega \hat{a}^\dagger = \frac{1}{2\omega}\hat{a}$.

In addition to this extra term in the partial derivative, when simulating a bosonic Hamiltonian with varying ω, a stationary basis such as $\hat{x}$ and $\hat{p}$ must be used. This is because the Schrödinger equation implicitly assumes the chosen basis is stationary, so anomalous results will otherwise occur. For example, if you simulate the harmonic oscillator with the Hamiltonian $\omega\hat{a}^\dagger\hat{a}$, you will find the simulation has no diabatic excitation. However when simulated in the $\hat{x}$ and $\hat{p}$ basis, there will be diabatic excitations

that occur [139].

5.1.2 Infinite sized Hilbert space

The other major difference to the spin AGP that we have seen previously, is that the Hilbert space of bosonic operators is infinite in size. This affects two parts of the computation of the AGP: taking the trace, and the effect of commutation. As the trace involves a sum over all diagonal elements in a given basis, for infinite sized operators this can lead to infinite values of the trace. If the number of non-zero diagonal values are finite, and the values themselves are finite, then the trace will also be finite. In fact, even if the number of non-zero diagonal values is infinite, if the infinite sum of these values converges, then the trace will be finite, for example $\frac{1}{\left(\hat{a}^\dagger \hat{a}\right)^2}$. However many operators that appear during the computation do not abide by this, for example $\hat{a}^\dagger \hat{a}$.

To overcome this problem, we first evaluate the trace for a finite number N of Fock states in the truncated bosonic Hilbert space. We can then normalise this partial trace by some factor that converges with respect to N to zero, faster or equally, making the limit $\lim_{N\to\infty}$ of this renormalised trace to be finite. Taking the example of $\mathrm{Tr}\left(\hat{a}^\dagger \hat{a}\right)$ again, we can compute the the trace up to N values being $\sum_{n=1}^{N} n = \frac{N(N+1)}{2}$. This expression scales quadratically with N, so we can normalise the trace by a factor $\frac{1}{N^2}$, such that the result is now $\frac{1}{N^2}\sum_{n=1}^{N} n = \frac{(N+1)}{2N}$, which has a limit $\lim_{N\to\infty} \frac{(N+1)}{2N} = \frac{1}{2}$. As such $\frac{1}{N^2}\mathrm{Tr}\left(\hat{a}^\dagger \hat{a}\right)$ is finite, and can be used to compute the AGP. This step of normalisation leads to extra computations in the calculations, but fundamentally just changes the process of computing the coefficients of the AGP, which can be accounted for.

However, the problem with commutators is much more fundamental, the results for commutation of bosonic operators is only true in the infinite Hilbert space size limit. Lets take the simplest bosonic commutation relation

$$\left[\hat{a}, \hat{a}^\dagger\right] = 1. \tag{5.2}$$

If we instead take any two operators in a finite Hilbert space, we call $\hat{O}^a$ and $\hat{O}^b$, we can

find the trace of their commutator must always be zero. This can be shown by using the fact that the trace is a linear mapping and its cyclic property, giving the result

$$\begin{aligned}\mathrm{Tr}\left(\left[\hat{O}^a,\hat{O}^b\right]\right) &= \mathrm{Tr}\left(\hat{O}^a\hat{O}^b-\hat{O}^b\hat{O}^a\right)\\ &= \mathrm{Tr}\left(\hat{O}^a\hat{O}^b\right)-\mathrm{Tr}\left(\hat{O}^b\hat{O}^a\right)\\ &= \mathrm{Tr}\left(\hat{O}^a\hat{O}^b\right)-\mathrm{Tr}\left(\hat{O}^a\hat{O}^b\right)\\ &= 0. \end{aligned} \tag{5.3}$$

However clearly $\mathrm{Tr}\{1\}\neq 0$, so something is wrong.

The way this commutation is normally derived is to expand the commutator in terms of its operators. By then multiplying the matrices we find

$$\begin{aligned}\left[\hat{a},\hat{a}^\dagger\right] =& \hat{a}\hat{a}^\dagger-\hat{a}^\dagger\hat{a}\\ =& \begin{pmatrix}0&1&0&\dots\\0&0&\sqrt{2}&\dots\\0&0&0&\dots\\\vdots&\vdots&\vdots&\ddots\end{pmatrix}\begin{pmatrix}0&0&0&\dots\\1&0&0&\dots\\0&\sqrt{2}&0&\dots\\\vdots&\vdots&\vdots&\ddots\end{pmatrix}\\ &-\begin{pmatrix}0&0&0&\dots\\1&0&0&\dots\\0&\sqrt{2}&0&\dots\\\vdots&\vdots&\vdots&\ddots\end{pmatrix}\begin{pmatrix}0&1&0&\dots\\0&0&\sqrt{2}&\dots\\0&0&0&\dots\\\vdots&\vdots&\vdots&\ddots\end{pmatrix}\\ =& \begin{pmatrix}1&0&0&\dots\\0&2&0&\dots\\0&0&3&\dots\\\vdots&\vdots&\vdots&\ddots\end{pmatrix}-\begin{pmatrix}0&0&0&\dots\\0&1&0&\dots\\0&0&2&\dots\\\vdots&\vdots&\vdots&\ddots\end{pmatrix}\\ =& \begin{pmatrix}1&0&0&\dots\\0&1&0&\dots\\0&0&1&\dots\\\vdots&\vdots&\vdots&\ddots\end{pmatrix}\end{aligned} \tag{5.4}$$

If these operators are truly infinite then each diagonal entry of $\hat{a}\hat{a}^\dagger$ is exactly one more than $\hat{a}^\dagger\hat{a}$. However if there is a maximum mode N, then the final diagonal entry of $\hat{a}\hat{a}^\dagger$ shall be zero because $\hat{a}^\dagger |N-1\rangle = 0$ as $|N\rangle$ does not exist. This means the final diagonal entry will be $1-N$ from the final diagonal element of $\hat{a}^\dagger - \hat{a}$. In this finite case, we see that now the trace is indeed zero, but the operator is no longer the identity.

This fact about the commutation plays a pivotal role in simulating these systems, as truncating the bosonic mode and treating it as a large spin, makes the Hamiltonian finite. This means diagonalization and other numerical techniques can be used. This approximation is extremely useful for simplifying bosonic physics, and can be well applied if the state of the system stays near to the vacuum state. To help illustrate this and the other complications mentioned in this section, we will now have a look at a simple bosonic model, to show examples of these complications in action.

5.2 Example model: a driven bosonic mode

We now wish to apply the ideas from the previous section into a model to see the complications in practice. This will help further the understanding of computing the AGP for bosonic Hamiltonians, giving example to the ideas we have just laid out. We will use a bosonic mode with the addition of a position based driving, which is given by the Hamiltonian in the Fock basis as

$$\hat{H} = \omega\hat{a}^\dagger\hat{a} + \epsilon\left(\hat{a} + \hat{a}^\dagger\right) \tag{5.5}$$

where ω is the energy gap, ϵ is the strength of the driving. We refer to this as position based driving, as the driving operator is proportional to the position operator $\left(\hat{a} + \hat{a}^\dagger\right) \propto \hat{x}$. As such when $\epsilon \ll \omega$ the ground state is the vacuum state $|0\rangle$, but when $\epsilon \gg \omega$ the ground state is given by the position state $|x = -\infty\rangle = \delta(x + \infty)$. This means the driving localises the ground state towards the negative x direction, and has maximal uncertain for value of momentum p.

5.2.1 The zero driving limit: harmonic oscillator

For the first case, we will take $\epsilon = 0$, such that the Hamiltonian is the same as the harmonic oscillator. As there is only one parameter, we will choose ω to be our control parameter, and compute the AGP with respect to it.

As with all the calculations of the AGP, we start by taking a partial derivate of the Hamiltonian, $\partial_\omega \hat{H}$ in this case. We have discussed how the creation and annihilation operators are not stationary basis, and instead depend on the cavity frequency ω. To illustrate this point, lets follow through with the **false** assumption of $\partial_\omega \hat{a} = 0$, and see if the calculation works. If $\partial_\omega \hat{a} = 0$ is true then $\partial_\omega \hat{H} = \hat{a}^\dagger \hat{a}$, and $[\hat{H}, \partial_\omega \hat{H}] = 0$. This instantly leads to the AGP being zero, which can be seen from Eq. (2.65), however the harmonic oscillator is in fact affected by diabatic dynamics which generates excitations [140]. This shows a clear example of the problem of the non stationary basis.

If we use the correct derivate of $\hat{a}$ and $\hat{a}^\dagger$ given in Eq. (5.1), we get

$$\partial_\omega \hat{H} = \hat{a}^\dagger \hat{a} + \frac{1}{2}(\hat{a}^\dagger \hat{a}^\dagger + \hat{a}\hat{a}). \tag{5.6}$$

We then commute with the Hamiltonian to get the first AGP operators

$$\begin{aligned}
\left[\hat{H}, \partial_\omega \hat{H}\right] &= \left[\omega \hat{a}^\dagger \hat{a}, \hat{a}^\dagger \hat{a} + \frac{1}{2}(\hat{a}^\dagger \hat{a}^\dagger + \hat{a}\hat{a})\right] \\
&= \frac{\omega}{2}\left(\left[\hat{a}^\dagger \hat{a}, \hat{a}^\dagger \hat{a}^\dagger\right] + \left[\hat{a}^\dagger \hat{a}, \hat{a}\hat{a}\right]\right) \\
&= \frac{\omega}{2}\left(2\hat{a}^\dagger \hat{a}^\dagger - 2\hat{a}\hat{a}\right) \\
&= \omega\left(\hat{a}^\dagger \hat{a}^\dagger - \hat{a}\hat{a}\right).
\end{aligned} \tag{5.7}$$

As the $\hat{a}^\dagger \hat{a}$ part commutes with the Hamiltonian, only the double creation/annihilation operator part remains. Notably outside of extra factors, the operator only changes by the sign of $\hat{a}\hat{a}$, meaning it forms a closed two cycle of commutation

$$\left[\hat{H}, \left(\hat{a}^\dagger \hat{a}^\dagger \pm \hat{a}\hat{a}\right)\right] = \omega\left(\hat{a}^\dagger \hat{a}^\dagger \mp \hat{a}\hat{a}\right). \tag{5.8}$$

As the AGP must be fully imaginary and Hermitian, we can conclude that only

$i\left(\hat{a}^\dagger\hat{a}^\dagger - \hat{a}\hat{a}\right)$ is the only operator in the AGP. As such we can then solve the problem using the ansatz

$$\hat{\mathcal{A}}_\omega = i\alpha\left(\hat{a}^\dagger\hat{a}^\dagger - \hat{a}\hat{a}\right). \tag{5.9}$$

We then solve for α using the variational approach, by computing the action

$$\begin{aligned}\hat{G}_\omega &= \partial_\omega\hat{H} - i\left[\hat{H}, \hat{\mathcal{A}}_\omega\right] \\ &= \hat{a}^\dagger\hat{a} + \frac{1}{2}(\hat{a}^\dagger\hat{a}^\dagger + \hat{a}\hat{a}) + 2\omega\alpha\left(\hat{a}^\dagger\hat{a}^\dagger + \hat{a}\hat{a}\right), \qquad (5.10)\\ S &= \mathrm{Tr}\left\{\hat{G}_\omega^2\right\} \\ &= \sum_{n=0}^{\infty} n^2 + \left(2\alpha\omega + \frac{1}{2}\right)^2\left(\sum_{n=0}^{\infty} n(n-1) + \sum_{n=0}^{\infty}(n+2)(n+1)\right). \qquad (5.11)\end{aligned}$$

The first term in this expression is independent of α, and as such we focus on the second term. The infinite sums are both positive, meaning we need to minimise the coefficient of this term. The α that minimises the second term, and as such the action, is then given by

$$\alpha = -\frac{1}{4\omega}. \tag{5.12}$$

We can transform to the $\hat{x}$,$\hat{p}$ basis, by expressing $\hat{a}\hat{a}$ as

$$\begin{aligned}\hat{a}\hat{a} =& \left(\sqrt{\frac{m\omega}{2\hbar}}\left(\hat{x} + \frac{i}{m\omega}\hat{p}\right)\right)\left(\sqrt{\frac{m\omega}{2\hbar}}\left(\hat{x} + \frac{i}{m\omega}\hat{p}\right)\right) \\ =& \frac{m\omega}{2\hbar}\left(\hat{x}^2 + \frac{i}{m\omega}\left(\hat{x}\hat{p} + \hat{p}\hat{x}\right) - \frac{1}{m^2\omega^2}\hat{p}^2\right). \qquad (5.13)\end{aligned}$$

As such the AGP can be written as

$$\begin{aligned}\hat{\mathcal{A}}_\omega =& -\frac{i}{4\omega}\left(\hat{a}^\dagger\hat{a}^\dagger - \hat{a}\hat{a}\right) \\ =& -\frac{i}{4\omega}\left(\frac{m\omega}{2\hbar}\left(\hat{x}^2 - \frac{i}{m\omega}\left(\hat{x}\hat{p} + \hat{p}\hat{x}\right) - \frac{1}{m^2\omega^2}\hat{p}^2\right)\right. \\ & \left. -\frac{m\omega}{2\hbar}\left(\hat{x}^2 + \frac{i}{m\omega}\left(\hat{x}\hat{p} + \hat{p}\hat{x}\right) - \frac{1}{m^2\omega^2}\hat{p}^2\right)\right) \\ =& -\frac{i}{4\omega}\frac{m\omega}{\hbar}\left(-\frac{i}{m\omega}\left(\hat{x}\hat{p} + \hat{p}\hat{x}\right)\right) \\ =& -\frac{1}{4\omega\hbar}\left(\hat{x}\hat{p} + \hat{p}\hat{x}\right). \qquad (5.14)\end{aligned}$$

This result then agrees with the standard result for counter diabatic terms of the harmonic oscillator [140].

5.2.2 Varying the positional driving

Now that we have given example of the non-stationary basis affecting the results, we now look at the effects of the infinite basis. We now choose to vary ϵ, such that we change the strength of the driving. We find the partial derivate to be

$$\partial_\epsilon \hat{H} = \left(\hat{a} + \hat{a}^\dagger\right). \tag{5.15}$$

From this we can see that no complications will arise from the basis being non-stationary, as ω is kept constant.

We shall then commute this derivate with the Hamiltonian to generate the first order AGP terms. This gives

$$\begin{aligned}\left[\omega\hat{a}^\dagger\hat{a} + \epsilon\left(\hat{a} + \hat{a}^\dagger\right), \hat{a} + \hat{a}^\dagger\right] =& -\omega\hat{a}^\dagger + \omega\hat{a} - \epsilon + \epsilon \\ =& \omega\left(\hat{a}^\dagger - \hat{a}\right).\end{aligned} \tag{5.16}$$

Repeating this commutation on $\left(\hat{a}^\dagger - \hat{a}\right)$ now, finds

$$\begin{aligned}\left[\omega\hat{a}^\dagger\hat{a} + \epsilon\left(\hat{a} + \hat{a}^\dagger\right), \hat{a}^\dagger - \hat{a}\right] =& \omega\hat{a} + \omega\hat{a} + \epsilon + \epsilon \\ =& \omega\left(\hat{a} + \hat{a}^\dagger\right) + 2\epsilon.\end{aligned} \tag{5.17}$$

The only new operator generated is $2\epsilon\hat{\mathbb{I}}$, which trivially commutes with any other operator.

Using this information, the AGP of this model has the form

$$\hat{\mathcal{A}}_\epsilon = i\alpha\left(\hat{a}^\dagger - \hat{a}\right). \tag{5.18}$$

Like before, we can use the variational approach to solve for α. We have already

calculated the commutator in Eq. (5.17), so substituting this into the action we get

$$\begin{aligned}\hat{G}_\epsilon &= \partial_\epsilon \hat{H} - i\left[\hat{H}, \hat{\mathcal{A}}_\epsilon\right] \\ &= \hat{a} + \hat{a}^\dagger + \omega\alpha\left(\hat{a}^\dagger + \hat{a}\right) + 2\alpha\epsilon \\ &= (1+\omega\alpha)\left(\hat{a}^\dagger + \hat{a}\right) + 2\alpha\epsilon, \qquad (5.19)\\ S &= \mathrm{Tr}\left\{\hat{G}_\omega^2\right\} \\ &= (1+\omega\alpha)^2 \sum_{n=0}^{\infty}(n+(n+1)) + \sum_{n=0}^{\infty} 4\alpha^2\epsilon^2. \qquad (5.20)\end{aligned}$$

Unlike with the case of the harmonic oscillator, both terms now are dependent on α, so we need to be a bit more careful minimising the expression. As the first term scales with n, we can expect that minimising the first coefficient will minimise the overall expression, which we will now verify. We can evaluate the sums for a finite maximum value of n which we denote as N and then take the limit of $N \to \infty$. The expression now looks like

$$S = \lim_{N\to\infty} (1+\omega\alpha)^2 \left(N(N+1)+N\right) + N4\alpha^2\epsilon^2. \qquad (5.21)$$

By dividing both sides by N^2 we get

$$\begin{aligned}\lim_{N\to\infty}\frac{S}{N^2} &= \lim_{N\to\infty}(1+\omega\alpha)^2\left(\frac{N(N+1)}{N^2}\right) + \frac{1}{N}\left((1+\omega\alpha)^2 + 4\alpha^2\epsilon^2\right) \\ &= (1+\omega\alpha)^2, \qquad (5.22)\end{aligned}$$

showing clearly that minimising the first coefficient will minimise the overall expression. The α that minimises the action is then

$$\alpha = -\frac{1}{\omega}. \qquad (5.23)$$

Surprisingly, this value is not dependent on ϵ, although the counterdiabatic Hamiltonian will of course involve $\dot{\epsilon}$ as $\hat{H}_{CD} = \hat{H} + \dot{\epsilon}\hat{\mathcal{A}}_\epsilon$. This occurs because of the linear nature of the ϵ driving that appears in the Hamiltonian, meaning $\partial_\epsilon \hat{H}$ is independent of ϵ. If the functional form of the driving was any different in the Hamiltonian, the

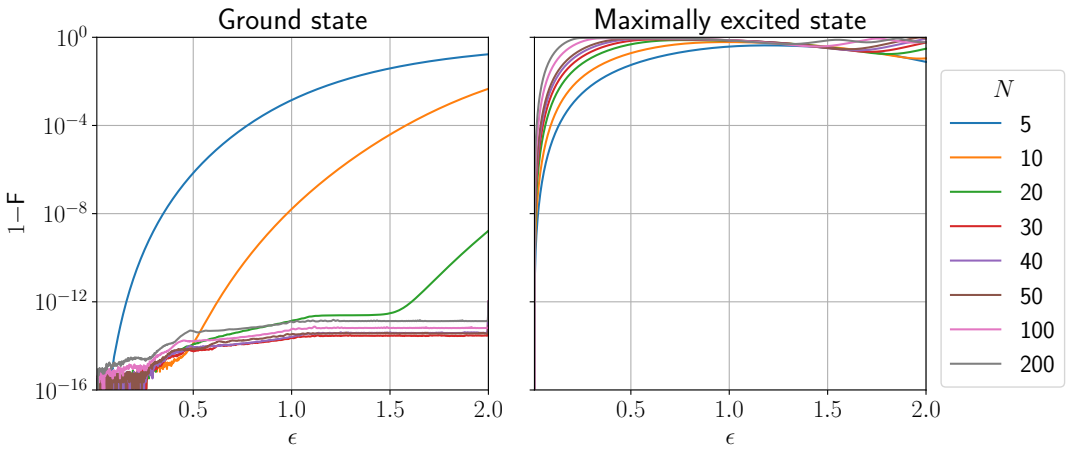

Figure 5.1: Plots showing control sequences of a linear $\dot{\epsilon} = 1$ ramping between two values of ϵ. The left plot initialises in the ground state, and then 1 - F is then measured against the instantaneous ground states of the system. The right plot show similar but instead with the maximally excited state.

result would be different. Let $\epsilon = f(\gamma)$, and $f'(\gamma)$ be the derivative with respect to γ, then if we repeated the above steps we would find Eq. (5.22) would become

$$\lim_{N\to\infty} \frac{S_f}{N^2} = \left(f'(\gamma) + \omega\alpha_f\right)^2. \tag{5.24}$$

This would lead to a result

$$\alpha = -\frac{f'(\gamma)}{\omega}. \tag{5.25}$$

As such, the independence of the AGP to the driving strength, was purely a result of our choice of functional form for the driving in Hamiltonian.

This AGP is exact for a truly bosonic system, where the commutation relation $\left[\hat{a}, \hat{a}^\dagger\right] = 1$ holds. However as previously mentioned, when simulating these models we often truncate the system to a large number of modes. This effectively simulates a large spin, where this commutation relation does not apply.

In Fig 5.1 we see the difference of trying to follow the ground state or the maximally excited state for a different size of truncated levels N. As expected the ground state improves as N is increased, however it is never truly exact for any finite N, but does reach near machine precision for $N = 200$. This shows that the approximation can be

well used to simulate counter diabatic driving to the ground state. On the other hand, for the maximally excited state the result is extremely diabatic, with it getting worse in general as N grows. This is because the difference between the approximate and the true finite commutation is equal to $1 - N$, so the result gets worse are N increases. This shows that it is vital that the value of N is sufficiently larger than any chosen state for counterdiabatic driving, such that any finite size effects are reduced.

During this section we have computed the AGP for a coherently driven bosonic mode, and effectively the harmonic oscillator. Whilst there are complications that arise like all bosonic models, the form of the AGP in the end is rather simple, both times being only a single term. Whilst this may not be surprising as the model is rather simple, this in fact points to a more general result. In bosonic physics quadratic models can be simplified using the Bogoliubov transformation [141]. We will now discuss these models to show how the AGP is rather simple in this case, and has a near closed form solution.

5.3 Exact AGP in quadratic bosonic models

Suppose we have a bosonic model with operators of at most order 2, which in general can be written as

$$\hat{H}_{\mathrm{Q}} = c_2^0 \hat{a}^2 + c_1^1 \hat{a}^\dagger \hat{a} + c_0^2 (\hat{a}^\dagger)^2 + c_1^0 \hat{a} + c_0^1 \hat{a}^\dagger + c_0^0 \hat{\mathbb{I}}. \tag{5.26}$$

For this section we assume the operators have an infinite sized Hilbert space such that the commutator $[\hat{a}, \hat{a}^\dagger] = 1$ is exact. This also means that we can always write the operators in normal order, as such we only include $\hat{a}^\dagger \hat{a}$ in the Hamiltonian and not $\hat{a}\hat{a}^\dagger$

If we calculate the commutation relations of such a model, we get

$[\downarrow, \rightarrow]$	$\hat{a}^2$	$\hat{a}^\dagger\hat{a}$	$(\hat{a}^\dagger)^2$	$\hat{a}$	$\hat{a}^\dagger$	$\hat{\mathbb{I}}$
$\hat{a}^2$	0	$2\hat{a}^2$	$4\hat{a}^\dagger\hat{a} + 2\hat{\mathbb{I}}$	0	$2\hat{a}$	0
$\hat{a}^\dagger\hat{a}$	$-2\hat{a}^2$	0	$2(\hat{a}^\dagger)^2$	$-\hat{a}$	$\hat{a}^\dagger$	0
$(\hat{a}^\dagger)^2$	$-4\hat{a}^\dagger\hat{a} - 2\hat{\mathbb{I}}$	$-2(\hat{a}^\dagger)^2$	0	$-2\hat{a}^\dagger$	0	0
$\hat{a}$	0	$\hat{a}$	$2\hat{a}^\dagger$	0	$\hat{\mathbb{I}}$	0
$\hat{a}^\dagger$	$-2\hat{a}$	$-\hat{a}^\dagger$	0	$-\hat{\mathbb{I}}$	0	0
$\hat{\mathbb{I}}$	0	0	0	0	0	0

From this we can see that all operators are mapped within the same set of operators the Hamiltonian is defined on, and as such the dynamical Lie algebra of this model contains at most these six operators. The dimension of the AGP being so small allows a calculation of the exact AGP, meaning we can use the exact condition of the AGP in Eq. (2.39) to avoid any problems with infinite traces.

We then need to compute $\hat{G}_\lambda$, which means defining the coefficients to now be functions of some control parameter λ

$$\hat{H}_{\mathrm{Q}}(\lambda) = c_2^0(\lambda)\hat{a}^2 + c_1^1(\lambda)\hat{a}^\dagger\hat{a} + c_0^2(\lambda)(\hat{a}^\dagger)^2 + c_1^0(\lambda)\hat{a} + c_0^1(\lambda)\hat{a}^\dagger + c_0^0(\lambda)\hat{\mathbb{I}}. \tag{5.27}$$

Then a derivative can be taken to give

$$\begin{aligned}\partial_\lambda \hat{H}_{\mathrm{Q}}(\lambda) =& \partial_\lambda c_2^0(\lambda)\hat{a}^2 + \partial_\lambda c_1^1(\lambda)\hat{a}^\dagger\hat{a} + \partial_\lambda c_0^2(\lambda)(\hat{a}^\dagger)^2 \\ &+ \partial_\lambda c_1^0(\lambda)\hat{a} + \partial_\lambda c_0^1(\lambda)\hat{a}^\dagger + \partial_\lambda c_0^0(\lambda)\hat{\mathbb{I}}.\end{aligned} \tag{5.28}$$

As we have seen previously, bosonic operators are not always independent of the control parameter λ. For simplicity, in the following calculations we assume $\partial_\lambda \hat{a} = \partial_\lambda \hat{a}^\dagger = 0$, however the following results can be generalised for different cases of partial derivate.

So to begin let's apply the left hand commutator of the Hamiltonian to each operator in the dynamical Lie algebra

$$\left[\hat{H}_{\mathrm{Q}}, \hat{a}^2\right] = -2c_1^1\hat{a}^2 - 4c_0^2\hat{a}^\dagger\hat{a} - 2c_0^1\hat{a} - 2c_0^2\hat{\mathbb{I}}, \tag{5.29}$$

$$\left[\hat{H}_{\mathrm{Q}}, \hat{a}^{\dagger}\hat{a}\right] = 2c_2^0\hat{a}^2 - 2c_0^2(\hat{a}^{\dagger})^2 + c_1^0\hat{a} - c_0^1\hat{a}^{\dagger}, \tag{5.30}$$

$$\left[\hat{H}_{\mathrm{Q}}, (\hat{a}^{\dagger})^2\right] = 4c_2^0\hat{a}^{\dagger}\hat{a} + 2c_1^1(\hat{a}^{\dagger})^2 + 2c_1^0\hat{a}^{\dagger} + 2c_2^0\hat{\mathbb{I}}, \tag{5.31}$$

$$\left[\hat{H}_{\mathrm{Q}}, \hat{a}\right] = -c_1^1\hat{a} - 2c_0^2\hat{a}^{\dagger} - c_0^1\hat{\mathbb{I}}, \tag{5.32}$$

$$\left[\hat{H}_{\mathrm{Q}}, \hat{a}^{\dagger}\right] = 2c_2^0\hat{a} + c_1^1\hat{a}^{\dagger} + c_1^0\hat{\mathbb{I}}, \tag{5.33}$$

$$\left[\hat{H}_{\mathrm{Q}}, \hat{\mathbb{I}}\right] = 0. \tag{5.34}$$

As was already clear, the AGP will not contain $\hat{\mathbb{I}}$ as it always commutes with any other operator. We will keep the coefficients in this extremely generic form, to allow for non-Hermitian Hamiltonians and complex valued Hamiltonians, although we shall also provide a simplified result for the specific case of a Hermitian real valued Hamiltonian.

We then define the AGP to be

$$\hat{\mathcal{A}}_{\mathrm{Q}} = \alpha_2^0\hat{a}^2 + \alpha_1^1\hat{a}^{\dagger}\hat{a} + \alpha_0^2(\hat{a}^{\dagger})^2 + \alpha_1^0\hat{a} + \alpha_0^1\hat{a}^{\dagger}, \tag{5.35}$$

We can setup a matrix equation to solve for the coefficients of this AGP. For the full derivation of this matrix equation please see App. A.6. The matrix equation is of the form

$$-i\mathbf{M}_{\mathrm{Q}}\vec{\alpha}_{\mathrm{Q}} = \vec{u}_{\mathrm{Q}} \tag{5.36}$$

where $\mathbf{M}_{\mathrm{Q}}$ is given by

$$\begin{pmatrix}
4(c_1^1)^2 - 8c_2^0c_0^2 & -4c_1^1c_2^0 & 8(c_2^0)^2 & 0 & 0 \\
8c_0^2c_1^1 & -16c_2^0c_0^2 & 8c_2^0c_1^1 & 0 & 0 \\
8(c_0^2)^2 & -4c_1^1c_0^2 & -8c_0^2c_2^0 + 4(c_1^1)^2 & 0 & 0 \\
6c_0^1c_1^1 - 4c_1^0c_0^2 & -6c_0^1c_2^0 - c_1^1c_1^0 & 8c_2^0c_1^0 & (c_1^1)^2 - 4c_2^0c_0^2 & 0 \\
8c_0^1c_0^2 & -6c_1^0c_0^2 - c_1^1c_0^1 & -4c_0^1c_2^0 + 6c_1^0c_1^1 & 0 & -4c_0^2c_2^0 + (c_1^1)^2 \\
4c_0^2c_1^1 + 2(c_0^1)^2 & -8c_0^2c_2^0 - 2c_0^1c_1^0 & 4c_2^0c_1^1 + 2(c_1^0)^2 & c_0^1c_1^1 - 2c_1^0c_0^2 & -2c_0^1c_2^0 + c_1^0c_1^1
\end{pmatrix} \tag{5.37}$$

$\vec{\alpha}$ is a column vector of the α values

$$\vec{\alpha}_{\mathrm{Q}}^T = \begin{pmatrix} \alpha_2^0 & \alpha_1^1 & \alpha_0^2 & \alpha_1^0 & \alpha_0^1 \end{pmatrix}. \tag{5.38}$$

and $\vec{u}_{\mathrm{Q}}$ is a column vector determined by the rate of change of all the variables, given by

$$\vec{u}_{\mathrm{Q}} = \begin{pmatrix} 2c_1^1 c_2'^0 - 2c_2^0 c_1'^1 \\ 4c_0^2 c_2'^0 - 4c_2^0 c_0'^2 \\ 2c_0^2 c_1'^1 - 2c_1^1 c_0'^2 \\ 2c_0^1 c_2'^0 - c_1^0 c_1'^1 + c_1^1 c_1'^0 - 2c_2^0 c_0'^1 \\ c_0^1 c_1'^1 - 2c_1^0 c_0'^2 + 2c_0^2 c_1'^0 - c_1^1 c_0'^1 \\ 2c_0^2 c_2'^0 - 2c_2^0 c_0'^2 + c_0^1 c_1'^0 - c_1^0 c_0'^1 \end{pmatrix}, \tag{5.39}$$

where the partial derivate is written as $c_b'^a = \frac{\partial c_b^a}{\partial \lambda}$.

We see that there are more rows than columns for the matrix making the solution overdetermined. This means unless there is linear dependence amongst the rows, there is no solution to the matrix. However we expect in that in any physical case, there is a solution to the AGP. Likely the inclusion of the identity operator in the Hamiltonian has lead to this overdetermined set of equations, as it only affects the eigenvalues of a Hamiltonian and not the eigenstates. Another observation that can be made is that because we have let the c coefficients be complex, there are actually twelve equations and ten AGP operators, if we take the real and imaginary parts separately.

5.3.1 Simplifications from real valued and Hermitian Hamiltonians

The matrix equation given in Eq. (5.36) is the most general form of the Hamiltonian that can be possible. However, there are great simplifications that can be made by imposing conditions on the Hamiltonian. We shall discuss the two main conditions of real valued c coefficients and enforcing the Hamiltonian to be hermitian.

If the coefficients are all real valued, then we know the AGP must be completely imaginary. This can be applied by taking all α values to be real, and adding a factor of i ($\vec{\alpha} \to i\vec{\alpha}$). This leads to the matrix equation becoming

$$\begin{aligned} -i\mathbf{M}_{\mathrm{Q}} i\vec{\alpha}_{\mathrm{Q}} &= \vec{u}_{\mathrm{Q}} \\ \mathbf{M}_{\mathrm{Q}}\vec{\alpha}_{\mathrm{Q}} &= \vec{u}_{\mathrm{Q}}. \end{aligned} \tag{5.40}$$

This means there can only be at most five AGP operators, and greatly simplifying the solution to the matrix equation.

The other case of the Hamiltonian being Hermitian means we must have

$$(c_2^0)^\dagger(\hat{a}^\dagger)^2 + (c_1^1)^\dagger\hat{a}^\dagger\hat{a} + (c_0^2)^\dagger\hat{a}^2 + (c_1^0)^\dagger\hat{a}^\dagger + (c_0^1)^\dagger\hat{a} + (c_0^0)^\dagger\hat{\mathbb{I}} = c_2^0\hat{a}^2 + c_1^1\hat{a}^\dagger\hat{a} + c_0^2(\hat{a}^\dagger)^2 + c_1^0\hat{a} + c_0^1\hat{a}^\dagger + c_0^0\hat{\mathbb{I}}, \tag{5.41}$$

which imposes on the coefficients the conditions

$$(c_2^0)^\dagger = c_0^2, \quad (c_1^1)^\dagger = c_1^1, \quad (c_1^0)^\dagger = c_0^1, \quad (c_0^0)^\dagger = c_0^0. \tag{5.42}$$

Additionally as discussed in Sec. 3.2, if the Hamiltonian is Hermitian then the AGP must also be Hermitian. This means

$$\alpha_2^0\hat{a}^2+\alpha_1^1\hat{a}^\dagger\hat{a}+\alpha_0^2(a^\dagger)^2+\alpha_1^0a+\alpha_0^1\hat{a}^\dagger = (\alpha_2^0)^\dagger(\hat{a}^\dagger)^2+(\alpha_1^1)^\dagger\hat{a}^\dagger\hat{a}+(\alpha_0^2)^\dagger\hat{a}^2+(\alpha_1^0)^\dagger\hat{a}^\dagger+(\alpha_0^1)^\dagger\hat{a}, \tag{5.43}$$

imposing the conditions

$$\alpha_2^0 =(\alpha_0^2)^\dagger, \tag{5.44}$$

$$\alpha_1^1 =(\alpha_1^1)^\dagger, \tag{5.45}$$

$$\alpha_1^0 =(\alpha_0^1)^\dagger. \tag{5.46}$$

This will reduce the number of equations that need to be solved, along with simplifying the form of the matrix.

Now if we combine these two results together, and impose the Hamiltonian is real and Hermitian, we can get the non trivial conditions

$$c_2^0 =c_0^2, \tag{5.47}$$

$$c_1^0 =c_0^1, \tag{5.48}$$

$$\alpha_2^0 = -\alpha_0^2, \tag{5.49}$$

$$\alpha_1^0 = -\alpha_0^1. \tag{5.50}$$

Note that the α values have a minus sign, due to the extra factor of i applied.

In App. A.7 we apply these conditions to the matrix equation, leading to the simplified form

$$\begin{pmatrix} 4(c_1^1)^2 - 16(c_2^0)^2 & 0 \\ 6c_1^0(c_1^1 - 2c_2^0) & (c_1^1)^2 - 4(c_2^0)^2 \end{pmatrix} \begin{pmatrix} \alpha_2^0 \\ \alpha_1^0 \end{pmatrix} = \begin{pmatrix} 2c_1^1 c_2'^0 - 2c_2^0 c_1'^1 \\ 2\left(c_1^0 c_2'^0 - c_1'^0 c_2^0\right) + c_1'^0 c_1^1 - c_1^0 c_1'^1 \end{pmatrix} \tag{5.51}$$

Then to simplify the notation, we define the constant $\gamma_\pm$ as

$$\gamma_\pm = c_1^1 \pm 2c_2^0, \tag{5.52}$$

and an anti product rule operator $\bar{\Delta}_\lambda$, between two scalar values a and b as

$$\bar{\Delta}_\lambda(a, b) = \frac{\partial a}{\partial \lambda} b - a \frac{\partial b}{\partial \lambda}. \tag{5.53}$$

With these, the matrix equation becomes

$$\begin{pmatrix} 4\gamma_+\gamma_- & 0 \\ 6c_1^0\gamma_- & \gamma_+\gamma_- \end{pmatrix} \begin{pmatrix} \alpha_2^0 \\ \alpha_1^0 \end{pmatrix} = \begin{pmatrix} 2\bar{\Delta}_\lambda(c_2^0, c_1^1) \\ 2\bar{\Delta}_\lambda(c_2^0, c_1^0) + \bar{\Delta}_\lambda(c_1^0, c_1^1) \end{pmatrix} \tag{5.54}$$

The solution to this matrix equation is then given by

$$\alpha_2^0 = \frac{1}{2} \frac{\bar{\Delta}_\lambda(c_2^0, c_1^1)}{\gamma_+\gamma_-}, \tag{5.55}$$

$$\alpha_1^0 = 2\frac{\bar{\Delta}_\lambda(c_2^0, c_1^0)}{\gamma_+\gamma_-} + \frac{\bar{\Delta}_\lambda(c_1^0, c_1^1)}{\gamma_+\gamma_-} - 3c_1^0 \frac{\bar{\Delta}_\lambda(c_2^0, c_1^1)}{\gamma_+^2\gamma_-}. \tag{5.56}$$

We can then test this result by computing the AGP for the driven bosonic mode we discussed in the previous section. The non zero coefficients that correspond to the Hamiltonian given in Eq. (5.5) are $c_1^1 = \omega$, $c_1^0 = c_0^1 = \epsilon$, and we vary the cavity (ϵ) such that the only non zero derivate is $c_1'^0 = c_0'^1 = 1$. With this we find the result

$$\alpha_2^0 = 0, \tag{5.57}$$

$$\alpha_1^0 = \frac{\omega}{(\omega)^2} = \frac{1}{\omega}, \tag{5.58}$$

which agrees with our previous calculation.

5.3.2 Extending to multiple quadratic bosonic modes

We can extend the idea of quadratic models to include multiple bosonic modes, where the coupling between modes is at most order two. By quadratic here we do not mean quadratic for each mode, but instead the total sum of creation/annihilation operators is less than two, meaning $\hat{a}_n^2 \otimes \hat{a}_m^2$ is not considered to be quadratic. The key coupling operators that this allows to be added then are: $\hat{a}_n \otimes \hat{a}_m$, $\hat{a}_n \otimes \hat{a}_m^\dagger$, $\hat{a}_n^\dagger \otimes \hat{a}_m$, $\hat{a}_n^\dagger \otimes \hat{a}_m^\dagger$, for coupling between the nth and mth modes. All other operators are effectively the single mode operators with identity operators acting on all other modes. When these coupling operators interact with a single mode operator, they only commute with either $\hat{a}$ or $\hat{a}^\dagger$ on that particular mode, which from Table 5.3 we see always results in either $\hat{a}$,$\hat{a}^\dagger$ or $\hat{\mathbb{I}}$ on the mode. This means the commutation relations between the coupling operators and single mode operators are always at most quadratic, so the closed commutation relations is not broken by them.

This leaves only commutations between coupling operators. For simplicity of notation, we enforce $n < m$ so we don't have any confusion over whether $\hat{a}_1 \otimes \hat{a}_2^\dagger = \hat{a}_2^\dagger \otimes \hat{a}_1$. If none of the modes are shared then it is clear the commutation will be zero. As such we either have one or two shared modes. For each shared mode the commutator is always between single excitation operators ($\hat{a}$ or $\hat{a}^\dagger$) and as such the commutator is either equal to 1 or 0 or -1. This means the operator will always be an identity on a shared mode, so for coupling operator between l, k and k, p the new operators will couple the non shared sites l, p, notably again preserving the quadratic nature. If there are two shared modes, then the there will be an anti-commutator involving non identity operators, as seen in Sec. 3.3.1. The anti-commutators of the bosonic operators are

$$\{\hat{a}, \hat{a}\} = 2\hat{a}^2, \tag{5.59}$$

$$\{\hat{a}, \hat{a}^\dagger\} = \hat{a}\hat{a}^\dagger + \hat{a}^\dagger\hat{a} = 2\hat{a}^\dagger\hat{a} + \hat{\mathbb{I}}, \tag{5.60}$$

$$\{\hat{a}^\dagger, \hat{a}\} = \hat{a}^\dagger\hat{a} + \hat{a}\hat{a}^\dagger = 2\hat{a}^\dagger\hat{a} + \hat{\mathbb{I}}, \tag{5.61}$$

$$\{\hat{a}^\dagger, \hat{a}^\dagger\} = 2(\hat{a}^\dagger)^2. \tag{5.62}$$

These again do not break the quadratic nature of the model, as they always combine with a identity operator on the other shared mode.

This shows that the same results can be derived for an arbitrary number of quadratic coupled bosonic modes. We do not provide a closed solution to this model, but similar steps that we took in the derivation of a single mode can be applied. Again these multimode quadratic models can also be solved using the Bogoliubov transformation, so it is expected that these results have a finite number of operators.

This concludes the chapter computing the AGP in bosonic models. The main takeaways for this chapter is the inherent differences between bosonic and spin operators that should be kept in mind during computation. We have also provided the matrix equation for all quadratic single mode bosonic models, which can be used directly to solve for the AGP. The results of this chapter can hopefully be used in further research to expand the scope of bosonic AGP physics. For the next chapter, we will further these results by combing together with the results from the previous chapter, to have a look at hybrid systems.

Chapter 6

The AGP in hybrid models

In the previous chapters, we have described how to compute the AGP for both spin and bosonic systems, and now we aim to combine these results together. Systems that include both spins and bosonic modes are referred to as hybrid systems, and appear in many areas of physics [142–145]. We look at the family of models that describe atoms in a cavity [146], with calculations for the Jaynes-Cummings and Rabi model in particular. We will see the results for the Jaynes-Cummings to be simple when the problem is laid out correctly, but intractable if approached naively. With the Rabi model we shall see how to apply different approximations to the model to allow computation, and how these lead to differences in the results. By the end of this chapter the reader will have some understanding of hybrid models, which can be thought of as the strongest type of open system as there is a full system and environment description. Hybrid systems as such show the next step towards a open system description, where we trace of the bath degrees of freedom and are left with only the system Hilbert space.

The most common collection of hybrid systems studied are spin-1/2 particles inside a cavity, which causes a coupling between the bosonic mode of the cavity and the spins. The coupling arises from interaction between the atomic dipole of the spin and the light field, this leads to the general form

$$\hat{H}_{int} = \sum_{j,n} g_{j,n}\hat{\sigma}_j^x \left(\hat{a}_n^\dagger + \hat{a}_n\right) = \sum_{j,n} g_{j,n}(\hat{a}_n^\dagger\hat{\sigma}_j^- + \hat{a}_n\hat{\sigma}_j^+) + g_{j,n}(\hat{a}_n^\dagger\hat{\sigma}_j^+ + \hat{a}_n\hat{\sigma}_j^-), \quad (6.1)$$

where $\hat{\sigma}_j^+$, $\hat{\sigma}_j^-$ are the spin raising and lowering operators on site j, and n labels the the nth bosonic mode. The splitting up of $\hat{\sigma}_j^x$, gives rise to what is referred to as the rotating term $(\hat{a}_n^\dagger \hat{\sigma}_j^- + \hat{a}_n \hat{\sigma}_j^+)$ and counter rotation term $(\hat{a}_n^\dagger \hat{\sigma}_j^+ + \hat{a}_n \hat{\sigma}_j^-)$. The rotating term arises from the component of the atomic dipole and light field that rotate in the same direction, leading to an effective slow rotation dependent on the difference in frequencies. On the other hand, the counter rotating term depend on the sum of the frequencies, as it arise from the dipoles rotating against each other. Due to this, the counter rotating term oscillates much faster than the rotating term, meaning it affects the dynamics much less. Jaynes and Cummings proposed the rotating wave approximation (RWA), where the counter rotating term is excluded entirely from the model [147], which is well justified for small coupling strengths. Depending on the number of spins and whether the RWA is applied, this collection of systems is split into four different models

	RWA	No RWA
$N = 1$	The Jaynes Cummings model	The Rabi model
$N > 1$	The Tavis Cummings model	The Dicke model

where N is the number of spin-1/2 particles. We shall focus on the case of $N = 1$ for this thesis, as such looking at both The Jaynes Cummings and Rabi models.

As mentioned, the first section of this chapter will focus of the Jaynes Cummings model, looking at the AGP for varying each of the parameters of the model. We provide exact results for a given excitation manifold, and show how producing a full operator description of the AGP is problematic for the Jaynes Cummings model. We then will move our focus towards the Rabi model, where we will treat the problem in terms of generalised Gell-Mann matrices to provide an exact description of the truncated model. This will involve developing an understanding the effect of the commutator in the Rabi model, allowing an analytical form of the matrix equation required to solve for the coefficients of the AGP.

6.1 The Jaynes Cummings model

In this section we look at the Jaynes Cummings (JC) model [147], which can be written as the Hamiltonian

$$\hat{H}_{JC} = \frac{\Delta}{2}\hat{\sigma}_z + \omega\hat{a}^\dagger\hat{a} + g(\hat{a}^\dagger\hat{\sigma}^- + \hat{a}\hat{\sigma}^+). \tag{6.2}$$

In this model there are three parameters that can be varied: the splitting between the spin energy levels (Δ), frequency of the cavity mode (ω) and coupling strength (g). Depending on which of these parameters are varied, the AGP will be different so we shall focus on each of the cases separately.

Before we get to computing the AGP, it is extremely useful to note that this Hamiltonian can be solved analytically. This is done by identifying the number of excitations, defined as

$$\hat{N}_e = \hat{a}^\dagger\hat{a} + \hat{\sigma}^+\hat{\sigma}^-, \tag{6.3}$$

is a conserved quantity ($[\hat{H}, \hat{N}_e] = 0$), as the rotating term in the coupling operator always swaps between a spin and bosonic excitation. This means we can split up the Hilbert space of the problem into each of the excitation numbers, N_e such that $\hat{N}_e |\psi\rangle = N_e |\psi\rangle$. As the spin can only be either in the ground or excited states, the only states with N_e excitations will be $|N_e, \downarrow\rangle$ and $|N_e - 1, \uparrow\rangle$. It is important to note that the zero excitation manifold has only one state, $|0, \downarrow\rangle$, meaning there is no pair, and as such it is already an adiabatic state, however we shall see later this is not the case when varying the cavity frequency ω, for the reasons we highlighted in the previous chapter (Sec. 5.1.1).

If we omit the zero excitation manifold for now, we can write the reduced Hamiltonian in the N_e excitation manifold as

$$\hat{H}_{JC}^{(N_e)} = \begin{pmatrix} \frac{\Delta}{2} + \omega(N_e - 1) & g\sqrt{N_e} \\ g\sqrt{N_e} & -\frac{\Delta}{2} + \omega N_e \end{pmatrix}, \tag{6.4}$$

which acts of the column vector of states

$$\begin{pmatrix} |N_e - 1, \uparrow\rangle \\ |N_e, \downarrow\rangle \end{pmatrix}. \tag{6.5}$$

This Hamiltonian is diagonalised by the eigenenergies and eigenstates (For details see App. A.8)

$$E_{N_e,\pm} = \omega\left(N_e - \frac{1}{2}\right) \pm \frac{1}{2}\sqrt{(\Delta-\omega)^2 + 4g^2 N_e}, \tag{6.6}$$

$$|N_e, +\rangle = \cos(\beta_{N_e})\,|N_e - 1, \uparrow\rangle + \sin\left(\frac{\beta_{N_e}}{2}\right)|N_e, \downarrow\rangle\,, \tag{6.7}$$

$$|N_e, -\rangle = \sin(\beta_{N_e})\,|N_e - 1, \uparrow\rangle - \cos(\beta_{N_e})\,|N_e, \downarrow\rangle\,, \tag{6.8}$$

where $\beta_{N_e} = \frac{1}{2}\arctan\left(\frac{2g\sqrt{N_e}}{\Delta-\omega}\right)$.

As we have an analytical form of the eigenstates and eigenenergies, we will compute the off diagonal elements of the AGP in the eigenbasis using Eq. (2.34), remembering that the diagonal elements of the AGP are set to zero. Of the three parameters in the system, the basis $|N_e - 1, \uparrow\rangle$, $|N_e, \downarrow\rangle$ is independent for both the spin energy (Δ) and the coupling (g) leading to simple diabatic excitations between the pairs of eigenstates, and the conservation of N_e shall hold. However as we have previously discussed, the bosonic basis is non-stationary when varying the cavity frequency ω, which will lead to an effective diabatic term that breaks the RWA.

6.1.1 Varying spin energy

We begin by varying the spin energy level (Δ). As the basis is stationary with respect to Δ, we simply find

$$\partial_\Delta \hat{H}_{JC} = \frac{1}{2}\hat{\sigma}^z. \tag{6.9}$$

We start the calculation by applying this operator to each of the eigenstates

$$\partial_\Delta \hat{H}_{JC}\,|N_e, +\rangle = \frac{1}{2}\left(\cos(\beta_{N_e})\,|N_e - 1, \uparrow\rangle - \sin(\beta_{N_e})\,|N_e, \downarrow\rangle\right), \tag{6.10}$$

$$\partial_\Delta \hat{H}_{JC}\,|N_e, -\rangle = \frac{1}{2}\left(\sin(\beta_{N_e})\,|N_e - 1, \uparrow\rangle + \cos(\beta_{N_e})\,|N_e, \downarrow\rangle\right). \tag{6.11}$$

These new states are all still within the same excitation manifold, which is to be expected as $\partial_\Delta \hat{H}_{JC}$ obeys the RWA, so there are no diabatic excitations between different excitation manifolds. This also confirms that the ground state is completely adiabatic when varying Δ.

We know that the AGP is skew symmetric, as it is fully imaginary and Hermitian, so $\langle N_e, -| \hat{\mathcal{A}}_\Delta |N_e, +\rangle = -\langle N_e, +| \hat{\mathcal{A}}_\Delta |N_e, -\rangle$. As such we only need to compute one element, which can be computed to be

$$\langle N_e, -| \hat{\mathcal{A}}_\Delta |N_e, +\rangle = i\frac{1}{2}\frac{\sin(2\beta_{N_e})}{\sqrt{(\Delta-\omega)^2 + 4g^2(N_e)}}. \tag{6.12}$$

We can further simplify this by using the definition of β_{N_e}, we can find

$$\tan(2\beta_{N_e}) = \frac{2g\sqrt{N_e}}{\Delta-\omega}, \tag{6.13}$$

$$\sin(2\beta_{N_e}) = \frac{2g\sqrt{N_e}}{\sqrt{4g^2N_e + (\Delta-\omega)^2}}, \tag{6.14}$$

$$\cos(2\beta_{N_e}) = \frac{\Delta-\omega}{\sqrt{4g^2N_e + (\Delta-\omega)^2}}, \tag{6.15}$$

where the denominator of $\sin(2\beta_{N_e})$ and $\cos(2\beta_{N_e})$ are chosen such that $\sin(2\beta_{N_e})^2 + \cos(2\beta_{N_e})^2 = 1$ holds.

We can then substitute this into the matrix elements to give the AGP for Δ as

$$\hat{\mathcal{A}}_\Delta^{(N_e)} = i\frac{g\sqrt{N_e}}{(\Delta-\omega)^2 + 4g^2(N_e)}\begin{pmatrix} 0 & -1 \\ 1 & 0 \end{pmatrix}. \tag{6.16}$$

To be able to apply this to a simulation, we need to transform back to the stationary $|N_e - 1, \uparrow\rangle, |N_e, \downarrow\rangle$ basis. From Eqs. (6.7),(6.8) we can write the transformation from $|N_e - 1, \uparrow\rangle, |N_e, \downarrow\rangle$ to $|N_e, +\rangle, |N_e, -\rangle$ as

$$= \begin{pmatrix} \cos(\beta_{N_e}) & \sin(\beta_{N_e}) \\ \sin(\beta_{N_e}) & -\cos(\beta_{N_e}) \end{pmatrix}\begin{pmatrix} |N_e - 1, \uparrow\rangle \\ |N_e, \downarrow\rangle \end{pmatrix} = \begin{pmatrix} |N_e, +\rangle \\ |N_e, -\rangle \end{pmatrix}. \tag{6.17}$$

This transformation matrix is involutory, as such the transform from $|N_e, +\rangle, |N_e, -\rangle$

to $|N_e-1,\uparrow\rangle, |N_e,\downarrow\rangle$ has the same matrix

$$= \begin{pmatrix} \cos(\beta_{N_e}) & \sin(\beta_{N_e}) \\ \sin(\beta_{N_e}) & -\cos(\beta_{N_e}) \end{pmatrix} \begin{pmatrix} |N_e,+\rangle \\ |N_e,-\rangle \end{pmatrix} = \begin{pmatrix} |N_e-1,\uparrow\rangle \\ |N_e,\downarrow\rangle \end{pmatrix}. \tag{6.18}$$

To transform $\hat{\mathcal{A}}_\Delta^{(N_e)}$ into the stationary basis we simply apply the transformation matrix to either side

$$\begin{aligned} \hat{\mathcal{A}}_\Delta^{(N_e),\text{stationary}} =& \begin{pmatrix} \cos(\beta_{N_e}) & \sin(\beta_{N_e}) \\ \sin(\beta_{N_e}) & -\cos(\beta_{N_e}) \end{pmatrix} \mathcal{A}_\Delta^{(N_e)} \begin{pmatrix} \cos(\beta_{N_e}) & \sin(\beta_{N_e}) \\ \sin(\beta_{N_e}) & -\cos(\beta_{N_e}) \end{pmatrix} \\ =& i\frac{g\sqrt{N_e}}{(\Delta-\omega)^2+4g^2N_e} \begin{pmatrix} 0 & 1 \\ -1 & 0 \end{pmatrix}. \end{aligned} \tag{6.19}$$

This analytical form of the AGP, allows us to learn some details about the diabatic behaviour in the Jaynes Cummings model when we vary the spin energy. The first detail to point out, is that for $g=0$ the AGP is exactly zero and as such there are no diabatic transitions. We present two explanations for this result: one physical, and one mathematical. Firstly, when $g=0$ there is no coupling between the spin and boson, and as such the two systems decouple and are independent, leaving just a varying spin-1/2 which is purely adiabatic. The other explanation can be found by looking at the eigenstates, namely β_{N_e} for which $g=0 \implies \beta_{N_e}=0$, meaning the mixing between the eigenstates is minimal and constant.

We can also observe for large values of N_e, the AGP can be approximated as

$$\hat{\mathcal{A}}_\Delta^{(N_e),\text{stationary}} \approx i\frac{1}{4g\sqrt{N_e}} \begin{pmatrix} 0 & 1 \\ -1 & 0 \end{pmatrix}, \tag{6.20}$$

showing how the diabatic effects lessen as N_e increases. This approximate form is in fact shared for the case of $g \gg \Delta, \omega$, showing in that limit the largest diabatic excitation occur for $N_e=1$. However if we find the stationary point with respect to N_e we find

the maximal value of the AGP to be when

$$N_e = \frac{(\Delta - \omega)^2}{4g^2}. \tag{6.21}$$

This shows that in the small coupling limit $g \ll \Delta, \omega$, the excitation manifold most susceptible to diabatic excitations is larger than one but still finite as the previous limit still holds as N_e increases.

Lastly the operator form of the AGP will likely be very familiar by this stage of the thesis, as it is effectively a $\hat{\sigma}^y$ type operator acting between the two states. This is expected as it is the only operators form that can appear for a two level system, which the Jaynes Cummings model effectively is.

6.1.2 Varying the coupling strength

We next look at varying the coupling strength (g), which is very similar to the previous result for varying Δ. We again start by taking the partial derivate, this time with respect to g

$$\partial_g \hat{H}_{JC} = \hat{a}^\dagger \hat{\sigma}^- + \hat{a}\hat{\sigma}^+. \tag{6.22}$$

We then apply this to the eigenstates

$$\partial_g \hat{H}_{JC} \left|N_e, +\right\rangle = \sqrt{N_e} \left(\sin\left(\beta_{N_e}\right) \left|N_e - 1, \uparrow\right\rangle + \cos\left(\beta_{N_e}\right) \left|N_e, \downarrow\right\rangle\right), \tag{6.23}$$

$$\partial_g \hat{H}_{JC} \left|N_e, -\right\rangle = \sqrt{N_e} \left(-\cos\left(\beta_{N_e}\right) \left|N_e - 1, \uparrow\right\rangle + \sin\left(\beta_{N_e}\right) \left|N_e, \downarrow\right\rangle\right). \tag{6.24}$$

Likewise, the operator respects the RWA, so there are only diabatic excitations between $|N_e, +\rangle$ and $|N_e, -\rangle$. We compute these to be

$$\left\langle N_e, -\right| \hat{\mathcal{A}}_g \left|N_e, +\right\rangle = -i \frac{(\Delta - \omega)\sqrt{N_e}}{(\Delta - \omega)^2 + 4g^2 N_e}. \tag{6.25}$$

This then gives an AGP in the form

$$\hat{\mathcal{A}}_g^{(N_e)} = i \frac{(\Delta - \omega)\sqrt{N_e}}{(\Delta - \omega)^2 + 4g^2 N_e} \begin{pmatrix} 0 & 1 \\ -1 & 0 \end{pmatrix}. \tag{6.26}$$

The last step we need to do to apply this counterdiabatic term is to transform back into the stationary basis. The form of the matrix is identical to Eq. (6.19) up to a minus sign, and as such we can see the result will be

$$\hat{\mathcal{A}}_g^{(N_e),\text{stationary}} = i\sqrt{N_e}\frac{\Delta-\omega}{(\Delta-\omega)^2+4g^2N_e}\begin{pmatrix}0 & -1\\ 1 & 0\end{pmatrix}. \tag{6.27}$$

Again this analytical expression allows the study of some details of the Jaynes Cummings model, this time for varying the coupling strength. There is another zero point, this time for $\Delta = \omega$ and not $g = 0$, as $\dot{g} \neq 0$ so the coupling strength cannot stay zero. This zero point can be easiest explained by looking at the eigenstates again and seeing β_{N_e} is always $\frac{\pi}{4}$ when $\Delta = \omega$, meaning the basis is stationary again and maximally mixed. interestingly when the energy scale of the spin and boson are equal the splitting between the eigenstates is only dependent on the coupling strength, which even if it is varying plays no role in the diabatic excitations in this case.

The limiting case of large excitation manifold, again decays down for large N_e

$$\hat{\mathcal{A}}_g^{(N_e),\text{stationary}} \approx i\frac{(\Delta-\omega)}{4g^2\sqrt{N_e}}\begin{pmatrix}0 & 1\\ -1 & 0\end{pmatrix}, \tag{6.28}$$

in a similar form to what we saw with varying the spin energy, where it scales inverses with the square root. With the functional form being so similar to Eq. (6.19), up to factors of Δ, ω and g, it may not be surprising that the stationary point is also the same at

$$N_e = \frac{(\Delta-\omega)^2}{4g^2}. \tag{6.29}$$

Likewise the functional form of the operator is the same as for varying the spin energy, up to a factor of -1 depending on if $\Delta > \omega$ or $\Delta < \omega$. So even though the coupling between the modes is what leads to the interesting results in the Jaynes Cummings model (as otherwise the two subsystems are independent), varying the strength has the same effect as varying the spin energy. As such we would expect similar for varying ω in the following subsection, however the effect of the non-stationary creation and

annihilation operators will distinguish that case.

6.1.3 Varying the cavity frequency

Next we shall discus the AGP for changing the frequency of the cavity photons (ω). Similar to the previous subsection, we can compute the partial derivative with respect to ω, remembering to take the derivatives of $\hat{a}$ and $\hat{a}^\dagger$

$$\partial_\omega \hat{H}_{JC} = \hat{a}^\dagger \hat{a} + \frac{1}{2}\left(\hat{a}^\dagger \hat{a}^\dagger + \hat{a}\hat{a}\right) + \frac{g}{2\omega}\left(\hat{a}\hat{\sigma}^- + \hat{a}^\dagger \hat{\sigma}^+\right). \tag{6.30}$$

If we apply the first term in this expression to our eigenstates we get

$$\hat{a}^\dagger \hat{a}\,|N_e, +\rangle = \left((N_e - 1)\cos\left(\beta_{N_e}\right)|N_e - 1, \uparrow\rangle + N_e \sin\left(\beta_{N_e}\right)|N_e, \downarrow\rangle\right), \tag{6.31}$$

$$\hat{a}^\dagger \hat{a}\,|N_e, -\rangle = \left((N_e - 1)\sin\left(\beta_{N_e}\right)|N_e - 1, \uparrow\rangle - N_e \cos\left(\beta_{N_e}\right)|N_e, \downarrow\rangle\right). \tag{6.32}$$

These stay within the manifold with N_e excitations, and leads to a similar result seen with varying Δ and g.

However if we apply the next two terms in the derivative, we instead get

$$\begin{aligned}
\frac{1}{2}\hat{a}^\dagger \hat{a}^\dagger\,|N_e, +\rangle =& \frac{1}{2}\Big(\sqrt{N_e + 1}\sqrt{N_e}\cos\left(\beta_{N_e}\right)|N_e + 1, \uparrow\rangle \\
&+ \sqrt{N_e + 2}\sqrt{N_e + 1}\sin\left(\beta_{N_e}\right)|N_e + 2, \downarrow\rangle\Big), \qquad (6.33)\\
\frac{1}{2}\hat{a}^\dagger \hat{a}^\dagger\,|N_e, -\rangle =& \frac{1}{2}\Big(\sqrt{N_e + 1}\sqrt{N_e}\sin\left(\beta_{N_e}\right)|N_e + 1, \uparrow\rangle \\
&- \sqrt{N_e + 2}\sqrt{N_e + 1}\cos\left(\beta_{N_e}\right)|N_e + 2, \downarrow\rangle\Big), \qquad (6.34)\\
\frac{1}{2}\hat{a}\hat{a}\,|N_e, +\rangle =& \frac{1}{2}\Big(\sqrt{N_e - 2}\sqrt{N_e - 1}\cos\left(\beta_{N_e}\right)|N_e - 3, \uparrow\rangle \\
&+ \sqrt{N_e - 1}\sqrt{N_e}\sin\left(\beta_{N_e}\right)|N_e - 2, \downarrow\rangle\Big), \qquad (6.35)\\
\frac{1}{2}\hat{a}\hat{a}\,|N_e, -\rangle =& \frac{1}{2}\Big(\sqrt{N_e - 2}\sqrt{N_e - 1}\sin\left(\beta_{N_e}\right)|N_e - 3, \uparrow\rangle \\
&- \sqrt{N_e - 1}\sqrt{N_e}\cos\left(\beta_{N_e}\right)|N_e - 2, \downarrow\rangle\Big). \qquad (6.36)
\end{aligned}$$

These states are outside of the excitation manifold, and as such the operator appears to break the RWA. This suggests that by varying the cavity frequency, the initial

assumption of ignoring the counter rotating terms is no longer valid, and the Jaynes-Cummings Hamiltonian as such is also invalid in this case. For the interest of the calculation, we will continue by assuming the Hamiltonian given in Eq. (6.2) is valid even when varying the frequency. We shall also continue referring to this as the Jaynes-Cummings model, although this is fundamentally a different model. For a more accurate description of the underlying physical model, we suggest using the full Rabi model as we shall discuss in Sec. 6.2.

So when varying ω, there are non-zero excitations between excitation manifolds and N_e is no longer a conserved quantity. Similarly if we apply the final term in the derivative, we get

$$\begin{aligned}\frac{g}{2\omega}\left(\hat{a}\hat{\sigma}^- + \hat{a}^\dagger\hat{\sigma}^+\right)|N_e,+\rangle =& \frac{g}{2\omega}\left(\sqrt{N_e+1}\sin\left(\beta_{N_e}\right)|N_e+1,\uparrow\rangle\right.\\ &\left.+\sqrt{N_e-1}\cos\left(\beta_{N_e}\right)|N_e-2,\downarrow\rangle\right), \qquad (6.37)\\ \frac{g}{2\omega}\left(\hat{a}\hat{\sigma}^- + \hat{a}^\dagger\hat{\sigma}^+\right)|N_e,-\rangle =& \frac{g}{2\omega}\left(-\sqrt{N_e+1}\cos\left(\beta_{N_e}\right)|N_e+1,\uparrow\rangle\right.\\ &\left.+\sqrt{N_e-1}\sin\left(\beta_{N_e}\right)|N_e-2,\downarrow\rangle\right). \qquad (6.38)\end{aligned}$$

Again this term does not preserve the excitation number.

One detail however is that the parity of the excitation is maintained, as the above shows that only states with two more or two fewer excitations are present. This means the AGP can be written in either the odd or even parity subsection, but both of these still has an infinite Hilbert space. In general the AGP will defined on a chain like system, where there are diabatic excitations between consecutive even or odd parity sectors. However if we focus on a given eigenstate $|N_e,\pm\rangle$, we have coupling only to $|N_e,\mp\rangle$ via $a^\dagger a$, and coupling to $|N_e+2,\pm\rangle$,$|N_e-2,\pm\rangle$ from the other non RWA terms. This means a state dependent AGP can be found in this local six dimensional Hilbert space, but this will only be valid if the AGP is exact, as a small excitation into one of the other states will couple to the next consecutive parity sector (jump of two eg. $N_e\pm 2$), breaking the assumption. In particular for the zero excitation state $|0,\downarrow\rangle$, there are only couplings to $|2,+\rangle$ and $|2,-\rangle$ which make it far simpler to compute. This zero excitation state is in fact the ground state of the model with energy $E_0=-\frac{\Delta}{2}$, whilst

the energy in Eq. (6.6) stays larger than this value. The state $|1,-\rangle$ will be the first state to cross the energy value of E_0, and as such we can find the inequality for where $|0,\downarrow\rangle$ is the ground state changes to be

$$\begin{aligned} E_0 <& E_{1,-} \\ -\frac{\Delta}{2} <& \frac{\omega}{2} - \frac{1}{2}\sqrt{(\Delta-\omega)^2+4g^2} \\ (\Delta+\omega)^2 >& (\Delta-\omega)^2+4g^2 \\ \Delta\omega >& g^2. \end{aligned} \tag{6.39}$$

As the most common application of the AGP is for ground state following, we shall avoid the full AGP and instead create a state specific AGP for the zero excitation state. We implicitly assume Eq. (6.39) holds by referring to this state as the ground state interchangeably.

For a state specific AGP, we only need to compute the rows and columns of the AGP that involve that state, and we set all other values to zero. This is because, if implemented exactly, the state will not change during the dynamics, so we only need to counteract the diabatic excitations to this specific state. As such we write the groundstate AGP as

$$\hat{\mathcal{A}}_\omega^{GS} = \begin{pmatrix} 0 & \langle 0,\downarrow|\,\hat{\mathcal{A}}_\omega^{GS}\,|2,+\rangle & \langle 0,\downarrow|\,\hat{\mathcal{A}}_\omega^{GS}\,|2,-\rangle \\ -\langle 0,\downarrow|\,\hat{\mathcal{A}}_\omega^{GS}\,|2,+\rangle & 0 & 0 \\ -\langle 0,\downarrow|\,\hat{\mathcal{A}}_\omega^{GS}\,|2,-\rangle & 0 & 0 \end{pmatrix}. \tag{6.40}$$

Using Eq. (2.34) again, we can compute these elements by applying $\langle 0,g|$ to the previous calculations with setting $N_e = 2$. Doing so gives the result

$$\begin{aligned} \langle 0,\downarrow|\,\hat{\mathcal{A}}_\omega^{GS}\,|2,+\rangle =& i\frac{\langle 0,\downarrow|\,\partial_\omega \hat{H}_{JC}\,|2,+\rangle}{E_{2,+}-E_{0,\downarrow}} \\ =& i\frac{\frac{1}{\sqrt{2}}\sin(\beta_2)+\frac{g}{2\omega}\cos(\beta_2)}{(\frac{1}{2}\Delta+\frac{3}{2}\omega+\frac{1}{2}\sqrt{(\Delta-\omega)^2+8g^2})}, \\ \langle 0,\downarrow|\,\hat{\mathcal{A}}_\omega^{GS}\,|2,-\rangle =& i\frac{\langle 0,\downarrow|\,\partial_\omega \hat{H}_{JC}\,|2,-\rangle}{E_{2,-}-E_{0,\downarrow}} \end{aligned} \tag{6.41}$$

$$=i\frac{-\frac{1}{\sqrt{2}}\cos(\beta_2)+\frac{g}{2\omega}\sin(\beta_2)}{(\frac{1}{2}\Delta+\frac{3}{2}\omega-\frac{1}{2}\sqrt{(\Delta-\omega)^2+8g^2})}, \tag{6.42}$$

$$\tag{6.43}$$

This is then the groundstate AGP for varying ω, whilst Eq. 6.39 holds, which is true also for adding varying Δ and g as they do not cause any diabatic excitations to $\langle 0,\downarrow|$.

Now we need to transform into a stationary basis, which for the spin part is similar to before when we computed the AGP for varying Δ or g, by converting from $|+\rangle, |-\rangle$ to $|\downarrow\rangle, |\uparrow\rangle$. This is slightly different to before as the ground state is already in the spin stationary basis $|\downarrow\rangle$. We wish a matrix in the form

$$\hat{\mathcal{A}}^{GS}_{\omega}=\begin{pmatrix} 0 & \langle 0,\downarrow|\hat{\mathcal{A}}^{GS}_{\omega}|1,\uparrow\rangle & \langle 0,\downarrow|\hat{\mathcal{A}}^{GS}_{\omega}|2,\downarrow\rangle \\ -\langle 0,\downarrow|\hat{\mathcal{A}}^{GS}_{\omega}|1,\uparrow\rangle & 0 & 0 \\ -\langle 0,\downarrow|\hat{\mathcal{A}}^{GS}_{\omega}|2,\downarrow\rangle & 0 & 0 \end{pmatrix}, \tag{6.44}$$

so we can re write this in terms of the previous matrix elements. We can calculate the first matrix element as

$$\begin{aligned}\langle 0,\downarrow|\hat{\mathcal{A}}^{GS}_{\omega}|1,\uparrow\rangle &= \langle 0,\downarrow|\hat{\mathcal{A}^{GS}_{\omega}}(\cos(\beta_2)|2,+\rangle+\sin(\beta_2)|2,-\rangle)\\ &=\cos(\beta_2)\langle 0,\downarrow|\hat{\mathcal{A}}^{GS}_{\omega}|2,+\rangle+\sin(\beta_2)\langle 0,\downarrow|\hat{\mathcal{A}}^{GS}_{\omega}|2,-\rangle.\end{aligned} \tag{6.45}$$

To help the clarity of the following steps, we define

$$\Omega=\frac{1}{2}\Delta+\frac{3}{2}\omega,\quad \zeta=\frac{1}{2}\sqrt{(\Delta-\omega)^2+8g^2}. \tag{6.46}$$

Using this we can compute the element to be

$$\langle 0,\downarrow|\hat{\mathcal{A}}^{GS}_{\omega}|1,\uparrow\rangle=i\frac{-\frac{1}{\sqrt{2}}\zeta\sin(2\beta_2)-\zeta\frac{g}{2\omega}\cos(2\beta_2)+\Omega\frac{g}{2\omega}}{\Omega^2-\zeta^2}. \tag{6.47}$$

The trigonometric functions can be simplified using Eqs. (6.14),(6.15) with $N_e=2$, to

give

$$\sin(2\beta_2) = \frac{g2\sqrt{2}}{\sqrt{(\Delta-\omega)^2+8g^2}} = \frac{g\sqrt{2}}{\zeta}. \tag{6.48}$$

$$\cos(2\beta_2) = \frac{\Delta-\omega}{\sqrt{(\Delta-\omega)^2+8g^2}} = \frac{\Delta-\omega}{2\zeta}. \tag{6.49}$$

We can also substitute in the values of Ω and ζ into the denominator to get

$$\begin{aligned}\Omega^2-\zeta^2 =& \left(\frac{1}{2}\Delta+\frac{3}{2}\omega\right)^2 - \frac{1}{4}\left((\Delta-\omega)^2+8g^2\right)\\ =& 2\omega(\Delta+\omega)-2g^2.\end{aligned} \tag{6.50}$$

Combining these together gives the result

$$\begin{aligned}\langle 0,\downarrow|\hat{\mathcal{A}}^{GS}_{\omega}|1,\uparrow\rangle =& i\frac{-g-\frac{g(\Delta-\omega)}{4\omega}+\left(\frac{1}{2}\Delta+\frac{3}{2}\omega\right)\frac{g}{2\omega}}{2\omega(\Delta+\omega)-2g^2}\\ =& i\frac{\frac{\Delta g}{4\omega}-\frac{\Delta g}{4\omega}+\frac{g}{4}-g+\frac{3g}{4}}{2\omega(\Delta+\omega)-2g^2}.\\ =& 0\end{aligned} \tag{6.51}$$

Surprisingly this results in a value of zero, indicating there are no diabatic excitations from $\langle 0,\downarrow|$ to $|1,\uparrow\rangle$. This occurs because the diabatic excitations to $|2,+\rangle$ exactly cancels out the diabatic excitation to $|2,-\rangle$, meaning the spin stationary basis is in fact simpler to compute.

A similar set of steps can be done for the other matrix element, which we expect to be non zero this time. We first substitute in $|2,\downarrow\rangle$ in terms of $|2,\pm\rangle$, to get

$$\langle 0,\downarrow|\hat{\mathcal{A}}^{GS}_{\omega}|2,\downarrow\rangle = \sin(\beta_2)\langle 0,\downarrow|\hat{\mathcal{A}}^{GS}_{\omega}|2,+\rangle - \cos(\beta_2)\langle 0,\downarrow|\hat{\mathcal{A}}^{GS}_{\omega}|2,-\rangle. \tag{6.52}$$

Then substituting in the matrix elements leads to the expression

$$\langle 0,\downarrow|\hat{\mathcal{A}}^{GS}_{\omega}|2,\downarrow\rangle = i\frac{\frac{1}{\sqrt{2}}\zeta\cos(2\beta_2)-\zeta\frac{g}{2\omega}\sin(2\beta_2)+\Omega\frac{1}{\sqrt{2}}}{\Omega^2-\zeta^2}. \tag{6.53}$$

We then use the expressions for the trigonometric functions and the denominator to

get

$$\begin{aligned}\langle 0,\downarrow|\,\mathcal{A}_\omega^{GS}\,|2,\downarrow\rangle =& i\frac{\frac{\Delta-\omega}{2\sqrt{2}}-\frac{g^2\sqrt{2}}{2\omega}+\left(\frac{1}{2}\Delta+\frac{3}{2}\omega\right)\frac{1}{\sqrt{2}}}{2\omega\left(\Delta+\omega\right)-2g^2}\\ =& i\frac{1}{2\sqrt{2}}\frac{1}{\omega}.\end{aligned} \tag{6.54}$$

This results in a rather simple expression, that as we show in App. A.9 is identical to the case of the groundstate AGP of the Harmonic oscillator. Unlike the other results for varying Δ and g, the coupling and the spin part play no role in the diabatic dynamics for varying ω. As such the only contribution to the diabatic excitations, come from the non-stationary nature of the creation and annihilation operators. We can make sense of this as we know the zero excitation state $\langle 0,\downarrow|$ has no pair, so only the coupling to the $N_e = 2$ excitation manifold can cause the diabatic excitations, which is only dependent on ω. For the same reasons, we can reason that for excitation manifold with $N_e \neq 0$, the result will be more complicated and likely be dependent on Δ and g.

Now we have an expression with stationary basis states for the spin, however we know that these basis states are not stationary for the bosonic part, because the creation and annihilation operators are non-stationary. To circumvent this problem one way to proceed is to write the cavity part of the AGP and Hamiltonian in the position basis. We can convert the Hamiltonian by replacing $\hat{a}, \hat{a}^\dagger \to \hat{x}, \hat{p}$ using the relation

$$\hat{a} = \sqrt{\frac{m\omega}{2\hbar}}\left(\hat{x}+\frac{i}{m\omega}\hat{p}\right), \tag{6.55}$$

$$\hat{a}^\dagger = \sqrt{\frac{m\omega}{2\hbar}}\left(\hat{x}-\frac{i}{m\omega}\hat{p}\right). \tag{6.56}$$

The Hamiltonian can then be re expressed, with setting $m = 1, \hbar = 1$, as

$$\begin{aligned}\hat{H}_{JC} =& \frac{\Delta}{2}\hat{\sigma}^z+\frac{\omega^2}{2}\left(\hat{x}^2-\frac{1}{\omega}+\frac{1}{\omega^2}\hat{p}^2\right)+g\sqrt{\frac{\omega}{2}}(\hat{x}\left(\hat{\sigma}^+ +\hat{\sigma}^-\right)+\frac{i}{\omega}\hat{p}\left(\hat{\sigma}^+ -\hat{\sigma}^-\right))\\ =& \frac{\Delta}{2}\hat{\sigma}^z+\frac{\omega^2}{2}\left(\hat{x}^2-\frac{1}{\omega}+\frac{1}{\omega^2}\hat{p}^2\right)+g\sqrt{\frac{\omega}{2}}(\hat{x}\hat{\sigma}^x-\frac{1}{\omega}\hat{p}\hat{\sigma}^y)\\ =& \frac{\Delta}{2}\hat{\sigma}^z+\frac{\omega^2}{2}\hat{x}^2-\frac{\omega}{2}+\frac{1}{2}\hat{p}^2+g\sqrt{\frac{\omega}{2}}\hat{x}\hat{\sigma}^x-g\sqrt{\frac{1}{2\omega}}\hat{p}\hat{\sigma}^y.\end{aligned} \tag{6.57}$$

We can then express the momentum operator $\hat{p}$ as the partial derivative of position, $\hat{p} = -i\frac{\hat{\partial}}{\partial x}$, and write everything in terms of the positon basis. Doing so we get

$$\hat{H}_{JC} = \frac{\omega^2}{2}\hat{x}^2 - \frac{\omega}{2} + g\sqrt{\frac{\omega}{2}}\hat{x}\hat{\sigma}^x + \frac{\Delta}{2}\hat{\sigma}^z + ig\sqrt{\frac{1}{2\omega}}\hat{\sigma}^y\frac{\hat{\partial}}{\partial x} - \frac{1}{2}\frac{\hat{\partial}^2}{\partial x^2} \tag{6.58}$$

The final step is a position basis representation of the Fock state $|n\rangle$. This is equal to the nth eigenstate of the harmonic oscillator, which in the position basis is [148]

$$\langle x|n\rangle = \psi_n(x) = \frac{1}{\sqrt{2^n n!}}\left(\frac{\omega}{\pi}\right)^{\frac{1}{4}} e^{-\frac{\omega x^2}{2}} \mathrm{H}_n\left(\sqrt{\omega}x\right), \tag{6.59}$$

with H_n being the n-th Hermite polynomial [149]. We wish to know the position basis representation of $|0\rangle$ and $|2\rangle$, so we need only H_0 and H_2, which are given as

$$\mathrm{H}_0(z) = 1, \tag{6.60}$$

$$\mathrm{H}_2(z) = 4z^2 - 2. \tag{6.61}$$

Then we can write the groundstate AGP in terms of ket-bra outer products, which only has one non zero Hermitian term

$$\hat{\mathcal{A}}_\omega^{GS} = i\frac{1}{2\sqrt{2}\omega}\left(|0,\downarrow\rangle\langle 2,\downarrow| - |2,\downarrow\rangle\langle 0,\downarrow|\right). \tag{6.62}$$

These ket and bra states can be expressed using Eq. (6.59) as $|0,\downarrow\rangle = \psi_0(x)|x,\downarrow\rangle$ and $|2,\downarrow\rangle = \psi_2(x)|x,\downarrow\rangle$. Combining this all together we can simulate the Jaynes Cummings model in a stationary basis, such that the diabatic excitations that occur are correct.

6.1.4 Simulation results of counterdiabatic driving

We now wish to simulate the Jaynes Cummings model for each of the different parameters being varied, to see the effect of counterdiabatic driving in each of the cases. For varying Δ and g we can use truncated creation and annihilation operators to represent the system, as the operators are stationary. However as we just discussed in Sec. 6.1.3, when varying the cavity we need to use a position basis. To numerically simulate this

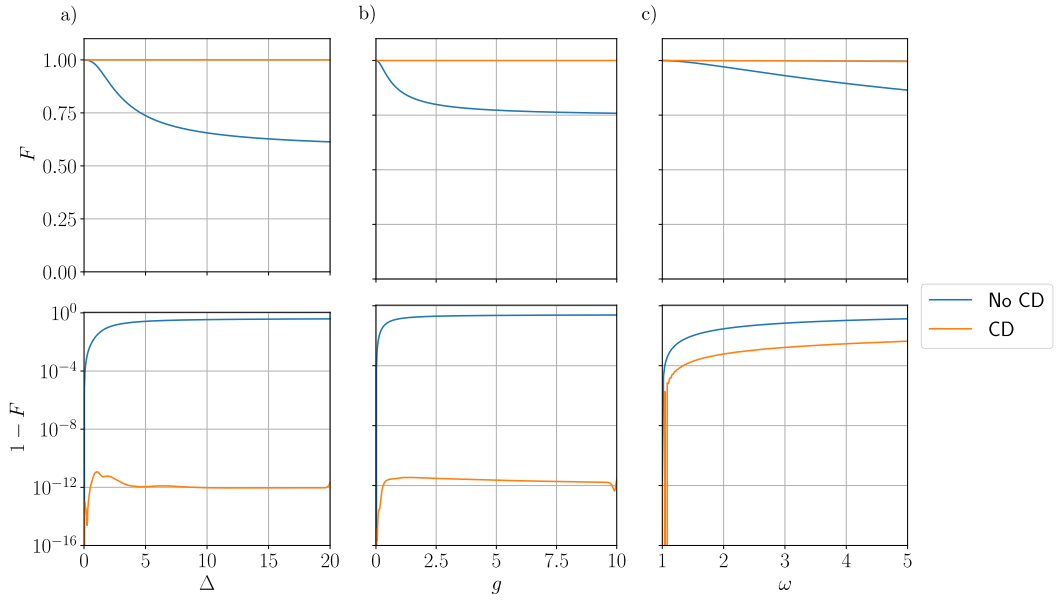

Figure 6.1: Panel a) shows the average fidelity across all eigenstates for the JC model, with and without applying the counterdiabatic driving for driving the spin energy Δ, for $N = 10$, $\omega = 1$, $g = 1$ and $\dot{\Delta} = 1000$. Panel b) shows the average fidelity across all eigenstates for the JC model, with and without applying the counterdiabatic driving for driving the coupling strength g, for $N = 10$, $\Delta = 0.1$, $\omega = 1$ and $\dot{g} = 1000$. Panel c) show the fidelity with the ground state for varying ω in Jaynes Cummings model, with the simulation parameters $\Delta = 10$, $g = 10$ and $\dot{\omega} = 100$ simulated on a one dimensional grid between $-5 \leq x \leq 5$ with a difference between consecutive points $\Delta x = 0.01$.

case, we can use finite differences to compute the partial derivative of the position operator. We use the central finite difference to approximate the first and second order derivatives as

$$\frac{\partial f(x)}{\partial x} \approx \frac{f(x + \Delta x) - f(x - \Delta x)}{2\Delta x}, \tag{6.63}$$

$$\frac{\partial^2 f(x)}{\partial x^2} \approx \frac{f(x + \Delta x) - 2f(x) + f(x - \Delta x)}{\Delta x^2}. \tag{6.64}$$

We then plot the results of our simulation in Fig. 6.1 for all the parameters. In Fig. 6.1-a we see the average fidelity of all eigenstates for varying Δ, where we compare

to the case of no driving at all. Without counterdiabatic driving, there are large diabatic excitations, leading to an average fidelity $F \approx 0.6$, compared to the near perfect fidelity $1 - F \approx 10^{-11}$ with the counterdiabatic driving. In Fig. 6.1-b we show results of average fidelity again now for varying g, where we now get a fidelity $F \approx 0.7$ without counterdiabatic driving, and again with the counterdiabatic driving $1 - F \approx 10^{-11}$. Finally in Fig. 6.1-c we plot the fidelity whilst varying ω found between the ground state and the dynamic state with and without counterdiabatic driving. We find as expected that the counterdiabatic case outperforms the case with no driving, with good fidelity with the ground state during the dynamics, however it does not reach the levels of precision we have seen in the simulations of other parameters. This is because the method of finite differences we have applied is not particularly precise for the simulation parameters we use, as such a more detailed simulation potentially using a different more accurate method would see better results. As this simulation is just to test the results from Eqs. (6.51),(6.54), we are not as worried about machine level precision of simulation, and instead we test the same simulation method to the Harmonics oscillator in App. A.9, and find similar levels of error margins. We as such are confident that the result for the AGP here is correct, and leave the more accurate and precise simulation of the model to later research.

6.1.5 Operator form of the Jaynes Cummings AGP

In this section so far we have computed the matrix elements of the AGP for the Jaynes Cummings model, and given these as small operators acting on either a specific excitation manifold for Δ and g or the first order diabatic coupling to the ground state for ω. When the diabatic excitations are within the same excitation manifold, the operator form is

$$\hat{\mathcal{A}}_{\Delta,g} = \sum_{N_e=0}^{\infty} i\alpha_{N_e}^{(\Delta,g)} \left(|N_e, +\rangle \langle N_e, -| - |N_e, -\rangle \langle N_e, +| \right), \tag{6.65}$$

Where $\alpha_{N_e}^{(\Delta,g)}$ is the coefficient from the previous results. This operator is effectively a $\hat{\sigma}^y$ within each excitation manifold, so we can write it by using a projector operator instead.

We define the projector $\hat{\mathcal{P}}_{N_e}$ as

$$\hat{\mathcal{P}}_{N_e} |n, \pm\rangle = \delta_{N_e,n} |N_e, \pm\rangle , \tag{6.66}$$

where $\delta_{N_e,n}$ is the Kronecker delta function. This means we can write the AGP in operator form as

$$\hat{\mathcal{A}}_{\Delta,g} = \sum_{N_e=0}^{\infty} \frac{i\alpha_{N_e}^{(\Delta,g)}}{N_e} \hat{\mathcal{P}}_{N_e}^{\dagger} \left(\hat{a}^{\dagger}\hat{\sigma}^{-} - \hat{a}\hat{\sigma}^{+} \right) \hat{\mathcal{P}}_{N_e}. \tag{6.67}$$

A similar expression would be able to be computed for the ground state AGP as well, by projecting into the subsystem of first order diabatic coupling to the ground state instead.

However because the AGP has this simple form with projection operators, it also means that computing these in terms of purely creation and annihilation operators is much more complicated. If we try and get an expression for a projector to a specific bosonic excitation, in terms of powers of $\hat{a}$ and $\hat{a}^{\dagger}$, we get

$$\hat{\mathcal{P}}_n = \sum_{l}^{\infty} A_l^n \left((\hat{a}^{\dagger})^l \hat{a}^l \right) \tag{6.68}$$

Note this is a different projection operator to $\mathcal{P}_{N_e}$, which would be a combination of two of these projection operators and spin raising/lowering operators. To ensure the states with less excitations than n are zero, we can simply set $A_l^n = 0$ for $l < n$, then we set $A_n^n = \frac{1}{n!}$ to normalise the nth bosonic excitation. Then we need to set each A_l^n for $l > n$, to negate the contributions from higher bosonic modes. This means all A_l^n for $l \geq n$ are non zero, as there is always a small error on large bosonic modes left over whenever a finite number is taken, similar to how $\left[\hat{a}, \hat{a}^{\dagger}\right] \neq 1$ for a finite truncation. As such, if you compute the AGP using the commutator approach on a creation and annihilation basis, you shall end up with an infinite sum of results that only cancel each other out for all modes other than n, masking the actual simplicity of the result when the projected basis is used.

6.2 The Rabi model

The last model we shall discuss in this thesis, is the Rabi model [150]. As described at the beginning of this chapter, this model is the same as the Jaynes Cummings model but with no rotating wave approximation, leading to counter rotating terms being present. Unlike the JC model, the Rabi model has no simple diagonalization, but there are exact solutions to the model [151]. Working with these exact solutions can be difficult, so numerical simulation is often used to study the model, or specific parameter regimes where approximations can be made [152]. As we have seen before, the bosonic mode has an infinite sized basis so it needs to be truncated to a maximum occupation, leading to it being effectively a large spin up to frequency dependence on the operators. In Sec. 5.1.2, we showed that this approximation does fundamentally change the physics of the AGP from the change in the commutator, however it is still expected to converge to the same result for a large enough truncation. In this thesis we do not study this convergence, and instead focus purely on the large spin approximation.

The Hamiltonian for the Rabi model can be written as

$$\hat{H}_{Rabi} = \frac{\Delta}{2}\hat{\sigma}^z + \omega\hat{a}^\dagger\hat{a} + g\hat{\sigma}^x\left(\hat{a}^\dagger + \hat{a}\right). \tag{6.69}$$

As there is not exact solution that is easy to use, we choose to truncate the bosonic mode into a spin of size N, using the generalised Gell-Mann basis (GGM Sec. 3.4.3) to represent this. The bosonic operators present can be expressed as

$$\hat{a} + \hat{a}^\dagger = 2\sum_{n=2}^{N}\sqrt{n-1}\hat{S}_{S_{n,n-1}}, \tag{6.70}$$

$$\hat{a}^\dagger\hat{a} = \frac{(N-1)}{2}\hat{\mathbb{I}} - \sum_{n=2}^{N}\sqrt{\frac{n(n-1)}{2}}\hat{S}_{D_n}, \tag{6.71}$$

which can then be applied to the Hamiltonian to give

$$\hat{H}_{Rabi} = \frac{\Delta}{2}\left(\hat{\sigma}^z \otimes \hat{\mathbb{I}}\right) + \omega\frac{(N-1)}{2}\left(\hat{\mathbb{I}} \otimes \hat{\mathbb{I}}\right) + \sum_{n=2}^{N}\omega\sqrt{\frac{n(n-1)}{2}}\left(\hat{\mathbb{I}} \otimes \hat{S}_{D_n}\right)$$

$$+ 2g \sum_{n=2}^{N} \sqrt{n-1} \left(\hat{\sigma}^x \otimes \hat{S}_{S_{n,n-1}} \right). \tag{6.72}$$

From here onwards, whenever we shall always be referring to this spin truncated Hamiltonian for the Rabi model. The reader may find it helpful to treat this section as more of a coupling between a two level spin and a large spin, as this is technically what we are doing, even if in the large N limit this represents the Rabi Hamiltonian. We shall not make any assumption about N being large during the calculations, so the results are also valid for the smaller N spin case.

Now whilst the standard GGM basis will work for the Rabi model, this leads to slightly overcomplicated commutation relations in some parts. For example, an anti-commutator of the form $\left\{ \hat{S}_{S_{n+1,n}}, \hat{S}_{S_{n+1,n}} \right\}$ is given by

$$\begin{aligned} \left\{ \hat{S}_{S_{n+1,n}}, \hat{S}_{S_{n+1,n}} \right\} =& \frac{1}{N} \hat{\mathbb{I}} - \sqrt{\frac{n-1}{2n}} \hat{S}_{D_n} + \frac{1-n}{\sqrt{2n(n+1)}} \hat{S}_{D_{n+1}} \\ &+ \sum_{k=n+2}^{N} \sqrt{\frac{2}{k(k-1)}} \hat{S}_{D_k}, \end{aligned} \tag{6.73}$$

with diagonal elements going all the way up to $\hat{S}_{D_N}$, leading to a massive number of operators appearing. However, if we compute this directly in a matrix form, showing only the n and $n+1$ matrix elements (as all others are zero), we get

$$\left\{ \hat{S}_{S_{n+1,n}}, \hat{S}_{S_{n+1,n}} \right\} = 2 \begin{pmatrix} 0 & \frac{\hbar}{2} \\ \frac{\hbar}{2} & 0 \end{pmatrix} \begin{pmatrix} 0 & \frac{\hbar}{2} \\ \frac{\hbar}{2} & 0 \end{pmatrix} \tag{6.74}$$

$$= \begin{pmatrix} \frac{\hbar^2}{2} & 0 \\ 0 & \frac{\hbar^2}{2} \end{pmatrix}. \tag{6.75}$$

This is a significantly simpler appearing result than when represented by $\hat{S}_{D_k}$, even thought the two results are equivalent. In fact similar cases repeatedly appear, where a sum over many $\hat{S}_{D_k}$ is required to cancel out diagonal elements that need to be zero. Whilst in general, $\hat{S}_{D_k}$ is useful as it can represent the $\mathfrak{su}(N)$ group, in this case we only wish to simplify our results as much as possible.

If we write this anti-commutator in terms of projectors, we need only write

$$\left\{\hat{S}_{n,n-1}, \hat{S}_{n,n-1}\right\} = \hat{\mathcal{P}}_n \frac{\hbar^2}{2} + \hat{\mathcal{P}}_{n+1} \frac{\hbar^2}{2}, \tag{6.76}$$

where

$$\hat{\mathcal{P}}_n = |n\rangle \langle n| . \tag{6.77}$$

These projectors are not traceless, however we only require our basis to be trace orthonormal. We can check this by computing the trace products

$$\mathrm{Tr}\left(\hat{\mathcal{P}}_l, \hat{S}_{S_{n,m}}\right) = \mathrm{Tr}\left(\hat{\mathcal{P}}_l, \hat{S}_{A_{n,m}}\right) = 0, \quad \mathrm{Tr}\left(\hat{\mathcal{P}}_l, \hat{\mathcal{P}}_k\right) = \delta_{l,k}, \quad \mathrm{Tr}\left(\hat{\mathcal{P}}_l, \hat{\mathbb{I}}\right) = 1,$$

which means they are in fact trace orthonormal, except with the identity operator ($\hat{\mathbb{I}}$). However this is because the identity operator is linearly dependent on the delta functions, $\hat{\mathbb{I}} = \sum_l \hat{\mathcal{P}}_l$, so we can remove the identity operator from the basis and express it purely in terms of the projectors.

This means for the Rabi model we use an adjusted Gell-Mann basis, given by

$$\hat{S}_j \in \left\{\hat{S}_{S_{n,m}}, \hat{S}_{A_{n,m}}, \hat{\mathcal{P}}_n\right\}. \tag{6.78}$$

This means Eq. (6.72) can now be written as

$$\hat{H}_{Rabi} = \frac{\Delta}{2} \sum_{n=1}^{N} \left(\hat{\sigma}^z \otimes \hat{\mathcal{P}}_n\right) + \omega \sum_{n=2}^{N} (n-1) \left(\hat{\mathbb{I}} \otimes \hat{\mathcal{P}}_n\right) + 2g \sum_{n=2}^{N} \sqrt{n-1} \left(\hat{\sigma}^x \otimes \hat{S}_{S_{n,n-1}}\right). \tag{6.79}$$

This change of basis will greatly reduce the complexity of the coming calculations, without changing the final result.

6.2.1 The Lie basis and general commutation in the Rabi model

For the following calculations it will be helpful to specify exactly what the effect of applying the commutator $[\hat{H}_{Rabi}, \cdot]$ is, rather than having to use the full structure constants of the GGM. To solve for the AGP, we only ever need to apply the commutator to the AGP operator, so we shall also limit to this case. As the Hamiltonian is real, we

know the AGP must be completely imaginary, so we get a splitting into

$$\left\{\hat{\mathbb{I}}, \hat{\sigma}^x, \hat{\sigma}^z\right\} \otimes \left\{\hat{S}_{A_{l,k}}\right\}, \tag{6.80}$$

$$\{\hat{\sigma}^y\} \otimes \left\{\hat{S}_{S_{l,k}}, \hat{\mathcal{P}}_l\right\}, \tag{6.81}$$

depending on with subspace is imaginary.

As we have two subspaces, we have commutation of the form

$$\left[\hat{\sigma}^a \otimes \hat{S}_\alpha, \hat{\sigma}^b \otimes \hat{S}_\beta\right] = \frac{1}{2}\left[\hat{\sigma}^a, \hat{\sigma}^b\right] \otimes \left\{\hat{S}_\alpha, \hat{S}_\beta\right\} + \frac{1}{2}\left\{\hat{\sigma}^a, \hat{\sigma}^b\right\} \otimes \left[\hat{S}_\alpha, \hat{S}_\beta\right]. \tag{6.82}$$

Due to the commutation and anti-commutation relations of the Pauli matrices (Eqs. (3.61) and (3.62)), only one of the commutator and anti-commutator can be non-zero at a time. As such we can rewrite Eq. (6.82) as

$$\left[\hat{\sigma}^a \otimes \hat{S}_\alpha, \hat{\sigma}^b \otimes \hat{S}_\beta\right] = \begin{cases} i\epsilon^c_{ab}\hat{\sigma}^c \otimes \left\{\hat{S}_\alpha, \hat{S}_\beta\right\}, & a \neq b \\ \hat{\mathbb{I}} \otimes \left[\hat{S}_\alpha, \hat{S}_\beta\right], & a = b \end{cases} \tag{6.83}$$

$$\left[\hat{\sigma}^a \otimes \hat{S}_\alpha, \hat{\mathbb{I}} \otimes \hat{S}_\beta\right] = \hat{\sigma}_a \otimes \left[\hat{S}_\alpha, \hat{S}_\beta\right]. \tag{6.84}$$

We will treat the spin, bosonic and interaction parts of the Hamiltonian as separate cases, which have the form

$$\hat{H}_S = \frac{\Delta}{2}\sum_{n=1}^{N} \hat{\sigma}^z \otimes \hat{\mathcal{P}}_n, \tag{6.85}$$

$$\hat{H}_B = \omega \sum_{n=2}^{N} (n-1)\hat{\mathbb{I}} \otimes \hat{\mathcal{P}}_n, \tag{6.86}$$

$$\hat{H}_I = 2g \sum_{n=2}^{N} \sqrt{n-1}\hat{\sigma}^x \otimes \hat{S}_{S_{n,n-1}}. \tag{6.87}$$

For the spin and bosonic parts, they only affect their respective subspace, so we can simply commute across the separate parts

$$\left[\hat{H}_S, \hat{\sigma}^i \otimes \hat{S}_j\right] = \frac{\Delta}{2}\left[\hat{\sigma}^z, \hat{\sigma}^i\right] \otimes \hat{S}_j, \tag{6.88}$$

$$\left[\hat{H}_B, \hat{\sigma}^i \otimes \hat{S}_j\right] = \omega \sum_{n=2}^{N} (n-1)\hat{\sigma}^i \otimes \left[\hat{\mathcal{P}}_n, \hat{S}_j\right]. \tag{6.89}$$

We note that because the identity operator has been replaced by a sum over projection operators for $\hat{H}_S$, this may not be as clear for this step, but remember the summation over all the projection operators results in the identity operator.

As for the interaction Hamiltonian, we find

$$\left[\hat{H}_I, \hat{\sigma}^i \otimes \hat{S}_j\right] = 2g \sum_{n=2}^{N} \sqrt{n-1} \begin{cases} \frac{1}{2}\left\{\hat{\sigma}^x, \hat{\sigma}^i\right\} \otimes \left[\hat{S}_{S_{n,n-1}}, \hat{S}_j\right], & \hat{\sigma}^i = \hat{\sigma}^x, \hat{\mathbb{I}} \\ \frac{1}{2}\left[\hat{\sigma}^x, \hat{\sigma}^i\right] \otimes \left\{\hat{S}_{S_{n,n-1}}, \hat{S}_j\right\}, & \hat{\sigma}^i = \hat{\sigma}^y, \hat{\sigma}^z \end{cases} \tag{6.90}$$

For the first case of $\hat{\sigma}^i = \hat{\sigma}^x, \hat{\mathbb{I}}$, this forces $\hat{S}_j \in \left\{\hat{S}_{A_{l,k}}\right\}$, whereas the second case is split, $\hat{\sigma}^i = \hat{\sigma}^z \to \hat{S}_j \in \left\{\hat{S}_{A_{l,k}}\right\}$ or $\hat{\sigma}^i = \hat{\sigma}^y \to \hat{S}_j \in \left\{\hat{\mathcal{P}}_l, \hat{S}_{S_{l,k}}\right\}$. This limits which indices we need to compute from the symmetric and anti-symmetric structure constants.

6.2.2 Commuting with the GGM

Looking at the GGM side of the commutation, the commutators and anti-commutators we need to compute are

$$\left[\hat{\mathcal{P}}_n, \hat{S}_{S_{l,k}}\right] = ?\,, \quad \left[\hat{\mathcal{P}}_n, \hat{S}_{A_{l,k}}\right] = ?\,, \quad \left[\hat{\mathcal{P}}_n, \hat{\mathcal{P}}_l\right] = ?\,, \quad \left[\hat{S}_{S_{n,n-1}}, \hat{S}_{A_{l,k}}\right] = ?\,, \tag{6.91}$$

$$\left\{\hat{S}_{S_{n,n-1}}, \hat{S}_{S_{l,k}}\right\} = ?\,, \quad \left\{\hat{S}_{S_{n,n-1}}, \hat{S}_{A_{l,k}}\right\} = ?\,, \quad \left\{\hat{S}_{S_{n,n-1}}, \hat{\mathcal{P}}_l\right\} = ?\,. \tag{6.92}$$

For the commutation with the projectors, and symmetric or anti-symmetric GGM we get

$$\left[\hat{\mathcal{P}}_n, \hat{S}_{S_{l,k}}\right] = \delta_{n,k} i \hat{S}_{A_{l,k}} - \delta_{n,l} i \hat{S}_{A_{l,k}}, \tag{6.93}$$

$$\left[\hat{\mathcal{P}}_n, \hat{S}_{A_{l,k}}\right] = -\delta_{n,k} i \hat{S}_{S_{l,k}} + \delta_{n,l} i \hat{S}_{S_{l,k}}. \tag{6.94}$$

The commutators between projectors are zero due to the fact that diagonal matrices

(such as the projectors) always commute. This means

$$\left[\hat{\mathcal{P}}_n, \hat{\mathcal{P}}_l\right] = 0. \tag{6.95}$$

For the final commutation in Eq. (6.91), between symmetric and anti-symmetric GGM there are two separate cases with non-zero commutation. By studying the structure constants in Sec. 3.4.3, we we find that the resulting operator can either be a diagonal GGM, which we write as a projector ($\hat{\mathcal{P}}_n$), or another symmetric GGM ($\hat{S}_{S_{n,m}}$). For the projector case, we can find the result

$$\left[\hat{S}_{S_{n,n-1}}, \hat{S}_{A_{n,n-1}}\right] = \frac{i}{2}\hat{\mathcal{P}}_{n-1} - \frac{i}{2}\hat{\mathcal{P}}_n, \tag{6.96}$$

which is notably simpler than expressing with diagonal GGM.

The case where we get another symmetric GGM, is itself split up into four separate cases

$$\left[\hat{S}_{S_{n,n-1}}, \hat{S}_{A_{l,k}}\right] = \begin{cases} if^{S_{n-1,k}}_{S_{n,n-1},A_{n,k}} \hat{S}_{S_{n-1,k}}, & l = n \\ if^{S_{n,k}}_{S_{n,n-1},A_{n-1,k}} \hat{S}_{S_{n,k}}, & l = n-1 \\ if^{S_{l,n-1}}_{S_{n,n-1},A_{l,n}} \hat{S}_{S_{l,n-1}}, & k = n \\ if^{S_{l,n}}_{S_{n,n-1},A_{l,n-1}} \hat{S}_{S_{l,n}}, & k = n-1 \end{cases}, \tag{6.97}$$

where the restriction on the final index can be found via ensuring the second index of each GGM operator is smaller than the first. This can be given explicitly as

$$\left[\hat{S}_{S_{n,n-1}}, \hat{S}_{A_{l,k}}\right] = \begin{cases} i\frac{1}{2}\hat{S}_{S_{n-1,k}}, & l = n \\ i\frac{1}{2}\hat{S}_{S_{n,k}}, & l = n-1 \\ -i\frac{1}{2}\hat{S}_{S_{l,n-1}}, & k = n \\ -i\frac{1}{2}\hat{S}_{S_{l,n}}, & k = n-1 \end{cases}. \tag{6.98}$$

The resulting effect on the second operator $\hat{S}_{A_{l,k}}$ is a swap from anti-symmetric to symmetric GGM, and an increase or decease by one to either index, with a change of sign if the second index is changed.

Now that the commutators have been computed, we must find all the non-zero anti-commutators containing $S_{S_{n,n-1}}$, which are listed in Eq. (6.92). Firstly we compute the anti-commutators between two symmetric GGM, which can result in either another symmetric GGM or a projector. These can be computed to get the result

$$\left\{\hat{S}_{S_{n,n-1}}, \hat{S}_{S_{l,k}}\right\} = \frac{1}{2}\begin{cases} \hat{S}_{S_{n-1,k}}, & l = n \\ \hat{S}_{S_{n,k}}, & l = n-1 \\ \hat{S}_{S_{l,n-1}}, & k = n \\ \hat{S}_{S_{l,n}}, & k = n-1 \end{cases}, \tag{6.99}$$

$$\left\{\hat{S}_{S_{n,n-1}}, \hat{S}_{S_{n,n-1}}\right\} = \frac{1}{2}\hat{\mathcal{P}}_n + \frac{1}{2}\hat{\mathcal{P}}_{n-1}. \tag{6.100}$$

Then for the anti-commutator with an anti-symmetric GGM, the resulting operator can only be another anti-symmetric GGM. This result turns out to be very similar to the commutator seen in Eq. (6.98), and is given by

$$\left\{\hat{S}_{S_{n,n-1}}, \hat{S}_{A_{l,k}}\right\} = \frac{1}{2}\begin{cases} \hat{S}_{A_{n-1,k}}, & l = n \\ \hat{S}_{A_{n,k}}, & l = n-1 \\ \hat{S}_{A_{l,n-1}}, & k = n \\ \hat{S}_{A_{l,n}}, & k = n-1 \end{cases}. \tag{6.101}$$

Finally the anti-commutator with a projector, results in a symmetric GGM, given by the result

$$\left\{\hat{S}_{S_{n,n-1}}, \hat{\mathcal{P}}_l\right\} = \delta_{l,n-1}\hat{S}_{S_{n,n-1}} + \delta_{l,n}\hat{S}_{S_{n,n-1}}. \tag{6.102}$$

With this we have now computed all the possible relevant non-zero commutators and anti-commutators, and now we need to combine these with the spin-1/2 to get the full commutation with the Hamiltonian.

6.2.3 Full commutation with Rabi Hamiltonian

So we now wish to group together all the results, with the respective coefficients from the different parts of the Hamiltonian. We shall do this operator by operator, starting with $\hat{\sigma}^y \otimes \hat{\mathcal{P}}_l$

$$\left[\hat{H}_S, \hat{\sigma}^y \otimes \hat{\mathcal{P}}_l\right] = -i\Delta\hat{\sigma}^x \otimes \hat{\mathcal{P}}_l, \tag{6.103}$$

$$\left[\hat{H}_I, \hat{\sigma}^y \otimes \hat{\mathcal{P}}_l\right] = 2ig\sqrt{l}\hat{\sigma}^z \otimes \hat{S}_{S_{l+1,l}} + 2ig\sqrt{l-1}\hat{\sigma}^z \otimes \hat{S}_{S_{l,l-1}}, \tag{6.104}$$

$$\left[\hat{H}_B, \hat{\sigma}^y \otimes \hat{\mathcal{P}}_l\right] = 0. \tag{6.105}$$

Now with $\hat{\sigma}^y \otimes \hat{S}_{S_{l,k}}$, assuming $k < l-1$ such that we can break up the case of $\hat{\sigma}^y \otimes \hat{S}_{S_{l,l-1}}$, we get

$$\left[\hat{H}_S, \hat{\sigma}^y \otimes \hat{S}_{S_{l,k}}\right] = -i\Delta\hat{\sigma}^z \otimes \hat{S}_{S_{l,k}}, \tag{6.106}$$

$$\begin{aligned}\left[\hat{H}_I, \hat{\sigma}^y \otimes \hat{S}_{S_{l,l-1}}\right] =& ig\sqrt{l}\hat{\sigma}^z \otimes \hat{S}_{S_{l+1,l-1}} + ig\sqrt{l-1}\hat{\sigma}^z \otimes \hat{\mathcal{P}}_l \\ &+ ig\sqrt{l-1}\hat{\sigma}^z \otimes \hat{\mathcal{P}}_{l-1} + ig\sqrt{l-2}\hat{\sigma}^z \otimes \hat{S}_{S_{l,l-2}},\end{aligned} \tag{6.107}$$

$$\begin{aligned}\left[\hat{H}_I, \hat{\sigma}^y \otimes \hat{S}_{S_{l,k}}\right] =& ig\sqrt{l}\hat{\sigma}^z \otimes \hat{S}_{S_{l+1,k}} + ig\sqrt{l-1}\hat{\sigma}^z \otimes \hat{S}_{S_{l-1,k}} \\ &+ ig\sqrt{k}\hat{\sigma}^z \otimes \hat{S}_{S_{l,k+1}} + ig\sqrt{k-1}\hat{\sigma}^z \otimes \hat{S}_{S_{l,k-1}}\end{aligned} \tag{6.108}$$

$$\left[\hat{H}_B, \hat{\sigma}^y \otimes \hat{S}_{S_{l,k}}\right] = -i\omega\left(l-k\right)\hat{\sigma}^y \otimes \hat{S}_{A_{l,k}}. \tag{6.109}$$

Similar again, now with $\hat{\mathbb{I}} \otimes \hat{S}_{A_{l,k}}$

$$\left[\hat{H}_S, \hat{\mathbb{I}} \otimes \hat{S}_{A_{l,k}}\right] = 0, \tag{6.110}$$

$$\begin{aligned}\left[\hat{H}_I, \hat{\mathbb{I}} \otimes \hat{S}_{A_{l,l-1}}\right] =& ig\sqrt{l}\hat{\sigma}^x \otimes \hat{S}_{S_{l+1,l-1}} - ig\sqrt{l-2}\hat{\sigma}^x \otimes \hat{S}_{S_{l,l-2}} \\ &+ ig\sqrt{l-1}\hat{\sigma}^x \otimes \hat{\mathcal{P}}_{l-1} - ig\sqrt{l-1}\hat{\sigma}^x \otimes \hat{\mathcal{P}}_l,\end{aligned} \tag{6.111}$$

$$\begin{aligned}\left[\hat{H}_I, \hat{\mathbb{I}} \otimes \hat{S}_{A_{l,k}}\right] =& ig\sqrt{l-1}\hat{\sigma}^x \otimes \hat{S}_{S_{l-1,k}} + ig\sqrt{l}\hat{\sigma}^x \otimes \hat{S}_{S_{l+1,k}} \\ &- ig\sqrt{k-1}\hat{\sigma}^x \otimes \hat{S}_{S_{l,k-1}} - ig\sqrt{k}\hat{\sigma}^x \otimes \hat{S}_{S_{l,k+1}},\end{aligned} \tag{6.112}$$

$$\left[\hat{H}_B, \hat{\mathbb{I}} \otimes \hat{S}_{A_{l,k}}\right] = i\omega(l-k)\mathbb{I} \otimes \hat{S}_{S_{l,k}}. \tag{6.113}$$

Likewise with $\hat{\sigma}^x \otimes \hat{S}_{A_{l,k}}$

$$\left[\hat{H}_S, \hat{\sigma}^x \otimes \hat{S}_{A_{l,k}}\right] = i\Delta\hat{\sigma}^y \otimes \hat{S}_{A_{l,k}} \tag{6.114}$$

$$\begin{aligned}\left[\hat{H}_I, \hat{\sigma}^x \otimes \hat{S}_{A_{l,l-1}}\right] =& ig\sqrt{l}\hat{\mathbb{I}} \otimes \hat{S}_{S_{l+1,l-1}} - ig\sqrt{l-2}\hat{\mathbb{I}} \otimes \hat{S}_{S_{l,l-2}} \\ &+ ig\sqrt{l-1}\hat{\mathbb{I}} \otimes \hat{\mathcal{P}}_{l-1} - ig\sqrt{l-1}\hat{\mathbb{I}} \otimes \hat{\mathcal{P}}_l,\end{aligned} \tag{6.115}$$

$$\begin{aligned}\left[\hat{H}_I, \hat{\sigma}^x \otimes \hat{S}_{A_{l,k}}\right] =& ig\sqrt{l-1}\hat{\mathbb{I}} \otimes \hat{S}_{S_{l-1,k}} + ig\sqrt{l}\hat{\mathbb{I}} \otimes \hat{S}_{S_{l+1,k}} \\ &- ig\sqrt{k-1}\hat{\mathbb{I}} \otimes \hat{S}_{S_{l,k-1}} - ig\sqrt{k}\hat{\mathbb{I}} \otimes \hat{S}_{S_{l,k+1}},\end{aligned} \tag{6.116}$$

$$\left[\hat{H}_B, \hat{\sigma}^x \otimes \hat{S}_{A_{l,k}}\right] = i\omega(l-k)\hat{\sigma}^x \otimes \hat{S}_{S_{l,k}}. \tag{6.117}$$

Finally with $\hat{\sigma}^z \otimes \hat{S}_{A_{l,k}}$

$$\left[\hat{H}_S, \hat{\sigma}^z \otimes \hat{S}_{A_{n,m}}\right] = 0 \tag{6.118}$$

$$\left[\hat{H}_I, \hat{\sigma}^z \otimes \hat{S}_{A_{l,l-1}}\right] = -ig\sqrt{l}\hat{\sigma}^y \otimes \hat{S}_{A_{l+1,l-1}} - ig\sqrt{l-2}\hat{\sigma}^y \otimes \hat{S}_{A_{l,l-2}}, \tag{6.119}$$

$$\begin{aligned}\left[\hat{H}_I, \hat{\sigma}^z \otimes \hat{S}_{A_{l,k}}\right] =& -ig\sqrt{l}\hat{\sigma}^y \otimes \hat{S}_{A_{l+1,k}} - ig\sqrt{l-1}\hat{\sigma}^y \otimes \hat{S}_{A_{l-1,k}} \\ &- ig\sqrt{k}\hat{\sigma}^y \otimes \hat{S}_{A_{l,k+1}} - ig\sqrt{k-1}\hat{\sigma}^y \otimes \hat{S}_{A_{l,k-1}},\end{aligned} \tag{6.120}$$

$$\left[\hat{H}_B, \hat{\sigma}^z \otimes \hat{S}_{A_{l,k}}\right] = i\omega(l-k)\hat{\sigma}^z \otimes \hat{S}_{S_{l,k}}. \tag{6.121}$$

With this, all of the possible relevant commutations have been computed with the necessary coefficients present. However this is still a lot of information to process, so we shall now move to a visual presentation to figure out some more details.

6.2.4 Visualising the AGP operators

Firstly we group together all operators with shared off diagonals for the cavity. This means we define

$$\vec{S}_k = \begin{pmatrix} \hat{S}_{S_{k,0}} \\ \hat{S}_{S_{1+k,1}} \\ \vdots \\ \hat{S}_{S_{(N-1),(N-k-1)}} \\ \hat{S}_{S_{N,(N-k)}} \end{pmatrix}, \quad \vec{A}_k = \begin{pmatrix} \hat{S}_{A_{k,0}} \\ \hat{S}_{A_{1+k,1}} \\ \vdots \\ \hat{S}_{A_{(N-1),(N-k-1)}} \\ \hat{S}_{A_{N,(N-k)}} \end{pmatrix}. \tag{6.122}$$

Additionally we will use the shorthand

$$\vec{S}_0 = \vec{A}_0 = \begin{pmatrix} \hat{\mathcal{P}}_1 \\ \hat{\mathcal{P}}_2 \\ \vdots \\ \hat{\mathcal{P}}_{N-1} \\ \hat{\mathcal{P}}_N \end{pmatrix}, \tag{6.123}$$

such that k is defined for the main diagonal as well.

By defining these quantities, we can plot the different operators in 3D space with one axis defining $\vec{S}_k$ or $\vec{A}_k$, another defining the spin-1/2 operator, and the final axis showing the k diagonal/off diagonal. We then draw lines between operators that have non zero commutations between them, which is shown in Fig. 6.2-a-d from a few angles to help visibility. We see that the spin Hamiltonian flips between spin-1/2 operators, and similarly the bosonic part flips between symmetric and anti-symmetric GGM. Then the interaction part of the Hamiltonian is the only part to shift k, always by ± 1. The key takeaway from these visualisations, is there are two disjoint sets of operators, which arise from the parity symmetry in the Rabi model.

As the AGP has the starting condition of $\partial_\Delta \hat{H}_{Rabi} = \sum_n \hat{\sigma}^z \otimes \hat{\mathcal{P}}_n$, we can show only operators that have a path back to this condition. Doing so produces a reduced set of relevant operators, shown in Fig. 6.2-e. With this we can identify the operators need

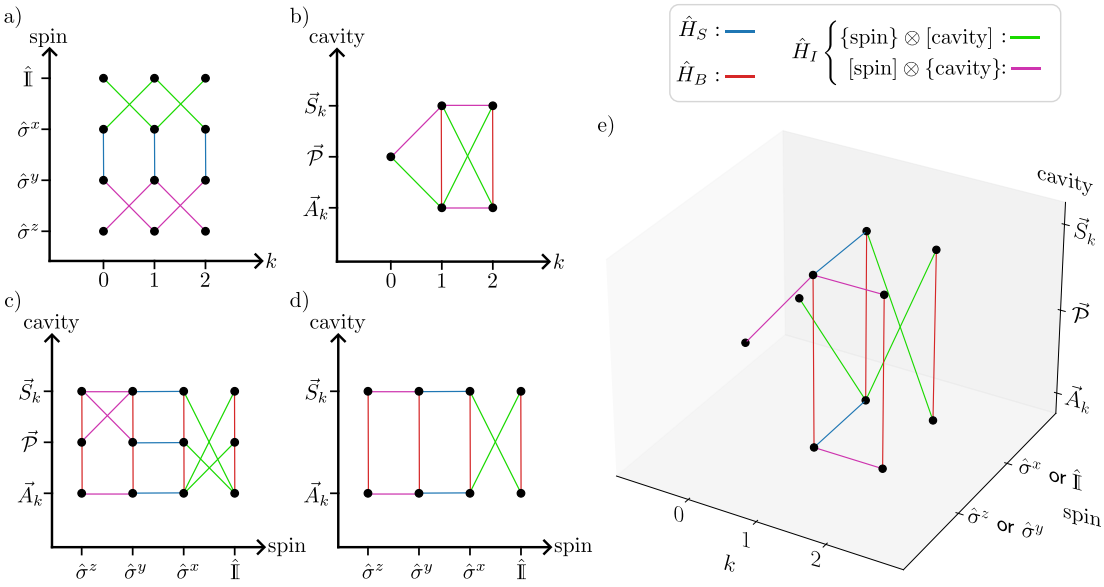

Figure 6.2: Different visualisations of the AGP operators (dots) and the commutations between them (lines), the different types of commutation are colour coded with a splitting of $\left[\hat{H}_I, \cdot\right]$ into $\{\hat{\sigma}^x, \cdot\} \otimes \left[\hat{S}^x, \cdot\right]$ and $[\hat{\sigma}^x, \cdot] \otimes \left\{\hat{S}^x, \cdot\right\}$ to help clarity. Panels a), b) and c) shows three different 2D projections of the operators, with d) repeating the showing the same angle as c) but without $k = 0$ such that $\vec{\mathcal{P}}$ can be omitted. Panel e) shows a 3D viewpoint of the operators, with only operators connected to the starting condition of $\partial_\Delta \hat{H}_{Rabi}$, as such this plot shows only the relevant operators to build the AGP and to optimise teh coefficients over.

to represent the AGP, by starting from $\partial_\Delta \hat{H}_{Rabi}$, and taking any operator that first appears first after an odd numbers of commutators. The general form of the operators that are found are

$$\begin{cases} \hat{\mathbb{I}} \otimes \vec{A}_k, \hat{\sigma}^z \otimes \vec{A}_k, & k \in even \\ \hat{\sigma}^x \otimes \vec{A}_k, \hat{\sigma}^y \otimes \vec{S}_k, & k \in odd \end{cases}, \tag{6.124}$$

where $k > 0$, for all $k < N$. These are all the possible operators in this basis needed to represent the exact AGP, up to to a truncation fo the Nth bosonic level. This means the scaling of the number of operators in the exact AGP is given by

$$2\left(N - 1 + N - 2 + \cdots + 1\right) = (N - 1)\, N. \tag{6.125}$$

This assumes all the $\vec{S}_k, \vec{A}_k$ vectors require all $N - k$ entries to be independent, however

there may be cases where the form of each vector stays constant, and as such the scaling can be reduced.

6.2.5 Mapping and ordering the AGP

Now that we have a reduced set of operators and vector collections of similar operators, we can also simplify the commutation expressions. To be able to solve for the AGP, each operator will need an associated coefficient to solve for. For a given vector operator $\hat{\sigma}^j \otimes \vec{S}_k, \hat{\sigma}^j \otimes \vec{A}_k$ we define a corresponding vector of coefficients $\vec{\alpha}^{(S,j,k)}, \vec{\alpha}^{(A,j,k)}$ such that the AGP is expressed by

$$\begin{aligned}\hat{\mathcal{A}}_\Delta = &\sum_{k\in\mathcal{K}_{even}} \left(\hat{\mathbb{I}} \otimes \left(\vec{\alpha}^{(A,I,k)} \cdot \vec{A}_k\right) + \hat{\sigma}^z \otimes \left(\vec{\alpha}^{(A,z,k)} \cdot \vec{A}_k\right)\right) \\ &\sum_{k\in\mathcal{K}_{odd}} \left(\hat{\sigma}^x \otimes \left(\vec{\alpha}^{(A,x,k)} \cdot \vec{A}_k\right) + \hat{\sigma}^y \otimes \left(\vec{\alpha}^{(S,y,k)} \cdot \vec{S}_k\right)\right),\end{aligned} \tag{6.126}$$

with $\mathcal{K}_{even}$,$\mathcal{K}_{odd}$ being the even,odd values respectively, of k for $0 < k \leq N$.

Then we can do a similar definition for all the operators one commutation away, which will define the action operators over which the coefficients will be minimised. To distinguish from the AGP operators/coefficients, we use $\vec{\beta}^{(S,j,k)}, \vec{\beta}^{(A,j,k)}$ for the action. This means that the commutation can be represented as linear super operators from $\vec{\alpha} \to \vec{\beta}$. If we rewrite Eqs. (6.103)-(6.121) in these super operators, we get

From → To	Super operator
$\vec{\alpha}^{(A,I,k)} \to \vec{\beta}^{(S,I,k)}$	$i\omega k\hat{\mathbb{I}}$
$\vec{\alpha}^{(A,I,k)} \to \vec{\beta}^{(S,z,k+1)}$	$ig(\hat{R}_k - \hat{U}_k)$
$\vec{\alpha}^{(A,I,k)} \to \vec{\beta}^{(S,z,k-1)}$	$ig(\hat{L}_k - \hat{D}_k)$
$\vec{\alpha}^{(A,x,k)} \to \vec{\beta}^{(A,y,k)}$	$i\Delta\hat{\mathbb{I}}$
$\vec{\alpha}^{(A,x,k)} \to \vec{\beta}^{(S,x,k)}$	$i\omega k\hat{\mathbb{I}}$
$\vec{\alpha}^{(A,x,k)} \to \vec{\beta}^{(S,I,k+1)}$	$-ig(\hat{R}_k - \hat{U}_k)$
$\vec{\alpha}^{(A,x,k)} \to \vec{\beta}^{(S,I,k-1)}$	$-ig(\hat{L}_k - \hat{D}_k)$
$\vec{\alpha}^{(S,y,k)} \to \vec{\beta}^{(S,x,k)}$	$-i\Delta\hat{\mathbb{I}}$
$\vec{\alpha}^{(S,y,k)} \to \vec{\beta}^{(A,y,k)}$	$-i\omega k\hat{\mathbb{I}}$
$\vec{\alpha}^{(S,y,k)} \to \vec{\beta}^{(S,x,k+1)}$	$ig(\hat{R}_k + \hat{U}_k)$
$\vec{\alpha}^{(S,y,k)} \to \vec{\beta}^{(S,x,k-1)}$	$ig(\hat{L}_k + \hat{D}_k)$
$\vec{\alpha}^{(A,z,k)} \to \vec{\beta}^{(S,z,k)}$	$i\omega k\hat{\mathbb{I}}$
$\vec{\alpha}^{(A,z,k)} \to \vec{\beta}^{(A,y,k+1)}$	$-ig(\hat{R}_k + \hat{U}_k)$
$\vec{\alpha}^{(A,z,k)} \to \vec{\beta}^{(A,y,k-1)}$	$-ig(\hat{L}_k + \hat{D}_k)$

where the super operators have the forms

Super operator	Square operator form	Reduced size
$\hat{R}_k$	$\left(\hat{n} + (k+1)\hat{\mathbb{I}}\right)^{\circ\frac{1}{2}}$	$(N-k-1)\times(N-k)$
$\hat{L}_k$	$\left(\hat{n} + k\hat{\mathbb{I}}\right)^{\circ\frac{1}{2}}$	$(N-k+1)\times(N-k)$
$\hat{U}_k$	$\hat{a}$	$(N-k-1)\times(N-k)$
$\hat{D}_k$	$\hat{a}^\dagger$	$(N-k+1)\times(N-k)$

with $\hat{n}$ being the number operator, and $^{\circ\frac{1}{2}}$ represents the Hadamard root (element wise square root).

These super operators allow an abstract view of the commutation, that shows the general effect of each of the Hamiltonian parts. We can see that $\hat{H}_S$ flips between $\hat{\sigma}^x$ and $\hat{\sigma}^y$, and similarly $\hat{H}_B$ flips between anti-symmetric ($\hat{S}_A$) and symmetric ($\hat{S}_S$) GGM. The real strength of this notation appears from describing the commutation of interaction Hamiltonian ($\hat{H}_I$). The super operators $\hat{R}_k$, $\hat{L}_k$, $\hat{U}_k$ and $\hat{D}_k$ can be thought of as shifting the kth diagonal 'Right', 'Left', 'Up' and 'Down' respectively. This arises

from commutations like Eq. (6.98), where the shift of an index of one can be thought of as a direction in the matrix.

6.2.6 The Hessian

Now to compute the Hessian, it is useful to define an ordering from the starting condition $\partial_\Delta \hat{H}_{Rabi}$. We give the ordering of the AGP coefficients/operators as

Group 1: $\quad \mathrm{y} : \vec{\alpha}^{(S,y,1)}$

Group 2: $\quad \mathrm{x} : \vec{\alpha}^{(A,x,1)}, \quad \mathrm{y} : \vec{\alpha}^{(S,y,3)}, \ \mathrm{z} : \vec{\alpha}^{(A,z,2)}, \ \mathrm{I} : \vec{\alpha}^{(A,I,2)}$

Group 3: $\quad \mathrm{x} : \vec{\alpha}^{(A,x,3)}, \quad \mathrm{y} : \vec{\alpha}^{(S,y,35)}, \ \mathrm{z} : \vec{\alpha}^{(A,z,4)}, \ \mathrm{I} : \vec{\alpha}^{(A,I,4)}$

Group j: $\quad \mathrm{x} : \vec{\alpha}^{(A,x,2j-3)}, \quad \mathrm{y} : \vec{\alpha}^{(S,y,2j-1)}, \ \mathrm{z} : \vec{\alpha}^{(A,z,2j-2)}, \ \mathrm{I} : \vec{\alpha}^{(A,I,2j-2)}$

(even N) Group $N/2+1$: $\quad \mathrm{x} : \vec{\alpha}^{(A,x,N-1)}$

(odd N) Group $(N-1)/2+1$: $\quad \mathrm{x} : \vec{\alpha}^{(A,x,N-2)}, \quad \mathrm{z} : \vec{\alpha}^{(A,z,N-1)}, \ \mathrm{I} : \vec{\alpha}^{(A,I,N-1)}$

Using this we can group together coefficients that need to be computed for each matrix. There are only two separated terms $\vec{\beta}^{(\mathcal{P},z,0)}$ and $\vec{\beta}^{(\mathcal{P},I,0)}$, which affect term 1y and term 2x. Also there is the effect of $\partial_\Delta \hat{H}$ that makes the initial condition that needs to be taken into account.

The product of maps that end on the same basis give the block form of the Hessian. As such let's group the β terms that represent G and the maps onto them

Term	Super operators	From
$\vec{\beta}^{(\delta,z,0)}$	$ig(\hat{L}_1+\hat{D}_1)$	$\vec{\alpha}^{(S,y,1)}$
$\vec{\beta}^{(\delta,I,0)}$	$ig(\hat{L}_1-\hat{D}_1)$	$\vec{\alpha}^{(A,x,1)}$
$\vec{\beta}^{(S,z,2)}$	$ig(\hat{R}_1+\hat{U}_1)$	$\vec{\alpha}^{(S,y,1)}$
	$i2\omega\hat{\mathbb{I}}$	$\vec{\alpha}^{(A,z,2)}$
	$ig(\hat{L}_3+\hat{D}_3)$	$\vec{\alpha}^{(S,y,3)}$
$\vec{\beta}^{(S,x,1)}$	$-i\Delta\hat{\mathbb{I}}$	$\vec{\alpha}^{(S,y,1)}$
	$i\omega\hat{\mathbb{I}}$	$\vec{\alpha}^{(A,x,1)}$
	$ig(\hat{L}_2-\hat{D}_2)$	$\vec{\alpha}^{(A,I,2)}$
$\vec{\beta}^{(A,y,1)}$	$-i\omega\hat{\mathbb{I}}$	$\vec{\alpha}^{(S,y,1)}$
	$i\Delta\hat{\mathbb{I}}$	$\vec{\alpha}^{(A,x,1)}$
	$-ig(\hat{L}_2+\hat{D}_2)$	$\vec{\alpha}^{(A,z,2)}$
$\vec{\beta}^{(S,z,2j)}$	$ig(\hat{R}_{2j-1}+\hat{U}_{2j-1})$	$\vec{\alpha}^{(S,y,2j-1)}$
	$i\omega(2j)\hat{\mathbb{I}}$	$\vec{\alpha}^{(A,z,2j)}$
	$ig(\hat{L}_{2j+1}+\hat{D}_{2j+1})$	$\vec{\alpha}^{(S,y,2j+1)}$
$\vec{\beta}^{(S,I,2j-2)}$	$-ig(\hat{R}_{2j-1}+\hat{U}_{2j-1})$	$\vec{\alpha}^{(A,x,2j-3)}$
	$i\omega(2j-2)\hat{\mathbb{I}}$	$\vec{\alpha}^{(A,I,2j)}$
	$ig(\hat{L}_{2j-1}+\hat{D}_{2j-1})$	$\vec{\alpha}^{(A,x,2j-1)}$
$\vec{\beta}^{(S,x,2j-1)}$	$-i\Delta\hat{\mathbb{I}}$	$\vec{\alpha}^{(S,y,2j-1)}$
	$i\omega(2j-1)\hat{\mathbb{I}}$	$\vec{\alpha}^{(A,x,2j-1)}$
	$ig(\hat{L}_{2j}-\hat{D}_{2j})$	$\vec{\alpha}^{(A,I,2j)}$
	$ig(\hat{R}_{2j-2}-\hat{U}_{2j-2})$	$\vec{\alpha}^{(A,I,2j-2)}$
$\vec{\beta}^{(A,y,2j-1)}$	$-i(2j-1)\omega\hat{\mathbb{I}}$	$\vec{\alpha}^{(S,y,2j-1)}$
	$i\Delta\hat{\mathbb{I}}$	$\vec{\alpha}^{(A,x,2j-1)}$
	$-ig(\hat{L}_{2j}+\hat{D}_{2j})$	$\vec{\alpha}^{(A,z,2j)}$
	$-ig(\hat{R}_{2j-2}+\hat{U}_{2j-2})$	$\vec{\alpha}^{(A,z,2j-2)}$

Clearly the final term j group will have no contributions from $j+1$, so this has to be adjusted at the end. With this we can write out the Hessian, remembering the form

$$\hat{G} = \partial_\Delta \hat{H_{Rabi}} - i\left[\hat{H_{Rabi}}, \hat{\mathcal{A}}\right], \tag{6.127}$$

means we can multiply every term by $-i$, which basically removes the imaginary nature of each term. There then will be a square and trace leaving just the square on each coefficient. Then we differentiate so a shared factor of 2 appears which we can cancel out. Not that the projectors have trace 1 when squared, but the GGM have $\frac{1}{2}$ (which could be fixed by redefining the projector basis, and some square roots appear) so we need to adjust all the parts with projectors to have double effect. We will solve this by multiplying every term that comes from projectors by two to remain consistent, which includes the initial condition.

The Hessian will be able to be written in block form, with blocks between different groups of the AGP operators

$$\mathbf{A} = \begin{pmatrix} \mathbf{A}_{(1,1)} & \mathbf{A}_{(1,2)} & 0 & 0 & \cdots & & 0 \\ \mathbf{A}_{(2,1)} & \mathbf{A}_{(2,2)} & \mathbf{A}_{(2,3)} & 0 & \cdots & & 0 \\ 0 & \mathbf{A}_{(3,2)} & \mathbf{A}_{(3,3)} & \mathbf{A}_{(3,4)} & \cdots & & 0 \\ 0 & 0 & \mathbf{A}_{(4,3)} & \mathbf{A}_{(4,4)} & \ddots & & 0 \\ \vdots & \vdots & \vdots & \ddots & \ddots & \ddots & \vdots \\ & & & & \ddots & \ddots & \mathbf{A}_{(\frac{N}{2},\frac{N}{2}+1)} \\ 0 & 0 & 0 & 0 & \cdots & \mathbf{A}_{(\frac{N}{2}+1,\frac{N}{2})} & \mathbf{A}_{(\frac{N}{2}+1,\frac{N}{2}+1)} \end{pmatrix} \tag{6.128}$$

These will be computed by combinations of the different super operators, that result in the same $\vec{\beta}$ term. During the middle sections these are of a generic form, but there are special cases for $\mathbf{A}_{(1,1)}$, $\mathbf{A}_{(1,2)} = \mathbf{A}^T_{(2,1)}$, $\mathbf{A}_{(2,2)}$, $\mathbf{A}_{(\frac{N}{2},\frac{N}{2})}$, $\mathbf{A}_{(\frac{N}{2},\frac{N}{2}+1)} = \mathbf{A}^T_{(\frac{N}{2}+1,\frac{N}{2})}$, $\mathbf{A}_{(\frac{N}{2}+1,\frac{N}{2}+1)}$. The full calculation of these results are shown in App. A.10, and can then be used to create the Hessian from the different matrices.

6.2.7 Applying the results

Using the Hessian to find the coefficients of the AGP, we can apply this to a simulation to find the fidelity with the final ground state is one, to a very good approximation, independent of the speed of driving. We have focused on varying Δ, but varying g is also very similar with a small change in the initial conditions. However as we have seen varying ω can be quite a lot trickier. For this case it will not change the operators as

much as previous cases, as the Rabi model already contains many of the operators that come from $\partial_\omega \hat{H}_{Rabi}$.

If we simulate the CD Hamiltonian and the base Hamiltonian with varying Δ and plot the fidelity between the simulated state and the ground state, we get the results shown in Fig. 6.3-a. We can see that the base Hamiltonian has a rather significant drop in fidelity, so there are diabatic excitations as expected. Then comparing to the CD Hamiltonian which has near perfect ground state following (error of $\approx 10^{-10}$ in fidelity), we can conclude that the form of the Hessian is indeed correct.

Now without an analytical form of the AGP, we cannot get quite as much information out of the result as we did with the Jaynes Cummings model, however we can plot the AGP norm to see where the diabatic excitations are strongest. In Fig. 6.3-b-c we plot the norm for both the Rabi model and the Jaynes Cummings model, to be able to compare the two results. It is clear that the diabatic dynamics in the Rabi model are far more complicated than in the JC model, with multiple peaks appearing. As g increases, the norm decreases in value similar to how we saw the magnitude of the AGP in JC model drop. However at smaller values of g, the peaks that appear in the result appear around Δ being an odd valued integer. We suggest this occurs due to resonances from higher order excitations, as we know that N_e is not a conversed quantity in the Rabi model, there are couplings to multi bosonic modes with the same parity. As g increases the peaks shift towards smaller Δ, creating curves that slowly fade off. Notably the AGP norm is small outside of these values, so it may be possible to follow a path that avoids these peak, although as we have only calculated the AGP with respect to Δ here, so the contribution from changing g will also be required.

This result allows understanding of the effective operators that arise from driving the Rabi model, by looking at the different magnitudes of the AGP coefficients. By doing so, any adiabatic pulse sequences on the Rabi model would be able to be sped up, by including some of the operators present. Like with previous results, further work needs to be done to find approximate forms of the AGP, but this gives an exact solution of the AGP in this model to use as a starting point.

With this, we arrive at the conclusion of this chapter on Hybrid systems, making

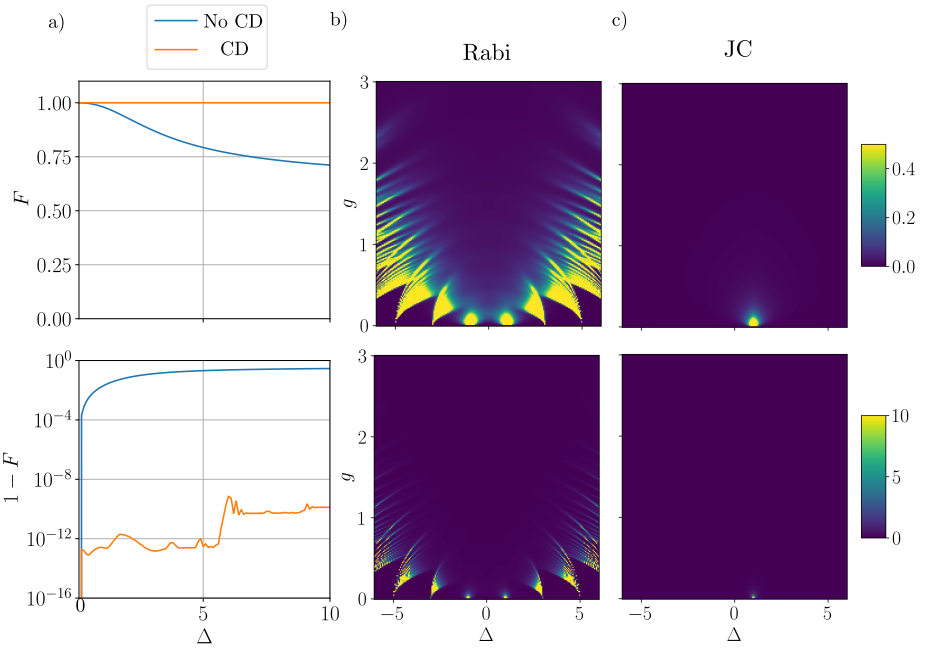

Figure 6.3: In panel a) we show the fidelity with ground state for varying Δ in the Rabi model, with parameters $\omega = g = 1$, $N = 50$, $\dot{\Delta} = 10^4$. There is near perfect groundstate following for the CD Hamiltonian, with only deviations of around 10^{-10} in the fidelity, which result from numerical errors. Panels b) and c) show the the AGP norm, with $\omega = 1$ and $N = 20$, for both the Rabi (b) and Jaynes Cummings (c) models for varying Δ. The top row has a smaller scale of 0.5 to be able to see more detail, whilst the bottom row has a higher scale up to to 10, although still far off from the maximum value which is 1.4×10^4 for the Rabi model and ∞ for the JC model.

this the final result of this thesis. During this chapter we have managed to compute the exact AGP for the Jaynes Cummings model, although we do not present a general AGP for varying the cavity frequency due to the infinite size. As such there are still areas of study in the Jaynes Cummings model for the AGP of larger excitation numbers (N_e), although results so far indicate that diabatic excitations are strongest for small N_e, so there may be only a small diabatic effect at larger N_e. The main area of improvement we see to our results, is more accurate simulations of the dynamics, as we only used a simple finite differences approach. This would be of particular importance for studying the effect of varying the cavity frequency in the Rabi model, where the simpler dynamics

for only varying spin energy are already relatively complex.

Another key recurring point in this thesis, is the results in this chapter have been purely focused on the theoretical results, and have not taken into account the complexity of actually realising the required counterdiabatic driving. As such further work into approximate AGP in these models would be of interest, which will also continue the path towards open systems where the bath (cavity) degrees of freedom are traced out. For these reasons we believe the results in this chapter, act as a solid starting point to further research of the AGP in Hybrid systems, and further bases beyond the typical spin-1/2.

Chapter 7

Conclusions and outlook

Over the course of this thesis we have explained the functionality of the adiabatic gauge potential, and explored how to compute it in different physical systems. In Chapters 2 and 3 we discussed the previously and currently existing methods for computing the AGP, trying to explain the similarities and differences alongside strengths and weaknesses. We showed how there are two key choices for each method of computing the AGP: what basis states are used, and how the optimal coefficients for each operator is computed. As such there does not need to be a rigid adherence to a specific methodology, and instead one method can be used for determining a basis and another for how to optimise it. We found that there is a significant advantage in understating when a simple basis is used, like with the Pauli matrices or the generalised Gell-Mann matrices, as results can be interpreted far easier than purely numerical operators. Whilst it would be most efficient to have one method that can be used for every problem, currently there is no method that gets around the fundamental complexity of computing the AGP due to its scaling with Hilbert space. This means that often symmetries need to be identified model by model, although sometimes this process can be semi automated like with graph symmetries we found in Sec. 4.1. While an ideal method could automatically make use of symmetries of the model, and be able to easily transform between human readable and numerical operators, as of yet such a method has not been developed, with further advances in both our understanding of symmetries and numerical techniques needed.

Even with the limitations in current methodology, we have still been able to explore results in interesting models. We first showed in Chapter 4 how different graph geometries lead to vastly different scaling of the number of operators needed to represent the AGP in the Ising model, with a closed form solution for the Ring graph and exponential scaling for asymmetric graphs. This highlighted a need for approximations to the graphs to be able to explore larger system sizes, or to focus on simple relevant graph geometries for implementation in experiment. When discussing the XXZ model, we saw how the scaling with geometry is fundamentally linked with the specific Hamiltonian, with the Complete graph having the best scaling overall and even showing a zero valued AGP for spin-1/2 meaning there are no diabatic excitations. When using Gell-Mann matrices for the spin-1 XXZ model, we highlighted the jump in complexity from the increased base in exponential scaling ($4^N \rightarrow 9^N$), meaning only very small sized systems were able to be studied. To be able to reach some of the unique phenomena to larger spin models, like the triple point in the phase diagram of the spin-1 XXZ model, approximate forms of the AGP will need to be created. This can help further the study of the AGP as a measure of phase transitions, and try to link what critical exponent it is related to.

We showed in Chapter 5 that it is possible to compute the AGP in bosonic systems, although there are problems with non-stationary basis vectors and infinite sized Hilbert spaces that need to be treated carefully. We found that even in the infinite size of bosonic models, there are many cases where the AGP is finite, with quadratic models having a particularly small operator space for the AGP. With this being the case, it would be of particular interest if the AGP can be used to improve control procedures in quadratic bosonic models, or whether the level of control over the AGP operators raises more problems than it fixes.

The main application we have seen of using bosonic AGP, is the use within hybrid systems which are so vital to our understanding of quantum optics. Whilst the results are preliminary at this stage of research, we believe they are promising beginnings. In the Jaynes Cummings model we saw how varying the cavity frequency can lead to a completely different effective Hamiltonian that breaks the excitation symmetry. Whilst

the Rabi model really highlighted how much information is lost to diabatic excitations even when just varying system parameters. Understanding what the effective Hamiltonian is when varying parameters allows for more sophisticated algorithms to avoid losses or make use of the new effective operators. The next vital step towards a open system AGP, is to understand the formulation of the AGP when the cavity mode is traced out. It is possible that due to how chaos and phase transitions are measured by the AGP in closed systems, open system could have analogous measures and be used as a measure of dissipative phase transitions.

With the results of this thesis, we now have numerical, and in some special cases analytical expressions, of the AGP in many new models. To be able to apply this knowledge to specific quantum control operations we would suggest the use of Counterdiabatic Optimised Local Driving (COLD), which shows that the AGP can be used as a cost function to efficiently optimise a control procedure without requiring a full simulation. This will provide results on which operators are most effective at reducing the diabatic losses, and as such will suggest the most effective basis of the AGP for Counterdiabatic driving. There are many directions this research can be taken further, many of which are currently being pursed by different groups. The field of shortcuts to adiabaticity has produced very promising results so far, especially for being a relatively new area of study, and we look forward to seeing where the field stands in the future.

Appendix A

Appendix

> "Albert grunted. "Do you know what happens to lads who ask too many questions?"
> Mort thought for a moment.
> "No," he said eventually, "what?"
> There was silence.
> Then Albert straightened up and said, "Damned if I know. Probably they get answers, and serve 'em right."
>
> Terry Pratchett, *Mort (1987)*

A.1 Binary symplectic form commutation proofs

Firstly we can find the possible operator form by using XOR on the bit registers of the X and Z components of the operators [103]. This means we can write a new operator $\hat{C}$ as the commutator of $\hat{A}$ and $\hat{B}$ as

$$\hat{C} = \left[\hat{A}, \hat{B}\right], \tag{A.1}$$

$$C^x = A^x \oplus B^x, \tag{A.2}$$

$$C^z = A^z \oplus B^z. \tag{A.3}$$

Taking the results for Pauli matrices in Sec. 3.3.1, we can see that only when both the operators on a site are different Pauli operators does the phase change at all, and

either gains i if they are cyclically ordered ($x \to y \to z$) or $-i$ if anti-cyclic ordered ($x \to z \to y$). The second term will always be exactly opposite in sign, and as such the commutator is exactly zero if there is an even number of non trivial products (anywhere where the commutator on each site would be non-zero). As we can count how many non zero commutations on each site we have.

This is done by noting that taking an AND operation on $A^x \wedge B^z$ will differ to $B^x \wedge A^z$ only where two different Pauli operators occur on that site. To have this explicitly clear, we can write a truth table of $A^x \wedge B^z$ (rows for A, columns for B)

	I	X	Y	Z
I	0	0	0	0
X	0	0	1	1
Y	0	0	1	1
Z	0	0	0	0

We can clearly see if we reflect in the diagonal axis only the cases (X, Y),(Y, Z),(Z, X) will vary. So if we count the number of 1's that appears in the each of the resulting binary numbers ($A^x \wedge B^z$ and $B^x \wedge A^z$) , take modulo 2 on the result and compare if the numbers are different or not. If they are equal then there is an even number of commutations and as such the commutator is zero. If they are different then we get a non zero commutation. We can write this in a single logical expression as

$$\text{not}\,(\text{countones}(A^x \wedge B^z) \mod 2 == \text{countones}(B^x \wedge A^z) \mod 2) \tag{A.4}$$

This will be True if the commutator is non zero.

Finally we need to figure out what the sign of operator is. As we noted, we ignore the imaginary phase of the term, and instead only focus on whether a commutation has a plus or minus sign eg. is the resulting phase $p = \{0, 3\}$ for plus or $p = \{1, 2\}$ for minus. If we look at the previous truth table, we see that (X,Y) and (Y,Z) both have 1 when $+i$, and 0 when $-i$, whereas (Z,X) has the opposite of 0 when $+i$ and 1 when $-i$. Notably this case also is the only situation where the output is a Y term. So if we compute where every commutation takes place, then look for spots where there is a Y

term at that location in the resulting operator, we can figure out how many plus and minuses there are.

The binary number that represents where sites flipped is given by

$$F_{\text{locs}} = (A^x \wedge B^z) \oplus (B^x \wedge A^z) \tag{A.5}$$

We can then figure out the number of flips by taking the number of ones here

$$N_{\text{coms}} = \text{countones}(F_{\text{locs}}) \tag{A.6}$$

The location of Y's in resulting term is

$$Y_{\text{locs}} = (A^x \oplus B^x) \wedge (A^z \oplus B^z) = C^x \wedge C^z \tag{A.7}$$

We can then flip the values where both a flip and a y occur

$$P_{\text{locs}} = ((A^x \wedge B^z) \oplus (F_{\text{locs}} \wedge Y_{\text{locs}})) \wedge F_{\text{locs}} \tag{A.8}$$

noting an additional AND with F_{locs} to remove the cases of YY. We can then count the number of $+i$ cases

$$N_{\text{positive}} = \text{countones}(P_{\text{locs}}), \tag{A.9}$$

and as the total flips should equal number of $+i$ and $-i$ cases, we have $N_{\text{coms}} - N_{\text{positive}}$ number of $-i$ cases.

With this we can finally write the phase as

$$\theta_C = \theta_A \cdot \theta_B \cdot (+i)^{N_{\text{positive}}} (-i)^{N_{\text{coms}} - N_{\text{positive}}}. \tag{A.10}$$

A.2 Spin Z operator to GGM

Given from the main text, the matrix elements of $\hat{S}_z$ is

$$\left(\hat{S}^z\right)_{ab} = \hbar(s+1-a)\delta_{a,b} = \hbar(s+1-b)\delta_{a,b} \tag{A.11}$$

we can represent this in terms of GGM as

$$\hat{S}^z = \hbar \sum_{k=2}^{N} \alpha_k \hat{S}_{D_k} = \sum_{k=2}^{N} \alpha'_k \sqrt{2k(k-1)} \hat{S}_{D_k}, \tag{A.12}$$

where α'_k are renormalised to make the equation simpler as now everything is just integers. Note that no identity matrix is required as $\hat{S}^z$ is traceless and the identity is not (and all gell mann matrices are also traceless). With these renormalised coefficients we get the equation

$$(1-k)\alpha'_k + \sum_{j=k+1}^{N} \alpha'_j = s + 1 - k. \tag{A.13}$$

Then by using $s = \frac{N-1}{2}$ we can rewrite the equation only in terms of N

$$(1-k)\alpha'_k + \sum_{j=k+1}^{N} \alpha'_j = \frac{N+1}{2} - k. \tag{A.14}$$

This can be simply solved by back substitution from $k = N$ down. In fact it will become very quickly clear that the solution is $\alpha'_k = \frac{1}{2} \forall k$. With this information we can write

$$\hat{S}^z = \hbar \sum_{k=2}^{N} \sqrt{\frac{k(k-1)}{2}} \hat{S}_{D_k}. \tag{A.15}$$

A.3 Functional forms of limits on AGP operators

In the main text we quote a simplified form of Eq. (4.3), which we repeat here for clarity as

$$N_{\mathcal{A}}^{\max} = \sum_{n_y}^{N} \sum_{n_z}^{N-n_y} \frac{N!}{n_y! n_z! (N - n_y - n_z)!} 2^{N-n_y-n_z}, \tag{A.16}$$

with simplified form

$$N_{\mathcal{A}}^{\max} = 2^{N-1}(2^{N-1} - 1). \tag{A.17}$$

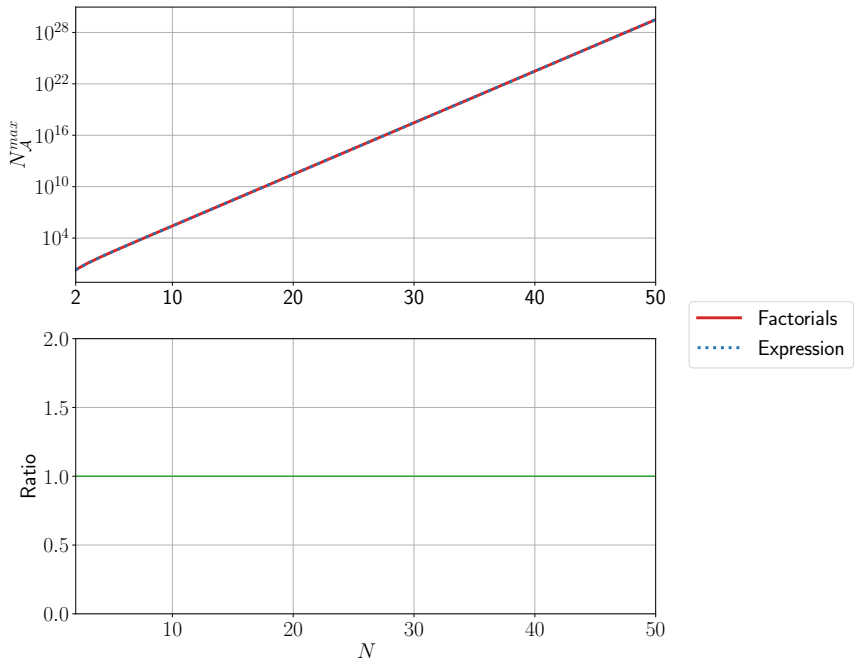

Figure A.1: Comparing the two forms of the maximum scaling number for the AGP in the Ising model. We find the functional expression matches the factorial result exactly within the range plotted.

Now whilst we are sure combinatorics can be used to match these two forms together, we found this simplification based on numerical results. We noticed that the value quickly approaches 4^{N-1}, and is exactly two for $N = 2$ so we made guesses at the functional form, assuming that the form is exponential of some form. In Fig. A.1 we show the numerics we found between these two expressions, where we see an exact agreement within the range plotted. Whilst this is in no way a true proof, we see no physical reason why the scaling form would change at some larger N, and the result agree at smaller values of N. In fact the asymptotic result of 4^{N-1} can be found by looking at the proportion of even and odd numbers of $\hat{\sigma}^y$ and $\hat{\sigma}^z$, as approximately half the operators should be even and half odd, so taking the full hilbert space dimension 4^N and dividing this twice by two gives 4^{N-1}. As such this result satisfies the level our rigour needed for our results, but we would not state this as a true mathematical proof.

A.4 Letter based derivation of Ring/Chain lie algebra

We can represent our Ising Hamiltonian by

$$\hat{H} = Jz\text{–}z + \lambda x, \tag{A.18}$$

$$\partial_\lambda \hat{H} = x. \tag{A.19}$$

We have used the symmetries of the graph to group together all the ZZ and X operators, as all sites are equivalent here, allowing a simpler representation where we do not need to write unnecessary identities. Ignoring the coefficients, we define a truth table to show us how to apply commutation

$$\begin{aligned}
[x, z] &= y, \\
[x, y] &= z, \\
[z\text{–}z, I\text{–}x] &= z\text{–}y, \\
[z\text{–}z, I\text{–}y] &= z\text{–}x, \\
[z\text{–}z, z\text{–}x] &= I\text{–}y, \\
[z\text{–}z, z\text{–}y] &= I\text{–}x.
\end{aligned}$$

The final non zero commutations can be found by the sites of the final four relations, eg. $y\text{–}I \to I\text{–}y$. This can give nice intuition that we can think of the commutators as just swapping colours. We can then compute the first seven applications of the commutator, retaining only new operators

$$(l = 1) \qquad [z\text{–}z + x, x] = z\text{–}y + y\text{–}z, \tag{A.20}$$

$$(l = 2) \qquad [z\text{–}z + x, (l = 1)] = x + y\text{–}y + z\text{–}z + z\text{–}x\text{–}z, \tag{A.21}$$

$$(l = 3) \qquad [z\text{–}z + x, (l = 2)] = z\text{–}x\text{–}y + y\text{–}x\text{–}z, \tag{A.22}$$

$$(l = 4) \qquad [z\text{–}z + x, (l = 3)] = y\text{–}x\text{–}y + z\text{–}x\text{–}x\text{–}z, \tag{A.23}$$

$$(l = 5) \qquad [z\text{–}z + x, (l = 4)] = y\text{–}x\text{–}x\text{–}z + z\text{–}x\text{–}x\text{–}y, \tag{A.24}$$

$$(l = 6) \qquad [z\text{–}z + x, (l = 5)] = y\text{–}x\text{–}x\text{–}y + z\text{–}x\text{–}x\text{–}x\text{–}z, \tag{A.25}$$

$$(l=7) \qquad [z\text{–}z+x,(l=6)] = y\text{–}x\text{–}x\text{–}x\text{–}z + z\text{–}x\text{–}x\text{–}x\text{–}y. \tag{A.26}$$

$$\tag{A.27}$$

We see that the operators are limited to chains with $\hat{\sigma}^x$ operators in the bulk, and either $\hat{\sigma}^y$ or $\hat{\sigma}^z$ on the ends.

A.5 Details of Calculations for the Ring Graph

In this Appendix, we give more details of the calculation of the AGP for the ring graph described in Sec. 4.1.2. This graph is special as we can get a full analytical solution, allowing a thermodynamic limit to be taken. In this graph, each spin is connected to its neighbours, with the first and last spins also being connected. It is important to note that $N = 2$ is a special case, and we focus here on $N \geq 3$ where the ring is clearly defined. This gives an adjacency matrix of the form

$$\begin{pmatrix} 0 & 1 & 0 & \dots & \dots & 0 & 1 \\ 1 & 0 & 1 & \ddots & \ddots & \ddots & 0 \\ 0 & 1 & 0 & \ddots & \ddots & \ddots & \vdots \\ \vdots & \ddots & \ddots & \ddots & \ddots & \ddots & \vdots \\ \vdots & \ddots & \ddots & \ddots & 0 & 1 & 0 \\ 0 & \ddots & \ddots & \ddots & 1 & 0 & 1 \\ 1 & 0 & \dots & \dots & 0 & 1 & 0 \end{pmatrix}. \tag{A.28}$$

We can define the symmetries of the graph with two generators, a clockwise rotation of all the spins, and a mirror around the central point. In addition, the one-dimensional nature of the ring, the terms become limited to having $\hat{\sigma}^x$ terms in the bulk, with $\hat{\sigma}^y$ and $\hat{\sigma}^z$ on either end. This used in addition to the symmetries means we can group together terms with an equal number of terms. The easiest way to show the operators are of this form is to define the connections for each operator. We can represent these operator connections like so

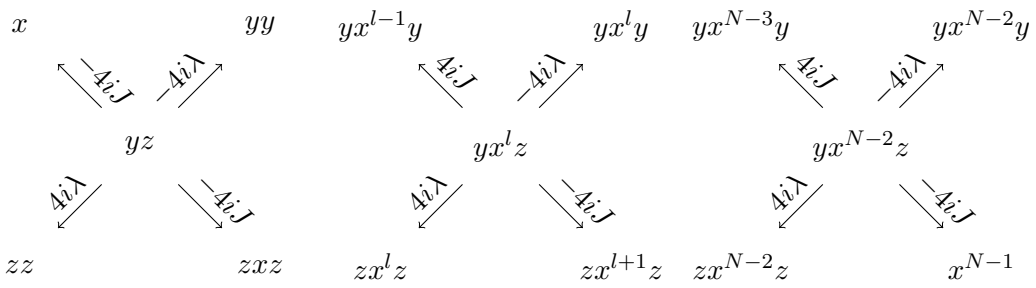

Here we see that the starting point $\partial_\lambda \hat{H} = \sum_i^N \hat{\sigma}_i^x$ is included, and each only has connections to $\hat{\sigma}^y\hat{\sigma}^z$ operators. Otherwise, all connections are explored, and there is no way to break away to different operators. Note, that the coefficient of the connections is doubled to four in every case because there are always two different operators (that have been grouped together) that map to the same thing. With these connections, we can write out the matrix equation for the graph as

$$\begin{pmatrix} \lambda^2+J^2 & -J\lambda & 0 & & \\ -J\lambda & \lambda^2+J^2 & -J\lambda & & \\ & \ddots & \ddots & \ddots & \\ & & -J\lambda & \lambda^2+J^2 & -J\lambda \\ & & 0 & -J\lambda & \lambda^2+J^2 \end{pmatrix} \begin{pmatrix} \alpha_1 \\ \alpha_2 \\ \vdots \\ \alpha_{N-2} \\ \alpha_{N-1} \end{pmatrix} = \begin{pmatrix} \frac{J}{8} \\ 0 \\ \vdots \\ 0 \\ 0 \end{pmatrix}. \tag{A.29}$$

There are many ways of solving such a system of equations, and in this case, we shall simply compute the inverse of the matrix. We suggest this approach because the vector on the right-hand side of the equation only contains a single non-zero value, meaning we have a solution of the form

$$\alpha_k = \frac{J}{8} M^{-1}_{k,1}, \tag{A.30}$$

Where $\mathbf{M}$ is our matrix, which is a symmetric Toeplitz tridiagonal matrix that is known to have a analytical inverse [153], and $M^{-1}_{k,1}$ is the kth element of the first row of the inverse matrix. To use this approach, we divide everything by $-J\lambda$ to get the off

diagonals to equal 1, giving the new equation

$$\begin{pmatrix} -\frac{\lambda^2+J^2}{J\lambda} & 1 & 0 & & \\ 1 & -\frac{\lambda^2+J^2}{J\lambda} & 1 & & \\ & \ddots & \ddots & \ddots & \\ & & 1 & -\frac{\lambda^2+J^2}{J\lambda} & 1 \\ & & 0 & 1 & -\frac{\lambda^2+J^2}{J\lambda} \end{pmatrix} \begin{pmatrix} \alpha_1 \\ \alpha_2 \\ \vdots \\ \alpha_{N-2} \\ \alpha_{N-1} \end{pmatrix} = \begin{pmatrix} -\frac{1}{8\lambda} \\ 0 \\ \vdots \\ 0 \\ 0 \end{pmatrix}, \tag{A.31}$$

and adjusted α_k:

$$\alpha_k = -\frac{1}{8\lambda} M'^{-1}_{k,1}, \tag{A.32}$$

where $\mathbf{M}'$ is this rescaled matrix. This means we have a diagonal element $D = -\frac{\lambda^2+J^2}{J\lambda}$. Depending on the value of D the form of the substitution required to find the inverse changes:

$$D = \begin{cases} 2\cosh\omega, & D \geq 2 \\ 2\cos\omega, & -2 < D < 2 \\ -2\cosh\omega, & D \leq -2 \end{cases} \tag{A.33}$$

This gives a result in operators of the new parameter ω. If we limit our parameters to $\lambda > 0$ and $J = \pm 1$ we have the following cases for D:

$$D = \begin{cases} -\frac{\lambda^2+1}{\lambda}, & J = 1 \\ \frac{\lambda^2+1}{\lambda}, & J = -1 \end{cases} \tag{A.34}$$

These functions for $\lambda > 0$ have stationary points at $\lambda = 1$, for $J = 1$ this is a maximum value of -2, whereas for $J = -1$ this is a minimum value of 2. This then gives us the value of omega for both cases $J = \pm 1$ as:

$$\omega = \operatorname{arccosh} \frac{\lambda^2 + 1}{2\lambda}. \tag{A.35}$$

However, the inverse of the matrix (and as such the solution to the AGP) is still dependent on the sign of J, as expected due to this physically being the difference between ferromagnetic and antiferromagnetic behaviour. We can then write down the

first column of the inverse of the matrix as:

$$M'^{-1}_{k,1} = \begin{cases} -\frac{\cosh\omega(N+1-k)-\cosh\omega(N-1-k)}{2\sinh\omega\sinh\omega N}, & J=1 \\ \\ (-1)^{k+1}\frac{\cosh\omega(N+1-k)-\cosh\omega(N-1-k)}{2\sinh\omega\sinh\omega N}, & J=-1 \end{cases} \tag{A.36}$$

This gives us for α_k

$$\alpha_k = \begin{cases} \frac{\cosh\omega(N+1-k)-\cosh\omega(N-1-k)}{16\lambda\sinh\omega\sinh\omega N}, & J=1 \\ \\ (-1)^{k}\frac{\cosh\omega(N+1-k)-\cosh\omega(N-1-k)}{16\lambda\sinh\omega\sinh\omega N}, & J=-1 \end{cases} \tag{A.37}$$

This expression is now able to be used but can be simplified further to remove the dependence on ω. The first step is to note that the value of ω can be expressed as:

$$\omega = \ln\lambda, \tag{A.38}$$

which then gives the same result as in equation (A.35). Using this and the exponential definitions of cosh and sinh we can expand the hyperbolic functions:

$$\cosh\omega(N+1-k) = \frac{\lambda^{2(N+1-k)}+1}{2\lambda^{N+1-k}}, \tag{A.39}$$

$$\cosh\omega(N-1-k) = \frac{\lambda^{2(N-1-k)}+1}{2\lambda^{N-1-k}}, \tag{A.40}$$

$$\sinh\omega = \frac{\lambda^2-1}{2\lambda}, \tag{A.41}$$

$$\sinh\omega N = \frac{\lambda^{2N}-1}{2\lambda^N}. \tag{A.42}$$

Substituting these into the expression for α_k and rearranging gives us the final result, quoted in the main text, for α_k:

$$\alpha_k = \begin{cases} \frac{\lambda^{k-1}}{8}\frac{\lambda^{2(N-k)}-1}{\lambda^{2N}-1}, & J=1 \\ \\ (-1)^k\frac{\lambda^{k-1}}{8}\frac{\lambda^{2(N-k)}-1}{\lambda^{2N}-1}, & J=-1 \end{cases} \tag{A.43}$$

An interesting limit to look at is what happens at the critical point $\lambda \to 1$, which we can compute using L'Hôpital's rule:

$$\lim_{\lambda\to 1}\alpha_k = \begin{cases} \frac{(1)^{k-1}}{8}\frac{2(N-k)(1)^{2(N-k)-1}}{2N(1)^{2N-1}}, & J=1 \\ \\ (-1)^k\frac{(1)^{k-1}}{8}\frac{2(N-k)(1)^{2(N-k)-1}}{2N(1)^{2N-1}}, & J=-1 \end{cases} \tag{A.44}$$

which can be simplified to:

$$\lim_{\lambda\to 1}\alpha_k = \begin{cases} \frac{1}{8}\frac{N-k}{N}, & J=1 \\ \\ (-1)^k\frac{1}{8}\frac{N-k}{N}, & J=-1 \end{cases} \tag{A.45}$$

We can then compute the AGP norm by squaring the operator, multiplying by the multiplicity of the type of operator (always $2N$ for ring operators) and sum over k, giving (for both $J=1$ and $J=-1$):

$$\begin{aligned} \lim_{\lambda\to 1}||\mathcal{A}_\lambda||^2 =& 2N\sum_{k=1}^{N-1}\frac{1}{64}\frac{(N-k)^2}{N^2} \\ =& \frac{1}{32N}\left(\sum_{k=1}^{N-1}N^2 - 2\sum_{k=1}^{N-1}Nk + \sum_{k=1}^{N-1}k^2\right) \\ =& \frac{1}{32N}\left(N^2(N-1) - N^2(N-1) + \frac{N}{6}(N-1)(2N-1)\right) \\ =& \frac{(N-1)(2N-1)}{192}. \end{aligned} \tag{A.46}$$

This shows that exactly at the critical point the norm diverges as N^2 compared to at all other values of λ where it diverges as N instead.

A.6 Derivation of matrix equation for quadratic bosonic models

Here we shall discus in more detail each of the steps of computing the matrix equation for the quadratic bosonic AGP. Starting from the form of the AGP given in the main text

$$\hat{\mathcal{A}}_{\mathrm{Q}} = \alpha_2^0 \hat{a}^2 + \alpha_1^1 \hat{a}^\dagger \hat{a} + \alpha_0^2 (\hat{a}^\dagger)^2 + \alpha_1^0 \hat{a} + \alpha_0^1 \hat{a}^\dagger, \tag{A.47}$$

where each α value is a function of λ for a specific pulse, or more generally a function of all the c coefficients. We can then begin computing $\hat{G}_{c_j^i}$

$$\begin{aligned}
\hat{G}_{c_j^i} =& \partial_{c_j^i} \hat{H}_{\mathrm{Q}} - i \left[\hat{H}_{\mathrm{Q}}, \hat{\mathcal{A}}_{\mathrm{Q}} \right] \\
=& \partial_{c_j^i} \hat{H}_{\mathrm{Q}} - i \Bigg(\left(-2c_1^1 \alpha_2^0 + 2c_2^0 \alpha_1^1 \right) \hat{a}^2 \\
&+ \left(-4c_0^2 \alpha_2^0 + 4c_2^0 \alpha_0^2 \right) \hat{a}^\dagger \hat{a} \\
&+ \left(-2c_0^2 \alpha_1^1 + 2c_1^1 \alpha_0^2 \right) (\hat{a}^\dagger)^2 \\
&+ \left(-2c_0^1 \alpha_2^0 + c_1^0 \alpha_1^1 - c_1^1 \alpha_1^0 + 2c_2^0 \alpha_0^1 \right) \hat{a} \\
&+ \left(-c_0^1 \alpha_1^1 + 2c_1^0 \alpha_0^2 - 2c_0^2 \alpha_1^0 + c_1^1 \alpha_0^1 \right) \hat{a}^\dagger \\
&+ \left(-2c_0^2 \alpha_2^0 + 2c_2^0 \alpha_0^2 - c_0^1 \alpha_1^0 + c_1^0 \alpha_0^1 \right) \hat{\mathbb{I}} \Bigg).
\end{aligned} \tag{A.48}$$

Now there are already many different coefficients, α values and operators in this expression, but we are required to do another commutation to fulfil the condition $[\hat{H}_{\mathrm{Q}}, \hat{G}_{c_j^i}] = 0$. However we can reuse the previous steps, by now writing

$$\hat{G}_{c_j^i} = G_2^0 \hat{a}^2 + G_1^1 \hat{a}^\dagger \hat{a} + G_0^2 (\hat{a}^\dagger)^2 + G_1^0 \hat{a} + G_0^1 \hat{a}^\dagger + G_0^0 \hat{\mathbb{I}}, \tag{A.49}$$

where each G_j^i can be computed from Eq. (A.48). Then again using Eq. (A.48), we can

swap $\hat{\mathcal{A}}_{\mathrm{Q}} \to \hat{G}_{c_j^i}$, $\alpha_j^i \to G_j^i$ and take the section within the large brackets to compute $[\hat{H}_{\mathrm{Q}}, \hat{G}_{c_j^i}]$. To be explicit we get

$$\begin{aligned}
0 &= \left[H_{\mathrm{Q}}, \hat{G}_{c_j^i}\right] \\
&= \left(-2c_1^1 G_2^0 + 2c_2^0 G_1^1\right) \hat{a}^2 \\
&\quad + \left(-4c_0^2 G_2^0 + 4c_2^0 G_0^2\right) \hat{a}^\dagger \hat{a} \\
&\quad + \left(-2c_0^2 G_1^1 + 2c_1^1 G_0^2\right) (\hat{a}^\dagger)^2 \\
&\quad + \left(-2c_0^1 G_2^0 + c_1^0 G_1^1 - c_1^1 G_1^0 + 2c_2^0 G_0^1\right) \hat{a} \\
&\quad + \left(-c_0^1 G_1^1 + 2c_1^0 G_0^2 - 2c_0^2 G_1^0 + c_1^1 G_0^1\right) \hat{a}^\dagger \\
&\quad + \left(-2c_0^2 G_2^0 + 2c_2^0 G_0^2 - c_0^1 G_1^0 + c_1^0 G_0^1\right) \hat{\mathbb{I}}.
\end{aligned} \tag{A.50}$$

The only way to satisfy all the above conditions simultaneously for all values, is that each individual operator contribution is equal to zero. We can use each of these conditions as lines in a matrix equation, which is equivalent to in some way to the algebraic approach but we have avoided taking any traces. The partial derivate will be the only term not involving any α values, so this will make up the initial conditions of the matrix equation, and the rest of the matrix equation is equivalent for all cases.

First we substitute the values of G_j^i back in to give

$$\begin{aligned}
0 =& -2c_1^1 \left(c_2'^0 - i\left(-2c_1^1\alpha_2^0 + 2c_2^0\alpha_1^1\right)\right) \\
&+ 2c_2^0 \left(c_1'^1 - i\left(-4c_0^2\alpha_2^0 + 4c_2^0\alpha_0^2\right)\right) \\
=& -2c_1^1 c_2'^0 + 2c_2^0 c_1'^1 \\
&- i\Bigg(\left(4(c_1^1)^2 - 8c_2^0 c_0^2\right)\alpha_2^0 + \left(-4c_1^1 c_2^0\right)\alpha_1^1 + \left(8(c_2^0)^2\right)\alpha_0^2\Bigg),
\end{aligned} \tag{A.51}$$

$$\begin{aligned}
0 =& -4c_0^2 \left(c_2'^0 - i\left(-2c_1^1\alpha_2^0 + 2c_2^0\alpha_1^1\right)\right) \\
&+ 4c_2^0 \left(c_0'^2 - i\left(-2c_0^2\alpha_1^1 + 2c_1^1\alpha_0^2\right)\right) \\
=& -4c_0^2 c_2'^0 + 4c_2^0 c_0'^2
\end{aligned}$$

$$- i\Bigg(\left(8c_0^2c_1^1\right)\alpha_2^0 + \left(-16c_2^0c_0^2\right)\alpha_1^1 + \left(8c_2^0c_1^1\right)\alpha_0^2 \Bigg), \tag{A.52}$$

$$\begin{aligned}
0 =& - 2c_0^2\left(c_1'^1 - i\left(-4c_0^2\alpha_2^0 + 4c_2^0\alpha_0^2\right)\right) \\
&+ 2c_1^1\left(c_0'^2 - i\left(-2c_0^2\alpha_1^1 + 2c_1^1\alpha_0^2\right)\right) \\
=& - 2c_0^2c_1'^1 + 2c_1^1c_0'^2 \\
&- i\Bigg(\left(8(c_0^2)^2\right)\alpha_2^0 + \left(-4c_1^1c_0^2\right)\alpha_1^1 + \left(-8c_0^2c_2^0 + 4(c_1^1)^2\right)\alpha_0^2 \Bigg),
\end{aligned} \tag{A.53}$$

$$\begin{aligned}
0 =& - 2c_0^1\left(c_2'^0 - i\left(-2c_1^1\alpha_2^0 + 2c_2^0\alpha_1^1\right)\right) \\
&+ c_1^0\left(c_1'^1 - i\left(-4c_0^2\alpha_2^0 + 4c_2^0\alpha_0^2\right)\right) \\
&- c_1^1\left(c_1'^0 - i\left(-2c_0^1\alpha_2^0 + c_1^0\alpha_1^1 - c_1^1\alpha_1^0 + 2c_2^0\alpha_0^1\right)\right) \\
&+ 2c_2^0\left(c_0'^1 - i\left(-c_0^1\alpha_1^1 + 2c_1^0\alpha_0^2 - 2c_0^2\alpha_1^0 + c_1^1\alpha_0^1\right)\right) \\
=& - 2c_0^1c_2'^0 + c_1^0c_1'^1 - c_1^1c_1'^0 + 2c_2^0c_0'^1 \\
&- i\Bigg(\left(6c_0^1c_1^1 - 4c_1^0c_0^2\right)\alpha_2^0 \\
&+ \left(-6c_0^1c_2^0 - c_1^1c_1^0\right)\alpha_1^1 \\
&+ \left(8c_2^0c_1^0\right)\alpha_0^2 \\
&+ \left((c_1^1)^2 - 4c_2^0c_0^2\right)\alpha_1^0 \\
&+ (0)\,\alpha_0^1 \Bigg),
\end{aligned} \tag{A.54}$$

$$\begin{aligned}
0 =& - c_0^1\left(c_1'^1 - i\left(-4c_0^2\alpha_2^0 + 4c_2^0\alpha_0^2\right)\right) \\
&+ 2c_1^0\left(c_0'^2 - i\left(-2c_0^2\alpha_1^1 + 2c_1^1\alpha_0^2\right)\right) \\
&- 2c_0^2\left(c_1'^0 - i\left(-2c_0^1\alpha_2^0 + c_1^0\alpha_1^1 - c_1^1\alpha_1^0 + 2c_2^0\alpha_0^1\right)\right) \\
&+ c_1^1\left(c_0'^1 - i\left(-c_0^1\alpha_1^1 + 2c_1^0\alpha_0^2 - 2c_0^2\alpha_1^0 + c_1^1\alpha_0^1\right)\right) \\
=& - c_0^1c_1'^1 + 2c_1^0c_0'^2 - 2c_0^2c_1'^0 + c_1^1c_0'^1
\end{aligned}$$

$$
\begin{aligned}
&- i\Bigg(\left(8c_0^1c_0^2\right)\alpha_2^0 \\
&+ \left(-6c_1^0c_0^2 - c_1^1c_0^1\right)\alpha_1^1 \\
&+ \left(-4c_0^1c_2^0 + 6c_1^0c_1^1\right)\alpha_0^2 \\
&+ (0)\,\alpha_1^0 \\
&+ \left(-4c_0^2c_2^0 + (c_1^1)^2\right)\alpha_0^1\Bigg),
\end{aligned} \tag{A.55}
$$

$$
\begin{aligned}
0 =& - 2c_0^2\left(c_2'^0 - i\left(-2c_1^1\alpha_2^0 + 2c_2^0\alpha_1^1\right)\right) \\
&+ 2c_2^0\left(c_0'^2 - i\left(-2c_0^2\alpha_1^1 + 2c_1^1\alpha_0^2\right)\right) \\
&- c_0^1\left(c_1'^0 - i\left(-2c_0^1\alpha_2^0 + c_1^0\alpha_1^1 - c_1^1\alpha_1^0 + 2c_2^0\alpha_0^1\right)\right) \\
&+ c_1^0\left(c_0'^1 - i\left(-c_0^1\alpha_1^1 + 2c_1^0\alpha_0^2 - 2c_0^2\alpha_1^0 + c_1^1\alpha_0^1\right)\right) \\
=& - 2c_0^2c_2'^0 + 2c_2^0c_0'^2 - c_0^1c_1'^0 + c_1^0c_0'^1 \\
&- i\Bigg(\left(4c_0^2c_1^1 + 2(c_0^1)^2\right)\alpha_2^0 \\
&+ \left(-8c_0^2c_2^0 - 2c_0^1c_1^0\right)\alpha_1^1 \\
&+ \left(4c_2^0c_1^1 + 2(c_1^0)^2\right)\alpha_0^2 \\
&+ \left(c_0^1c_1^1 - 2c_1^0c_0^2\right)\alpha_1^0 \\
&+ \left(-2c_0^1c_2^0 + c_1^0c_1^1\right)\alpha_0^1\Bigg).
\end{aligned} \tag{A.56}
$$

We can then write the matrix equation as

$$
-i\mathbf{M}_{\mathrm{Q}}\vec{\alpha} = \vec{u}_{\mathrm{Q}} \tag{A.57}
$$

where $\mathbf{M}_{\mathrm{Q}}$ is given by

$$\begin{pmatrix} 4(c_1^1)^2 - 8c_2^0c_0^2 & -4c_1^1c_2^0 & 8(c_2^0)^2 & 0 & 0 \\ 8c_0^2c_1^1 & -16c_2^0c_0^2 & 8c_2^0c_1^1 & 0 & 0 \\ 8(c_0^2)^2 & -4c_1^1c_0^2 & -8c_0^2c_2^0 + 4(c_1^1)^2 & 0 & 0 \\ 6c_0^1c_1^1 - 4c_1^0c_0^2 & -6c_0^1c_2^0 - c_1^1c_1^0 & 8c_2^0c_1^0 & (c_1^1)^2 - 4c_2^0c_0^2 & 0 \\ 8c_0^1c_0^2 & -6c_1^0c_0^2 - c_1^1c_0^1 & -4c_0^1c_2^0 + 6c_1^0c_1^1 & 0 & -4c_0^2c_2^0 + (c_1^1)^2 \\ 4c_0^2c_1^1 + 2(c_0^1)^2 & -8c_0^2c_2^0 - 2c_0^1c_1^0 & 4c_2^0c_1^1 + 2(c_1^0)^2 & c_0^1c_1^1 - 2c_1^0c_0^2 & -2c_0^1c_2^0 + c_1^0c_1^1 \end{pmatrix} \tag{A.58}$$

$\vec{\alpha}$ is a column vector of the alphas values

$$\vec{\alpha} = \begin{pmatrix} \alpha_2^0 \\ \alpha_1^1 \\ \alpha_0^2 \\ \alpha_1^0 \\ \alpha_0^1 \end{pmatrix}. \tag{A.59}$$

and $\vec{u}_{\mathrm{Q}}$ is a column vector determined by the rate of change of all the variables, given by

$$\vec{u}_{\mathrm{Q}} = \begin{pmatrix} 2c_1^1c_2'^0 - 2c_2^0c_1'^1 \\ 4c_0^2c_2'^0 - 4c_2^0c_0'^2 \\ 2c_0^2c_1'^1 - 2c_1^1c_0'^2 \\ 2c_0^1c_2'^0 - c_1^0c_1'^1 + c_1^1c_1'^0 - 2c_2^0c_0'^1 \\ c_0^1c_1'^1 - 2c_1^0c_0'^2 + 2c_0^2c_1'^0 - c_1^1c_0'^1 \\ 2c_0^2c_2'^0 - 2c_2^0c_0'^2 + c_0^1c_1'^0 - c_1^0c_0'^1 \end{pmatrix}. \tag{A.60}$$

A.7 Applying the simplifications to quadratic model AGP

By applying the simplifications of a real valued hermitian Hamiltonian, we can reduce the previous matrix equation to a simpler one.

We first apply the conditions on the c coefficients to the matrix $\mathbf{M}_{\mathrm{Q}}$ to give the

simplification

$$\begin{pmatrix} 4(c_1^1)^2 - 8(c_2^0)^2 & -4c_1^1c_2^0 & 8(c_2^0)^2 & 0 & 0 \\ 8c_2^0c_1^1 & -16(c_2^0)^2 & 8c_2^0c_1^1 & 0 & 0 \\ 8(c_2^0)^2 & -4c_1^1c_2^0 & -8(c_2^0)^2 + 4(c_1^1)^2 & 0 & 0 \\ 6c_1^0c_1^1 - 4c_1^0c_2^0 & -6c_1^0c_2^0 - c_1^1c_1^0 & 8c_2^0c_1^0 & (c_1^1)^2 - 4(c_2^0)^2 & 0 \\ 8c_1^0c_2^0 & -6c_1^0c_2^0 - c_1^1c_1^0 & -4c_1^0c_2^0 + 6c_1^0c_1^1 & 0 & -4(c_2^0)^2 + (c_1^1)^2 \\ 4c_2^0c_1^1 + 2(c_1^0)^2 & -8(c_2^0)^2 - 2(c_1^0)^2 & 4c_2^0c_1^1 + 2(c_1^0)^2 & c_1^0c_1^1 - 2c_1^0c_2^0 & -2c_1^0c_2^0 + c_1^0c_1^1 \end{pmatrix} \tag{A.61}$$

and to $\vec{u}_{\mathrm{Q}}$ giving

$$\vec{u}_{\mathrm{Q}} = \begin{pmatrix} 2c_1^1c_2'^0 - 2c_2^0c_1'^1 \\ 0 \\ 2c_0^2c_1'^1 - 2c_1^1c_2'^0 \\ 2c_1^0c_2'^0 - c_1^0c_1'^1 + c_1^1c_1'^0 - 2c_2^0c_1'^0 \\ c_1^0c_1'^1 - 2c_1^0c_2'^0 + 2c_2^0c_1'^0 - c_1^1c_1'^0 \\ 0 \end{pmatrix}. \tag{A.62}$$

Next we can apply the α conditions by combing the columns that are now equivalent ($1 \to 1-3$ and $4 \to 4-5$). This will give

$$\begin{pmatrix} 4(c_1^1)^2 - 16(c_2^0)^2 & -4c_1^1c_2^0 & 0 \\ 0 & -16(c_2^0)^2 & 0 \\ 16(c_2^0)^2 - 4(c_1^1)^2 & -4c_1^1c_2^0 & 0 \\ 6c_1^0c_1^1 - 12c_1^0c_2^0 & -6c_1^0c_2^0 - c_1^1c_1^0 & (c_1^1)^2 - 4(c_2^0)^2 \\ 12c_1^0c_2^0 - 6c_1^0c_1^1 & -6c_1^0c_2^0 - c_1^1c_1^0 & 4(c_2^0)^2 - (c_1^1)^2 \\ 0 & -8(c_2^0)^2 - 2(c_1^0)^2 & 0 \end{pmatrix}. \tag{A.63}$$

We can now see that for rows two and six to be in general true, the only solution is $\alpha_1^1 = 0$. This means we can reduce further by completely removing the second column,

and rows two and six. We shall also write in $\vec{u}_{\text{Quad}}$ as we now have the space

$$\begin{pmatrix} 4(c_1^1)^2 - 16(c_2^0)^2 & 0 \\ 16(c_2^0)^2 - 4(c_1^1)^2 & 0 \\ 6c_1^0c_1^1 - 12c_1^0c_2^0 & (c_1^1)^2 - 4(c_2^0)^2 \\ 12c_1^0c_2^0 - 6c_1^0c_1^1 & 4(c_2^0)^2 - (c_1^1)^2 \end{pmatrix} \begin{pmatrix} \alpha_2^0 \\ \alpha_1^0 \end{pmatrix} = \begin{pmatrix} 2c_1^1c_2'^0 - 2c_2^0c_1'^1 \\ 2c_0^2c_1'^1 - 2c_1^1c_2'^0 \\ 2c_1^0c_2'^0 - c_1^0c_1'^1 + c_1^1c_1'^0 - 2c_2^0c_1'^0 \\ c_1^0c_1'^1 - 2c_1^0c_2'^0 + 2c_2^0c_1'^0 - c_1^1c_1'^0 \end{pmatrix} \tag{A.64}$$

The above equation shows that the rows one and two, are equivalent up to a sign difference, similarly for rows three and four. We can as such remove the redundant rows, to give the final simplified matrix equation

$$\begin{pmatrix} 4(c_1^1)^2 - 16(c_2^0)^2 & 0 \\ 6c_1^0c_1^1 - 12c_1^0c_2^0 & (c_1^1)^2 - 4(c_2^0)^2 \end{pmatrix} \begin{pmatrix} \alpha_2^0 \\ \alpha_1^0 \end{pmatrix} = \begin{pmatrix} 2c_1^1c_2'^0 - 2c_2^0c_1'^1 \\ 2\left(c_1^0c_2'^0 - c_1'^0c_2^0\right) + c_1'^0c_1^1 - c_1^0c_1'^1 \end{pmatrix} \tag{A.65}$$

A.8 Diagonalising the Jaynes Cummings model

To diagonalise the Hamiltonian given in the main text (Sec.6.1), we first rearrange the terms into the form

$$\hat{H}_{JC}^{(N_e)} = \begin{pmatrix} \frac{1}{2}(\Delta - \omega) & g\sqrt{N_e} \\ g\sqrt{N_e} & -\frac{1}{2}(\Delta - \omega) \end{pmatrix} + \begin{pmatrix} \omega(N_e - \frac{1}{2}) & 0 \\ 0 & \omega(N_e - \frac{1}{2}) \end{pmatrix}. \tag{A.66}$$

The second matrix here is proportional to identity, meaning it will only adjust the eigenvalues by adding the value $\omega(N_e - \frac{1}{2})$, so we can ignore it for now.

We can solve for the eigenvalues λ of the first matrix, using the characteristic equation

$$\begin{aligned} \begin{vmatrix} \frac{1}{2}(\Delta - \omega) - \lambda & g\sqrt{N_e} \\ g\sqrt{N_e} & -\frac{1}{2}(\Delta - \omega) - \lambda \end{vmatrix} &= 0 \\ \lambda^2 - \frac{1}{4}(\Delta - \omega)^2 - g^2N_e &= 0 \\ \lambda &= \pm\frac{1}{2}\sqrt{(\Delta - \omega)^2 + 4g^2N_e}. \end{aligned} \tag{A.67}$$

Then as this is a two level system, we can introduce mixing angles $\theta_\pm$ and write the eigenstates as

$$|\lambda_\pm\rangle = \cos(\theta_\pm)\,|N_e - 1, \uparrow\rangle + \sin(\theta_\pm)\,|N_e, \downarrow\rangle\,. \tag{A.68}$$

We then solve for θ using

$$\begin{pmatrix} \frac{1}{2}(\Delta-\omega) & g\sqrt{N_e} \\ g\sqrt{N_e} & -\frac{1}{2}(\Delta-\omega) \end{pmatrix} \begin{pmatrix} \cos(\theta_\pm) \\ \sin(\theta_\pm) \end{pmatrix} = \lambda_\pm \begin{pmatrix} \cos(\theta_\pm) \\ \sin(\theta_\pm) \end{pmatrix}. \tag{A.69}$$

We note that as $\lambda_\pm$ are only different by a sign, the transformation $\sin(\theta_-) \to -\cos(\theta_+)$, $\cos(\theta_-) \to \sin(\theta_+)$ also satisfies this equation. This means that $\theta_- = \theta_+ - \frac{\pi}{2}$, and we can solve for just θ_+ and adjust the form of $|\lambda_-\rangle$.

The two rows of the matrix equation are equal, so we just look at the first one to solve for θ_+

$$\begin{aligned} \frac{1}{2}(\Delta-\omega)\cos(\theta_+) + g\sqrt{N_e}\sin(\theta_+) &= \cos(\theta_+)\lambda_+ \\ (\Delta-\omega) + 2g\sqrt{N_e}\tan(\theta_+) &= 2\lambda_+ \\ \tan(\theta_+) &= \frac{2\lambda_+ - (\Delta-\omega)}{2g\sqrt{N_e}}. \end{aligned} \tag{A.70}$$

This value of $\tan(\theta_+)$ can be used, however a slightly simpler form can be given by computing $\tan(2\theta_+)$ [154]

$$\begin{aligned} \tan^2\theta_+ &= \frac{2\lambda_+ - (\Delta-\omega)}{2g\sqrt{N_e}} \frac{2\lambda_+ - (\Delta-\omega)}{2g\sqrt{N_e}} \left(\frac{2\lambda_+ + (\Delta-\omega)}{2\lambda_+ + (\Delta-\omega)}\right) \\ &= \frac{2\lambda_+ - (\Delta-\omega)}{2g\sqrt{N_e}} \frac{4\lambda_+^2 - (\Delta-\omega)^2}{2g\sqrt{N_e}\,(2\lambda_+ + (\Delta-\omega))} \\ &= \frac{2\lambda_+ - (\Delta-\omega)}{2g\sqrt{N_e}} \frac{\left(4g^2N_e + (\Delta-\omega)^2\right) - (\Delta-\omega)^2}{2g\sqrt{N_e}\,(2\lambda_+ + (\Delta-\omega))} \\ &= \frac{2\lambda_+ - (\Delta-\omega)}{2\lambda_+ + (\Delta-\omega)} \end{aligned} \tag{A.71}$$

$$\tan(2\theta_+) = \frac{2\tan\theta_+}{1-\tan^2\theta_+}$$

$$
\begin{aligned}
&= \frac{2\frac{2\lambda_+ - (\Delta-\omega)}{2g\sqrt{N_e}}}{1 - \left(\frac{2\lambda_+ - (\Delta-\omega)}{2\lambda_+ + (\Delta-\omega)}\right)} \\
&= \frac{2\frac{2\lambda_+ - (\Delta-\omega)}{2g\sqrt{N_e}}}{\frac{2\lambda_+ + (\Delta-\omega) - 2\lambda_+ + (\Delta-\omega)}{2\lambda_+ + (\Delta-\omega)}} \\
&= \frac{2\frac{2\lambda_+ - (\Delta-\omega)}{2g\sqrt{N_e}}}{\frac{2(\Delta-\omega)}{2\lambda_+ + (\Delta-\omega)}} \\
&= 2\frac{4\lambda_+^2 - (\Delta-\omega)^2}{2g\sqrt{N_e}2(\Delta-\omega)} \\
&= 2\frac{4g^2 N_e}{2g\sqrt{N_e}2(\Delta-\omega)} \\
&= \frac{2g\sqrt{N_e}}{(\Delta-\omega)}
\end{aligned} \tag{A.72}
$$

We will then use the notation $\beta_{N_e} = \theta_+ = \frac{1}{2}\arctan\left(\frac{2g\sqrt{N_e}}{\Delta-\omega}\right)$, such that the Hamiltonian is diagonalised by the eigenenergies and eigenstates

$$E_{N_e,\pm} = \omega\left(N_e - \frac{1}{2}\right) \pm \frac{1}{2}\sqrt{(\Delta-\omega)^2 + 4g^2 N_e}, \tag{A.73}$$

$$|N_e, +\rangle = \cos(\beta_{N_e})\,|N_e - 1, \uparrow\rangle + \sin(\beta_{N_e})\,|N_e, \downarrow\rangle\,, \tag{A.74}$$

$$|N_e, -\rangle = \sin(\beta_{N_e})\,|N_e - 1, \uparrow\rangle - \cos(\beta_{N_e})\,|N_e, \downarrow\rangle\,. \tag{A.75}$$

A.9 Harmonic oscillator double check

To verify that the Jaynes Cummings model cavity simulation works, we test for accuracy of the same method in the Harmonic oscillator. The Hamiltonian in the position basis can be written as

$$\hat{H}_{HO} = \frac{\omega^2}{2}\hat{x}^2 - \frac{1}{2}\frac{\partial^2}{\partial\hat{x}^2} - \frac{\omega}{2}. \tag{A.76}$$

We then simulate this with finite differences again, in three different cases: base with no counterdiabatic driving, exact operator AGP applied and lastly a groundstate AGP. The exact AGP for the Harmonic oscillator was given in the main text in the creation

and annihilation basis, which we can convert to the position basis

$$\begin{aligned}
\hat{\mathcal{A}}_\omega =& -i\frac{1}{4\omega}\left(\hat{a}^\dagger\hat{a}^\dagger - \hat{a}\hat{a}\right),\\
aa =& \frac{m\omega}{2\hbar}\left(\hat{x}+\frac{i}{m\omega}\hat{p}\right)\left(\hat{x}+\frac{i}{m\omega}\hat{p}\right)\\
=& \frac{m\omega}{2\hbar}\left(\hat{x}^2+\frac{i}{m\omega}\left(\hat{x}\hat{p}+\hat{p}\hat{x}\right)-\frac{1}{m^2\omega^2}\hat{p}^2\right),\\
a^\dagger a^\dagger =& \frac{m\omega}{2\hbar}\left(\hat{x}^2-\frac{i}{m\omega}\left(\hat{x}\hat{p}+\hat{p}\hat{x}\right)-\frac{1}{m^2\omega^2}\hat{p}^2\right),\\
\hat{\mathcal{A}}_\omega =& -i\frac{1}{4\omega}\frac{m\omega}{2\hbar}\left(-2\frac{i}{m\omega}\left(\hat{x}\hat{p}+\hat{p}\hat{x}\right)\right)\\
=& -\frac{1}{4\omega\hbar}\left(\hat{x}\hat{p}+\hat{p}\hat{x}\right)\\
=& \frac{i}{4\omega}\left(\hat{x}\frac{\hat{\partial}}{\partial x}+\frac{\hat{\partial}}{\partial x}\hat{x}\right).
\end{aligned} \tag{A.77}$$

Then for the groundstate AGP we only need to compute the matrix element between $|0\rangle$ and $|2\rangle$ similar to the Jaynes cummings model, which is given by

$$\begin{aligned}
\langle 0|\,\hat{\mathcal{A}}_\omega\,|2\rangle =& i\hbar\frac{\langle 0|\,\partial_\omega\hat{H}\,|2\rangle}{E_2-E_0}\\
=& i\hbar\frac{\langle 0|\,\hat{a}^\dagger\hat{a}+\frac{1}{2}\left(\hat{a}^\dagger\hat{a}^\dagger+\hat{a}\hat{a}\right)|2\rangle}{2\hbar\omega}\\
=& i\frac{1}{4\omega}\langle 0|\,\sqrt{2}\sqrt{1}\,|0\rangle\\
=& i\frac{1}{2\sqrt{2}\omega}.
\end{aligned}$$

This means the Groundstate AGP is given by

$$\hat{\mathcal{A}}_\omega^{GS} = i\frac{1}{2\sqrt{2}\omega}\left(|0\rangle\langle 2| - |2\rangle\langle 0|\right) \tag{A.78}$$

The results of this simulation is given in Fig. A.2, where we similar to the Jaynes cummings model the results do not get machines precision groundstate following. There is a difference between the groundstate AGP and the exact operator form, because the simulation has errors there is leakage into the higher eigenstates which is not mitigated at all by the groundstate AGP, whereas the exact AGP will reduce diabatic excitations

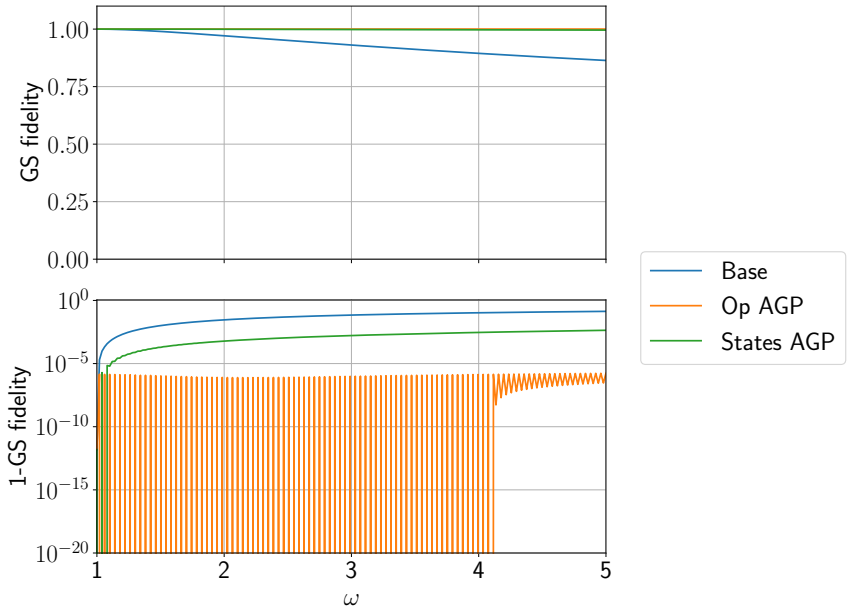

Figure A.2: Fidelity with the ground state for varying ω in the Harmonic oscillator, to verify the result seen in the Jaynes Cummings model. We see that the most accurate AGP is still given by the direct operator form, however the state AGP also gives a good result with similar error as seen in the JC model. The parameters for the simulation are $\dot{\omega} = 100$ simulated on a one dimensional grid between $-5 \leq x \leq 5$ with a difference between consecutive points $\Delta x = 0.01$.

for all eigenstates. Notably the errors seen here are comparable to the JC model, so we can confirm that the JC groundstate AGP is within the error margin we would expect. As said in the main text, to be completely sure of the result a more in depth simulation will need to be done.

A.10 Details of Rabi model Hessian

In the main text, we derive all the commutations needed for the rabi model AGP, and define blocks of the hessian to be computed. In this section we compute those blocks, simplifying the form to a reasonable stage.

The first block is the Group 1 onto 1

$$\mathbf{A}_{(1,1)} = 2\left(g(\hat{L}_1 + \hat{D}_1)^T\right)\left(g(\hat{L}_1 + \hat{D}_1)\right) + \left(g(\hat{R}_1 + \hat{U}_1)^T\right)\left(g(\hat{R}_1 + \hat{U}_1)\right)$$

$$+\left(-\Delta\hat{\mathbb{I}}\right)\left(-\Delta\hat{\mathbb{I}}\right)+\left(-\omega\hat{\mathbb{I}}\right)\left(-\omega\hat{\mathbb{I}}\right)$$

which is the only group with initial conditions

$$\mathbf{B}_{(1)}=\left(-2\left(g(\hat{L}_1+\hat{D}_1)^T\right)\left(\tfrac{1}{2}\text{ones}\right)\right), \tag{A.79}$$

where ones is a column vectors of N ones. All other $\mathbf{B}$ parts are zero ($\mathbf{B}_{(i)}=0,\forall i\neq 1$).

Next we have the connections between group 1 and 2, which we can first write out each connections

$$\mathbf{A}_{(1,2)}=\mathbf{A}_{(2,1)}^T=\begin{pmatrix}1y,2x & 1y,2y & 1y,2z & 1y,2I\end{pmatrix} \tag{A.80}$$

These have values

$$\begin{aligned}
(1y,2x)&=\left(-\Delta\hat{\mathbb{I}}\right)\left(\omega\hat{\mathbb{I}}\right)+\left(-\omega\hat{\mathbb{I}}\right)\left(\Delta\hat{\mathbb{I}}\right)\\
(1y,2y)&=\left(g(\hat{R}_1+\hat{U}_1)^T\right)\left(g(\hat{L}_3+\hat{D}_3)\right)\\
(1y,2z)&=\left(g(\hat{R}_1+\hat{U}_1)^T\right)\left(2\omega\hat{\mathbb{I}}\right)+\left(-\omega\hat{\mathbb{I}}\right)\left(-g(\hat{L}_2+\hat{D}_2)\right)\\
(1y,2I)&=\left(-\Delta\hat{\mathbb{I}}\right)\left(g(\hat{L}_2-\hat{D}_2)\right)
\end{aligned}$$

Then there is group 2 onto 2

$$\mathbf{A}_{(2,2)}=\begin{pmatrix}2x,2x & 0 & 2x,2z & 2x,2I\\ 0 & 2y,2y & 2y,2z & 2y,2I\\ 2z,2x & 2z,2y & 2z,2z & 0\\ 2I,2x & 2I,2y & 0 & 2I,2I\end{pmatrix} \tag{A.81}$$

These have values same values as the general case, expect for

$$\begin{aligned}
2x,2x=&\left(\Delta\hat{\mathbb{I}}\right)^T\left(\Delta\hat{\mathbb{I}}\right)+\left((1)\,\omega\hat{\mathbb{I}}\right)^T\left((1)\,\omega\hat{\mathbb{I}}\right)\\
&+2\left(g\left(\hat{L}_1-\hat{D}_1\right)\right)^T\left(g\left(\hat{L}_1-\hat{D}_1\right)\right)+\left(g\left(\hat{R}_1-\hat{U}_1\right)\right)^T\left(g\left(\hat{R}_1-\hat{U}_1\right)\right)
\end{aligned}$$

Appendix A. Appendix

We look at only even N here, so there is also group $\frac{N}{2}$ onto $\frac{N}{2}$

$$\mathbf{A}_{(\frac{N}{2},\frac{N}{2})} = \begin{pmatrix} \frac{N}{2}x, \frac{N}{2}x & 0 & \frac{N}{2}x, \frac{N}{2}z & \frac{N}{2}x, \frac{N}{2}I \\ 0 & \frac{N}{2}y, \frac{N}{2}y & \frac{N}{2}y, \frac{N}{2}z & \frac{N}{2}y, \frac{N}{2}I \\ \frac{N}{2}z, \frac{N}{2}x & \frac{N}{2}z, \frac{N}{2}y & \frac{N}{2}z, \frac{N}{2}z & 0 \\ \frac{N}{2}I, \frac{N}{2}x & \frac{N}{2}I, \frac{N}{2}y & 0 & \frac{N}{2}I, \frac{N}{2}I \end{pmatrix} \tag{A.82}$$

These have values same values as the general case, expect for

$$\begin{aligned} \frac{N}{2}y, \frac{N}{2}y = &\left(g\left(\hat{L}_{N-1} + \hat{D}_{N-1}\right)\right)^T \left(g\left(\hat{L}_{N-1} + \hat{D}_{N-1}\right)\right) \\ &+ \left(-\left(N-1\right)\omega\hat{\mathbb{I}}\right)^T \left(-\left(N-1\right)\omega\hat{\mathbb{I}}\right) \\ &+ \left(-\Delta\hat{\mathbb{I}}\right)^T \left(-\Delta\hat{\mathbb{I}}\right) \end{aligned}$$

Then group $\frac{N}{2}$ onto $\frac{N}{2}+1$

$$\mathbf{A}_{(\frac{N}{2},\frac{N}{2}+1)} = \begin{pmatrix} \frac{N}{2}x, \left(\frac{N}{2}+1\right)x \\ \frac{N}{2}y, \left(\frac{N}{2}+1\right)x \\ \frac{N}{2}z, \left(\frac{N}{2}+1\right)x \\ \frac{N}{2}I, \left(\frac{N}{2}+1\right)x \end{pmatrix} \tag{A.83}$$

These have values

$$\begin{aligned} \frac{N}{2}x, \left(\frac{N}{2}+1\right)x &= \left(g\left(\hat{R}_{N-3} - \hat{U}_{N-3}\right)\right)^T \left(g\left(\hat{L}_{N-1} - \hat{D}_{N-1}\right)\right) \\ \frac{N}{2}y, \left(\frac{N}{2}+1\right)x &= \left(-\left(N-1\right)\omega\hat{\mathbb{I}}\right)^T \left(\Delta\hat{\mathbb{I}}\right) + \left(-\Delta\hat{\mathbb{I}}\right)^T \left(\left(N-1\right)\omega\hat{\mathbb{I}}\right) \\ \frac{N}{2}z, \left(\frac{N}{2}+1\right)x &= \left(-g\left(\hat{R}_{N-2} + \hat{U}_{N-2}\right)\right)^T \left(\Delta\hat{\mathbb{I}}\right) \\ \frac{N}{2}I, \left(\frac{N}{2}+1\right)x &= \left(g\left(\hat{R}_{N-2} - \hat{U}_{N-2}\right)\right)^T \left(\left(N-1\right)\omega\hat{\mathbb{I}}\right) \\ &\quad + \left(\left(N-2\right)\omega\hat{\mathbb{I}}\right)^T \left(g\left(\hat{L}_{N-1} - \hat{D}_{N-1}\right)\right) \end{aligned}$$

Lastly we have the end point where we have $\frac{N}{2}+1$ onto $\frac{N}{2}+1$

$$\mathbf{A}_{(\frac{N}{2}+1,\frac{N}{2}+1)} = \left(\left(\tfrac{N}{2}+1\right)x, \left(\tfrac{N}{2}+1\right)x\right) \tag{A.84}$$

These have values

$$\begin{aligned}\left(\frac{N}{2}+1\right)x, \left(\frac{N}{2}+1\right)x = &\left(\omega(N-1)\hat{\mathbb{I}}^{\dagger}\right)\left(\omega(N-1)\hat{\mathbb{I}}\right) + \left(\Delta\hat{\mathbb{I}}^{\dagger}\right)\left(\Delta\hat{\mathbb{I}}\right) \\ &+ \left(g(\hat{L}_{N-1}-\hat{D}_{N-1})\right)^{\dagger}\left(g(\hat{L}_{N-1}-\hat{D}_{N-1})\right)\end{aligned}$$

A.10.0.1 General

For the rest of the matrix elements, we have a repeating structure for j onto $j+1$

$$\mathbf{A}_{(j,j+1)} = \mathbf{A}^{T}_{(j+1,j)} = \begin{pmatrix} jx,(j+1)x & 0 & 0 & 0 \\ jy,(j+1)x & jy,(j+1)y & jy,(j+1)z & jy,(j+1)I \\ jz,(j+1)x & 0 & jz,(j+1)z & 0 \\ jI,(j+1)x & 0 & 0 & jI,(j+1)I \end{pmatrix} \tag{A.85}$$

These have values

$$\begin{aligned}
jx,(j+1)x &= \left(g\left(\hat{R}_{2j-3}-\hat{U}_{2j-3}\right)\right)^{T}\left(g\left(\hat{L}_{2j-1}-\hat{D}_{2j-1}\right)\right) \\
jy,(j+1)x &= \left(-\left(2j-1\right)\omega\hat{\mathbb{I}}\right)^{T}\left(\Delta\hat{\mathbb{I}}\right) \\
&\quad + \left(-\Delta\hat{\mathbb{I}}\right)^{T}\left(\left(2j-1\right)\omega\hat{\mathbb{I}}\right) \\
jy,(j+1)y &= \left(g\left(\hat{R}_{2j-1}+\hat{U}_{2j-1}\right)\right)^{T}\left(g\left(\hat{L}_{2j+1}+\hat{D}_{2j+1}\right)\right) \\
jy,(j+1)z &= \left(g\left(\hat{R}_{2j-1}+\hat{U}_{2j-1}\right)\right)^{T}\left(\left(2j\right)\omega\hat{\mathbb{I}}\right) \\
&\quad + \left(-\left(2j-1\right)\omega\hat{\mathbb{I}}\right)^{T}\left(-g\left(\hat{L}_{2j}+\hat{D}_{2j}\right)\right) \\
jy,(j+1)I &= \left(-\Delta\hat{\mathbb{I}}\right)^{T}\left(g\left(\hat{L}_{2j}-\hat{D}_{2j}\right)\right) \\
jz,(j+1)x &= \left(-g\left(\hat{R}_{2j-2}+\hat{U}_{2j-2}\right)\right)^{T}\left(\Delta\hat{\mathbb{I}}\right) \\
jz,(j+1)z &= \left(-g\left(\hat{R}_{2j-2}+\hat{U}_{2j-2}\right)\right)^{T}\left(-g\left(\hat{L}_{2j}+\hat{D}_{2j}\right)\right)
\end{aligned}$$

$$
\begin{aligned}
jI,(j+1)x &= \left(g\left(\hat{R}_{2j-2}-\hat{U}_{2j-2}\right)\right)^{T}\left(\left(2j-1\right)\omega\hat{\mathbb{I}}\right)\\
&\quad+\left(\left(2j-2\right)\omega\hat{\mathbb{I}}\right)^{T}\left(g\left(\hat{L}_{2j-1}-\hat{D}_{2j-1}\right)\right)\\
jI,(j+1)I &= \left(g\left(\hat{R}_{2j-2}-\hat{U}_{2j-2}\right)\right)^{T}\left(g\left(\hat{L}_{2j}-\hat{D}_{2j}\right)\right)
\end{aligned}
$$

Then for j onto j we also have

$$
\mathbf{A}_{(j,j)}=\begin{pmatrix} jx,jx & 0 & jx,jz & jx,jI\\ 0 & jy,jy & jy,jz & jy,jI\\ jz,jx & jz,jy & jz,jz & 0\\ jI,jx & jI,jy & 0 & jI,jI \end{pmatrix} \tag{A.86}
$$

These have values

$$
\begin{aligned}
jx,jx &= \left(\Delta\hat{\mathbb{I}}\right)^{T}\left(\Delta\hat{\mathbb{I}}\right)+\left(\left(2j-3\right)\omega\hat{\mathbb{I}}\right)^{T}\left(\left(2j-3\right)\omega\hat{\mathbb{I}}\right)\\
&\quad+\left(g\left(\hat{L}_{2j-3}-\hat{D}_{2j-3}\right)\right)^{T}\left(g\left(\hat{L}_{2j-3}-\hat{D}_{2j-3}\right)\right)\\
&\quad+\left(g\left(\hat{R}_{2j-3}-\hat{U}_{2j-3}\right)\right)^{T}\left(g\left(\hat{R}_{2j-3}-\hat{U}_{2j-3}\right)\right)\\
jx,jz &= jz,jx^{T}\\
jx,jI &= \left(\left(2j-3\right)\omega\hat{\mathbb{I}}\right)^{T}\left(g\left(\hat{L}_{2j-2}-\hat{D}_{2j-2}\right)\right)\\
&\quad+\left(g\left(\hat{R}_{2j-3}-\hat{U}_{2j-3}\right)\right)^{T}\left(\left(2j-2\right)\omega\hat{\mathbb{I}}\right)\\
jy,jy &= \left(g\left(\hat{L}_{2j-1}+\hat{D}_{2j-1}\right)\right)^{T}\left(g\left(\hat{L}_{2j-1}+\hat{D}_{2j-1}\right)\right)\\
&\quad+\left(g\left(\hat{R}_{2j-1}+\hat{U}_{2j-1}\right)\right)^{T}\left(g\left(\hat{R}_{2j-1}+\hat{U}_{2j-1}\right)\right)\\
&\quad+\left(-\left(2j-1\right)\omega\hat{\mathbb{I}}\right)^{T}\left(-\left(2j-1\right)\omega\hat{\mathbb{I}}\right)+\left(-\Delta\hat{\mathbb{I}}\right)^{T}\left(-\Delta\hat{\mathbb{I}}\right)\\
jy,jz &= jz,jy^{T}\\
jy,jI &= \left(-\Delta\hat{\mathbb{I}}\right)^{T}\left(g\left(\hat{R}_{2j-2}-\hat{U}_{2j-2}\right)\right)\\
jz,jx &= \left(-g\left(\hat{L}_{2j-2}+\hat{D}_{2j-2}\right)\right)^{T}\left(\Delta\hat{\mathbb{I}}\right)\\
jz,jy &= \left(\left(2j-2\right)\omega\hat{\mathbb{I}}\right)^{T}\left(-g\left(\hat{L}_{2j-1}+\hat{D}_{2j-1}\right)\right)\\
&\quad+\left(-g\left(\hat{R}_{2j-2}+\hat{U}_{2j-2}\right)\right)^{T}\left(-\left(2j-1\right)\omega\hat{\mathbb{I}}\right)
\end{aligned}
$$

$$
\begin{aligned}
jz, jz =& \left((2j-2)\,\omega \hat{\mathbb{I}} \right)^T \left((2j-2)\,\omega \hat{\mathbb{I}} \right) \\
&+ \left(-g \left(\hat{L}_{2j-2} + \hat{D}_{2j-2} \right) \right)^T \left(-g \left(\hat{L}_{2j-2} + \hat{D}_{2j-2} \right) \right) \\
&+ \left(-g \left(\hat{R}_{2j-2} + \hat{U}_{2j-2} \right) \right)^T \left(-g \left(\hat{R}_{2j-2} + \hat{U}_{2j-2} \right) \right) \\
jI, jx =& jx, jI^T \\
jI, jy =& jy, jI^T \\
jI, jI =& \left(g \left(\hat{L}_{2j-2} - \hat{D}_{2j-2} \right) \right)^T \left(g \left(\hat{L}_{2j-2} - \hat{D}_{2j-2} \right) \right) \\
&+ \left(g \left(\hat{R}_{2j-2} - \hat{U}_{2j-2} \right) \right)^T \left(g \left(\hat{R}_{2j-2} - \hat{U}_{2j-2} \right) \right) \\
&+ \left((2j-2)\,\omega \hat{\mathbb{I}} \right)^T \left((2j-2)\,\omega \hat{\mathbb{I}} \right)
\end{aligned}
$$

Bibliography

[1] D. A. Neamen and D. Biswas, *Semiconductor physics and devices* (McGraw-Hill higher education New York, 2011).

[2] K. Seeger, *Semiconductor physics* (Springer Science & Business Media, 2013).

[3] S. M. Sze, Y. Li, and K. K. Ng, *Physics of semiconductor devices* (John wiley & sons, 2021).

[4] M. O. Scully and M. S. Zubairy, *Quantum optics* (Cambridge university press, 1997).

[5] P. R. Berman and V. S. Malinovsky, *Principles of laser spectroscopy and quantum optics* (Princeton University Press, 2011).

[6] W. Shi, Q. Fang, X. Zhu, R. A. Norwood, and N. Peyghambarian, Applied optics **53**, 6554 (2014).

[7] A. Uchida, *Optical communication with chaotic lasers: applications of nonlinear dynamics and synchronization* (John Wiley & Sons, 2012).

[8] H. A. Wigdor, J. T. Walsh Jr, J. D. Featherstone, S. R. Visuri, D. Fried, and J. L. Waldvogel, Lasers in surgery and medicine **16**, 103 (1995).

[9] Q. Peng, A. Juzeniene, J. Chen, L. O. Svaasand, T. Warloe, K.-E. Giercksky, and J. Moan, Reports on Progress in Physics **71**, 056701 (2008).

[10] C. L. Degen, F. Reinhard, and P. Cappellaro, Reviews of modern physics **89**, 035002 (2017).

[11] S. Pirandola, B. R. Bardhan, T. Gehring, C. Weedbrook, and S. Lloyd, Nature Photonics **12**, 724 (2018).

[12] A. D. Ludlow, M. M. Boyd, J. Ye, E. Peik, and P. O. Schmidt, Reviews of Modern Physics **87**, 637 (2015).

[13] J. Vanier, Applied Physics B **81**, 421 (2005).

[14] I. Hrvoic, G. M. Hollyer, and P. Eng, GEM Systems Technical Papers (2005).

[15] J. B. Brask, R. Chaves, and J. Kołodyński, Physical Review X **5**, 031010 (2015).

[16] N. Gisin and R. Thew, Nature photonics **1**, 165 (2007).

[17] S. Pirandola, U. L. Andersen, L. Banchi, M. Berta, D. Bunandar, R. Colbeck, D. Englund, T. Gehring, C. Lupo, C. Ottaviani, *et al.*, Advances in optics and photonics **12**, 1012 (2020).

[18] A. V. Sergienko, *Quantum communications and cryptography* (CRC press, 2018).

[19] R. Ursin, F. Tiefenbacher, T. Schmitt-Manderbach, H. Weier, T. Scheidl, M. Lindenthal, B. Blauensteiner, T. Jennewein, J. Perdigues, P. Trojek, *et al.*, Nature physics **3**, 481 (2007).

[20] A. Steane, Reports on Progress in Physics **61**, 117 (1998).

[21] J. Gruska *et al.*, *Quantum computing*, Vol. 2005 (McGraw-Hill London, 1999).

[22] B. Fauseweh, Nature Communications **15**, 2123 (2024).

[23] A. Smith, M. S. Kim, F. Pollmann, and J. Knolle, npj Quantum Information **5**, 106 (2019).

[24] A. Das and B. K. Chakrabarti, Reviews of Modern Physics **80**, 1061 (2008).

[25] E. Farhi and S. Gutmann, Physical Review A **57**, 2403 (1998).

[26] D. Dong and I. R. Petersen, IET control theory & applications **4**, 2651 (2010).

[27] M. Shapiro and P. Brumer, *Quantum control of molecular processes* (John Wiley & Sons, 2012).

[28] M. Plesch and Č. Brukner, Physical Review A—Atomic, Molecular, and Optical Physics **83**, 032302 (2011).

[29] X.-M. Zhang, T. Li, and X. Yuan, Physical Review Letters **129**, 230504 (2022).

[30] Y. R. Sanders, G. H. Low, A. Scherer, and D. W. Berry, Physical review letters **122**, 020502 (2019).

[31] A. Polkovnikov, K. Sengupta, A. Silva, and M. Vengalattore, Reviews of Modern Physics **83**, 863 (2011).

[32] T. Oka and S. Kitamura, Annual Review of Condensed Matter Physics **10**, 387 (2019).

[33] T. Yu and J. Eberly, Physical review letters **97**, 140403 (2006).

[34] I. Rotter and J. Bird, Reports on Progress in Physics **78**, 114001 (2015).

[35] M. Sarovar and K. C. Young, New Journal of Physics **15**, 125032 (2013).

[36] M. Kolodrubetz, D. Sels, P. Mehta, and A. Polkovnikov, Physics Reports **697**, 1 (2017).

[37] N. V. Vitanov, A. A. Rangelov, B. W. Shore, and K. Bergmann, Reviews of Modern Physics **89**, 015006 (2017).

[38] R. Unanyan, M. Fleischhauer, B. Shore, and K. Bergmann, Optics Communications **155**, 144 (1998).

[39] P. Marte, P. Zoller, and J. L. Hall, Physical Review A **44**, R4118 (1991).

[40] N. Ganesan and T.-J. Tarn, Physical Review A—Atomic, Molecular, and Optical Physics **75**, 032323 (2007).

[41] H. Wiseman, Modern Physics Letters B **9**, 629 (1995).

[42] C. P. Koch, Journal of Physics: Condensed Matter **28**, 213001 (2016).

[43] G. E. Fux, E. P. Butler, P. R. Eastham, B. W. Lovett, and J. Keeling, Physical Review Letters **126**, 200401 (2021).

[44] E. P. Butler, G. E. Fux, C. Ortega-Taberner, B. W. Lovett, J. Keeling, and P. R. Eastham, Physical Review Letters **132**, 060401 (2024).

[45] E. Crosson and D. Lidar, Nature Reviews Physics **3**, 466 (2021).

[46] A. Rahmani, B. Seradjeh, and M. Franz, Physical Review B **96**, 075158 (2017).

[47] H. Mabuchi, Physical Review A—Atomic, Molecular, and Optical Physics **78**, 032323 (2008).

[48] M. Yanagisawa and H. Kimura, IEEE Transactions on Automatic control **48**, 2107 (2003).

[49] T. Kato, Journal of the Physical Society of Japan **5**, 435 (1950).

[50] J. Du, N. Xu, X. Peng, P. Wang, S. Wu, and D. Lu, Physical review letters **104**, 030502 (2010).

[51] T. Albash and D. A. Lidar, Reviews of Modern Physics **90**, 015002 (2018).

[52] D. Guéry-Odelin, A. Ruschhaupt, A. Kiely, E. Torrontegui, S. Martínez-Garaot, and J. G. Muga, Reviews of Modern Physics **91**, 045001 (2019).

[53] E. Torrontegui, S. Ibáñez, S. Martínez-Garaot, M. Modugno, A. del Campo, D. Guéry-Odelin, A. Ruschhaupt, X. Chen, and J. G. Muga, in *Advances in atomic, molecular, and optical physics*, Vol. 62 (Elsevier, 2013) pp. 117–169.

[54] S. Deffner, C. Jarzynski, and A. del Campo, Physical Review X **4**, 021013 (2014).

[55] X. Chen, A. Ruschhaupt, S. Schmidt, A. del Campo, D. Guéry-Odelin, and J. G. Muga, Physical review letters **104**, 063002 (2010).

[56] S. Masuda and K. Nakamura, Proceedings of the Royal Society A: Mathematical, Physical and Engineering Sciences **466**, 1135 (2010).

[57] K. Nakamura, A. Khujakulov, S. Avazbaev, and S. Masuda, Physical Review A **95**, 062108 (2017).

[58] D. Sels and A. Polkovnikov, Proceedings of the National Academy of Sciences **114**, E3909 (2017).

[59] Y. Zheng, S. Campbell, G. De Chiara, and D. Poletti, Physical Review A **94**, 042132 (2016).

[60] M. Demirplak and S. A. Rice, The Journal of Physical Chemistry A **107**, 9937 (2003).

[61] M. V. Berry, Journal of Physics A: Mathematical and Theoretical **42**, 365303 (2009).

[62] T. Hatomura and K. Takahashi, Physical Review A **103**, 012220 (2021).

[63] S. Omanakuttan, K. Chinni, P. D. Blocher, and P. M. Poggi, Physical Review A **107**, 032418 (2023).

[64] M. Pandey, P. W. Claeys, D. K. Campbell, A. Polkovnikov, and D. Sels, Physical Review X **10**, 041017 (2020).

[65] C. Lim, K. Matirko, A. Polkovnikov, and M. O. Flynn, arXiv preprint arXiv:2401.01927 **10** (2024).

[66] P. W. Claeys, M. Pandey, D. Sels, and A. Polkovnikov, Phys. Rev. Lett. **123**, 090602 (2019).

[67] K. Takahashi and A. del Campo, arXiv (2023), 10.48550/ARXIV.2302.05460.

[68] B. Bhattacharjee, arXiv (2023), 10.48550/ARXIV.2302.07228.

[69] S. Morawetz and A. Polkovnikov, arXiv preprint arXiv:2503.01952 (2025).

[70] I. Čepaitė, A. Polkovnikov, A. J. Daley, and C. W. Duncan, PRX Quantum **4**, 010312 (2023).

[71] I. Čepaitė, arXiv preprint arXiv:2403.20267 (2024).

[72] M. Kolodrubetz, D. Sels, P. Mehta, and A. Polkovnikov, Physics Reports **697**, 1 (2017), geometry and non-adiabatic response in quantum and classical systems.

[73] P. Kok and B. W. Lovett, *Introduction to optical quantum information processing* (Cambridge university press, 2010).

[74] A. M. Souza, G. A. Alvarez, and D. Suter, Physical Review A—Atomic, Molecular, and Optical Physics **86**, 050301 (2012).

[75] G. Burkard, D. Loss, and D. P. DiVincenzo, Physical Review B **59**, 2070 (1999).

[76] D. P. DiVincenzo and D. Loss, Journal of Magnetism and Magnetic Materials **200**, 202 (1999).

[77] A. Klimov, R. Guzmán, J. Retamal, and C. Saavedra, Physical Review A **67**, 062313 (2003).

[78] P. Gokhale, J. M. Baker, C. Duckering, N. C. Brown, K. R. Brown, and F. T. Chong, in *Proceedings of the 46th International Symposium on Computer Architecture* (2019) pp. 554–566.

[79] A. Rivas and S. F. Huelga, *Open quantum systems*, Vol. 10 (Springer, 2012).

[80] E. D. C. Lawrence, S. F. J. Schmid, I. Čepaitė, P. Kirton, and C. W. Duncan, "A numerical approach for calculating exact non-adiabatic terms in quantum dynamics," (2024), arXiv:2401.10985 [quant-ph] .

[81] C. Leforestier, R. Bisseling, C. Cerjan, M. Feit, R. Friesner, A. Guldberg, A. Hammerich, G. Jolicard, W. Karrlein, H.-D. Meyer, *et al.*, Journal of Computational Physics **94**, 59 (1991).

[82] H. Tal-Ezer and R. Kosloff, The Journal of chemical physics **81**, 3967 (1984).

[83] R. MacKenzie, A. Morin-Duchesne, H. Paquette, and J. Pinel, Phys. Rev. A **76**, 044102 (2007).

[84] J.-P. Malrieu, J.-L. Heully, and A. Zaitsevskii, Theoretica chimica acta **90**, 167 (1995).

[85] A. Polkovnikov, Physical Review B—Condensed Matter and Materials Physics **72**, 161201 (2005).

[86] P. Hauke, H. G. Katzgraber, W. Lechner, H. Nishimori, and W. D. Oliver, Reports on Progress in Physics **83**, 054401 (2020).

[87] N. Mohseni, P. L. McMahon, and T. Byrnes, Nature Reviews Physics **4**, 363 (2022).

[88] S. Yarkoni, E. Raponi, T. Bäck, and S. Schmitt, Reports on Progress in Physics (2022), 10.1088/1361-6633/ac8c54.

[89] A. Rajak, S. Suzuki, A. Dutta, and B. K. Chakrabarti, Philosophical Transactions of the Royal Society A **381**, 20210417 (2023).

[90] S. R. Das, "Quantum quench and universal scaling," (2020).

[91] S. Omanakuttan, K. Chinni, P. D. Blocher, and P. M. Poggi, Phys. Rev. A **107**, 032418 (2023).

[92] M. Pandey, P. W. Claeys, D. K. Campbell, A. Polkovnikov, and D. Sels, Phys. Rev. X **10**, 041017 (2020).

[93] T. Hatomura and K. Takahashi, Phys. Rev. A **103**, 012220 (2021).

[94] D. Sels and A. Polkovnikov, PNAS **114**, E3909 (2017).

[95] W. Miller, *Symmetry groups and their applications* (Academic Press, 1973).

[96] S. Morawetz and A. Polkovnikov, "Efficient paths for local counterdiabatic driving," (2024), arXiv:2401.12287 [quant-ph] .

[97] K. Takahashi and A. del Campo, arXiv (2023), arXiv:2302.05460 [quant-ph] .

[98] S. G. Schirmer, I. C. H. Pullen, and A. I. Solomon, Journal of Physics A: Mathematical and General **35**, 2327–2340 (2002).

[99] D. D'Alessandro, "Lie algebraic analysis and control of quantum dynamics," (2009), arXiv:0803.1193 .

[100] R. T. Sayer, *Quantum dynamics using lie algebras, with explorations in the chaotic behavior of oscillators* (Brigham Young University, 2012).

[101] B. N. Datta, *Numerical Linear Algebra and Applications, Second Edition*, 2nd ed. (Society for Industrial and Applied Mathematics, USA, 2010).

[102] C. F. Van Loan, Journal of computational and applied mathematics **123**, 85 (2000).

[103] A. Calderbank, E. Rains, P. Shor, and N. Sloane, IEEE Transactions on Information Theory **44**, 1369 (1998).

[104] M. Gell-Mann, Phys. Rev. **125**, 1067 (1962).

[105] R. A. Bertlmann and P. Krammer, Journal of Physics A: Mathematical and Theoretical **41**, 235303 (2008).

[106] D. Bossion and P. Huo, "General formulas of the structure constants in the $\mathfrak{su}(n)$ lie algebra," (2021), arXiv:2108.07219 [math-ph] .

[107] D. J. Griffiths and D. F. Schroeter, *Introduction to quantum mechanics* (Cambridge university press, 2018).

[108] T. Kadowaki and H. Nishimori, Physical Review E **58**, 5355 (1998).

[109] S. Suzuki, J.-i. Inoue, and B. K. Chakrabarti, *Quantum Ising phases and transitions in transverse Ising models*, Vol. 862 (Springer, 2012).

[110] F. Sá Barreto, I. Fittipaldi, and B. Zeks, Ferroelectrics **39**, 1103 (1981).

[111] A. Lucas, Frontiers in Physics **2** (2014), 10.3389/fphy.2014.00005, arXiv:1302.5843 [cond-mat, physics:quant-ph].

[112] Z. Bian, F. Chudak, W. G. Macready, and G. Rose, D-wave systems **2**, 1 (2010).

[113] Y. Cen, D. Das, and X. Fong, Scientific Reports **12**, 14755 (2022).

[114] F. Glover, G. Kochenberger, and Y. Du, arXiv preprint arXiv:1811.11538 (2018).

[115] M. W. Johnson, M. H. Amin, S. Gildert, T. Lanting, F. Hamze, N. Dickson, R. Harris, A. J. Berkley, J. Johansson, P. Bunyk, *et al.*, Nature **473**, 194 (2011).

[116] T. F. Rønnow, Z. Wang, J. Job, S. Boixo, S. V. Isakov, D. Wecker, J. M. Martinis, D. A. Lidar, and M. Troyer, science **345**, 420 (2014).

[117] T. Albash and D. A. Lidar, Phys. Rev. X **8**, 031016 (2018).

[118] P. Hauke, L. Bonnes, M. Heyl, and W. Lechner, Frontiers in Physics **3**, 21 (2015).

[119] T. Graß, D. Raventós, B. Juliá-Díaz, C. Gogolin, and M. Lewenstein, Nature communications **7**, 11524 (2016).

[120] D. Raventós, T. Graß, B. Juliá-Díaz, and M. Lewenstein, Phys. Rev. A **97**, 052310 (2018).

[121] A. W. Glaetzle, R. M. van Bijnen, P. Zoller, and W. Lechner, Nature communications **8**, 15813 (2017).

[122] S. Ebadi, A. Keesling, M. Cain, T. T. Wang, H. Levine, D. Bluvstein, G. Semeghini, A. Omran, J.-G. Liu, R. Samajdar, X.-Z. Luo, B. Nash, X. Gao, B. Barak, E. Farhi, S. Sachdev, N. Gemelke, L. Zhou, S. Choi, H. Pichler, S.-T. Wang, M. Greiner, V. Vuletić, and M. D. Lukin, Science **376**, 1209 (2022).

[123] P. Erdős and A. Rényi, Acta Math. Hung. **14**, 295 (1963).

[124] A. del Campo, M. M. Rams, and W. H. Zurek, Phys. Rev. Lett. **109**, 115703 (2012).

[125] B. Damski, Journal of Statistical Mechanics: Theory and Experiment **2014**, P12019 (2014).

[126] H. J. Lipkin, N. Meshkov, and A. Glick, Nuclear Physics **62**, 188 (1965).

[127] W. Heisenberg, Zeitschrift für Physik **49**, 619 (1928).

[128] P. Fendley, *Modern Statistical Mechanics* (The University of Virginia, 2014).

[129] O. S. Sarıyer, Philosophical Magazine **99**, 1787 (2019).

[130] S. Mahdavifar, S. Mahdavifar, and R. Jafari, Physical Review A **96**, 052303 (2017).

[131] B. Narozhny, A. Millis, and N. Andrei, Physical Review B **58**, R2921 (1998).

[132] K. Kubo and T. Kishi, Physical review letters **61**, 2585 (1988).

[133] S.-J. Gu, G.-S. Tian, and H.-Q. Lin, Physical Review A—Atomic, Molecular, and Optical Physics **71**, 052322 (2005).

[134] Z. Maassarani and P. Mathieu, Nuclear Physics B **517**, 395 (1998).

[135] F. J. Dyson, E. H. Lieb, and B. Simon, Physical Review Letters **37**, 120 (1976).

[136] S.-J. Gu, H.-Q. Lin, and Y.-Q. Li, Physical Review A **68**, 042330 (2003).

[137] A. Malvezzi, . G. Karpat, B. Çakmak, F. Fanchini, T. Debarba, and R. Vianna, Physical Review B **93**, 184428 (2016).

[138] T. Lahaye, C. Menotti, L. Santos, M. Lewenstein, and T. Pfau, Reports on Progress in Physics **72**, 126401 (2009).

[139] S. Solimeno, P. Di Porto, and B. Crosignani, Journal of Mathematical Physics **10**, 1922 (1969).

[140] J. G. Muga, X. Chen, S. Ibáñez, I. Lizuain, and A. Ruschhaupt, Journal of Physics B: Atomic, Molecular and Optical Physics **43**, 085509 (2010).

[141] P. T. Nam, M. Napiórkowski, and J. P. Solovej, Journal of Functional Analysis **270**, 4340 (2016).

[142] J. Flick, N. Rivera, and P. Narang, Nanophotonics **7**, 1479 (2018).

[143] A. Frisk Kockum, A. Miranowicz, S. De Liberato, S. Savasta, and F. Nori, Nature Reviews Physics **1**, 19 (2019).

[144] P. Forn-Díaz, L. Lamata, E. Rico, J. Kono, and E. Solano, Reviews of Modern Physics **91**, 025005 (2019).

[145] N. Rivera and I. Kaminer, Nature Reviews Physics **2**, 538 (2020).

[146] J. Larson and E. K. Irish, Journal of Physics A: Mathematical and Theoretical **50**, 174002 (2017).

[147] E. Jaynes and F. Cummings, Proceedings of the IEEE **51**, 89 (1963).

[148] B. Zwiebach, *Mastering quantum mechanics: essentials, theory, and applications* (MIT Press, 2022).

[149] E. W. Weisstein, https://mathworld. wolfram. com/ (2002).

[150] I. I. Rabi, Phys. Rev. **51**, 652 (1937).

[151] Q. Xie, H. Zhong, M. T. Batchelor, and C. Lee, Journal of Physics A: Mathematical and Theoretical **50**, 113001 (2017).

[152] E. Twyeffort Irish, Physical review letters **99**, 173601 (2007).

[153] G. Y. Hu and R. F. O'Connell, Journal of Physics A: Mathematical and General **29**, 1511 (1996).

[154] C. Kapadia, "Standard mathematical tables," (1970).

Bibliography